DNA-MEDIATED CHARGE TRANSPORT DEVICES FOR PROTEIN DETECTION

Thesis by
Ariel L. Furst

In Partial Fulfillment of the Requirements
for the Degree of
Doctor of Philosophy in Chemistry

California Institute of Technology
Pasadena, CA
2015
(Defended May 28, 2015)

Acknowledgements

It is with immense gratitude that I acknowledge the many people who have supported and guided me in this work. First and foremost, I wish to thank my advisor, Prof. Jackie Barton. Your passion for science and continued optimism are a constant inspiration. Thank you for everything you have taught me, especially how to make beautiful figures. With your guidance, I have learned to take risks and push back scientific frontiers. Your unwavering enthusiasm has made me a strong, fearless scientist.

I cannot find words to express my appreciation for Prof. Mike Hill. Your collaboration throughout my time at Caltech has been invaluable. I have learned so much from you, both inside and outside of the lab. Your ability to break extremely complex ideas into manageable pieces combined with your infinite knowledge of electrochemistry has helped shape my graduate training. Your advice and support have enabled me to take risks in the laboratory, which, as you have taught me, leads to the most interesting discoveries. I also thank you for your friendship; your constant positivity has been an inspiration over the past five years, especially when I had trouble finding my own.

I would also like to thank my committee chair, Prof. Doug Rees, for your guidance throughout my graduate studies. It has been incredibly rewarding to work as a TA for you over the past four years. You have showed me how to be an effective teacher, especially your ability to weave real-world examples and demonstrations into your lectures. I am thankful for the support of my committee members, Profs. Harry

Gray and Theo Agapie; your genuine interest in my work and insightful questions during my exams have made me a better scientist.

To Maureen Renta, thank you for everything you have done for me. Your humor kept me sane, especially while waiting for meetings with my committee. Your friendship has meant so much to me, and your advice has been invaluable.

I am so thankful to have worked with so many wonderful Bartonites. You truly make the lab what it is. In particular, I would like to thank the Barton group members who have collaborated with me or provided me guidance throughout this journey. Natalie Muren, you took me under your wing when I first joined the group and taught me how to become a scientist. You showed me everything I would need to know in the Barton group, from techniques like DNA purification and human cell culture to keeping an impeccable notebook and fixing the DNA synthesizer. You have also been a constant source of both scientific and emotional support, especially during difficult periods in the lab. Your mentorship and friendship are the reasons for my success, and one of my proudest moments of graduate school was feeling that you trusted me with your experiments.

In addition, Eric Olmon, Pam Sontz, Katie Schaefer, Catrina Pheeney, and Anna Arnold, among others, have taught me so much. You have always been available to offer advice or train me on a new technique. I have considered it an honor to work with other members of the electrochemistry subgroup, who are always willing to lend a hand and troubleshoot when obstacles arise.

To my Caltech friends, thank you for lending an ear or a shoulder and for making the past five years so wonderful. Thank you to Alexis Komor and Andrew Wang, Myles

Herbert, Kathryn Perez, Mike Post, Guy Edouard, Kaycie Deyle, Adam Boynton, Anna and Seth Arnold, and so many others. Thanks especially to Phil Bartels for being an immense source of support both inside and outside of the lab. I must also thank my Occidental friends for your constant optimism, especially Lisa Pangilinan and Jeremy Kallick.

Thanks also to my non-Caltech friends; you are always able to keep things in perspective. Roy, Mike, and all of my friends at REKM have truly kept me grounded for the past three years. Lynn, Regina, and Linda: you have all added humor to my life and offered me so much insight and guidance. Molly, you have been my support since high school. Without you to talk to, I would have gone insane.

This thesis would not have been possible without my roommate and bestie, Alyson Weidmann. You have been a constant source of strength and advice. You truly are the reason I have stayed sane throughout graduate school. You have been there to congratulate me at the high points and pick me up at the low points. You are the only person who understands exactly what I am feeling from just a look.

I owe my deepest gratitude to my family for their endless love and support. Thank you to my Mom and Michael for all of the help and advice you have given me throughout the years and for reminding me about the importance of pursuing a career in something that truly inspires me. You both have showed me how to have an open mind while also thinking critically. Thank you for listening to me and providing unending understanding and support. I would also like to thank my brother, David, whose humor and insight have helped me throughout the years. I can always count on you to make me laugh. Finally, I would like to thank my grandparents for emphasizing the importance of

education. Your love and encouragement (and care packages) have helped more than I can say.

Finally, to my better half, Tim: your constant encouragement is truly the reason I am where I am today. You have solved any problem that has arisen for me, sat with me in lab on the weekends, read every draft I have written, and listened to all of my talks. You have always put my needs before your own. You are the most patient, kind person I know, and I honestly do not know what I would do without your support and advice. I am so lucky to have you in my life. Thank you.

Abstract

Detection of biologically relevant targets, including small molecules, proteins, DNA, and RNA, is vital for fundamental research as well as clinical diagnostics. Sensors with biological elements provide a natural foundation for such devices because of the inherent recognition capabilities of biomolecules. Electrochemical DNA platforms are simple, sensitive, and do not require complex target labeling or expensive instrumentation. Sensitivity and specificity are added to DNA electrochemical platforms when the physical properties of DNA are harnessed. The inherent structure of DNA, with its stacked core of aromatic bases, enables DNA to act as a wire via DNA-mediated charge transport (DNA CT). DNA CT is not only robust over long molecular distances of at least 34 nm, but is also especially sensitive to anything that perturbs proper base stacking, including DNA mismatches, lesions, or DNA-binding proteins that distort the π-stack. Electrochemical sensors based on DNA CT have previously been used for single-nucleotide polymorphism detection, hybridization assays, and DNA-binding protein detection. Here, improvements to (i) the structure of DNA monolayers and (ii) the signal amplification with DNA CT platforms for improved sensitivity and detection are described.

First, improvements to the control over DNA monolayer formation are reported through the incorporation of copper-free click chemistry into DNA monolayer assembly. As opposed to conventional film formation involving the self-assembly of thiolated DNA, copper-free click chemistry enables DNA to be tethered to a pre-formed mixed alkylthiol monolayer. The total amount of DNA in the final film is directly related to the amount of azide in the underlying alkylthiol monolayer. DNA monolayers formed with

this technique are significantly more homogeneous and lower density, with a larger amount of individual helices exposed to the analyte solution. With these improved monolayers, significantly more sensitive detection of the transcription factor TATA binding protein (TBP) is achieved.

Using low-density DNA monolayers, two-electrode DNA arrays were designed and fabricated to enable the placement of multiple DNA sequences onto a single underlying electrode. To pattern DNA onto the primary electrode surface of these arrays, a copper precatalyst for click chemistry was electrochemically activated at the secondary electrode. The location of the secondary electrode relative to the primary electrode enabled the patterning of up to four sequences of DNA onto a single electrode surface. As opposed to conventional electrochemical readout from the primary, DNA-modified electrode, a secondary microelectrode, coupled with electrocatalytic signal amplification, enables more sensitive detection with spatial resolution on the DNA array electrode surface. Using this two-electrode platform, arrays have been formed that facilitate differentiation between well-matched and mismatched sequences, detection of transcription factors, and sequence-selective DNA hybridization, all with the incorporation of internal controls.

For effective clinical detection, the two working electrode platform was multiplexed to contain two complementary arrays, each with fifteen electrodes. This platform, coupled with low density DNA monolayers and electrocatalysis with readout from a secondary electrode, enabled even more sensitive detection from especially small volumes (4 μL per well). This multiplexed platform has enabled the simultaneous

detection of two transcription factors, TBP and CopG, with surface dissociation constants comparable to their solution dissociation constants.

With the sensitivity and selectivity obtained from the multiplexed, two working electrode array, an electrochemical signal-on assay for activity of the human methyltransferase DNMT1 was incorporated. DNMT1 is the most abundant human methyltransferase, and its aberrant methylation has been linked to the development of cancer. However, current methods to monitor methyltransferase activity are either ineffective with crude samples or are impractical to develop for clinical applications due to a reliance on radioactivity. Electrochemical detection of methyltransferase activity, in contrast, circumvents these issues. The signal-on detection assay translates methylation events into electrochemical signals *via* a methylation-specific restriction enzyme. Using the two working electrode platform combined with this assay, DNMT1 activity from tumor and healthy adjacent tissue lysate were evaluated. Our electrochemical measurements revealed significant differences in methyltransferase activity between tumor tissue and healthy adjacent tissue.

As differential activity was observed between colorectal tumor tissue and healthy adjacent tissue, ten tumor sets were subsequently analyzed for DNMT1 activity both electrochemically and by tritium incorporation. These results were compared to expression levels of *DNMT1*, measured by qPCR, and total DNMT1 protein content, measured by Western blot. The only trend detected was that hyperactivity was observed in the tumor samples as compared to the healthy adjacent tissue when measured electrochemically. These advances in DNA CT-based platforms have propelled this class of sensors from the purely academic realm into the realm of clinically relevant detection.

Table of Contents

List of Figures

Chapter 1

Chapter 2

Chapter 3

Chapter 4

Chapter 5

Chapter 6

Chapter 7

Chapter 8

Chapter 1

Introduction

Adapted from: Barton, J. K., Furst, A. L., and Grodick, M. A. (2015) DNA Sensors using DNA Charge Transport Chemistry, in DNA in Supramolecular Chemistry and Nanotechnology, 1st Ed. Wiley & Sons *In Press*.

and Furst, A. L., Hill, M. G., and Barton, J. K. (2014) Electrocatalysis in DNA Sensors, *Polyhedron 84*, 150-159.

DNA Charge Transport

From the first proposal of the structure of DNA,[1, 2] debates about what properties DNA may hold beyond the simple transfer of genetic information have arisen. The structure of the stacked DNA bases within the double helix led many to predict that this macromolecular assembly could conduct charge. The stacked base pairs closely resemble the structure of graphene sheets, as both contain aromatic heterocycles stacked at 3.4 Å (Figure 1.1).[3] However, the notion that the DNA helix can conduct charge was long met with skepticism. Today, as a result of extensive experimentation, DNA charge transport (DNA CT) is well-established chemistry, though the full mechanistic understanding still requires development.[4]

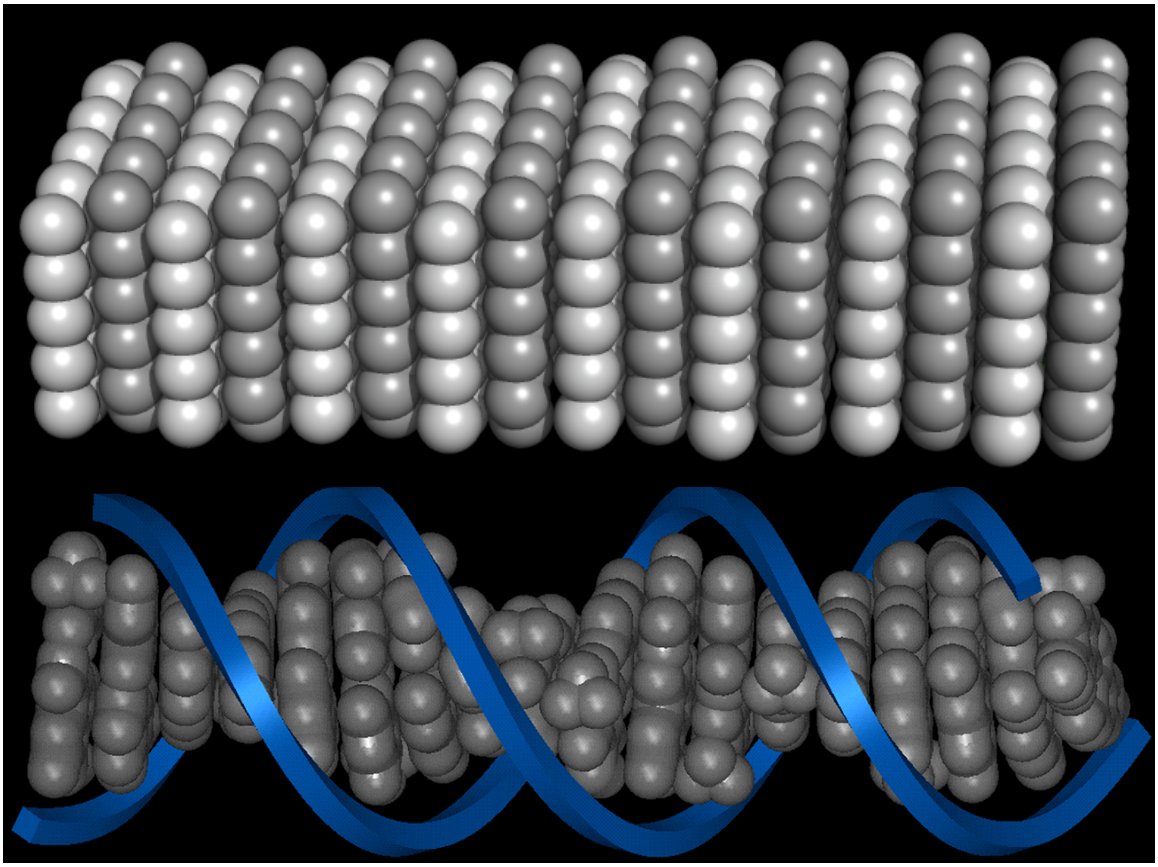

Figure 1.1 Schematic illustrations of the structures of graphene (top) and DNA (bottom). The planar sheets of graphene are shown in grey, as are the aromatic DNA bases; for the DNA, the sugar-phosphate backbone has been schematized as a ribbon (blue). In both cases, the layers are stacked at a distance of 3.4 Å, enabling orbital overlap, and therefore the flow of charge.

Experiments with DNA CT first involved the observation of long-range, excited-state charge transport through a DNA duplex between well-stacked donors and acceptors.[5-7] In an early experiment, electron transfer between covalently tethered metallointercalators was observed over a distance of 40 Å through DNA (Figure 1.2).[5] A 15-base DNA duplex was labeled at one terminus with $[Ru(phen)_2dppz]^{2+}$ (dppz = dipyrido[3,2-*a*:2',3'-*c*]phenazine), with the excited state acting as an electron donor, and $[Rh(phi)_2phen]^{3+}$ (phi = 9,10-phenanthrenequinone diimine) at the opposite terminus acting as an electron acceptor. In the absence of the electron acceptor, the ruthenium complex tethered to DNA luminesces. However, upon incorporation of the rhodium complex, the luminescence is completely quenched. In the years since this experiment, the ability of DNA to conduct charge through its π-stacked bases has been studied extensively using a variety of platforms.[5, 8-12] Moreover, as the power of this chemistry became apparent, experiments focused on biological applications of DNA CT chemistry came to the forefront.[13]

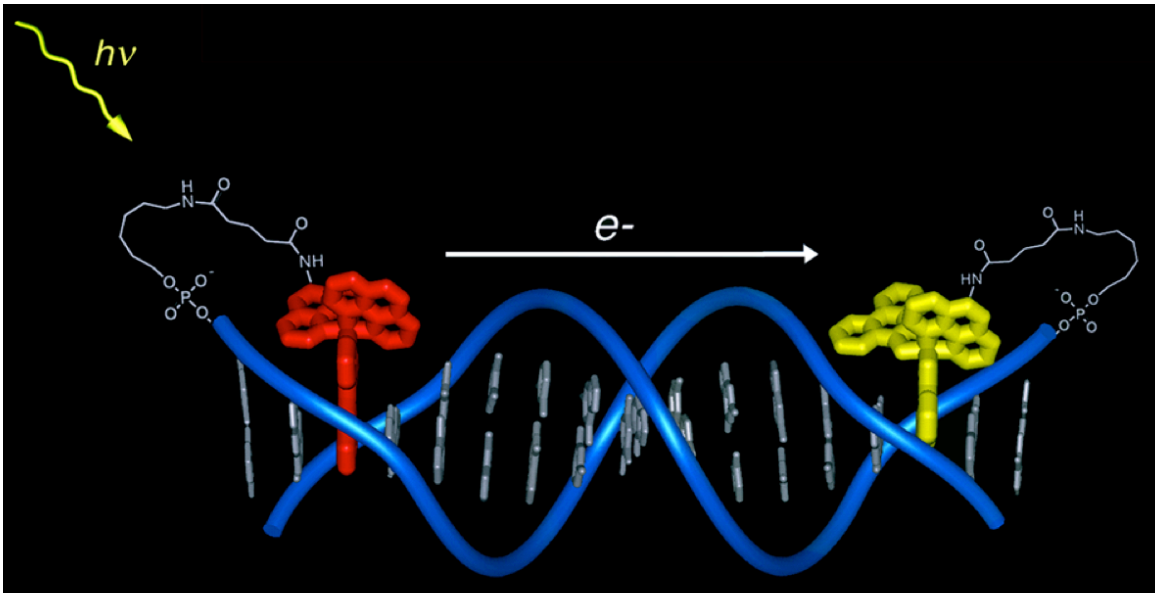

Figure 1.2 A DNA modified with two metallointercalators to test photoinduced DNA CT. Electron transfer over 40 Å was shown through DNA between covalently tethered metallointercalators, $[Ru(phen)_2dppz]^{2+}$ (red) as an electron donor and $[Rh(phi)_2phen]^{3+}$ (yellow) at the opposite terminus as an electron acceptor.[5]

The remarkable utility of this chemistry became evident as DNA CT was shown to be extremely efficient over long molecular distances on fast time scales, yet exquisitely sensitive to perturbations in base-base stacking.[14] Single base mismatches and other damaged products have been shown to significantly attenuate CT both in ground and excited state experiments.[15-17] DNA CT has also been directly measured in single molecule experiments in the ground state.[18] Using an oxygen plasma, molecular size gaps can be inserted into carbon nanotubes and individual DNA molecules functionalized with terminal amines covalently attached within the gaps using amide chemistry. These robust devices can then be used to measure the current flow in the nanotube containing the covalently attached molecule of interest versus that current in the original nanotube (Figure 1.3). In these devices, duplex DNA was attached either by functionalizing the 5'-end of both strands of the DNA with alkyl amines or both 3'- and 5'-ends of only one of the strands of the duplex, with the complementary strand non-covalently associated. Using this device, we found that the resistance generated in the gap with a DNA duplex inserted was quite similar to that expected for a stacked graphite insert (~ 1 megaohm resistance for a ~6 nm gap).

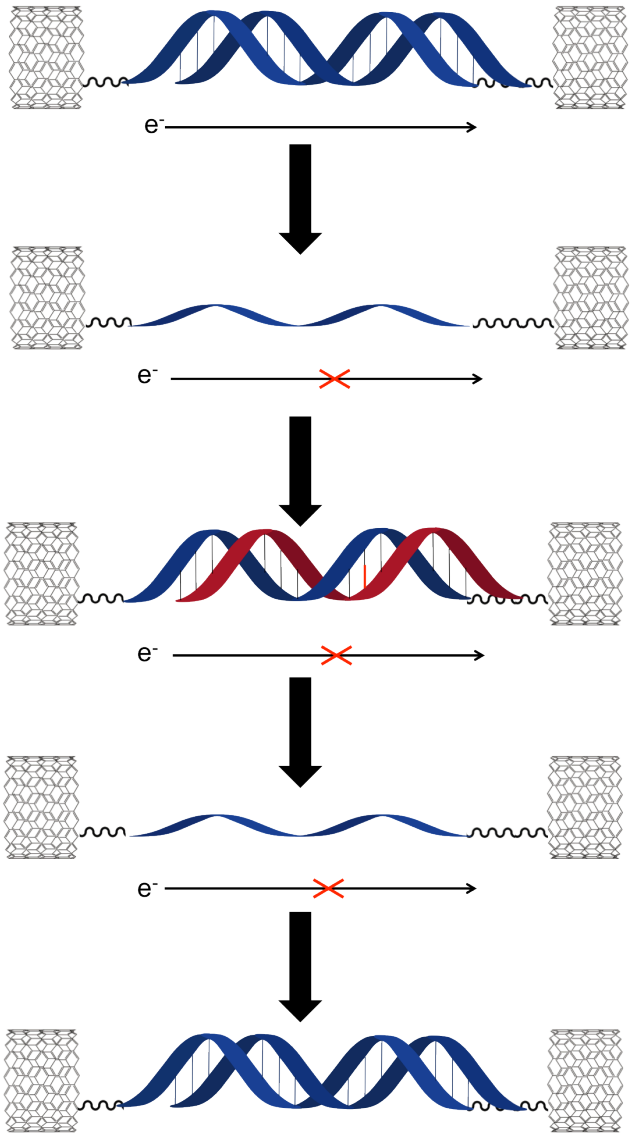

Figure 1.3 Illustration of a single molecule experiment with DNA tethered to carbon nanotubes to test ground state DNA CT.[18] Well matched DNA is covalently attached to carbon nanotubes through the termini of the DNA functionalized with amines. The DNA can then be denatured in the device so that only one strand remains covalently attached. A complementary strand that contains a single base mismatch can then be floated in and annealed to the covalently tethered strand. For the well matched duplex DNA (top), significant current is obtained, but this current is attenuated in the presence of a mismatch (middle with red mismatch); addition of the well matched complement (bottom) restores full current flow. This cycle of unannealing and reannealing alternative complements can be repeated and the conductivity reproducibly measured.

Even more interesting was how this assembly could be used to test the effect of a mismatch on DNA CT. With one strand covalently attached to the device through both the 5'- and 3'-ends, various complements, with or without a mismatch, could be interchanged into the duplex and the resultant current tested (Figure 1.3). Several different complements could be cycled in this robust device. The presence of a mismatch was found to yield a 300-fold attenuation in current relative to the current found for the well matched complement. Moreover, all current was lost upon DNA cleavage with a blunt-end restriction enzyme, illustrating that the conformation of the DNA duplex in the gap was intact and recognizable by the DNA-binding protein.

While early experiments focused on the distance dependence of DNA CT using largely spectroscopic experiments involving excited state transport, ground state measurements repeatedly illustrated the high sensitivity of DNA CT to intervening perturbations in stacking.[11] Although the shallow distance dependence of DNA CT was remarkable, so too was the exquisite sensitivity of DNA CT to perturbations in base stacking. This led to significant applications of DNA CT chemistry in bio-sensing. DNA CT has allowed the sensitive detection of a variety of biologically relevant targets, including single base mismatches irrespective of sequence context, the monitoring of binding of DNA transcription factors, and even following, electrochemically, the reactions of various enzymes on DNA. DNA CT-based platforms represent one example within a broad family of nucleic acid sensing platforms.

Nucleic Acid Biosensing

Detection of biologically relevant targets is vital for both fundamental research as well as clinical and field diagnostics. Sensing strategies that feature biological substrates for analyte capture provide a natural foundation for bioassays owing to the inherent molecular-recognition nature of substrate-ligand binding. Nucleic-acid-based platforms in particular comprise an especially robust and flexible class of sensors capable of detecting a variety of small-molecule, protein, and DNA/RNA targets.[19] Among the many different read-out strategies employed for DNA-based sensing (*e.g.,* fluorescence,[20-23] changes in conductivity,[24, 25] or mass[26-30] that accompany hybridization, *etc.*), we have focused on electrochemical methods.[31, 32] Electrochemical instrumentation is both low cost and portable, making this method of detection ideal for clinical diagnostics.

One of the first DNA electrochemical detection strategies involved the direct reduction of nucleic acid bases adsorbed onto a mercury electrode: hybridization of a target sequence increased the amount of adsorbed DNA, resulting in greater signals.[33] Similarly, sinusoidal voltammetry was used to measure the direct oxidation of the amine-containing nucleobases as well as the sugar-phosphate backbone of all nucleotides.[34] While this platform is potentially capable of detecting zeptomoles of DNA, it is impractical for biosensor applications due to its lack of specificity to differentiate between dissimilar sequences of DNA.

Alternative systems typically rely on indirect detection schemes, in which a redox-active mediator is employed either to report on the composition of target DNA or to induce redox reactions of the bases themselves.[35] Often, the target DNA is labeled with

a small, electrochemically active molecule; hybridization is then signaled by the appearance of an electrochemical signal. This technique mimics common fluorescence-based techniques in that the target, rather than the probe, is modified.[36] Target labeling has the advantage of presenting a 'signal on' method of detection—a hybridization event must successfully occur for an electrochemical signal to appear—yet is ultimately limited by the thermodynamic stability of the DNA duplexes formed. Non-specific hybridization can result in false positive signals, making the identification of subtle sequence variants, *e.g.,* single-nucleotide polymorphisms, impractical.

The probe sequence can also be labeled in electrochemical DNA sensors. One such system involves the application of a hairpin DNA construct as the probe molecule.[37] Hairpins are DNA architectures that are composed of a stem region containing a self-complementary sequence and a disordered loop region containing the target sequence. Upon hybridization to a complementary target, the hairpin opens. If the terminus of the stem region is modified with a redox-active moiety, the probe will be in close proximity to the surface in the hairpin form where it will be electrochemically active with no target bound. This signal will significantly diminish upon target binding.[38]

Finally, there are DNA-based electrochemical detection methods based on DNA 'sandwich' assemblies. These structures involve three sequences of DNA: a target molecule, a probe molecule tethered to the surface, and a reporter sequence.[39-42] The reporter sequence binds to an overhang of the probe-target duplex and can either directly generate an electrochemical signal or can be a component of an ancillary redox cycle. This method of detection negates the necessity of target labeling and maintains a 'signal on' detection scheme.

DNA-functionalized Electrochemical Sensors

The most common technique employed for electrochemical detection based on DNA CT involves the immobilization of duplexed DNA on a gold surface at one terminus and modified with a redox-active probe at the distal terminus (Figure 1.4). A range of redox-active probes have been employed, and, unsurprisingly, the most sensitive reporters of the integrity of the DNA duplex are those that are themselves well stacked and hence well coupled into the DNA π-stack.

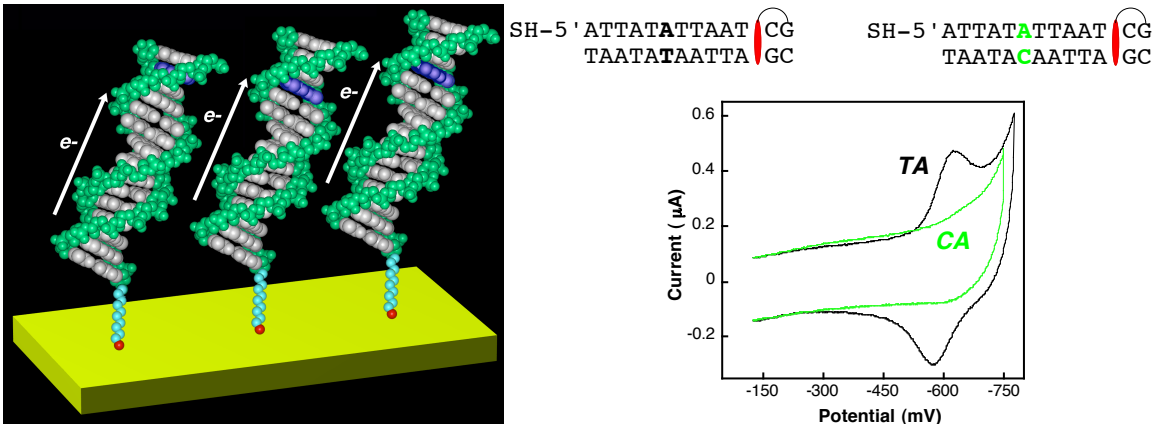

Figure 1.4 Electrochemical signal from well matched DNA and DNA containing a single-base mismatch using DNA-modified electrodes. DNA assembled on a gold electrode (left) containing a covalent redox reporter daunomycin was electrochemically monitored by cyclic voltammetry (right).[43] The well matched DNA produces a large, reversible signal. Upon incorporation of a single-base mismatch, the electrochemical signal is significantly attenuated.

In one electrochemical experiment, the DNA duplex was shown to carry out ground state charge transport over 100 base pairs, or 34 nm.[44] This experiment involved a particularly long molecular wire, but the extraordinary sensitivity of DNA to small perturbations in the base stack was demonstrated through the significant electrochemical effect of a single mismatched base incorporated into the DNA duplex. The 100-mer was terminally modified with a covalent Nile blue redox probe and assembled on the gold electrode. The incorporation of a single mismatched base pair resulted in a significant attenuation of signal, 0.8 ± 0.1 nC for the cathodic peak containing a single base mismatch, as compared to 1.7 ± 0.1 nC for that of the well-matched duplex.[44] Interestingly, the degree of signal attenuation observed through 100 base pairs for the single base mismatch was equal to that observed for the same mismatch incorporated into a 17-mer. Remarkably, while the effect of the mismatch is substantial and independent of duplex length and sequence context, no perturbation in current is observed with a nick in the DNA backbone. The 100-mer used in this experiment was actually constructed from the annealing of several smaller pieces of DNA containing sticky ends. What is essential for DNA CT is effective base stacking; CT is through the base pair stack, not the sugar-phosphate backbone.

DNA-modified Electrode Formation

Generally, a major challenge of DNA-based electrochemical sensors is the ability to detect bulky biomolecules specifically at a solid surface. Conventionally, DNA-modified electrodes are formed through the self-assembly of thiolated DNA onto a planar gold electrode.[45] However, this method provides only limited control over the spacing and total amount of DNA assembled on a surface. It has been shown, in fact, that DNA assembled in this manner clusters into regions of extremely high DNA density, leaving other areas on the electrode surface bare.[46, 47] This inhomogeneity can lead to issues with effective and consistent detection, as different regions of the electrode surface respond differently to the addition of analyte.[48] Additionally, upon inclusion of a shielding ion, such as $MgCl_2$, which neutralizes the negatively charged DNA backbone, DNA forms a fairly uniform but extremely dense monolayer. This type of morphology limits the access of targets to the surface probes, significantly decreasing the sensitivity of detection.[49] One major area of research, therefore, has been the development of methods to both better control the homogeneity of DNA-modified surfaces, as well as to increase the spacing between individual DNA helices. There are two main schools of thought as to how best to control the assembly of DNA helices: controlling the underlying electrode morphology through nanostructuring and attachment of DNA to pre-formed monolayers.

Nanostructured Microelectrodes

Nanostructured microelectrodes have been reported to yield better spacing of the DNA over conventional, planar electrodes by increasing the deflection angle between the DNA helices.[50, 51] Nanostructuring microelectrodes involves the preliminary formation

of patterned electrodes using conventional lithographic techniques onto a substrate. Subsequently, electrodeposition onto these pre-formed electrodes enables the formation of nanoscale structures that increase the overall surface area available for biomolecule attachment.[52] Multiple conditions for the addition of the nanostructured electrodes have been attempted, and small variations in the assembly conditions greatly affect the roughness of the resulting structures. [53] For example, applying higher deposition potentials leads to more highly patterned nanostructures, which reportedly enable greater access to individual DNA helices than their smooth counterparts. One consequence of the electrodeposition method, however, is that while the degree of patterning and the total amount of metal added can be controlled, the specific surface structure cannot. Thus, no two electrodeposited electrode surfaces will be identical, making direct comparisons potentially problematic.

Electrochemical detection with this platform involves the well known electrocatalytic signal amplification of $Fe(CN)_6^{3-}$ reduction mediated by the electrostatic reporter $Ru(NH_3)_6^{3+}$. Detection limits for hybridization assays using this technique have reached sub-femtomolar limits.[53] While this method of detection provides significant amplification, like all methods in which the electrochemical signals are monitored at the probe-modified surface, it also produces a large background signal, with relatively small electrochemical differentials between no hybridization to the target and full hybridization. While these small differentials can be translated into large percentage differentials, they have not yet been shown to be sufficiently reliable for clinical detection from crude samples.

Controlled Self-Assembly onto Flat Surfaces

Straightforward chemical methods can also be used to regulate the placement of DNA on planar electrodes and effectively control the homogeneity and spacing of the DNA duplexes within a sensing monolayer. Conventional DNA-modified electrode surfaces are formed through the self-assembly of thiolated DNA duplexes on gold surfaces. Owing to the restricted access of target molecules to sterically congested probe sequences, these monolayers are not ideal for the detection of large proteins, proteins that bind to specific sequences of DNA, or hybridization events. Although the surface density of the DNA monolayer can be controlled through the adjustment of the composition and ionic strength of the deposition solution—high ionic strength provides better Debye screening of the negative charges on DNA, enabling the DNA helices to pack closer together—the range of DNA surface coverages is narrow (~40 – 50 pmol/cm^2). Similarly, conventional DNA assembly methods do not allow control over the homogeneity of DNA dispersed within a multicomponent film. It is also known that thiol-modified DNA forms a heterogeneous monolayer when combined with a passivating agent such as mercaptohexanol. The DNA helices cluster into large domains of very high density, leaving large regions of the surface almost entirely devoid of DNA.[46, 47] This helix clustering is especially problematic for detection because it leads to variability across the electrode surface and makes access to specific base sequences difficult.

An alternative method of monolayer formation, based on azide/alkyne "click" coupling, provides significantly more control over both the homogeneity of DNA within a monolayer and the total amount of DNA assembled onto the surface. With this

assembly technique, alkyne-labeled DNA is coupled to a pre-formed mixed alkanethiol monolayer doped with azide-terminated functionalities. The underlying composition of the monolayer determines the bulk DNA loading onto the film. Shown in Figure 1.5 is a schematic representation of the difference in spacing between DNA helices formed by thiolated DNA self-assembly and DNA assembled *via* click chemistry to a pre-formed mixed monolayer. A schematic of DNA monolayer formation *via* copper-free click chemistry is shown in Figure 1.6.

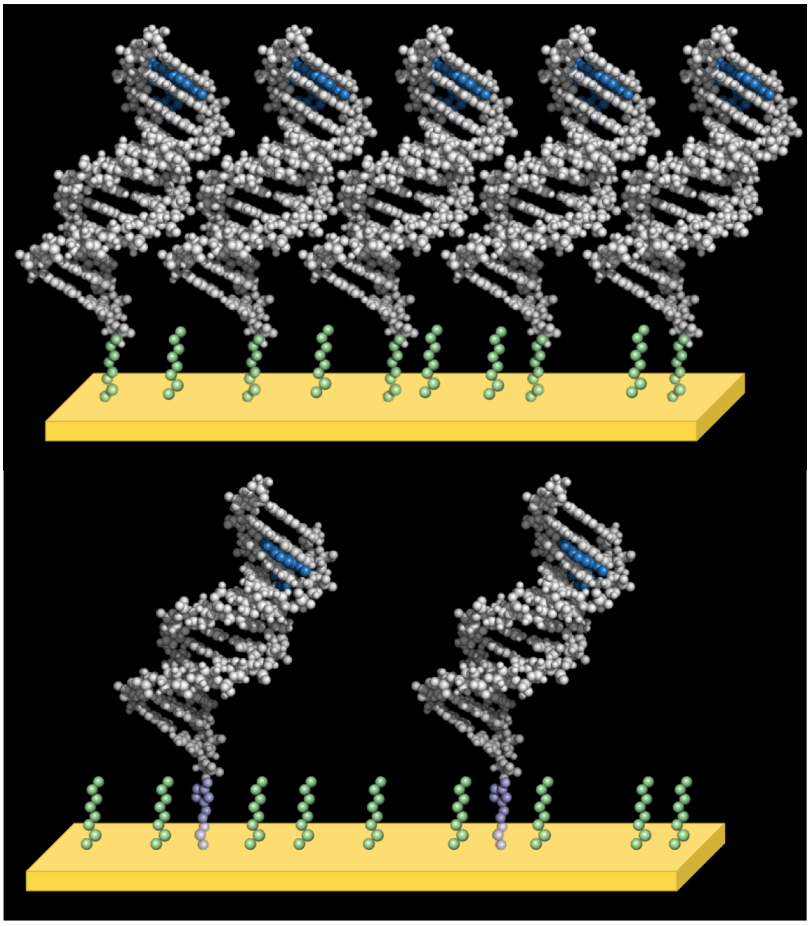

Figure 1.5 Representation of DNA monolayers formed conventionally and with click chemistry. DNA is shown tethered to a gold electrode surface with a terminally bound redox probe for efficient electrochemical readout. Self-assembled thiolated DNA (*top*) forms regions of very high DNA density, which can prevent access of large biomolecules to the probe sequences on the surface, with other regions of the electrode surface devoid of DNA. In contrast, DNA that is 'clicked' onto a pre-formed mixed alkanethiol monolayer has significantly more controlled spacing with more separation between the helices, enabling greater access to the individual probe DNA helices.

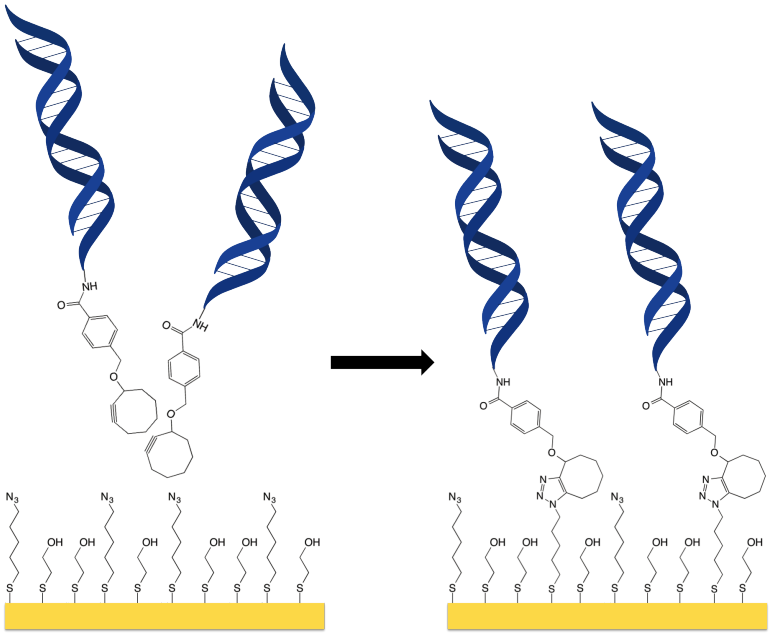

Figure 1.6 Assembly of DNA monolayers using copper-free click chemistry. DNA modified with a strained cyclooctyne moiety is added to pre-formed mixed alkanethiol monolayers containing 'active' azide head groups as well as 'passivating' alcohol head groups. The DNA can only attach to the points at which an azide has previously been immobilized. Because of the cyclooctyne ring strain, the reaction between the azide and the alkyne occurs spontaneously.

Redox Probes for DNA-mediated Charge Transport Detection

Effective detection by DNA CT is dependent on the interaction between a redox probe and the base stack, whether the molecule is covalently tethered to DNA or free in solution. There are multiple modes of non-covalent interaction between small molecules and DNA, including groove binding, electrostatic association, and intercalation. For effective DNA CT, the redox probes must be well coupled into the base pair stack. Intercalation, where the probe is itself p-stacked in the duplex, is a particularly sensitive coupling mode for electrochemical applications. A series of redox-active probes that interact with DNA through either intercalation or groove binding were tested for signal attenuation upon incorporation of a mismatch. The compounds capable of intercalation, including $[Ir(bpy)(phen)(phi)]^{3+}$, daunomycin, and methylene blue, lead to a differential in the electrochemical current between well-matched duplexes and duplexes containing a single-base mismatch. Ruthenium hexammine, however, which is only capable of hydrogen binding in the groove, shows no difference in current between the well-matched and mismatched DNA; here CT is not *through* the base stack. Moreover, the intercalative complexes that are less likely to groove bind, $[Ir(bpy)(phen)(phi)]^{3+}$ and daunomycin, have a significantly greater signal differential for mismatch discrimination (CA:TA signal ratio of 0.3) than methylene blue (CA:TA signal ratio of 0.5). Figure 1.7 shows the difference in specificity for mismatch discrimination between the small molecule ruthenium hexammine and the DNA intercalator daunomycin, which speaks to the sensitivity of the π-stack to perturbations to charge transport.

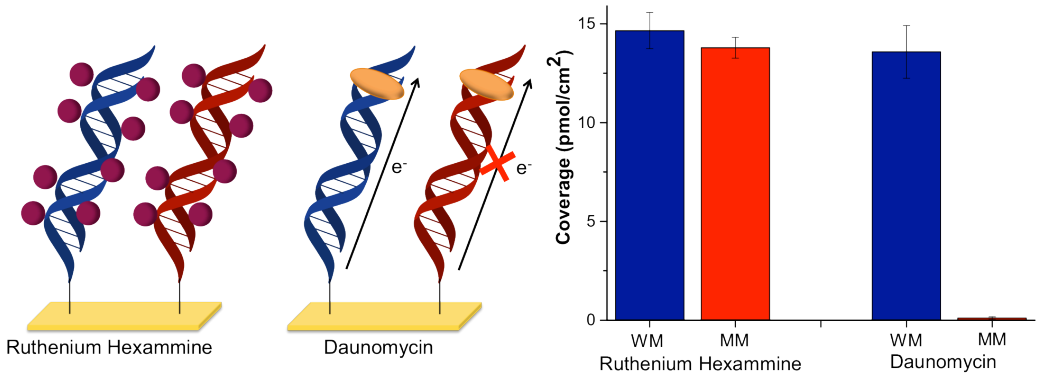

Figure 1.7 DNA monolayer coverage determined by ruthenium hexammine and daunomycin. Ruthenium hexammine electrostatically interacts with the DNA backbone (purple dots, left), and is therefore a good redox probe to determine the total amount of phosphate on the surface. Daunomycin, a redox-active DNA intercalator, is capable of interacting with the DNA base stack and reporting on perturbations therein (orange spheres, center). When DNA coverage on electrodes is determined by quantifying the redox signal from each of these probes with either well-matched DNA (blue bars, right) or mismatch-containing DNA (red bars, right), ruthenium hexammine yields the same total DNA coverage for both sequences. In contrast, a significant signal attenuation is observed for the daunomycin redox probe with mismatch-containing DNA, as compared to the well-matched sequence.[54]

Electrocatalysis for Signal Amplification

In order to detect low-abundance species, it may be necessary to amplify the electrochemical signal obtained directly from a DNA-interacting reporter, as these signals can be prohibitively small. To address the problem of small electrochemical signals, an electrocatalytic cycle can be incorporated into the detection platform for signal amplification. The most effective signal amplification system involves intercalated MB coupled to $Fe(CN)_6^{3-}$ freely diffusing in solution.[17] Owing to its negative charge, direct electrochemical reduction of $Fe(CN)_6^{3-}$ is inhibited at the highly (negatively) charged surfaces of DNA-modified electrodes, even at overpotentials as high as 1 V. On the other hand, reduction of $Fe(CN)_6^{3-}$ by leucomethylene blue (LB, the reduced form of MB), is thermodynamically favored by more than 0.5 eV, ensuring a rapid homogeneous electron transfer reaction. Thus, addition of micromolar MB to electrolyte solutions containing millimolar $Fe(CN)_6^{3-}$ leads to a dramatic increase in the electrochemical response at a DNA-modified electrode. Importantly, the onset of this response occurs at the reduction potential of MB (indicating MB as the electrochemical mediator), and the reduction is completely irreversible, as the reduced form of MB is oxidized rapidly by $Fe(CN)_6^{3-}$ and is therefore no longer available for electrochemical oxidation.

Methylene Blue as Electrocatalyst with Ferricyanide

Based on data collected at rotating disk electrodes,[55] we proposed the mechanism of electrocatalysis between MB and $Fe(CN)_6^{3-}$ illustrated in Figure 1.8 for this reaction. The cycle begins with MB intercalated into the DNA film. Upon sweeping the potential past the formal MB/LB reduction potential, MB is rapidly reduced through DNA CT to

LB, which subsequently dissociates from the film and reduces two equivalents of $Fe(CN)_6^{3-}$. Intercalation of regenerated MB back into the film completes the catalytic cycle. The kinetics of this process suggests that the overall catalytic rate is governed by the on/off dynamics of MB/LB into and out of the DNA film. As a consequence, as long as the on/off rates are fast on the electrochemical timescale, the overall current is limited no longer by the surface density of MB in the film, but by the concentration (and diffusion constant) of $Fe(CN)_6^{3-}$ in solution. Depending on the concentration of $Fe(CN)_6^{3-}$, this electrocatalysis results in absolute currents that are roughly an order of magnitude higher than those produced by direct electrochemical reduction of MB.

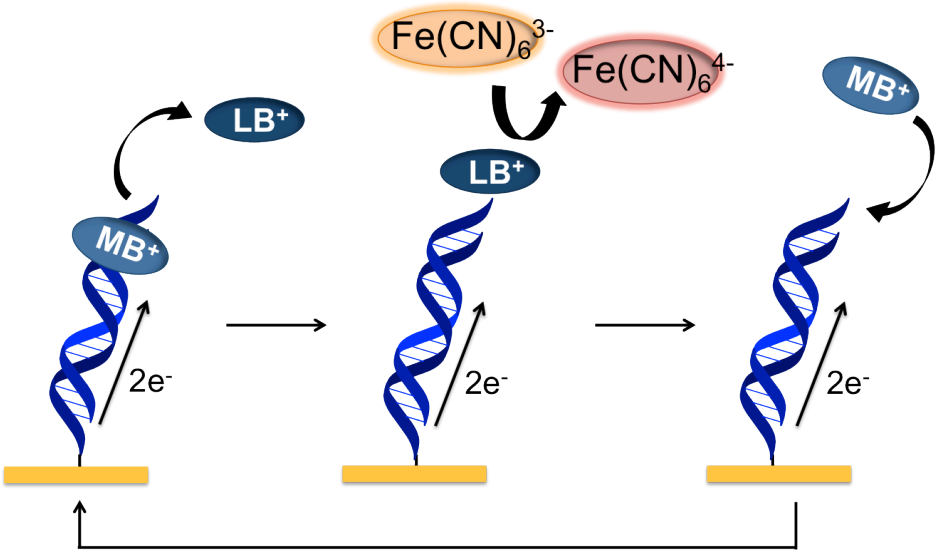

Figure 1.8 Electrocatalytic cycle between free methylene blue and ferricyanide on a DNA-modified electrode. Methylene blue in its oxidized form is intercalated into the DNA base stack. Upon reduction of methylene blue to leucomethylene blue via DNA-mediated charge transport, the affinity of the leucomethylene blue for DNA is lowered and leucomethylene blue is no longer intercalated. The reduced leucomethylene blue is capable of reducing ferricyanide that is freely diffusing in solution. The leucomethylene blue is then reoxidized to methylene blue and can reintercalate into the DNA. The ferricyanide acts as a diffusing electron sink in solution for the redox probe, methylene blue.

Single Base Mismatch and Lesion Detection with Electrocatalysis

With a successful catalytic cycle in hand, the question then became whether the presence of a mismatch or other DNA lesion would sufficiently attenuate the catalytic response. Several studies were therefore carried out to assess empirically electrocatalytic signal differentials at well matched versus mismatched helices using a series of different electrochemical mediators. These studies reinforced the importance of selecting redox probes with both the right binding mode and binding kinetics for use in DNA CT electrocatalytic assays. Figure 1.9 illustrates this point by showing the electrochemical response of 1 mM $Fe(CN)_6^{3-}$ at well matched and mismatched films in the presence of micromolar concentrations of MB, DM, and $Ru(NH_3)_6^{3+}$.[55] With relatively fast on/off intercalation dynamics, MB mediates $Fe(CN)_6^{3-}$ reduction efficiently at well-matched DNA films, but, because of attenuated DNA CT, yields a dramatically smaller catalytic reduction at films made up of mismatched helices. This differential signal enables MB to serve as a highly effective reporter for DNA base-stack perturbations using electrocatalysis. In contrast, the tightly intercalated DM probe, with very slow on/off dynamics, is unable to mediate $Fe(CN)_6^{3-}$ reduction at either type of electrode surface, rendering it unsuitable as an electrocatalyst. Finally, the $Ru(NH_3)_6^{3+}$ probe, which merely ion pairs to the DNA backbone, exhibits the fastest on/off dynamics, and correspondingly mediates the most efficient $Fe(CN)_6^{3-}$ reduction. However, because $Ru(NH_3)_6^{3+}$ reduction is not DNA mediated, the electrocatalytic waves are virtually identical at both matched and mismatched films.

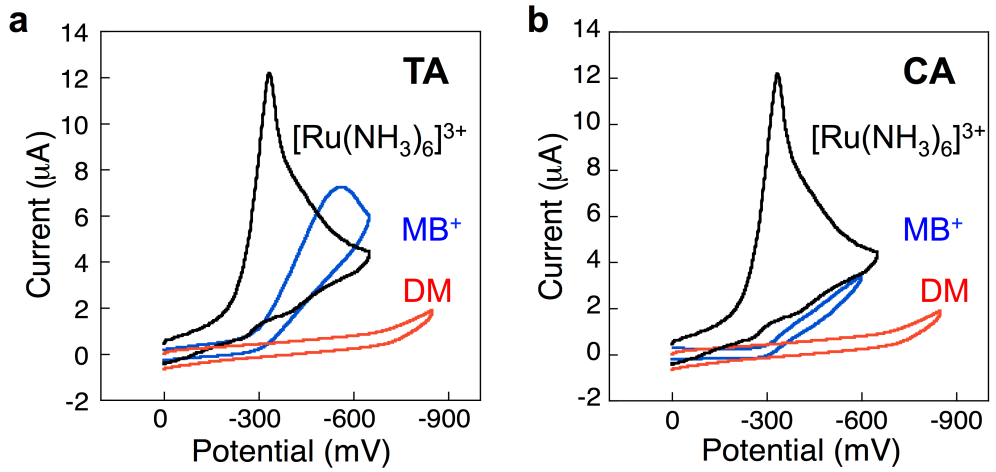

Figure 1.9 Electrocatalytic signals from DNA-modified electrodes and a variety of redox probes with $[Fe(CN)_6]^{3-}$. In black is the electrocatalytic signal from ruthenium hexammine interacting with $[Fe(CN)_6]^{3-}$; in blue is freely diffusing methylene blue with with $[Fe(CN)_6]^{3-}$, and in red is daunomycin with $[Fe(CN)_6]^{3-}$. In (a) is shown the signals for well-matched DNA, and (b) shows signals for DNA containing a C:A mismatch. As can be seen, no electrocatalytic turnover occurs between daunomycin and $[Fe(CN)_6]^{3-}$, and with ruthenium hexammine, no signal attenuation is observed upon the incorporation of a C:A mismatch. Only methylene blue and $[Fe(CN)_6]^{3-}$ produce a DNA mediated signal with electrocatalytic amplification that is attenuated upon incorporation of a mismatch.

Indeed, both the absolute currents for MB-mediated $Fe(CN)_6^{3-}$ reduction and, more importantly, the differential currents generated at matched versus mismatched DNA films are an order of magnitude greater than the corresponding currents observed for the direct electrochemical reduction of intercalated MB. Moreover, integrating the steady-state catalytic currents as a function of time yields differential charges at matched versus mismatched films that only get larger with time. This effect is illustrated in Figure 1.10, where the time-dependent electrocatalytic charge is plotted separately for MB-mediated $Fe(CN)_6^{3-}$ reduction at films featuring either matched or mismatched DNA helices. Significantly, this chronocoulometry assay allows ready detection of all of the possible single-base mismatches, including purine-purine base steps, without any manipulation of hybridization conditions.[16] The improved signal differentiation as a function of time is a direct consequence of the catalytic nature of this assay.

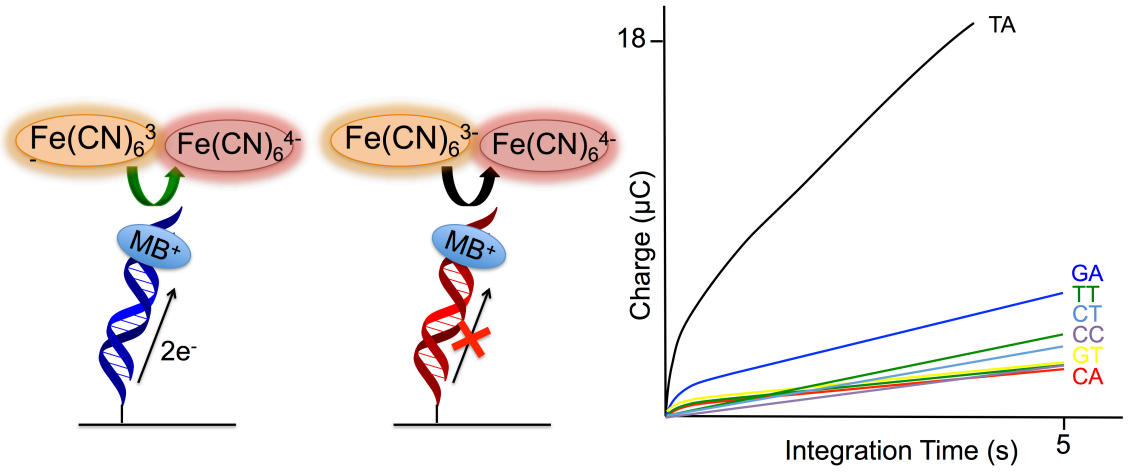

Figure 1.10 Chronocoulometry of well-matched DNA as well as the same mismatches previously tested with free daunomycin examined with methylene blue and $[Fe(CN)_6]^{3-}$. As can be seen, the difference in charge between well-matched DNA and each of the single base mismatch-containing duplexes is significantly larger for the signals amplified with electrocatalysis than those that do not.

The utility of this electrocatalytic chronocoulometry platform applied to biologically relevant targets was highlighted by the successful detection of different lesion products in DNA, as well as the detection of hot-spot mutations of the human p53 gene.[16] Cellular DNA lesions occur as a result of exposure to reactive-oxygen species and UV light, and this assay proved sufficiently sensitive to differentiate not only between undamaged DNA and DNA containing various lesions but also between the different lesions tested, including an abasic site, 8-oxo-adenine, 5,6-dihydroxy thymine, and deoxy-uracil.[16] Likewise, the assay enabled ready detection of several p53 mutations contained in tumor cell lines using a multiplexed chip featuring microelectrode sensors.[16]

Tethering Methylene Blue

One drawback of the $Fe(CN)_6^{3-}$-based electrocatalytic system is the stringent requirement for thoroughly passivated electrode surfaces: any direct $Fe(CN)_6^{3-}$ reduction at the bare electrode—even at pinholes—bypasses the DNA CT pathway and renders the assay incapable of sensing π-stack perturbations. This is especially problematic when detecting larger biomarkers, *e.g.,* protein transcription factors, which require lower DNA surface densities in order to gain access to specific sequences within the individual helices.[56] Low-density films additionally require that the redox mediator be prohibited from diffusing down into the DNA sequence and intercalating below the site of π-stack disruption.

A method was therefore developed to covalently tether methylene blue directly to the terminus of the DNA. The covalent MB reporter is coupled to a modified thymine base through a flexible molecular tether which maintains the capacity of MB to

intercalate into the DNA base stack and still dissociate upon reduction to LB.[57] In covalent linkage of methylene blue to the DNA, the linker length was of the most concern. The linker must be flexible enough and sufficiently long for the probe to intercalate into the base stack, while not so long that the probe can interact directly with the surface. The length of the tether was optimized to a 6-carbon chain because this length enabled the probe to destack from the bases upon reduction to leucomethylene blue and interact with the diffusing electron sink and to intercalate into the DNA base stack in the oxidized methylene blue form, while being sufficiently short to minimize direct surface interactions between the probe and the gold electrode. Additionally, unlike free methylene blue, with the covalent methylene blue probe, there is only a single redox reporter per DNA helix.

Various tethers for MB have been explored, and it was found that too short a tether did indeed limit access to solution, but a longer linker gave direct interaction with the gold electrode.[57, 58] We also considered whether intercalation was always intraduplex for the tethered probes. Here, clearly the extent of intraduplex intercalation depended upon how closely packed the DNA helices were. Most importantly, an essential element for all these characterizations was the assay for how effective a mismatch served to attenuate current flow. The key for efficient DNA detection was CT mediated by the full helix, as tested through the inclusion of intervening mismatches.

Covalent Methylene Blue with Hemoglobin as an Electrocatalysis Pair

To address the problem of direct-electrode $Fe(CN)_6^{3-}$ reduction, a metalloprotein-based electron sink was additionally employed to provide some inherent shielding from

the electrode surface. While a variety of redox-active proteins have been applied generally to electrocatalytic platforms, including glucose oxidase and horseradish peroxidase, many of these generate undesirable reactive oxygen species.[59-61] Hemoglobin, in contrast, is a fairly small protein that does not generate byproducts that can damage DNA.

Because of the iron center shielding afforded by hemoglobin's native protein conformation, passivation of the DNA-modified electrode is less of a stringent necessity when this protein is used as an electron sink (Figure 1.11).[62] The combination of a covalent MB mediator and hemoglobin electron sink enabled the ready detection of restriction enzyme activity at a low-density DNA film. Notably, using covalent MB and $Fe(CN)_6^{3-}$, detection of DNA was limited to greater than 500 fmol on the surface. In contrast, upon incorporation of hemoglobin, DNA was detectable at 5 fmol on the surface, increasing the sensitivity of detection by 100 fold.

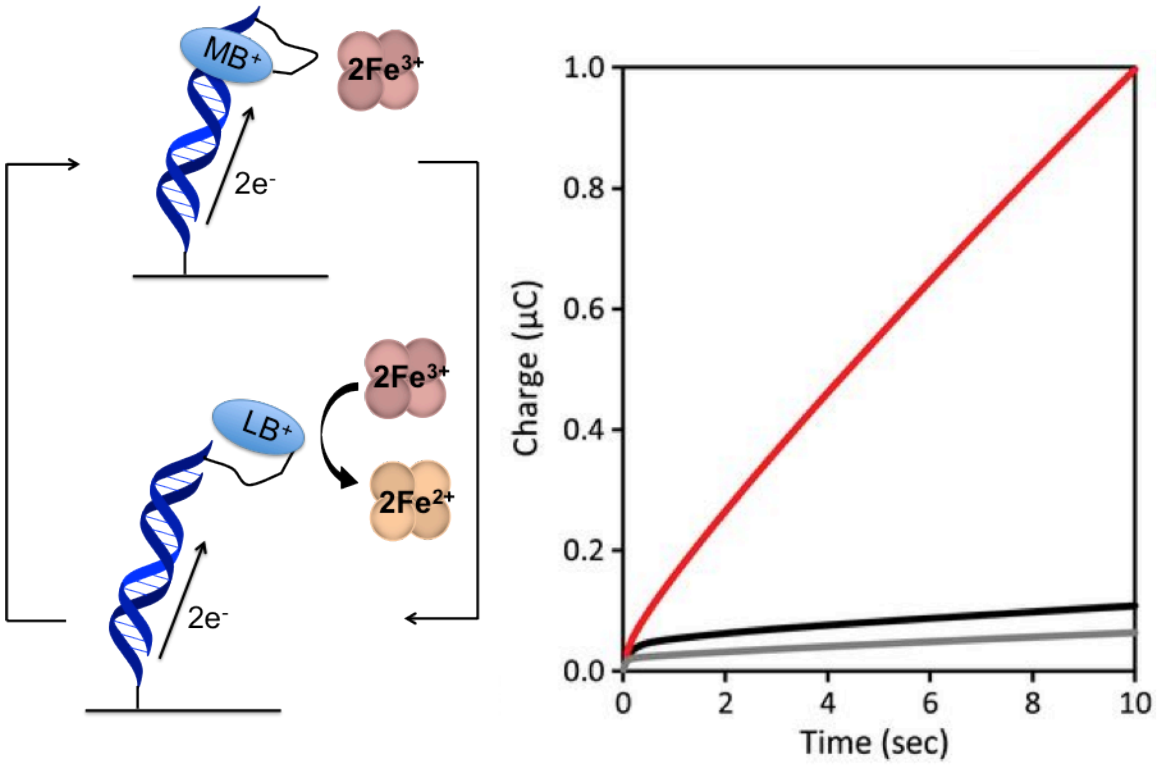

Figure 1.11 Electrocatalytic cycle between DNA tethered MB and freely-diffusing hemoglobin. As MB is reduced to LB, its affinity for DNA is significantly decreased, resulting in LB dissociation from the duplex. The LB is then reoxidized by hemoglobin in solution while maintaining surface passivation. The amino acids of the hemoglobin shell provide an inherent passivator between the iron center and electrode surface. The chronocoulometry of the system is shown. In red is the signal resulting from electrocatalysis, while in black is the MB-DNA without hemoglobin, and in grey is unmodified DNA duplex.

Platforms for DNA Electrochemistry

Sensitive detection of biomarkers is necessary for fundamental biological studies as well as for the development of effective diagnostic tools. As DNA can be used to specifically capture DNA, RNA, and proteins, nucleic acid sensors provide a flexible platform that can be easily manipulated to detect a variety of targets. Moreover, their structure is amenable to multiplexed formats.

Many modern DNA sensors involve modifying capture or target nucleic acids with fluorophores and observing changes in fluorescence upon a hybridization event.[63] Because these platforms rely solely on hybridization, probe sequences can be varied in an array that can contain hundreds of thousands of individual DNA sequences in a single square centimeter.[64, 65] While these platforms provide a significant amount of information, such as gene expression levels, and cannot currently be matched in information content with multiplexed electrochemical chips, the fluorescence assays lack the sensitivity and specificity required to directly detect biomarkers at low concentrations for both fundamental biological studies and diagnostic applications. Furthermore, these assays are expensive, require sophisticated instrumentation, and are thus not well suited for point of care diagnostics.

Electrochemically-based DNA platforms are very well suited for diagnostic applications, from the research lab to clinic, as they are generally very simple and sensitive, and do not require the complex labeling of targets.[31] Charge transport offers a powerful means to interrogate and report on the integrity and conformation of the base stack. Traditionally, DNA-modified electrodes are formed from thiolated DNA self-assembled onto a gold surface (Figure 1.4). The gold is then passivated with

mercaptohexanol to minimize direct interactions between redox-active moieties and the electrode surface. DNA CT sensors are based on the flow of electrons from the surface of electrodes through the DNA base stack to redox-active reporters. Importantly, the flow of electrons through DNA is inhibited by anything that perturbs the DNA base stack, including a single base mismatch, as described above, a DNA lesion, or the binding of a protein that disrupts the DNA base stack upon binding, as in proteins that kink DNA or flip bases out of the helix.[66] This sensitivity enables the detection of many classes of biomolecules, from single-stranded DNA to RNA and proteins.[67]

Electrochemical devices utilizing DNA CT have evolved over time. The first DNA CT-based detection platforms contained only a single electrode. This was advantageous, as devices were simple and could be constructed using commercially available materials. However, single-electrode platforms were limited because multiple experimental parameters could not be directly compared, making subtle differences between samples difficult to discern. More complex electrochemical systems have been developed to address this issue. A multiplexed platform allowing for the simultaneous analysis of different experimental conditions on the same chip was developed. The current multiplexed silicon chip is fabricated with 16 individually-addressable gold electrodes divided into four isolated quadrants.[68] This platform has enabled the incorporation of significantly more complex experiments due to the ability to run multiple experimental conditions in parallel.

We have also recently developed a two working electrode platform for sensing, which enables spatial addressing of many sequences of DNA on an electrode through the patterning of multiple sequences of DNA onto a single electrode surface.[69] This two-

electrode setup involves a large substrate electrode onto which DNA can be specifically patterned in an array via site-specific activation of a click catalyst at a secondary electrode. Detection is subsequently performed through scans across the array with a microelectrode to detect DNA-mediated electrochemistry. Through a simple method of fabrication, this platform allows uniformity in arrays as well as highly sensitive, localized detection with spatial resolution.

While patterning multiple DNA sequences onto a single electrode surface enables direct comparisons between those sequences upon treatment with one particular analyte solution, for clinically relevant detection, it may be necessary to detect differences between solutions. We therefore developed a platform that combines our low-density DNA monolayers with the capacity for multiplexing, as with our multiplexed DNA chips.[70] This platform contains two electrode arrays, a primary array to act as a multiplexed DNA-modified substrate, and a secondary array to function as a set of patterning and detection electrodes.

Detection of Single Base Mutations and DNA Lesions

DNA-modified electrodes thus provide a powerful technique to monitor mismatches in DNA and therefore also genomic mutations. Electrochemical signal attenuation has been shown with every possible base mismatch, irrespective of sequence context.[16, 17] Chronocoulometry, with signal amplification through electrocatalysis of ferricyanide by methylene blue, was used to observe all mismatched base pairs.[16] Purine-purine, pyrimidine-purine, and pyrimidine-pyrimidine mismatches all lead to significantly attenuated signals by electrocatalysis. This chemistry can also be applied to the detection of DNA lesions. The majority of DNA lesions have only a small thermodynamic and structural impact on the DNA helix, making them especially difficult to detect with many platforms. However, similarly to single-base mismatches, lesions disrupt the long-range π-stacking of the bases, making them detectable using DNA CT. With chronocoulometry, many common DNA lesions have been shown to significantly attenuate charge accumulation.[15] These include a hydroxylation product of thymine (5,6-hydroxy thymine), an abasic site, an adenine oxidation product (8-oxo-adenine), and a cytosine deamination product (deoxy-uracil). All lesions tested lead to signal attenuations on the order of those observed for mismatches.

Detection of DNA-Binding Proteins

DNA CT platforms are similarly advantageous for the detection of proteins that interact with DNA. Here we describe a variety of proteins that bind to DNA in different ways but can all be detected sensitively using DNA electrochemistry.

Detection of Transcriptional Regulators

Transcription factors are vital components of cellular genetic regulation. Transcriptional activators and repressors control the recruitment of RNA polymerase to commence RNA transcription. Many of these proteins primarily interact with DNA simply by bending the helix at the binding site. Because their binding is completely reversible and they do not permanently alter the DNA in any way, transcription factors can be difficult to detect with many DNA-based platforms. However, these proteins can be an important component of pathogenesis, as many influence regulation of tumor suppressor genes or oncogenes, making mutations to the sequences of these proteins potentially extremely deleterious in the cell.[71] As the primary mode of interaction between some of these proteins and DNA is significant helical bending, which distorts the π-stacking of the bases, DNA CT-based detection can be advantageous for their detection.

The transcriptional activator TATA-binding protein (TBP) has been easily detected on DNA-modified electrodes, given the large perturbation in DNA stacking associated with the binding of TBP. TBP binds to a TATA sequence in DNA and kinks the helix 80° at that location, leading to a significant DNA-mediated signal attenuation.[72] Figure 1.12 shows this result.[66] A DNA-modified electrode containing a covalently

bound redox probe shows a large accumulation in charge by chronocoulometry. In the presence of TBP, which binds to the specific 5'-TATA-3' site and kinks the DNA, the charge accumulation is significantly attenuated. Protein binding acts essentially as a switch, turning off DNA CT. In contrast, some proteins that regulate DNA expression bind without perturbing the DNA helix. Helix-turn-helix proteins are one example. These proteins have no significant effect on DNA CT.

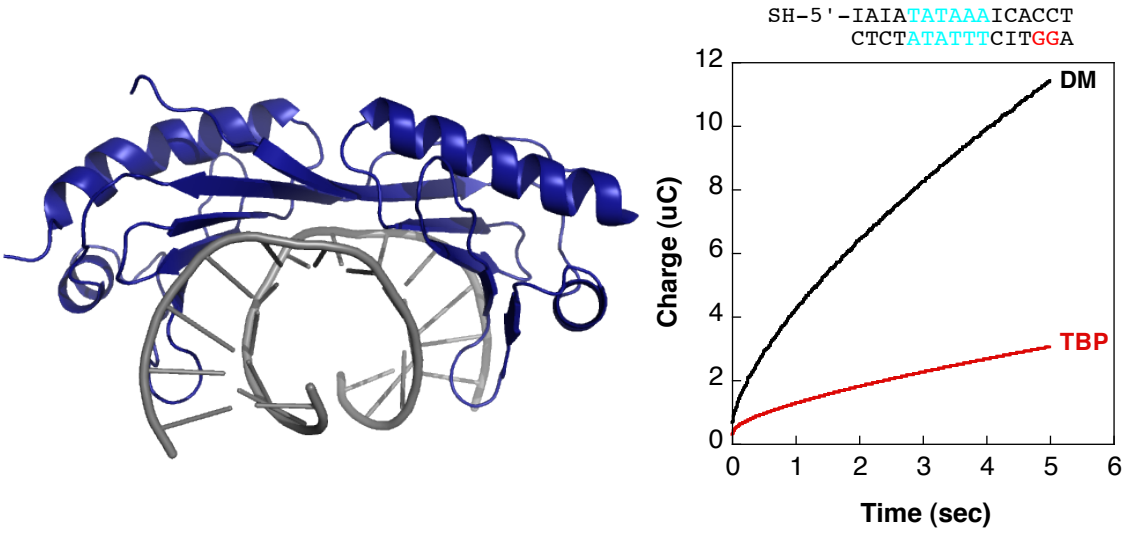

Figure 1.12 Electrochemistry of DNA with TATA-binding protein (TBP). Left: Illustration of the crystal structure of TBP (blue) bound to DNA (grey);[72] a significant kink in the DNA helix is observable. Right: Chronocoulometry of the DNA-modified electrode without protein (black) and with TBP bound (red).[66] As can be seen, the total charge accumulation in the presence of TBP is significantly smaller than in its absence.

Photolyase Activity and Detection

Photolyases repair UV damage to DNA, notably pyrimidine-pyrimidine dimers (thymine or cytosine dimers).[73] Thymine dimers (T<>T) are some of the most common lesions caused by UV damage and greatly distort the structure of DNA. They can result in mutagenesis and are linked to the development of melanomas. Photolyases repair such lesions in bacteria and fungi using visible light and a flavin cofactor. Because thymine dimers disrupt the π-stack, not surprisingly, they attenuate DNA CT. Upon photolyase repair, though, CT is restored through the repaired DNA. This result was shown on DNA-modified electrodes with DNA containing a pre-formed T<>T.[74] Rather than requiring the incorporation of a redox probe, a signal is observed from the flavin cofactor of the protein bound to the DNA. However, this signal is diminished when a T<>T is incorporated. As the protein-DNA complex is irradiated over time, facilitating DNA repair, the electrochemical signal increases and then levels off, consistent with the repair time for photolyase. Repair of photolyase was confirmed by HPLC. Thus, DNA repair by photolyase can be monitored electrochemically.

Methyltransferase and Methylation Detection

Methyltransferases are proteins responsible for methylation of the genome and are gaining wide interest given their importance in the regulation of gene expression. It has recently been shown that aberrant levels of methyltransferase protein are often early indicators of cancer.[75-77] Methyltransferases generally require the flipping of a base out of the π-stack in order to accomplish methylation; after the methyl group has been successfully added to the nucleotide, the base is returned to the DNA stack.[78] While the

methylated DNA base product does not hinder DNA CT, CT is significantly diminished when the base is flipped out of the π-stack and a non-aromatic protein residue is inserted into the base stack, seemingly as a placeholder for the flipped base while methylation occurs. This signal attenuation upon base flipping was shown through the detection of a methyltransferase on a DNA-modified electrode surface.[66] Interestingly, if a mutant methyltransferase is used in which an aromatic residue is inserted in the stack, no attenuation of CT is evident.

Methyltransferases have additionally been detected using the carbon nanotube devices, and a reduced affinity of the protein for the DNA after methylation was found.[79] When a single DNA helix containing the binding site for *Sss*I, a bacterial methyltransferase, was exposed to *Sss*I without the necessary cofactor, S-adenosyl methionine (SAM), a small attenuation in the current through the device was observed. However, upon the addition of the cofactor, the current dropped significantly. This decrease in current was attributed to the destacking of the bases, as the protein flips a base out of the π-stack in order for methylation to occur. Restoration of current occurs as the protein is washed from the DNA. Interestingly, given that this corresponds to a single molecule measurement, when the protein was again added to the duplex with its cofactor, no significant current attenuation was observed, as the DNA was already methylated. This result indicates that the affinity of the protein for methylated DNA is significantly lower than for its unmethylated counterpart.

Ideally, however, protein detection is performed with a 'signal-on' system, as many nonspecific events can cause signal attenuation. Such an assay has been developed in which DNA that has been successfully methylated maintains its electrochemical signal,

while DNA that remains unmethylated is cut by a methylation-specific restriction enzyme.[80] This assay has specifically been used for the detection of the human methyltransferase DNMT1 and the bacterial methyltransferase *Sss*I. DNMT1 is the methyltransferase responsible for both the establishment and maintenance of cytosine methylation patterns in the human genome. Aberrant methylation patterns caused by underexpression or overexpression of methyltransferases have been linked to the proliferation of cancers. A bacterial methyltransferase, *Sss*I, a SAM-dependent protein with a preference for unmethylated DNA, was first used, as *Sss*I has significantly higher activity than DNMT1. At 20 nM protein concentration, almost full signal protection is achieved upon addition of the restriction enzyme *BstU*I, which has a preference for unmethylated DNA. When surfaces were treated with either the SAM cofactor alone or the *Sss*I protein alone, large signal decreases were observed upon treatment with *BstU*I. The surfaces were then treated with the restriction enzyme *Rsa*I, which cuts both unmethylated and hemi-methylated DNA. All quadrants had significant signal decreases upon treatment, establishing that the DNA was hemi-methylated in the presence of *Sss*I and SAM (Figure 1.13).

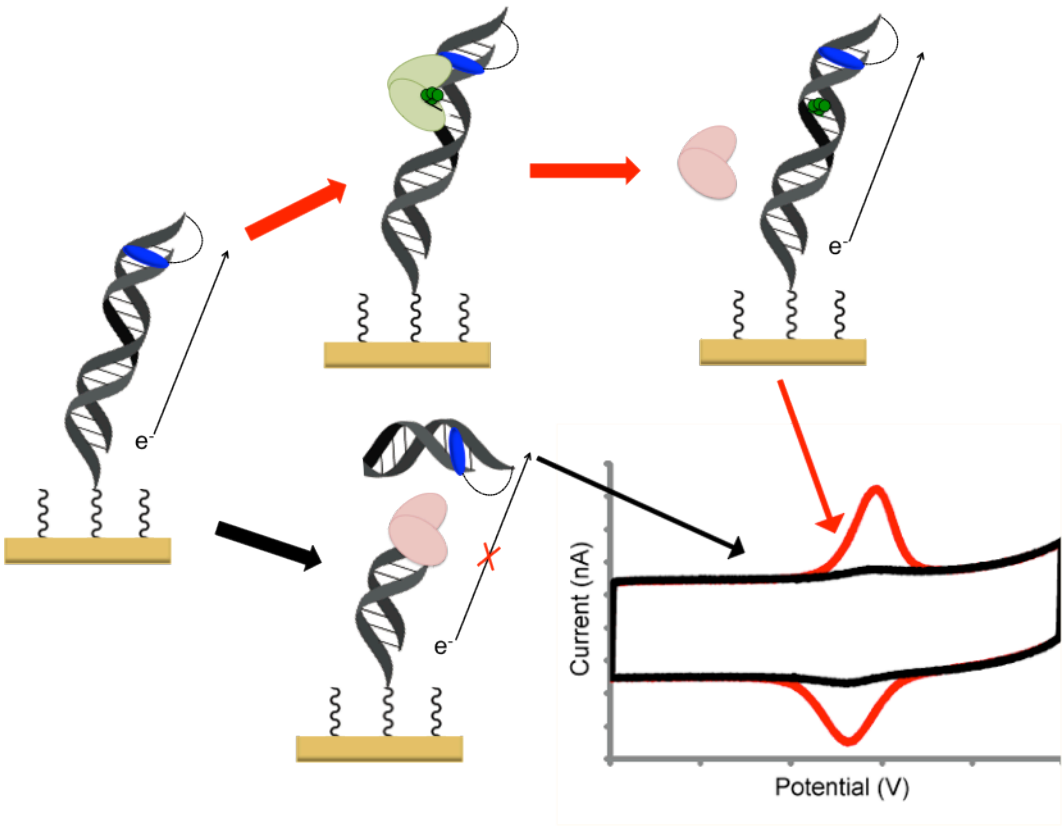

Figure 1.13 Electrochemical assay for methyltransferase activity. DNA duplexes that either contain a binding site for the methyltransferase protein (red arrow) or does not contain the binding site (black arrow) are assembled on electrodes. Methyltransferase protein (green) and S-adenosyl methionine (SAM) cofactor are added to the surface, and the protein is allowed to methylate the DNA. If the DNA is methylated, restriction enzymes (pink) selective for unmethylated DNA will not cut the DNA, maintaining an 'on' signal (red cyclic voltammogram). If the DNA remains unmethylated, upon addition of the restriction enzyme, the DNA is cleaved (bottom route), and the electrochemical signal turns off (black cyclic voltammogram).[80]

This assay was then tested with the human methyltransferase DNMT1, which only methylates hemi-methylated DNA and is associated with genomic methylation maintenance.[81] In a similar manner to *Sss*I, DNMT1 was allowed to methylate DNA on surfaces containing either unmethylated or hemimethylated DNA. *BssH*II, a restriction enzyme that cuts unmethylated or hemimethylated DNA but not fully methylated DNA, duplexes was then added. Hemimethylated surfaces that had DNMT1 and SAM added at protein concentrations as little as 10 nM saw protection from restriction enzyme cutting. Because genomic methylation patterns and the proteins responsible for this are linked to the development of cancers,[82-88] the further development of this assay is vital for the development of early cancer diagnostic tools.

Conclusions

The ability of DNA to conduct charge is a fascinating and powerful chemistry. Many electrochemical detection platforms have been developed to probe enzymatic activity and the fidelity of DNA. DNA CT can occur over long molecular distances, at least 34 nm, has a shallow distance dependence, and is exquisitely sensitive to perturbations to the DNA helix. The variety of biological elements that have been shown to affect DNA CT, including DNA lesions and mismatches, transcription factors, and proteins containing iron-sulfur clusters, speaks to the potential importance of DNA CT for biosensing applications.

The thesis work described herein utilizes DNA CT-based detection platforms to expand our biological detection capabilities. Chapter 2 describes the application of copper-free click chemistry to better control the density and homogeneity of DNA monolayers. This method of monolayer formation is expanded in Chapter 3 to form patterned DNA arrays. These arrays incorporate a secondary electrode with electrocatalytically-amplified signals for sensitive biomolecule detection. Chapters 4 and 5 describe the multiplexing of this platform to enable sensitive and selective detection of transcription factors and the application of a signal-on method for methyltransferase detection. The combination of the multiplexed, two working electrode platform with the signal-on methyltransferase assay enables detection of methyltransferase activity from tumor samples, which is further investigated for its clinical relevance in Chapter 6. In Chapter 7, the two working electrode platform is applied directly to a flow-through system for microfluidic detection. Finally, efforts toward applications of DNA CT for nanocircuitry are presented in Chapter 8.

This body of work reflects recent advances in DNA CT-based electrochemical sensors that significantly extend detection capabilities. With improvements to both the morphology of DNA monolayers and the methods used for signal amplification, specific protein detection is possible from crude tissue samples. These advances in DNA CT-based platforms have moved this class of sensors from purely academic to clinically relevant.

References

1. Neidle, S., Puvvada, M. S., and Thurston, D. E. (1994) The relevance of drug DNA sequence specificity to anti-tumour activity, *Eur. J. Cancer. 30A*, 567-568.

2. Watson, J. D., and Crick, F. H. (1953) Molecular structure of nucleic acids; a structure for deoxyribose nucleic acid, *Nature 171*, 737-738.

3. Eley, D. D., and Spivey, D. I. (1962) Semiconductivity of organic substances. Part 9.- Nucleic acid in the dry state, *Trans. Faraday Soc. 58*, 411-415.

4. Genereux, J. C., and Barton, J. K. (2010) Mechanisms for DNA charge transport, *Chem. Rev. 110*, 1642-1662.

5. Murphy, C. J., Arkin, M. R., Jenkins, Y., Ghatlia, N. D., Bossmann, S. H., Turro, N. J., and Barton, J. K. (1993) Long-range photoinduced electron transfer through a DNA helix, *Science 262*, 1025-1029.

6. O'Neill, M. A., Becker, H. C., Wan, C., Barton, J. K., and Zewail, A. H. (2003) Ultrafast dynamics in DNA-mediated electron transfer: base gating and the role of temperature, *Angew. Chem. Int. Ed. 42*, 5896-5900.

7. Wan, C., Fiebig, T., Kelley, S. O., Treadway, C. R., Barton, J. K., and Zewail, A. H. (1999) Femtosecond dynamics of DNA-mediated electron transfer, *Proc. Natl. Acad. Sci. USA 96*, 6014-6019.

8. Hall, D. B., Holmlin, R. E., and Barton, J. K. (1996) Oxidative DNA damage through long-range electron transfer, *Nature 382*, 731-735.

9. Holmlin, R. E., Dandliker, P. J., and Barton, J. K. (1997) Charge Transfer through the DNA Base Stack, *Angew. Chem. Int. Ed. 36*, 2714-2730.

10. Lewis, F. D., Liu, X., Miller, S. E., and Wasielewski, M. R. (1999) Electronic Interactions between π-Stacked DNA Base Pairs and Diphenylacetylene-4,4'-dicarboxamide in Hairpin DNA, *J. Am. Chem. Soc. 121*, 9746-9747.

11. Muren, N. B., Olmon, E. D., and Barton, J. K. (2012) Solution, surface, and single molecule platforms for the study of DNA-mediated charge transport, *Phys. Chem. Chem. Phys. 14*, 13754-13771.

12. Voityuk, A. A., Rösch, N., Bixon, M., and Jortner, J. (2000) Electronic Coupling for Charge Transfer and Transport in DNA, *J. Phys. Chem. B 104*, 9740-9745.

13. Sontz, P. A., Muren, N. B., and Barton, J. K. (2012) DNA charge transport for sensing and signaling, *Acc. Chem. Res. 45*, 1792-1800.

14. Kelley, S. O., Holmlin, R. E., Stemp, E. D. A., and Barton, J. K. (1997) Photoinduced Electron Transfer in Ethidium-Modified DNA Duplexes: Dependence on Distance and Base Stacking, *J. Am. Chem. Soc. 119*, 9861-9870.

15. Boal, A. K., and Barton, J. K. (2005) Electrochemical detection of lesions in DNA, *Bioconjug. Chem. 16*, 312-321.

16. Boon, E. M., Ceres, D. M., Drummond, T. G., Hill, M. G., and Barton, J. K. (2000) Mutation detection by electrocatalysis at DNA-modified electrodes, *Nat. Biotechnol. 18*, 1096-1100.

17. Kelley, S. O., Boon, E. M., Barton, J. K., Jackson, N. M., and Hill, M. G. (1999) Single-base mismatch detection based on charge transduction through DNA, *Nucleic Acids Res. 27*, 4830-4837.

18. Guo, X., Gorodetsky, A. A., Hone, J., Barton, J. K., and Nuckolls, C. (2008) Conductivity of a single DNA duplex bridging a carbon nanotube gap, *Nat. Nanotechnol. 3*, 163-167.

19. Sassolas, A., Leca-Bouvier, B. D., and Blum, L. J. (2008) DNA biosensors and microarrays, *Chem. Rev. 108*, 109-139.

20. Wang, R. E., Zhang, Y., Cai, J., Cai, W., and Gao, T. (2011) Aptamer-based fluorescent biosensors, *Current Med. Chem. 18*, 4175-4184.

21. Dai, N., and Kool, E. T. (2011) Fluorescent DNA-based enzyme sensors, *Chem. Soc. Rev. 40*, 5756-5770.

22. Dai, N., Guo, J., Teo, Y. N., and Kool, E. T. (2011) Protease probes built from DNA: multispectral fluorescent DNA-peptide conjugates as caspase chemosensors, *Angew. Chem. Int. Ed. 50*, 5105-5109.

23. Epstein, J. R., Leung, A. P., Lee, K. H., and Walt, D. R. (2003) High-density, microsphere-based fiber optic DNA microarrays, *Biosens. Bioelectron. 18*, 541-546.

24. Steel, A. B., Herne, T. M., and Tarlov, M. J. (1998) Electrochemical quantitation of DNA immobilized on gold, *Anal. Chem. 70*, 4670-4677.

25. Steel, A. B., Herne, T. M., and Tarlov, M. J. (1999) Electrostatic interactions of redox cations with surface-immobilized and solution DNA, *Bioconjug. Chem. 10*, 419-423.

26. Caruso, F., Rodda, E., Furlong, D. N., Niikura, K., and Okahata, Y. (1997) Quartz crystal microbalance study of DNA immobilization and hybridization for nucleic Acid sensor development, *Anal. Chem. 69*, 2043-2049.

27. Wang, J., Nielsen, P. E., Jiang, M., Cai, X., Fernandes, J. R., Grant, D. H., Ozsoz, M., Beglieter, A., and Mowat, M. (1997) Mismatch-sensitive hybridization detection by peptide nucleic acids immobilized on a quartz crystal microbalance, *Anal. Chem. 69*, 5200-5202.

28. Liss, M., Petersen, B., Wolf, H., and Prohaska, E. (2002) An aptamer-based quartz crystal protein biosensor, *Anal. Chem. 74*, 4488-4495.

29. Tang, W., Wang, D., Xu, Y., Li, N., and Liu, F. (2012) A self-assembled DNA nanostructure-amplified quartz crystal microbalance with dissipation biosensing platform for nucleic acids, *Chem. Commun. 48*, 6678-6680.

30. Fritz, J., Baller, M. K., Lang, H. P., Rothuizen, H., Vettiger, P., Meyer, E., Guntherodt, H., Gerber, C., and Gimzewski, J. K. (2000) Translating biomolecular recognition into nanomechanics, *Science 288*, 316-318.

31. Drummond, T. G., Hill, M. G., and Barton, J. K. (2003) Electrochemical DNA sensors, *Nat. Biotechnol. 21*, 1192-1199.

32. Odenthal, K. J., and Gooding, J. J. (2007) An introduction to electrochemical DNA biosensors, *Analyst 132*, 603-610.

33. Palecek, E. (1960) Oscillographic polarography of highly polymerized deoxyribonucleic acid, *Nature 188*, 656-657.

34. Singhal, P., and Kuhr, W. G. (1997) Ultrasensitive voltammetric detection of underivatized oligonucleotides and DNA, *Anal. Chem. 69*, 4828-4832.

35. Yang, I. V., and Thorp, H. H. (2001) Modification of indium tin oxide electrodes with repeat polynucleotides: electrochemical detection of trinucleotide repeat expansion, *Anal. Chem. 73*, 5316-5322.

36. Palecek, E., Fojta, M., and Jelen, F. (2002) New approaches in the development of DNA sensors: hybridization and electrochemical detection of DNA and RNA at two different surfaces, *Bioelectrochem. 56*, 85-90.

37. Lucarelli, F., Tombelli, S., Minunni, M., Marrazza, G., and Mascini, M. (2008) Electrochemical and piezoelectric DNA biosensors for hybridisation detection, *Anal. Chim. Acta 609*, 139-159.

38. Yang, W., and Lai, R. Y. (2011) Comparison of the stem-loop and linear probe-based electrochemical DNA sensors by alternating current voltammetry and cyclic voltammetry, *Langmuir 27*, 14669-14677.

39. Rosi, N. L., and Mirkin, C. A. (2005) Nanostructures in biodiagnostics, *Chem. Rev. 105*, 1547-1562.

40. Xia, F., White, R. J., Zuo, X., Patterson, A., Xiao, Y., Kang, D., Gong, X., Plaxco, K. W., and Heeger, A. J. (2010) An electrochemical supersandwich assay for sensitive and selective DNA detection in complex matrices, *J. Am. Chem. Soc. 132*, 14346-14348.

41. Zuo, X., Xiao, Y., and Plaxco, K. W. (2009) High specificity, electrochemical sandwich assays based on single aptamer sequences and suitable for the direct detection of small-molecule targets in blood and other complex matrices, *J. Am. Chem. Soc. 131*, 6944-6945.

42. Umek, R. M., Lin, S. W., Vielmetter, J., Terbrueggen, R. H., Irvine, B., Yu, C. J., Kayyem, J. F., Yowanto, H., Blackburn, G. F., Farkas, D. H., and Chen, Y. P. (2001) Electronic detection of nucleic acids: a versatile platform for molecular diagnostics, *J. Mol. Diagn. 3*, 74-84.

43. Kelley, S. O., Jackson, N. M., Hill, M. G., and Barton, J. K. (1999) Long-Range Electron Transfer through DNA Films, *Angew. Chem. Int. Ed. 38*, 941-945.

44. Slinker, J. D., Muren, N. B., Renfrew, S. E., and Barton, J. K. (2011) DNA charge transport over 34 nm, *Nat. Chem. 3*, 228-233.

45. Kelley, S. O., Barton, J. K., Jackson, N. M., and Hill, M. G. (1997) Electrochemistry of methylene blue bound to a DNA-modified electrode, *Bioconjug. Chem. 8*, 31-37.

46. Herne, T. M., and Tarlov, M. J. (1997) Characterization of DNA Probes Immobilized on Gold Surfaces, *J. Am. Chem. Soc. 119*, 8916-8920.

47. Hobara, D., Sasaki, T., Imabayashi, S.-i., and Kakiuchi, T. (1999) Surface Structure of Binary Self-Assembled Monolayers Formed by Electrochemical Selective Replacement of Adsorbed Thiols, *Langmuir 15*, 5073-5078.

48. Gorodetsky, A. A., Hammond, W. J., Hill, M. G., Slowinski, K., and Barton, J. K. (2008) Scanning electrochemical microscopy of DNA monolayers modified with Nile Blue, *Langmuir 24*, 14282-14288.

49. Peterson, A. W., Heaton, R. J., and Georgiadis, R. M. (2001) The effect of surface probe density on DNA hybridization, *Nucleic Acids Res. 29*, 5163-5168.

50. Lapierre, M. A., O'Keefe, M., Taft, B. J., and Kelley, S. O. (2003) Electrocatalytic detection of pathogenic DNA sequences and antibiotic resistance markers, *Anal. Chem. 75*, 6327-6333.

51. Kelley, S. O., Mirkin, C. A., Walt, D. R., Ismagilov, R. F., Toner, M., and Sargent, E. H. (2014) Advancing the speed, sensitivity and accuracy of biomolecular detection using multi-length-scale engineering, *Nat. Nanotechnol. 9*, 969-980.

52. Bin, X., Sargent, E. H., and Kelley, S. O. (2010) Nanostructuring of sensors determines the efficiency of biomolecular capture, *Anal. Chem. 82*, 5928-5931.

53. Das, J., and Kelley, S. O. (2013) Tuning the bacterial detection sensitivity of nanostructured microelectrodes, *Anal. Chem. 85*, 7333-7338.

54. Furst, A. L., Hill, M. G., and Barton, J. K. (2013) DNA-modified electrodes fabricated using copper-free click chemistry for enhanced protein detection, *Langmuir 29*, 16141-16149.

55. Boon, E. M., Barton, J. K., Bhagat, V., Nersissian, M., Wang, W., and Hill, M. G. (2003) Reduction of Ferricyanide by Methylene Blue at a DNA-Modified Rotating-Disk Electrode, *Langmuir 19*, 9255-9259.

56. Pheeney, C. G., Arnold, A. R., Grodick, M. A., and Barton, J. K. (2013) Multiplexed electrochemistry of DNA-bound metalloproteins, *J. Am. Chem. Soc. 135*, 11869-11878.

57. Pheeney, C. G., and Barton, J. K. (2012) DNA electrochemistry with tethered methylene blue, *Langmuir 28*, 7063-7070.

58. Pheeney, C. G., and Barton, J. K. (2013) Intraduplex DNA-mediated electrochemistry of covalently tethered redox-active reporters, *J. Am. Chem. Soc. 135*, 14944-14947.

59. Ju, H., and Shen, C. (2001) Electrocatalytic Reduction and Determination of Dissolved Oxygen at a Poly(nile blue) Modified Electrode, *Electroanalysis 13*, 789-793.

60. Pelossof, G., Tel-Vered, R., Elbaz, J., and Willner, I. (2010) Amplified biosensing using the horseradish peroxidase-mimicking DNAzyme as an electrocatalyst, *Anal. Chem. 82*, 4396-4402.

61. Xu, J.-Z., Zhu, J.-J., Wu, Q., Hu, Z., and Chen, H.-Y. (2003) An Amperometric Biosensor Based on the Coimmobilization of Horseradish Peroxidase and Methylene Blue on a Carbon Nanotubes Modified Electrode, *Electroanalysis 15*, 219-224.

62. Pheeney, C. G., Guerra, L. F., and Barton, J. K. (2012) DNA sensing by electrocatalysis with hemoglobin, *Proc. Natl. Acad. Sci. USA 109*, 11528-11533.

63. Heller, M. J. (2002) DNA microarray technology: devices, systems, and applications, *Annu. Rev. Biomed. Eng. 4*, 129-153.

64. Behr, M. A., Wilson, M. A., Gill, W. P., Salamon, H., Schoolnik, G. K., Rane, S., and Small, P. M. (1999) Comparative genomics of BCG vaccines by whole-genome DNA microarray, *Science 284*, 1520-1523.

65. Schena, M., Shalon, D., Davis, R. W., and Brown, P. O. (1995) Quantitative monitoring of gene expression patterns with a complementary DNA microarray, *Science 270*, 467-470.

66. Boon, E. M., Salas, J. E., and Barton, J. K. (2002) An electrical probe of protein-DNA interactions on DNA-modified surfaces, *Nat. Biotechnol. 20*, 282-286.

67. Gorodetsky, A. A., Buzzeo, M. C., and Barton, J. K. (2008) DNA-mediated electrochemistry, *Bioconjug. Chem. 19*, 2285-2296.

68. Slinker, J. D., Muren, N. B., Gorodetsky, A. A., and Barton, J. K. (2010) Multiplexed DNA-modified electrodes, *J. Am. Chem. Soc. 132*, 2769-2774.

69. Furst, A., Landefeld, S., Hill, M. G., and Barton, J. K. (2013) Electrochemical patterning and detection of DNA arrays on a two-electrode platform, *J. Am. Chem. Soc. 135*, 19099-19102.

70. Furst, A. L., Muren, N. B., Hill, M. G., and Barton, J. K. (2014) Label-free electrochemical detection of human methyltransferase from tumors, *Proc. Natl. Acad. Sci. USA 111*, 14985-14989.

71. Darnell, J. E., Jr. (2002) Transcription factors as targets for cancer therapy, *Nat. Rev. Cancer 2*, 740-749.

72. Juo, Z. S., Chiu, T. K., Leiberman, P. M., Baikalov, I., Berk, A. J., and Dickerson, R. E. (1996) How proteins recognize the TATA box, *J. Mol. Biol. 261*, 239-254.

73. Sancar, A. (2008) Structure and function of photolyase and in vivo enzymology: 50th anniversary, *J. Biol. Chem. 283*, 32153-32157.

74. DeRosa, M. C., Sancar, A., and Barton, J. K. (2005) Electrically monitoring DNA repair by photolyase, *Proc. Natl. Acad. Sci. USA 102*, 10788-10792.

75. Brueckner, B., Kuck, D., and Lyko, F. (2007) DNA methyltransferase inhibitors for cancer therapy, *Cancer J. 13*, 17-22.

76. Ghoshal, K., and Bai, S. (2007) DNA methyltransferases as targets for cancer therapy, *Drugs Today 43*, 395-422.

77. Robertson, K. D. (2001) DNA methylation, methyltransferases, and cancer, *Oncogene 20*, 3139-3155.

78. Smith, S. S., Kaplan, B. E., Sowers, L. C., and Newman, E. M. (1992) Mechanism of human methyl-directed DNA methyltransferase and the fidelity of cytosine methylation, *Proc. Natl. Acad. Sci. USA 89*, 4744-4748.

79. Wang, H., Muren, N. B., Ordinario, D., Gorodetsky, A. A., Barton, J. K., and Nuckolls, C. (2012) Transducing methyltransferase activity into electrical signals in a carbon nanotube-DNA device, *Chem. Sci. 3*, 62-65.

80. Muren, N. B., and Barton, J. K. (2013) Electrochemical assay for the signal-on detection of human DNA methyltransferase activity, *J. Am. Chem. Soc. 135*, 16632-16640.

81. Pradhan, S., Bacolla, A., Wells, R. D., and Roberts, R. J. (1999) Recombinant human DNA (cytosine-5) methyltransferase. I. Expression, purification, and comparison of de novo and maintenance methylation, *J. Biol. Chem. 274*, 33002-33010.

82. De Marzo, A. M., Marchi, V. L., Yang, E. S., Veeraswamy, R., Lin, X., and Nelson, W. G. (1999) Abnormal regulation of DNA methyltransferase expression during colorectal carcinogenesis, *Cancer Res. 59*, 3855-3860.

83. el-Deiry, W. S., Nelkin, B. D., Celano, P., Yen, R. W., Falco, J. P., Hamilton, S. R., and Baylin, S. B. (1991) High expression of the DNA methyltransferase gene characterizes human neoplastic cells and progression stages of colon cancer, *Proc. Natl. Acad. Sci. USA 88*, 3470-3474.

84. Esteller, M. (2007) Cancer epigenomics: DNA methylomes and histone-modification maps, *Nat. Rev. Genet. 8*, 286-298.

85. Esteller, M. (2008) Epigenetics in cancer, *New Engl. J. Med. 358*, 1148-1159.

86. Esteller, M., Corn, P. G., Baylin, S. B., and Herman, J. G. (2001) A gene hypermethylation profile of human cancer, *Cancer Res. 61*, 3225-3229.

87. Esteller, M., Fraga, M. F., Paz, M. F., Campo, E., Colomer, D., Novo, F. J., Calasanz, M. J., Galm, O., Guo, M., Benitez, J., and Herman, J. G. (2002) Cancer epigenetics and methylation, *Science 297*, 1807-1808; discussion 1807-1808.

88. Frigola, J., Song, J., Stirzaker, C., Hinshelwood, R. A., Peinado, M. A., and Clark, S. J. (2006) Epigenetic remodeling in colorectal cancer results in coordinate gene suppression across an entire chromosome band, *Nat. Genet. 38*, 540-549.

Chapter 2

DNA-modified Electrodes Fabricated using Copper-Free Click Chemistry for Enhanced Protein Detection

Adapted from: Furst, A. L., Hill, M. G., and Barton, J. K. (2013) DNA-Modified Electrodes Fabricated Using Copper-Free Click Chemistry for Enhanced Protein Detection, *Langmuir*, *29*, 16141-16149.

Introduction

Sensitive detection of biomarkers is essential for the development of effective diagnostic tools. Electrochemical biosensing platforms have the unique ability to convert biological events, including protein or ligand binding and DNA or RNA hybridization, directly into electronic signals, making them ideal tools for point-of-care diagnostics.[1-7] The ability of DNA to conduct charge, and more specifically, the sensitivity of DNA charge transport (DNA CT) to structural perturbations of the double helix, provides a robust signaling mechanism for DNA-modified electrode-based biosensing.[8] Exploiting DNA CT, we have developed highly sensitive electrochemical assays for nucleic acids and protein-DNA binding.[9-14]

Typically, DNA-modified surfaces are prepared through self-assembly of thiolated DNA duplexes on gold to form high-density monolayers. While straightforward to fabricate, these films pose challenges for the detection of very large proteins, proteins that target specific sequences of DNA, and hybridization/dehybridization events, owing to the limited accessibility to individual helices within the close-packed structure of the monolayer.[15, 16] Although some control over the surface density is possible by adjusting the ionic strength of the deposition solution with magnesium ions, the range of attainable DNA surface coverages is narrow (~ 30 – 50 pmol/cm^2).[17-20] Moreover, this method does not allow for control over the dispersion of DNA helices within the film; recent imaging studies have revealed that thiol-modified DNA forms a heterogeneous monolayer when combined with a passivating agent such as mercaptohexanol. In such films, the DNA helices cluster into exceedingly large domains of very high density within a sea of passivating thiol.[21, 22] This extensive clustering of helices is especially problematic for

biomolecule detection because it leads to variability across the electrode surface, with regions of close-packed helices in which access to specific base sequences may be inhibited.

The structural similarity of the components of a mixed monolayer-forming solution is a major determining factor for the degree of homogeneity within the resulting self-assembled monolayer (SAM).[23-29] Thus an alternative approach to a low-density DNA film is to prepare a homogeneous mixed SAM *without* DNA, followed by DNA conjugation to the functionalized mixed monolayer. Previous work by Chidsey and coworkers involved the preliminary formation of a mixed alkylthiol monolayer on gold containing azide-terminated thiols, followed by copper-catalyzed click chemistry to tether single-stranded oligonucleotides to gold surfaces. While copper-catalyzed click chemistry is efficient,[30] conventional copper(I) catalysts can damage DNA and are difficult to remove after the reaction has occurred.

In this work, we employ a catalyst-free method of DNA conjugation to a mixed monolayer that capitalizes on ring strain to drive the [3+2] cycloaddition.[31, 32] We first form a mixed azide-alcohol-terminated monolayer, then add cyclooctyne-labeled DNA, which, due to ring strain, spontaneously couples specifically to the azide. Because the loading and distribution of DNA are pre-fixed by the composition of the underlying monolayer, this labeling method enables very low surface concentrations of DNA to be evenly dispersed across the electrode, as verified by AFM imaging, and provides a significantly larger surface area-to-volume ratio for the DNA, increasing the accessibility of analyte in solution to individual helices. These low-density monolayers display all of the characteristics of DNA-mediated electrochemistry, including sensitivity to

mismatches and π-stack perturbations. Furthermore, the enhanced sensitivity of these monolayers to protein binding (as compared to conventional DNA-modified electrodes) makes them attractive platforms for biomolecule detection.

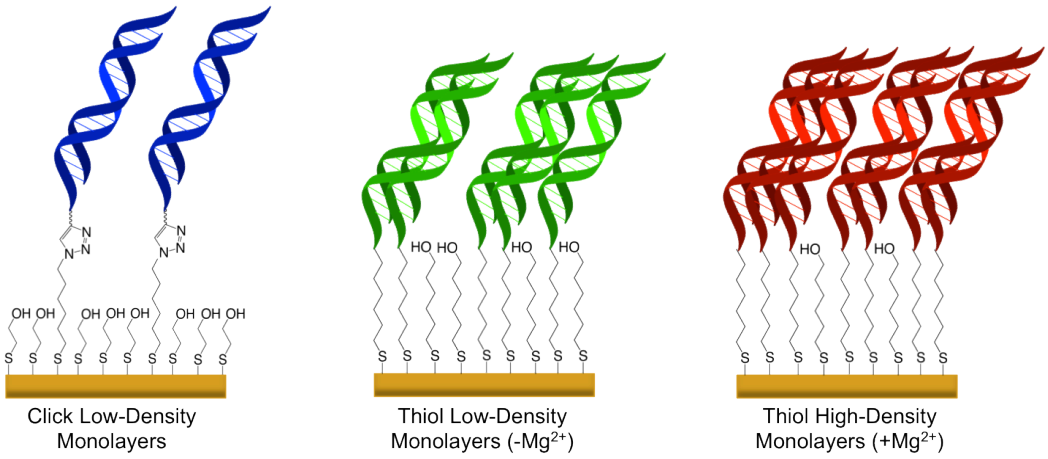

Figure 2.1 DNA monolayers of different densities. The ultra low-density DNA monolayers (*left*) are formed using click chemistry on surfaces. Both low-density DNA monolayers (*center*) and high-density DNA monolayers (*right*) are formed with self-assembly of thiolated DNA on surfaces. Click chemistry leads to significantly more homogeneous monolayers than either the low- or high-density thiol DNA monolayers.

Materials and Methods

Synthesis of NHS Ester Activated Cyclooctyne

9,9-Dibromobicyclo-[6.1.0]nonane was synthesized according to the procedure by Skattebøl et al.[33] The cyclooctyne was synthesized as described by Agard et al.[27] Cyclooctyne (OCT) was prepared for coupling to DNA by NHS ester activation. 5 mg (0.019 mmol) of OCT was combined with 7 mg (0.034 mmol) N,N'-dicyclohexylcarbodiimide and 3.7 mg (0.033 mmol) N-hydroxysuccinimide in 1 mL anhydrous DMF. The reaction was stirred for 1.5 h, followed by solvent removal under reduced pressure.

Oligonucleotide Synthesis and Purification

Oligonucleotides were synthesized on an Applied Biosystems 3400 DNA synthesizer. Terminal modifications incorporated into the 5' end of one of the strands were either a C6 S-S thiol linker or a C3 amine linker, purchased from Glen Research. Complementary unmodified strands were also synthesized. Each oligonucleotide was purified by high-performance liquid chromatography (HPLC) using a gradient of acetonitrile and 50 mM ammonium acetate. Preparation of all of the oligonucleotides followed a reported protocol.[34] Following purification, oligonucleotides were desalted by ethanol precipitation and quantified using ultraviolet-visible spectrophotometry based on their extinction coefficients at 260 nm (IDT Oligo Analyzer). The following sequences were prepared: well matched: 5'-NH_3-$(CH_2)_3$-GCT CAG TAC GAC GTC GA-3' with its unmodified complement, a mismatch-containing sequence with a CA mismatch at the 9th base pair, and a TBP-binding sequence: 5'-NH_3-$(CH_2)_3$-GGC GTC TAT AAA GCG

ATC GCG A-3' with its unmodified complement. DNA to be coupled to OCT was synthesized with a 5'-terminal C3 amino-modifier. The DNA was cleaved from solid support, deprotected, and HPLC-purified as previously described. The OCT-NHS ester was suspended in 20 uL of dry DMSO in preparation for coupling to DNA. Following desalting, the oligonucleotides were suspended in 100 μL of 0.5 M $NaHCO_3/Na_2CO_3$ buffer (pH 8.75) and the OCT-ester in DMSO was added to the oligonucleotides. The reaction was stirred for 24 h, followed by a final round of HPLC purification. The formation of the desired product was confirmed by a significant shift in the HPLC retention time and MALDI-TOF analysis of the product. MALDI-TOF: calc: 5592.1 obs: 5589.08.

DNA duplexes were formed by thermally annealing equimolar amounts of single-stranded oligonucleotides in deoxygenated phosphate buffer (5mM phosphate, 50 mM NaCl, pH 7.0) at 90° C for 5 minutes followed by slowly cooling to 25° C.

AFM Measurements

Silicon AFM tips (Nanosensors™ AdvancedTEC™) with a force constant of 0.2 N were first chemically modified by vapor deposition of a 10-nm layer of gold using a CVC Metal Physical Evaporator Deposition system, followed by soaking in a 10 mM solution of hexanethiol in ethanol for 1 h. Modified tips were thoroughly rinsed with 200-proof ethyl alcohol before use.

Scanning probe microscopy (SPM) images were acquired with a MultiMode Scanning Probe Microscope (Digital Instruments). DNA-modified surfaces were mounted on the SPM, and all images were collected with contact mode in phosphate

buffer (50 mM, pH 7.0) at ambient temperature. To obtain height measurements of the monolayers, a voltage of 10 V was applied to the tip, which was scanned repetitively over a 1 μm square area to physically remove the adsorbed monolayer. A portion of the mixed monolayer was removed, followed by measuring the depth profile of the hole produced. Holes were formed on several independent surfaces, and the height profiles of ten different holes were measured (Figure 2.2).

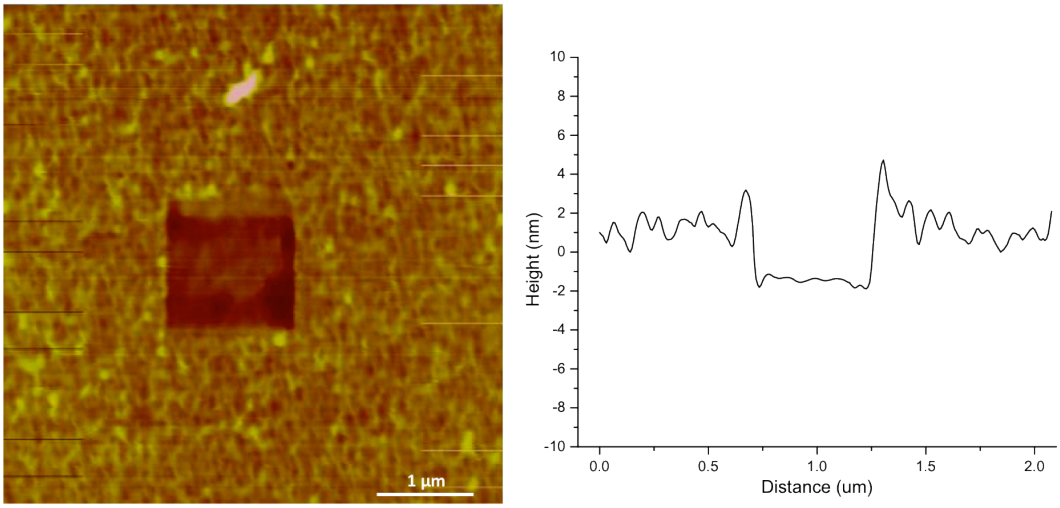

Figure 2.2 Depth measurement of OCT-DNA monolayer with AFM. The image shown is obtained in phosphate buffer (5 mM phosphate, 50 mM NaCl, pH 7.0) with a chemically-modified AFM tip. A hole is formed through the application of a force to the AFM tip in contact mode. When a force is no longer applied to the tip, the depth of the resulting hole is measured. When averaged over many measurements, the height of the monolayer is determined to be 3.5 nm.

Preparation of DNA-Modified Electrodes and AFM Surfaces

Stationary gold electrodes (1.6-mm diameter, BASi) and rotating disk electrodes, RDEs (5-mm diameter, Pine Instruments), were prepared for DNA monolayer formation by polishing with 0.05 μm alumina, followed by electrochemical cycling in 0.5 M H_2SO_4 between ~1.7 and -0.4 V.

High-density thiol-terminated DNA monolayers were formed by depositing 10 μL of 25 μM duplexed DNA in 5 mM phosphate buffer (pH 7.0) containing 100 mM $MgCl_2$ onto the electrode. The films were allowed to assemble for 12 h; the electrodes were then washed with phosphate buffer (5 mM phosphate, 50 mM NaCl, pH 7.0). The electrodes were subsequently backfilled with 1 mM 1-mercaptohexanol (MCH) in a 95:5 phosphate buffer (5 mM phosphate, 50 mM NaCl, pH 7.0)/glycerol solution for 45 minutes. The electrodes were again rinsed with phosphate buffer to ensure removal of residual MCH.

Monolayers featuring DNA-OCT were prepared using a two-step process. An initial mixed monolayer of mercaptoethanol (MCE) as the passivating agent and 6-Azido-1-hexanethiol ("thiol-azide") was formed by soaking the electrodes in an ethanol solution containing 1 mM MCE and 0.25 mM azide for 24 hours to form a monolayer composed of 20% azide. After washing with 5 mM phosphate buffer (pH 7.0), 10 μL of 50 μM DNA-OCT hybridized to its complement was deposited onto the electrode or gold AFM surface (Novascan), where the conjugation reaction was allowed to proceed for 24 hours before washing with phosphate buffer. The average DNA domain size of 25 nm was determined by measuring 15 islands on three different images, each 1 square micron in size.

Electrochemical Measurements

Electrochemical measurements were performed with a CH760B Electrochemical Analyzer (CH Instruments) using a AgCl/Ag reference electrode and Pt-wire counter electrode. Electrochemical measurements were recorded in the dark at ambient temperature in deoxygenated Tris buffer (10 mM Tris, 100 mM KCl, 2.5 mM $MgCl_2$, 1 mM $CaCl_2$, pH 7.6). Using methylene blue, covalently attached to the DNA by either a 2-carbon or 6-carbon alkyl tether, no electrochemical signal decrease was observed upon incorporation of a single base mismatch, indicating that signals are dominated by interactions of the probe with the passivating layer. Additionally, signals obtained from a covalent Nile blue reporter were too small to quantify. Daunomycin (MPBio) dissolved to a final concentration of 2 μM in Tris buffer (10 mM Tris, 100 mM KCl, 2.5 mM $MgCl_2$, 1 mM $CaCl_2$, pH 7.6) was successfully used as a redox probe. All of the DNA sequences used for electrochemical measurements contain a terminal GC sequence, the preferred intercalation site for daunomycin, to direct the redox probe to the terminus of the helix, thereby maximizing the electrochemical effects of helical distortions including incorporation of mismatches and protein binding events. At daunomycin concentrations higher than 6 μM, the DNA-free films exhibited weak surface signals. All experiments were therefore carried out with concentrations of daunomycin at 2 μM, above the saturation limit for DNA intercalation but well below the binding concentration to the mixed-monolayer surface.

TBP Binding Measurements

TATA-Binding Protein (TBP) was purchased from ProteinOne and stored at -80° C until use. MicroBiospin 6 columns (BioRad) were used to exchange the shipping buffer for Tris buffer (10 mM Tris, 100 mM KCl, 2.5 mM $MgCl_2$, 1 mM $CaCl_2$, pH 7.6). Prior to electrochemical measurements with TBP, electrodes were incubated with 1 μM Bovine serum albumin (BSA) for 30 min, followed by rinsing with Tris buffer. BSA binds non-specifically to modified electrodes, which acts to coat any regions where such non-specific binding could occur before the addition of TBP. Electrodes were scanned in the dark in deoxygenated Tris buffer (10 mM Tris, 100 mM KCl, 2.5 mM $MgCl_2$, 1 mM $CaCl_2$, pH 7.6) with 2 μM daunomycin and, unless otherwise noted, 150 nM TBP. In the case of RDEs, unless otherwise noted, electrodes were rotated at 400 rpm.

Results and Discussion

Formation of Low-Density Monolayers by Copper-Free Click Chemistry

Conventional DNA-modified electrodes are prepared by self-assembling thiol-modified DNA duplexes onto gold, followed by backfilling with an alkylthiol to passivate any remaining exposed surface. This method leaves little room for control over the density and spacing of the DNA molecules.[21, 22] Instead, we have labeled DNA with a cyclooctyne moiety (OCT) tethered to the 5' phosphate backbone (Figure 2.3); gold electrodes are then modified with an alcohol-terminated monolayer doped with an azide-capped alkyl thiol, followed by a copper-free click reaction in which cyclooctyne-labeled duplexes, OCT-DNA, are coupled to the film *via* azide-alkyne cycloaddition.[35] This approach offers several advantages over conventional preparations of DNA monolayers: (i) it allows for precise control over the total amount of DNA by simply changing the fraction of thiol-azide present in the preliminary monolayer; (ii) the preliminary self-assembly step results in a passivated surface before the addition of DNA, minimizing undesirable direct interactions between the gold surface and DNA helices; and (iii) because the underlying azide conjugation sites are more evenly distributed in the preliminary monolayer, DNA helices are less prone to cluster into large, high-density domains.

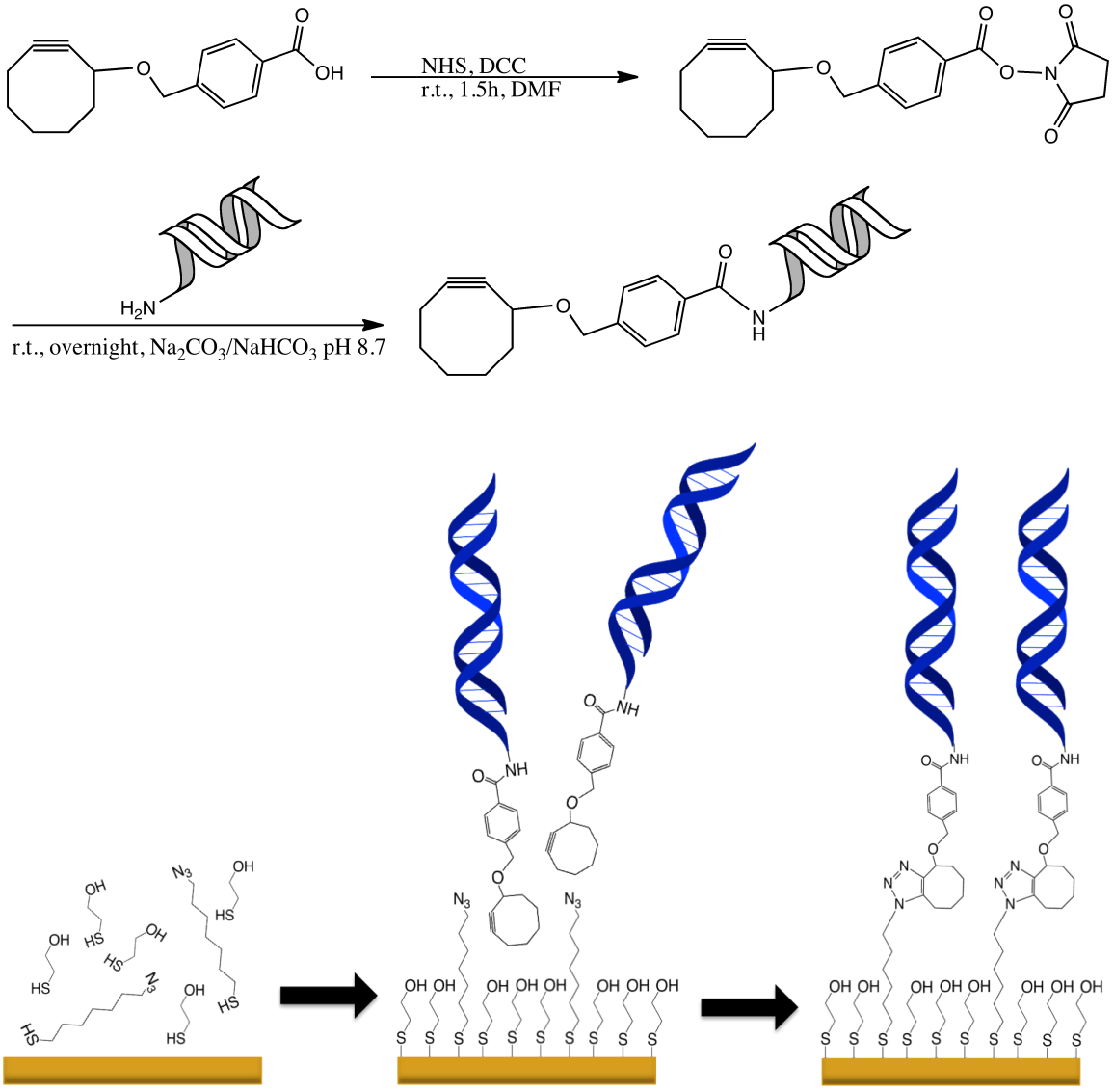

Figure 2.3 Synthesis of OCT-DNA and assembly of OCT-DNA monolayers. *(Above)* Synthetic scheme for OCT-DNA. *(Below)* A preliminary mixed monolayer of alcohol- and azide-terminated thiols is assembled on a gold surface. OCT-modified DNA is subsequently added and allowed to react with the azides to form a covalently tethered low-density DNA monolayer on gold.

Monolayer Characterization through AFM Imaging

OCT-DNA monolayers were examined by atomic force microscopy (AFM) under fluid conditions to visualize the DNA surface coverage and distribution of individual helices within the film. Previous AFM work on high-density monolayers revealed that DNA adheres to standard AFM tips, leading to disturbance of the DNA monolayer when the instrument is in contact mode.[18, 21, 22] We therefore employed tips modified with a hydrophobic film (mercaptohexane), which diminishes interactions with both the buffer and the negatively charged DNA on the surface.[18]

In contrast to low-density thiolated DNA monolayers, which show images consistent with quite densely packed monolayers,[21] images of OCT-DNA films on a 20% azide monolayer reveal no large-domain clustering (Figure 2.4). Notably, the images do show some monolayer stratification, consistent with extremely small clusters of DNA that are remarkably uniform in size and shape. Indeed, these mini-clusters likely indicate some sequestration of azide-thiol reagents in the underlying monolayer, presumably a result of small chain-length differences between the passivating molecules and the azide-containing thiols. While longer alcohol-terminated thiols were tested in an attempt to form a more evenly-dispersed mixed monolayer, DNA coupling efficiencies were extremely low for 3, 4, 5, and 6-carbon alcohol-terminated thiols, likely due to the size of the cyclooctyne.

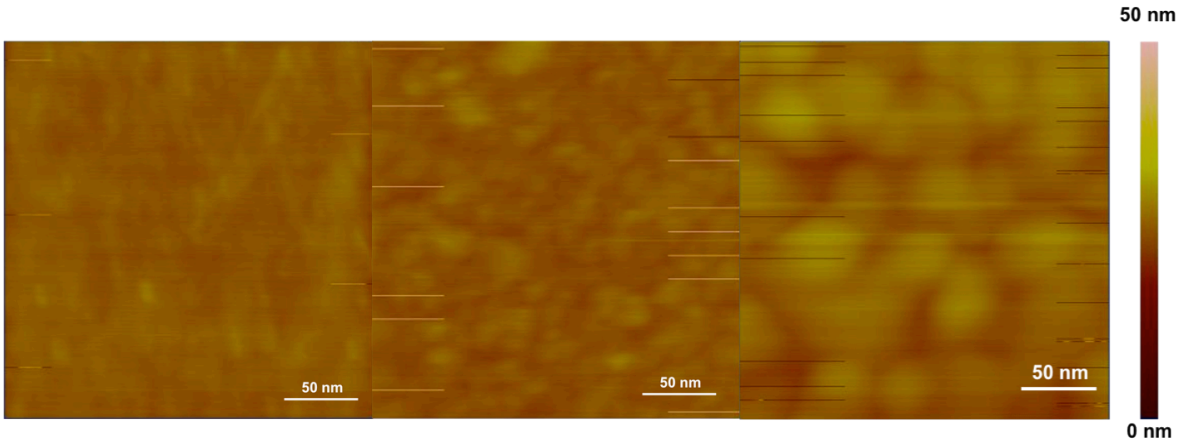

Figure 2.4 AFM images of the assembly of low-density OCT-DNA monolayers. Images are in phosphate buffer (5 mM phosphate, 50 mM NaCl, pH 7.0) and were obtained with chemically modified tips. *(Left)* Image of bare gold electrode. *(Center)* Self-assembled monolayer containing 20% thiol azide and 80% mercaptoethanol. *(Right)* Surface after incubation with OCT-DNA. The morphology of the surface changes with sequential modification steps. From the image on the right, it can be seen that the individual clusters of DNA on the surface are small; the number of DNA helices contained in a microcluster is approximately 150.

The height of these low-density DNA monolayers was also measured by AFM; we previously reported a film depth for densely packed 15-base-pair duplexes on gold of ~4.5 nm.[18] Analogous films prepared from OCT-DNA yield an average film height of ~3.5 nm ± 0.5 nm, consistent with a monolayer composed of a mixture of taller DNA mini-clusters and shorter underlying passivating agent (Figure 2.2). Notably, these regularly spaced bumps observed in the film-height profile are consistent with small aggregates of DNA homogeneously dispersed within the passivating film. The area of these bumps, attributed to mini-clusters of DNA, can be quantified. Based on the diameter of B-form DNA (2.0 nm) and the average diameter of the clusters (25 nm, an average of the size of clusters measured from three 1 μm^2 AFM images), each cluster contains ~ 150 individual helices, with the overall DNA surface coverage for the entire AFM field of view estimated as ~15 pmol/cm^2. Significantly, this implies that ~1/3 of the duplexes in the film have a solution-exposed edge, meaning that a much greater portion of DNA in these monolayers is directly accessible to analytes in solution as compared to films in which the DNA helices are closely packed into large islands.

Electrochemical Monolayer Characterization

OCT-DNA monolayers (5% - 90% azide in the underlying film) were also examined using electrochemical assays. For 20% azide films, the total surface coverage of DNA, G_{DNA}, was measured based on the electrochemical response of $Ru(NH_3)_6^{3+}$ electrostatically bound to the DNA.[20, 36, 37] 20% azide films that featured fully Watson-Crick base-paired duplexes, as well as 20% azide films with duplexes that possessed a single CA mismatch, were investigated. Voltammetry of micromolar solutions of

$Ru(NH_3)_6^{3+}$ yielded well defined $Ru^{3+/2+}$ surface waves; integrating the traces yielded an average value for DNA surface coverage of 13.5±1 pmol/cm^2, as determined by Eq.1 (where *z* is the charge on ruthenium, 3+, and *m* is the number of nucleotides in the duplex, 17).

$$\Gamma_{DNA} = \Gamma_{Ru}\left(\frac{m}{z}\right) \qquad (1)$$

This surface coverage is not only in excellent agreement with that calculated by AFM, but is the same regardless of whether the monolayers are formed from well matched or mismatched OCT-DNA duplexes. In comparison, high-density monolayers prepared from thiol-labeled DNA typically yield surface coverages in the range of 40 - 50 pmol/cm^2.[38] These data show that the coupling on a surface is essentially quantitative, as a preliminary monolayer composed of 20% azide yields a total DNA coverage that is 25% of the coverage of high-density monolayers, as measured with $Ru(NH_3)_6^{3+}$. Significantly, the amount of DNA on the surface increased linearly with the percentage of azide used to form the underlying monolayer (Figure 2.5). As the amount of DNA increased linearly with increasing solution concentrations of azide, the solution percentage of azide appears proportional to the amount that assembles on the electrode, which also indicates that OCT-DNA coupling appears essentially quantitative.

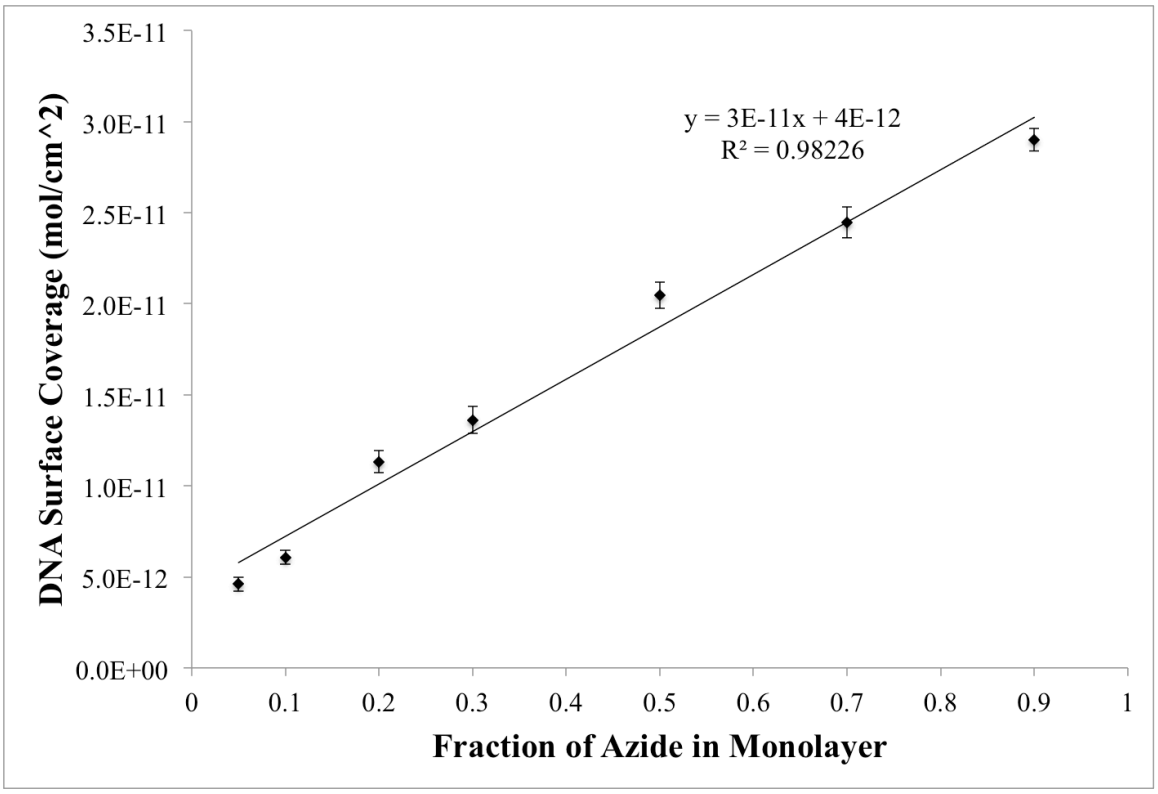

Figure 2.5 Quantification of DNA in OCT-DNA monolayers assembled with varying solution concentrations of azide. The amount of OCT-DNA that covalently attached to monolayers formed with varying concentrations of azide in the monolayer formation solution was determined by measuring electrochemical signals in a 20 μM ruthenium hexammine solution in Tris buffer (10 mM Tris, 100 mM KCl, 2.5 mM $MgCl_2$, 1 mM $CaCl_2$, pH 7.6). Concentrations of azide ranged from 5%-90%. A linear increase in amount of DNA on the surface with increasing percent of azide indicates that the solution concentration of azide is a valid approximation of the amount of azide assembled in the monolayer, and that the DNA coupling to the active head groups on the surface is essentially quantitative.

To assess OCT-DNA films for DNA CT-based biosensing applications, we carried out experiments using non-covalent intercalative probe molecules.[13] The anthraquinone-based drug daunomycin (DM) intercalates into DNA films where it undergoes a reversible 1 e^- reduction at pH values greater than ~7.3.[11, 39, 40] Figure 2.6 shows the background-subtracted cyclic voltammogram of DM at a well-matched OCT-DNA surface. Significantly, no signal is observed under identical conditions at a mixed alcohol/azide monolayer, confirming that the observed DM signals are due to the presence of intact DNA. Moreover, the presence of an intervening CA mismatch results in nearly complete loss of the DM electrochemical response, yet the electrode maintains a nearly identical $Ru(NH_3)_6^{3+}$ redox signal. This confirms that the attenuation of the DM signals at mismatched OCT-DNA is not due to dehybridization or less favorable monolayer assembly.

While DM undergoes efficient oxidation and reduction when intercalated into well-matched OCT-DNA duplexes, the incorporation of an intervening CA mismatch results in nearly complete loss of the electrochemical response (see Figures 2.6, 2.7). This sensitivity to mismatches is strong evidence for a DNA-mediated CT reaction. Importantly, both well matched and mismatched OCT-DNA films yield virtually identical $Ru(NH_3)_6^{3+}$ responses (Figure 2.6), confirming that the attenuation of the DM signals at mismatched OCT-DNA is not due to dehybridization or less favorable assembly of the mismatched monolayer versus the matched.

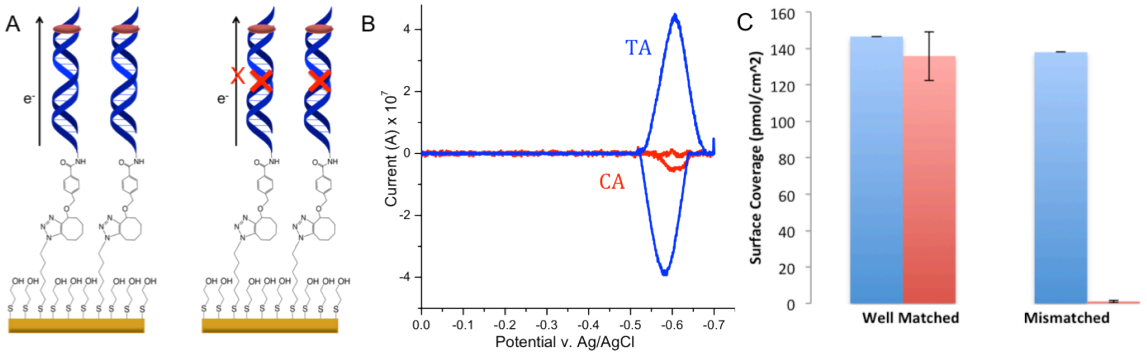

Figure 2.6 Electrochemical mismatch discrimination. (A) The incorporation of a single-base mismatch into the sequence of DNA assembled on an electrode prevents electrons from flowing to the redox probe as compared to the electron flow through the well-matched DNA. (B) A background-subtracted cyclic voltammogram (CV) of the electrochemical signal discrimination observed between well-paired helices in an OCT-DNA monolayer (blue) and an OCT-DNA monolayer with DNA containing a CA mismatch (red) is shown. The CV was obtained with a scan rate of 100 mV/s. Both DNA duplexes were 17 base pairs in length. Traces were obtained with 2 μM daunomycin in Tris buffer (10 mM Tris, 100 mM KCl, 2.5 mM $MgCl_2$, 1 mM $CaCl_2$, pH 7.6). Almost a complete signal loss is observed upon incorporation of a single CA mismatch. (C) DNA CT mismatch discrimination compared to quantified DNA surface coverage. The surface coverage determined from the DNA-mediated electrochemical signal obtained from daunomycin for well matched DNA and DNA containing a single-base mismatch (blue) is compared to coverage determined from the electrochemical signal of ruthenium hexammine (red), which electrostatically interacts the phosphates in the DNA and does not report on helix integrity. Surface coverages were calculated from the quantification of the area of the anodic peak of a CV obtained for both reporters at a scan rate of 100 mV/s in Tris buffer Tris buffer (10 mM Tris, 100 mM KCl, 2.5 mM $MgCl_2$, 1 mM $CaCl_2$, pH 7.6). Almost identical amounts of DNA are present for the well matched and mismatched sequences as quantified with ruthenium hexammine; the only observable difference is in the DNA-mediated daunomycin signal. Error bars are given for the standard deviation from three replicates for each experimental condition.

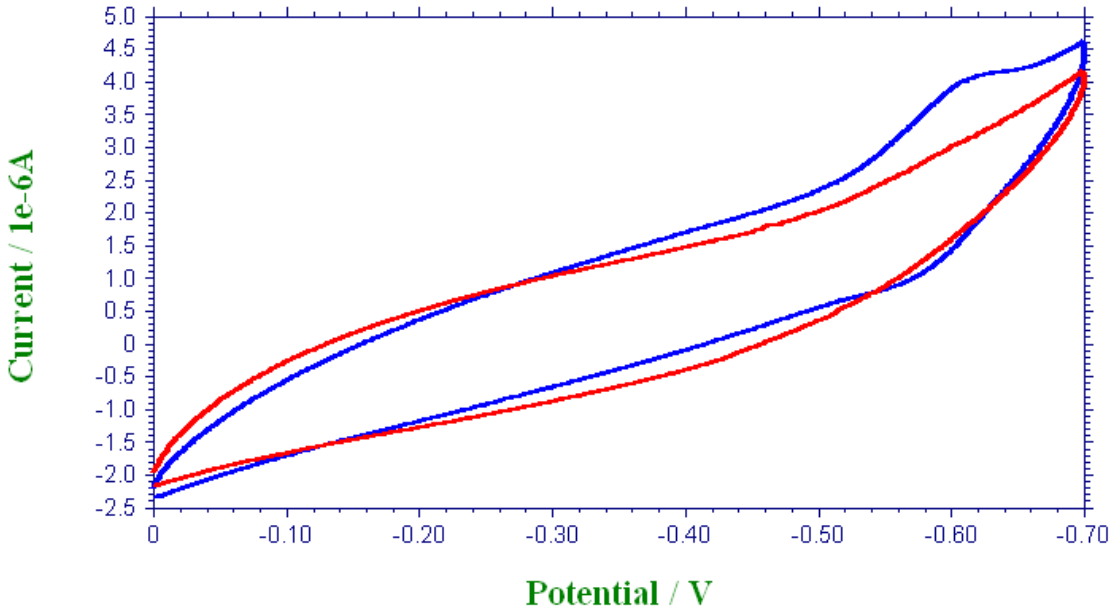

Figure 2.7 Raw cyclic voltammogram (CV) of mismatch discrimination. The electrochemical signal discrimination observed between well-paired helices in an OCT-DNA monolayer (blue) and an OCT-DNA monolayer with DNA containing a CA mismatch (red) is shown. The background-subtracted CV is shown in an additional figure. The CV was obtained with a scan rate of 100 mV/s. Both DNA duplexes were 17 base pairs in length. Traces were obtained with 2 μM daunomycin in Tris buffer (10 mM Tris, 100 mM KCl, 2.5 mM $MgCl_2$, 1 mM $CaCl_2$, pH 7.6). Almost a complete signal loss is observed upon incorporation of a single CA mismatch.

Electrochemistry of TBP Binding

To test whether the enhanced solution accessibility of DNA helices in OCT-DNA films allows for improved protein detection, we investigated the binding of TATA-binding protein, TBP. The electrochemistry of DM at OCT-DNA films with 20%, 50% and 90% azide, as well as conventional low- and high-density films in which the individual helices contained a TATA sequence, were examined in the presence of TBP. TBP, a subunit of the TFIID transcription factor in eukaryotes, kinks DNA (80°) when bound to its TATA target sequence and has been shown to attenuate DNA CT on DNA-modified electrodes.[11, 13, 41, 42] Before incubation with TBP, monolayers were incubated with BSA, a non-DNA binding protein. This protein adheres non-specifically to the electrode surfaces, ensuring that electrochemical changes after TBP addition are due to the specific binding of TBP to DNA.

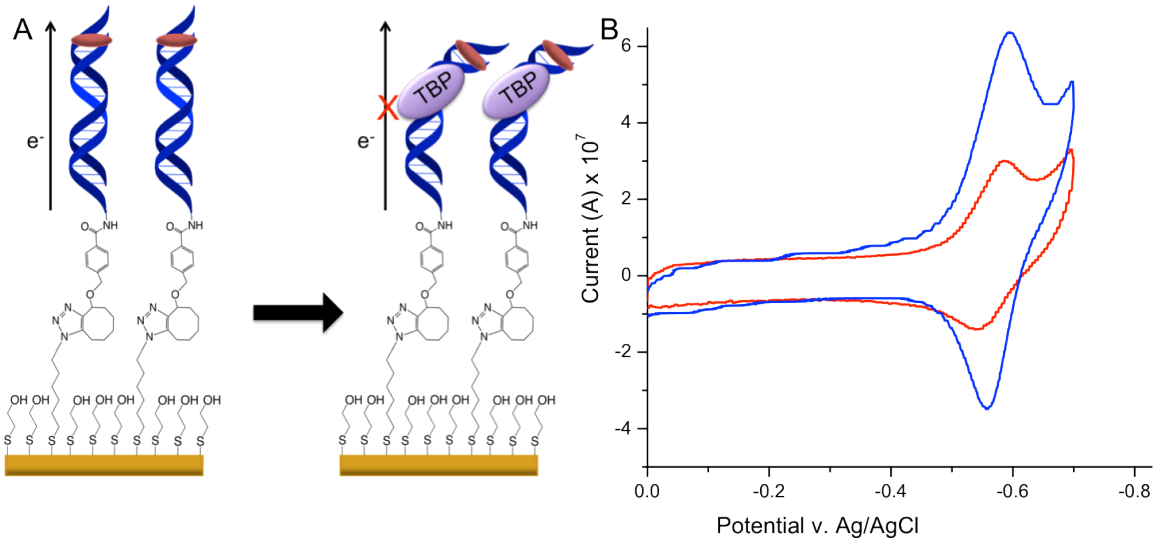

Figure 2.8 Electrochemical determination of TBP binding. *(A)* The binding and subsequent kinking of DNA by TBP prevents electrons from flowing to the daunomycin redox probe; before the protein is bound, there is a significant amount of electron flow through the DNA. *(B)* A cyclic voltammogram (CV) of the electrochemical signal reduction observed in an OCT-DNA monolayer with the TBP binding DNA sequence before the addition of protein (blue) and after the addition of 150 nM TBP that is allowed to incubate for 15 minutes (red) is shown. The CV was obtained with a scan rate of 100 mV/s. The TBP binding DNA duplex is 22 base pairs in length. Traces were obtained with 2 μM daunomycin in Tris buffer (10 mM Tris, 100 mM KCl, 2.5 mM $MgCl_2$, 1 mM $CaCl_2$, pH 7.6). Significant signal attenuation is observed upon TBP binding.

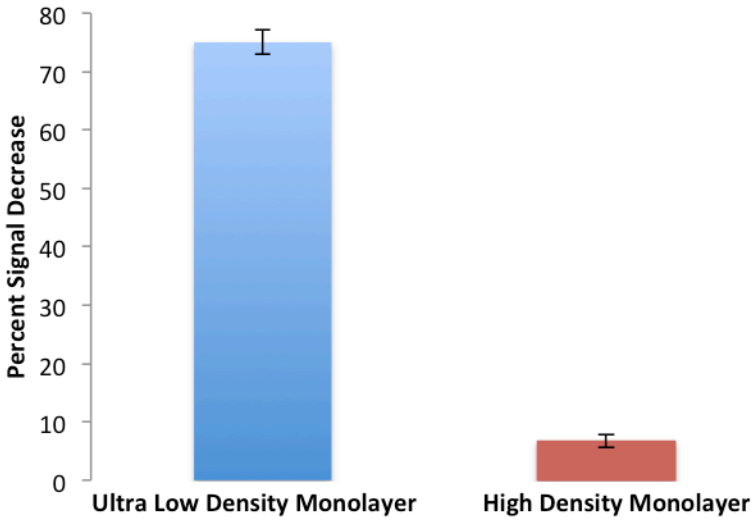

Figure 2.9 Percent signal decrease upon TBP binding for high- versus low-density DNA monolayers. Shown is the percent signal decrease from the DNA-mediated electrochemical signal obtained from daunomycin for TBP binding to DNA in an OCT-DNA monolayer (blue) and a high-density thiol monolayer (red) after addition of 75 nM TBP. Percent signal decreases are calculated from the quantification of the area of the anodic peak of a CV obtained for the signal before and after TBP addition at a scan rate of 100 mV/s in Tris buffer (10 mM Tris, 100 mM KCl, 2.5 mM $MgCl_2$, 1 mM $CaCl_2$, pH 7.6). Error bars are given for the standard deviation from three replicates.

No significant change in electrochemical signal was observed with either the well-matched sequence or the TBP-binding sequence after BSA incubation. After subsequent incubation with TBP, the presence of 150 nM protein causes a signal decrease of 75% at OCT-DNA films (20% azide), compared to a decrease of only 6% at high-density monolayers (Figures 2.8, 2.9). The preliminary addition of BSA ensures that ensuing signal decreases upon TBP addition are due to the specific binding of the protein. To further confirm that the signal decrease was due to a loss of DNA CT caused by TBP binding and subsequent kinking of the DNA, we measured the $Ru(NH_3)_6^{3+/2+}$ response, which gave nearly identical values for G_{DNA} regardless of whether the OCT-DNA sequences were matched, mismatched, or contained the TATA binding sequence (Figure 2.10).

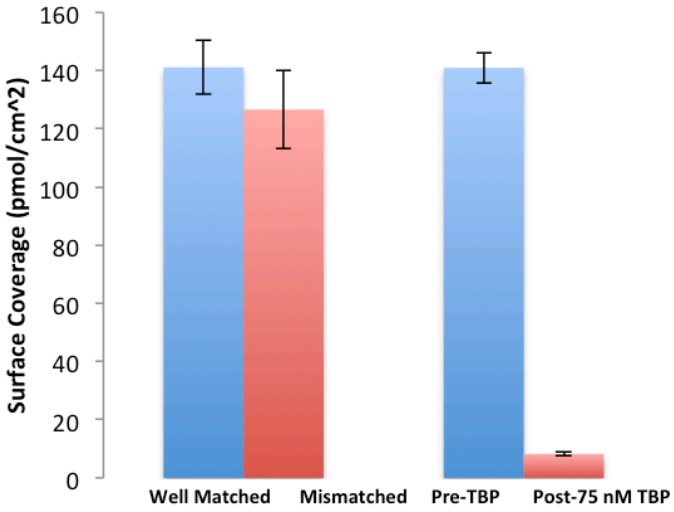

Figure 2.10 TBP DNA CT signal attenuation compared to quantified DNA surface coverage on an OCT-DNA monolayer. In red is the surface coverage determined from the DNA-mediated electrochemical signal obtained from daunomycin for the TBP binding DNA sequence before and after the addition of 75 nM TBP. In blue is the surface coverage determined from the electrochemical signal of ruthenium hexammine, which electrostatically interacts with the phosphates in the DNA and does not report on helix integrity. Surface coverages are calculated from the quantification of the area of the anodic peak of a CV obtained for both reporters at a scan rate of 100 mV/s in Tris buffer (10 mM Tris, 100 mM KCl, 2.5 mM $MgCl_2$, 1 mM $CaCl_2$, pH 7.6). As can be seen from the graph, the amount of DNA on the surface does not change upon addition of TBP, as quantified with ruthenium hexammine; the only observable difference in coverage is in the DNA-mediated daunomycin signal. Error bars are given for the standard deviation from three replicates for each experimental condition.

We also investigated detection limits of TBP binding at OCT-DNA films through the titration of TBP onto DNA-modified electrodes comprised of both OCT- and thiol-modified DNAs (Figure 2.11). Films formed from OCT-DNA are significantly more sensitive to TBP. A signal attenuation of over 10% is observed for both the 20% and 50% azide monolayers upon addition of 4 nM TBP protein, a concentration near the dissociation constant of TBP. The ability to detect proteins at such low concentrations is an important step in the development of DNA-modified films for diagnostic applications.

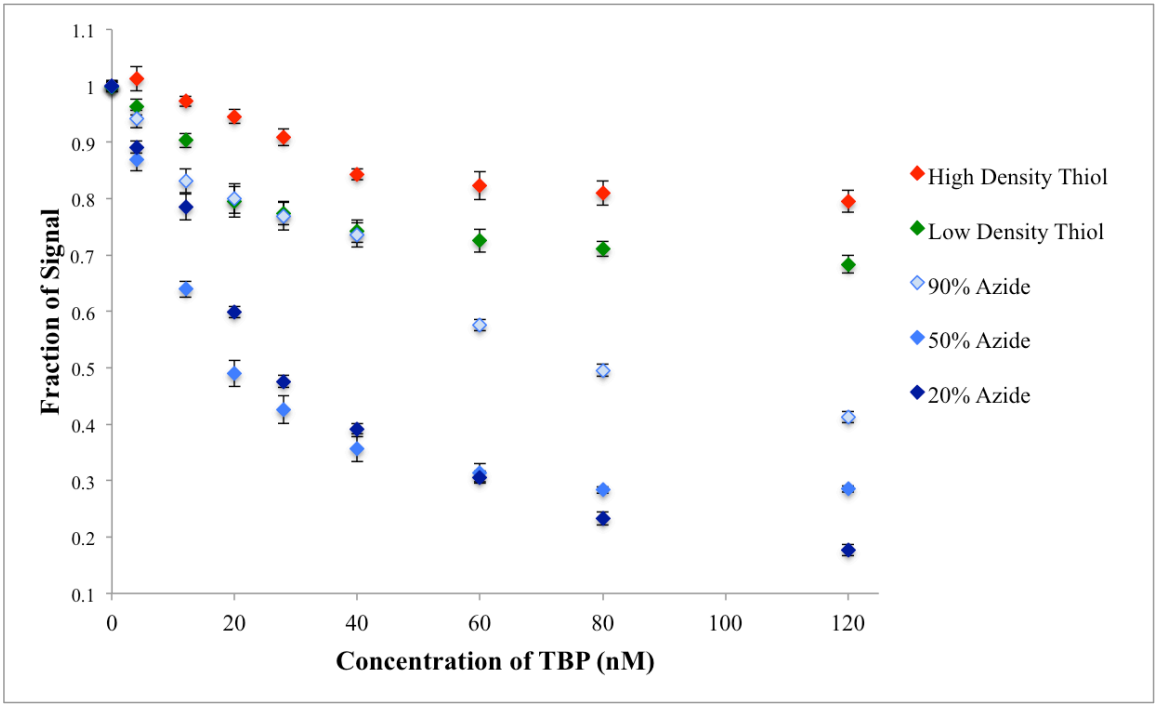

Figure 2.11 TBP titration onto DNA-modified electrodes. The plot shows the titration of TBP onto a 20% OCT-DNA monolayer (dark blue), a 50% OCT-DNA monolayer (blue) a 90% OCT-DNA monolayer (light blue), a low-density thiol monolayer (green), and a high-density thiol monolayer (red), as determined electrochemically. The signal remaining was determined through the quantification of the area of the anodic peak of a CV obtained at a scan rate of 100 mV/s. CVs were obtained with 2 μM daunomycin in Tris buffer (10 mM Tris, 100 mM KCl, 2.5 mM $MgCl_2$, 1 mM $CaCl_2$, pH 7.6). TBP is detectable with the OCT-DNA monolayer at concentrations as low as 4 nM (at which there is a greater than 15% signal decrease), which is near the K_D of the protein (3.3 nM); both high-density and low-density thiol monolayers have a negligible signal decrease at this protein concentration. Error bars represent the standard deviation obtained over nine replicates of each type of DNA-modified electrode.

The electrochemically derived TBP/OCT-DNA binding isotherm could not be fit well to a simple Langmuir thermodynamics model, indicating some form of cooperative TBP binding. We therefore analyzed the data according to the Frumkin-Fowler-Guggenheim (FFG) model,[33, 34, 43, 44] which accounts for lateral interactions on a surface. Using Eq. (2), a plot of log[θ/(1-θ)C] *vs.* θ gives a straight line (Figure 2.12).

$$\frac{\theta}{1-\theta}e^{2\theta a} = \beta C \qquad (2)$$

In this equation, θ is the fractional surface coverage (i.e., $\Gamma_{\text{TBP bound}}/\ \Gamma_{\text{TBP binding sites}}$), C is the solution concentration (M) of TBP, β is the adsorption equilibrium constant, and a is the lateral interaction or Frumkin coefficient. From this fit, values for the lateral interaction coefficient, a, and the adsorption equilibrium constant, β, were found to be 0.2 and 30 μM, respectively. The positive a value obtained indicates repulsive sorbent/sorbate lateral interactions. A repulsive lateral interaction on the surface is consistent with the steric presence that bound TBP exerts on DNA duplexes, impeding the binding of additional TBP proteins, as kinked TBP-bound helices likely impede binding of TBP to adjacent sequences. From the determined value of β (the adsorption equilibrium constant), $ln(\beta)$ can be used to characterize the free adsorption energy of the protein, ΔG_A, which provides the difference in free energy of TBP between its solution state and adsorbed state. The value for ΔG_A can be determined from Eq. (3):

$$\Delta G_A = -RTln(\beta) \qquad (3)$$

where R is the molar gas constant.[45-47] The free adsorption energy of the TBP protein on the low-density DNA monolayer is determined to be 42 kJ/mol. This positive free adsorption energy is not uncommon for charged molecules adsorbing onto a charged surface.[34]

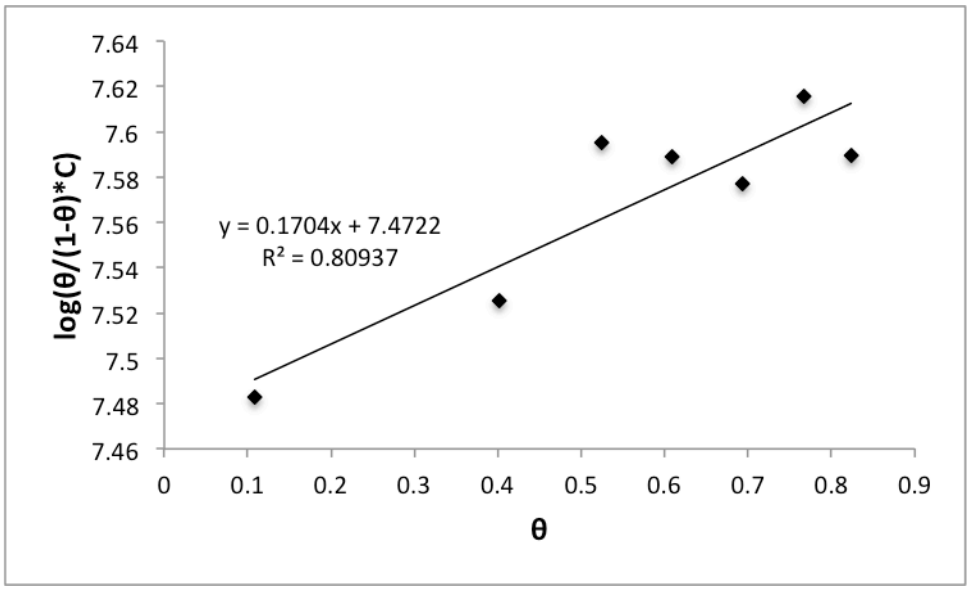

Figure 2.12 Linear fit of TBP titration data to the Frumkin-Fowler-Guggenheim adsorption isotherm. To determine the Frumkin coefficient (*a*) and the adsorption equilibrium constant (β) from the previous titration data, a plot of log[θ/(1-θ)C] versus the fractional surface coverage (θ), where C is the solution concentration of TBP is constructed. The linear fit of the data is shown, from which the two desired parameters are extrapolated.

Given the anti-cooperative nature of TBP binding observed upon thermodynamic investigations of this protein binding to OCT-DNA monolayers, we also investigated the relative kinetics of TBP binding to these monolayers and to thiolated DNA films. Rotating disk electrode (RDE) experiments were undertaken to determine the binding kinetics of TBP on both high density thiol-DNA and low-density OCT-DNA monolayers. RDEs remove diffusion as a factor when determining kinetics of a system.[44, 48] The loss of an electrochemical DM signal upon TBP binding over time therefore reports on the kinetics of protein binding. Because the number of TBP binding sites is fixed, the solution concentration of protein is in large enough excess to be unaffected by the amount of protein bound to the surface, and the rate of TBP diffusion to the surface is removed as a factor, we can analyze the kinetics of TBP binding to the surfaces with a Langmuir kinetics model. As is evident in Figure 2.13, which shows the decrease in charge determined from the area of the reductive peak plotted as a function of time, the rate of signal decrease for both the high density and ultra low-density monolayers upon TBP binding is almost identical. As is apparent in the figure, the RDEs produce similar overall signal attenuations to stationary electrodes for both types of DMEs. When the data are fit to this Langmuir equation for protein binding kinetics, the k_{obs} for high density monolayers was determined to be 6.1×10^{-3} s^{-1}; likewise, for the ultra low density monolayers, the k_{obs} was determined to be 6.1×10^{-3} s^{-1}. This indicates that protein binding to DMEs is a fairly slow process. Additionally, the rate of protein binding is unaffected by accessibility; only the amount of signal attenuation is dependent on DNA helix accessibility.

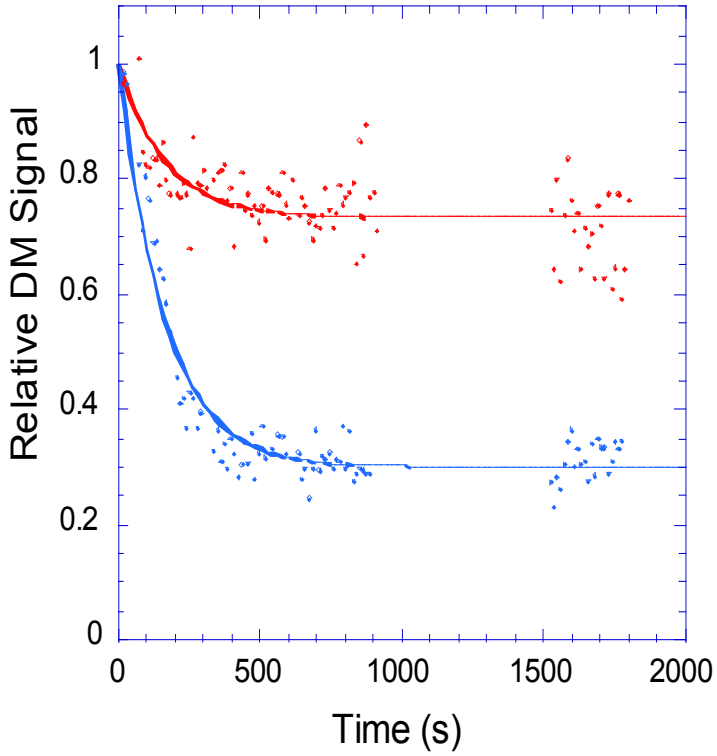

Figure 2.13 Kinetics of TBP binding to DNA-modified electrodes. The kinetics of TBP binding to both OCT-DNA monolayers and high density monolayers are determined electrochemically at a gold rotating disk electrode surface. Electrodes are rotated at 400 rpm, with 2 μM daunomycin in Tris buffer (10 mM Tris, 100 mM KCl, 2.5 mM $MgCl_2$, 1 mM $CaCl_2$, pH 7.6). TBP (75 nM) is added, and sequential CV scans are obtained at 100 mV/s. The relative DM signal is obtained through the quantification of the anodic CV peak and subsequent normalization to the value obtained for time=0. Curves for high-density thiol DNA (red) and low density OCT-DNA (blue) monolayers are shown. The data are fit to a Langmuir kinetics model based on exponential decay, which shows that the rates of TBP binding to both types of monolayers are essentially the same.

When thermodynamic and kinetic data are evaluated together, a model for TBP binding to DMEs becomes apparent. Based on the repulsive lateral interactions on the surface, the positive value for the free energy of adsorption and the relatively slow rate of TBP binding to both OCT-DNA and thiol-DNA films, TBP likely binds primarily to surface-exposed sequences. This conclusion is further supported by the significantly lower detection limits for the low-density OCT-DNA films as compared to the high-density thiol-DNA films. The low-density OCT-DNA monolayers have significantly more solution-exposed TBP binding sites than the thiol-DNA monolayers. This model for TBP binding is also consistent with the kinetics that are independent of surface coverage; only exposed sequences are available, and there are relatively fewer of them in tightly-packed films. This model of protein binding supports the utility of OCT-DNA monolayers for biomolecule detection, as the large amount of buffer-exposed helices aids TBP binding to the monolayers.

Conclusions

A novel method of DNA assembly to form DNA-modified surfaces for the electrochemical detection of biomolecules has been developed. The copper-free click-based strategy described here allows for the formation of low-density, more evenly spaced monolayers, while maintaining surface passivation against the redox reporter. Both electrochemical and imaging methods have been used to characterize these monolayers. This platform facilitates DNA-mediated CT and is thus extremely sensitive to perturbations in the DNA, providing exquisite electrochemical discrimination between well matched and mismatched DNA duplexes. Additionally, this platform provides greater sensitivity to protein binding events than conventional high-density films due to the larger number of accessible, solution-exposed binding sites. In particular, here, low-density films allow for the detection of as little as 4 nM TBP. The enhanced detection with OCT-DNA films adds another sensitive detection tool to the toolbox of electrochemical DNA CT-based detection strategies.

References

1. Cederquist, K. B., and Kelley, S. O. (2012) Nanostructured biomolecular detectors: pushing performance at the nanoscale, *Curr. Opin. Chem. Biol. 16*, 415-421.

2. Drummond, T. G., Hill, M. G., and Barton, J. K. (2003) Electrochemical DNA sensors, *Nat. Biotechnol. 21*, 1192-1199.

3. Gooding, J. J. (2002) Electrochemical DNA Hybridization Biosensors, *Electroanalysis 14*, 1149-1156.

4. Lord, H., and Kelley, S. O. (2009) Nanomaterials for ultrasensitive electrochemical nucleic acids biosensing, *J. Mat. Chem. 19*, 3127-3134.

5. Mikkelsen, S. R. (1996) Electrochecmical biosensors for DNA sequence detection, *Electroanalysis 8*, 15-19.

6. Slinker, J. D., Muren, N. B., Gorodetsky, A. A., and Barton, J. K. (2010) Multiplexed DNA-modified electrodes, *J. Am. Chem. Soc. 132*, 2769-2774.

7. Wang, J. (2006) Electrochemical biosensors: towards point-of-care cancer diagnostics, *Biosens. Bioelectron. 21*, 1887-1892.

8. Kelley, S. O., Boon, E. M., Barton, J. K., Jackson, N. M., and Hill, M. G. (1999) Single-base mismatch detection based on charge transduction through DNA, *Nucleic Acids Res. 27*, 4830-4837.

9. Boon, E. M., Ceres, D. M., Drummond, T. G., Hill, M. G., and Barton, J. K. (2000) Mutation detection by electrocatalysis at DNA-modified electrodes, *Nat. Biotechnol. 18*, 1096-1100.

10. Boon, E. M., Livingston, A. L., Chmiel, N. H., David, S. S., and Barton, J. K. (2003) DNA-mediated charge transport for DNA repair, *Proc. Natl. Acad. Sci. USA 100*, 12543-12547.

11. Boon, E. M., Salas, J. E., and Barton, J. K. (2002) An electrical probe of protein-DNA interactions on DNA-modified surfaces, *Nat. Biotechnol. 20*, 282-286.

12. Gorodetsky, A. A., Buzzeo, M. C., and Barton, J. K. (2008) DNA-mediated electrochemistry, *Bioconjug. Chem. 19*, 2285-2296.

13. Gorodetsky, A. A., Ebrahim, A., and Barton, J. K. (2008) Electrical detection of TATA binding protein at DNA-modified microelectrodes, *J. Am. Chem. Soc. 130*, 2924-2925.

14. Guo, X., Gorodetsky, A. A., Hone, J., Barton, J. K., and Nuckolls, C. (2008) Conductivity of a single DNA duplex bridging a carbon nanotube gap, *Nat. Nanotechnol. 3*, 163-167.

15. Chen, C., Wang, W., Ge, J., and Zhao, X. S. (2009) Kinetics and thermodynamics of DNA hybridization on gold nanoparticles, *Nucleic Acids Res. 37*, 3756-3765.

16. Peterson, A. W., Heaton, R. J., and Georgiadis, R. M. (2001) The effect of surface probe density on DNA hybridization, *Nucleic Acids Res. 29*, 5163-5168.

17. Chrisey, L. A., Lee, G. U., and O'Ferrall, C. E. (1996) Covalent attachment of synthetic DNA to self-assembled monolayer films, *Nucleic Acids Res. 24*, 3031-3039.

18. Kelley, S. O., Barton, J. K., Jackson, N. M., and Hill, M. G. (1997) Electrochemistry of methylene blue bound to a DNA-modified electrode, *Bioconjug. Chem. 8*, 31-37.

19. Levicky, R., Herne, T. M., Tarlov, M. J., and Satija, S. K. (1998) Using Self-Assembly To Control the Structure of DNA Monolayers on Gold: A Neutron Reflectivity Study, *J. Am. Chem. Soc. 120*, 9787-9792.

20. Yu, H. Z., Luo, C. Y., Sankar, C. G., and Sen, D. (2003) Voltammetric procedure for examining DNA-modified surfaces: quantitation, cationic binding activity, and electron-transfer kinetics, *Anal. Chem. 75*, 3902-3907.

21. Mui, S., Boon, E. M., Barton, J. K., Hill, M. G., and Spain, E. M. (2001) Morphology of 15-mer Duplexes Tethered to Au(111) Probed Using Scanning Probe Microscopy, *Langmuir. 17*, 5727-5730.

22. Murphy, J. N., Cheng, A. K., Yu, H. Z., and Bizzotto, D. (2009) On the nature of DNA self-assembled monolayers on Au: measuring surface heterogeneity with

electrochemical in situ fluorescence microscopy, *J. Am. Chem. Soc. 131*, 4042-4050.

23. Folkers, J. P., Laibinis, P. E., and Whitesides, G. M. (1992) Self-assembled monolayers of alkanethiols on gold: comparisons of monolayers containing mixtures of short- and long-chain constituents with methyl and hydroxymethyl terminal groups, *Langmuir 8*, 1330-1341.

24. Hobara, D., Sasaki, T., Imabayashi, S.-i., and Kakiuchi, T. (1999) Surface Structure of Binary Self-Assembled Monolayers Formed by Electrochemical Selective Replacement of Adsorbed Thiols, *Langmuir 15*, 5073-5078.

25. Love, J. C., Estroff, L. A., Kriebel, J. K., Nuzzo, R. G., and Whitesides, G. M. (2005) Self-assembled monolayers of thiolates on metals as a form of nanotechnology, *Chem. Rev. 105*, 1103-1169.

26. Sellers, H., Ulman, A., Shnidman, Y., and Eilers, J. E. (1993) Structure and binding of alkanethiolates on gold and silver surfaces: implications for self-assembled monolayers, *J. Am. Chem. Soc. 115*, 9389-9401.

27. Stranick, S. J., Parikh, A. N., Tao, Y. T., Allara, D. L., and Weiss, P. S. (1994) Phase Separation of Mixed-Composition Self-Assembled Monolayers into Nanometer Scale Molecular Domains, *J. Phys. Chem. 98*, 7636-7646.

28. Tamada, K., Hara, M., Sasabe, H., and Knoll, W. (1997) Surface Phase Behavior of n-Alkanethiol Self-Assembled Monolayers Adsorbed on Au(111): An Atomic Force Microscope Study, *Langmuir 13*, 1558-1566.

29. Ulman, A. (1996) Formation and Structure of Self-Assembled Monolayers, *Chem. Rev. 96*, 1533-1554.

30. Devaraj, N. K., Miller, G. P., Ebina, W., Kakaradov, B., Collman, J. P., Kool, E. T., and Chidsey, C. E. (2005) Chemoselective covalent coupling of oligonucleotide probes to self-assembled monolayers, *J. Am. Chem. Soc. 127*, 8600-8601.

31. Agard, N. J., Prescher, J. A., and Bertozzi, C. R. (2004) A strain-promoted [3 + 2] azide-alkyne cycloaddition for covalent modification of biomolecules in living systems, *J. Am. Chem. Soc. 126*, 15046-15047.

32. Baskin, J. M., and Bertozzi, C. R. (2007) Bioorthogonal Click Chemistry: Covalent Labeling in Living Systems, *QSAR & Comb. Sci. 26*, 1211-1219.

33. Trasatti, S. (1974) Acquisition and analysis of fundamental parameters in the adsorption of organic substances at electrodes, *J. Electroanal. Chem. and Interfacial Electrochem. 53*, 335-363.

34. Goyne, K. W., Chorover, J., Zimmerman, A. R., Komarneni, S., and Brantley, S. L. (2004) Influence of mesoporosity on the sorption of 2,4-dichlorophenoxyacetic acid onto alumina and silica, *J. Colloid Interface Sci 272*, 10-20.

35. Huisgen, R. (1961) Proceedings of the Chemical Society. October 1961, *Proc. Chem. Soc.* 357-396.

36. Ceres, D. M., Udit, A. K., Hill, H. D., Hill, M. G., and Barton, J. K. (2007) Differential ionic permeation of DNA-modified electrodes, *J. Phys. Chem. B 111*, 663-668.

37. Steel, A. B., Herne, T. M., and Tarlov, M. J. (1998) Electrochemical quantitation of DNA immobilized on gold, *Anal. Chem. 70*, 4670-4677.

38. Anson, F. C., and Rodgers, R. S. (1973) Electrode kinetics for a simple redox reaction with adsorbed reactant: The reduction of $Cr(OH_2)_3(NCS)_3$ at mercury electrodes, *J. Electroanal. Chem. and Interfacial Electrochem. 47*, 287-309.

39. Jackson, N. M., and Hill, M. G. (2001) Electrochemistry at DNA-modified surfaces: new probes for charge transport through the double helix, *Curr. Opin. Chem. Biol. 5*, 209-215.

40. Palanti, S., Marrazza, G., and Mascini, M. (1996) Electrochemical DNA Probes, *Anal. Lett. 29*, 2309-2331.

41. Nikolov, D. B., Hu, S. H., Lin, J., Gasch, A., Hoffmann, A., Horikoshi, M., Chua, N. H., Roeder, R. G., and Burley, S. K. (1992) Crystal structure of TFIID TATA-box binding protein, *Nature 360*, 40-46.

42. Gorodetsky, A. A., Hammond, W. J., Hill, M. G., Slowinski, K., and Barton, J. K. (2008) Scanning electrochemical microscopy of DNA monolayers modified with Nile Blue, *Langmuir 24*, 14282-14288.

43. Fowler, R., and Guggenheim, E. A. (1965) *Statistical Thermodynamics*, Cambridge Univ. Press: London.

44. Vendra, V. K., Wu, L., and Krishnan, S. (2010) Nanostructured Thin films and Surfaces, In *Nanomaterials for the Life Sciences* (Kumar, C. S. S. R., Ed.), pp 1-54, Wiley-VCH, Weinheim.

45. Bard, A. J., Inzelt, G., and Scholz, F. (2012) *Electrochemical Dictionary*, 2nd ed.

46. Butt, H. J., Graf, K., and Kappl, M. (2006) *Physics and Chemistry of Interfaces*, 2nd ed., Wiley-VCH, Federal Republic of Germany.

47. Herne, T. M., and Tarlov, M. J. (1997) Characterization of DNA Probes Immobilized on Gold Surfaces, *J. Am. Chem. Soc. 119*, 8916-8920.

48. Anson, F. C. (1968) Electrochemistry, *Annu. Rev. Phys. Chem. 19*, 83-110.

Chapter 3

Electrochemical Patterning and Detection of DNA Arrays on a Two-Electrode Platform

Adapted from: Furst, A. L., Landefeld, S., Hill, M. G., and Barton, J. K. (2013) Electrochemical Patterning and Detection of DNA Arrays on a Two-Electrode Platform, *J. Am. Chem. Soc. 135*, 19099-19102.

A. Furst synthesized DNA and collected and analyzed all data presented. S. Landefeld and M. G. Hill performed preliminary experiments with the platform.

Introduction

Nucleic acid sensors are critical for the detection of many biological markers of disease. An important diagnostic goal is the development of arrayed, multiplexed sensors, enabling different markers to be tested in parallel with high accuracy. Although fluorescence-based arrays have proven useful for high-throughput screening applications,[1, 2] they generally do not provide the accessibility, ease of use, and unambiguous readout required for clinical diagnostics.

DNA-based electrochemistry offers a promising alternative technology.[3-6] In particular, assays that capitalize on DNA-mediated charge transport (DNA CT) enable selective detection of protein binding events, hybridization, and mismatches and lesions, with near on/off specificity.[7-18] This level of specificity is possible largely because DNA CT-based assays do not rely on the subtle thermodynamic differences of duplex hybridization for the determination of mismatches or lesions, thus eliminating the need for stringent hybridization conditions required for many other DNA-based technologies.[19-21] Instead, DNA CT-based assays depend on the integrity of the π-stack of the nucleobases; disruption of the π-stacking by protein binding or mismatch incorporation attenuates DNA CT.

DNA-modified electrodes are generally prepared by the self-assembly of thiol-labeled duplexes onto gold, followed by passivation of the uncovered electrode surface with an alkylthiol.[22] This method of assembly offers little control over the density and dispersion of the DNA within the film.[23-26] Alternative assembly methods based on the preliminary formation of a mixed alkylthiol monolayer containing active head groups, followed by coupling of the DNA to this monolayer, offer a promising alternative

assembly method that provides more control over the final composition of the DNA monolayer.[27]

Independent of assembly conditions, electrochemical DNA sensors typically rely on electrochemical readout from the surface onto which the monolayers are assembled, providing a measurement of only bulk changes that occur over the entire electrode. Steps toward more complex detection with DNA-modified electrodes have been made through multiplexing, which enables multiple experimental conditions to be run simultaneously with redundancy.[28-30] Yet even these platforms measure average changes over an entire electrode surface. Moreover, comparing individual, isolated electrodes can be misleading, as small variations between monolayer conformations can lead to substantial differences in the electrochemical properties of the resulting DNA monolayer.

A two-electrode detection system enables the determination of more specific spatial information on a single substrate electrode surface. The most widely used two-electrode technique is scanning electrochemical microscopy (SECM).[31-34] This technique has previously been used to detect oligonucleotide hybridization events on DNA-modified surfaces.[35-37] We have previously shown that SECM of high-density DNA-modified electrodes allows for the identification of small imperfections on a surface that can lead to falsely high electrochemical signals when the bulk electrochemical response is measured.[15] Here, we report a simplified, macroscopic two-electrode detection system for analysis of DNA arrays composed of multiple DNA sequences assembled on a single substrate electrode surface.

Our arrays are formed through selective electrochemical patterning of multiple DNA sequences onto a single electrode surface containing a pre-formed mixed

monolayer. Electrochemical readout is then accomplished via amperometric detection at a spatially isolated probe electrode controlled by a bipotentiostat. Because multiple DNA sequences are patterned onto a single substrate, different sequences can be examined under identical experimental conditions. With our assay, we now have the ability to incorporate both redundancy and internal controls onto the same electrode surface.

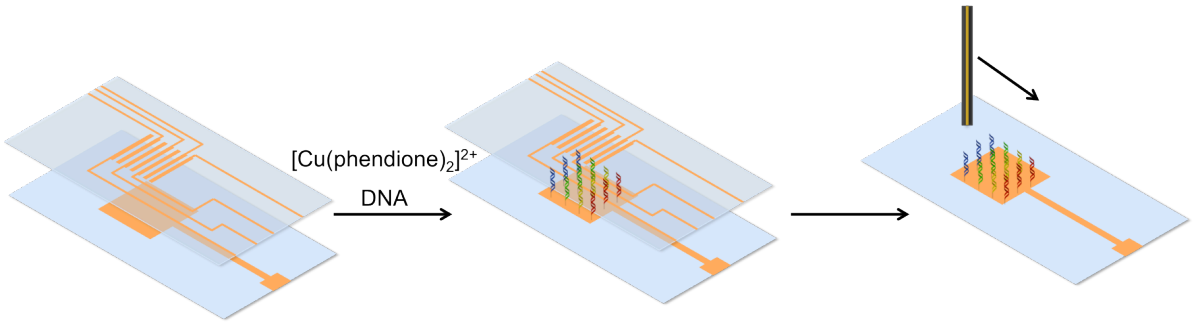

Figure 3.1 Two working electrode patterning and readout platform. DNA arrays are formed electrochemically through the activation of an inert copper complex to an active catalyst from a secondary set of electrodes. Using the current configuration, up to four individual sequences of DNA are patterned onto a single substrate electrode. Subsequent readout of the sequences on the surface is accomplished by manual scanning of a microelectrode across the secondary electrode.

Materials and Methods

DNA Synthesis and Purification

Oligonucleotides were synthesized on an Applied Biosystems 3400 DNA synthesizer. Terminal C6 alkyne moieties were incorporated into the 5' end of one of the strands and were purchased from Glen Research. Complementary unmodified strands were also synthesized. Preparation of all of the oligonucleotides followed a reported protocol. Each oligonucleotide was purified by high-performance liquid chromatography (HPLC) using a gradient of acetonitrile and 50 mM ammonium acetate. Following purification, oligonucleotides were desalted by ethanol precipitation and quantified using ultraviolet-visible spectrophotometry based on their extinction coefficients at 260 nm (IDT Oligo Analyzer). The following sequences were prepared: well matched: 5'-CC-$(CH_2)_6$-GCT CAG TAC GAC GTC GA-3' with its unmodified complement, a mismatch-containing sequence with a CA mismatch at the 9th base pair, and a TBP-binding sequence: 5'-CC-$(CH_2)_6$-GGC GTC TAT AAA GCG ATC GCG A-3' with its unmodified complement.

Preparation of Slides

Gold evaporation was accomplished using aluminum masks and a CVC Metal Physical Vapor Deposition system. Glass slides were coated in MPS ([3-mercaptopropyl]-trimethoxysilane). Slides were cleaned by boiling at 70° C for 10 minutes in Piranha solution (1:4 hydrogen peroxide: sulfuric acid), followed by baking for 10 minutes. Slides were then boiled in a 1:1:40 MPS: water: isopropyl alcohol solution for 10 minutes and then cured at 107° C for 8 minutes. A 150 nm gold

monolayer was formed on the slides with either the patterning or the substrate pattern using aluminum masks and a CVC Metal Physical Vapor Deposition system with 0.5 mm diameter gold wire.

DNA Patterning

Degassed $[Cu(phendione)_2]^{2+}$ was used as the inert catalytic precursor because of its aqueous solubility. $[Cu(phendione)_2]^{2+}$ was prepared by combining 1,10-phenanthroline-5,6-dione (Sigma Aldrich) (294.3 mg, 1.4 mmol) with $CuSO_4$ (Sigma Aldrich) (111.7 mg, 700 μmol) in 5 mL of deionized water. ESI-MS: 580.2 (calc: 580.0). The complex was isolated as the PF_6^- salt or used directly *in situ*. Before application to the electrode surface, the complex was diluted to a final concentration of 50 μM in Tris buffer (10 mM Tris, 100 mM KCl, 2.5 mM $MgCl_2$, 1 mM $CaCl_2$, pH 7.6) and thoroughly degassed. When a sufficiently negative potential is applied to this compound, Cu(II) is reduced to Cu(I), generating an active catalyst. A BAS Epsilon bipotentiostat was used both to apply potentials and record data. A constant potential was applied to the patterning electrodes that was sufficiently negative to continuously activate the copper at that location. For the constant applied potential, -250 mV v. AgCl/Ag was used, and application was allowed to proceed for 15 minutes. The 100 μM catalyst (20 μL) with 20 μL of 50 μM DNA in Tris buffer (10 mM Tris, 100 mM KCl, 2.5 mM $MgCl_2$, 1 mM $CaCl_2$, pH 7.6) was used to pattern each strip. Residual catalyst interaction with DNA was a concern, but no change in duplex melting temperatures in the presence of catalyst was observed. Neither protein binding nor hybridization was affected by catalyst.

Scanning Across Surface

The height of the probe electrode (z) was adjusted manually by lowering the electrode onto a 100-um teflon spacer placed on the corner of the substrate pad. No attempt was made to control for drift; while the measured currents were remarkably consistent for each substrate pad, the absolute signals varied somewhat from substrate to substrate. Electrochemical images of substrate surface are presented as scans from left to right. In all cases, the scanning origin is indicated by a distance of 0 on the x-axis, and the distance increases positively in the direction of scanning. Additionally, multiple scans can be obtained at different locations (y) on the substrate pad. Variation in current between different locations on the substrate pad enabled calculation of standard deviation.

TATA Binding Protein Experiments

TATA-Binding Protein (TBP) was purchased from ProteinOne and stored at -80° C until use. MicroBiospin 6 columns (BioRad) were used to exchange the shipping buffer for Tris buffer (10 mM Tris, 100 mM KCl, 2.5 mM $MgCl_2$, 1 mM $CaCl_2$, pH 7.6). Prior to electrochemical measurements with TBP, electrodes were incubated with 1 μM Bovine serum albumin (BSA) for 30 min, followed by rinsing with Tris buffer. TBP was titrated onto the surface in a range of 1 μM to 25 μM protein, with each concentration allowed to incubate for 15 minutes prior to scanning.

Hybridization Experiments

After a preliminary scan of duplex DNA on the electrode surface, dehybridization was induced through the heating of the surface in phosphate buffer (5 mM phosphate, 50 mM NaCl, pH 7.0) to 65°C for fifteen minutes. Subsequently, the surface was rinsed with 65°C phosphate buffer (pH 7.0). The complementary strand (25 μL of 50 μM strand) was then added to the surface and incubated for one hour while the surface cooled to ambient temperature. The surface was subsequently scanned again.

Results

Both substrate and patterning surfaces were prepared from glass microscope slides coated with MPS ([3-mercaptopropyl]-trimethoxysilane) using an established protocol.[38] MPS acts as a molecular adhesive between the glass microscope slide and a gold monolayer, forming an attachment to the glass through silanization and a bond to the gold through a thiol-metal bond. A gold layer (150 nm thick) was then deposited onto the slides in either a series of lines (the patterning surface) or a square (the substrate electrode; Figure 3.2), using aluminum masks and a CVC Metal Physical Vapor Deposition system. Mixed monolayers were formed on the substrate surfaces using an ethanolic solution of 1M 12-azidododecane-1-thiol (C_{12} thiol azide) and 1M 11-mercaptoundecylphosphoric acid, which forms a monolayer capable of passivation against ferricyanide and methylene blue, electrochemical reporters of DNA CT. Alkynyl-labeled DNA was then patterned onto the substrate by sandwiching 0.1 mM $[Cu(phendione)_2]^{2+}$ (phendione=1,10-phenanthroline-5,6-dione) and the DNA solution of choice between the substrate and patterning pads separated by a thin (200 μm) Teflon spacer (unpublished results). Subsequent electrochemical reduction of $[Cu(phendione)_2]^{2+}$ at specific working electrodes on the patterning pad results in the covalent attachment of DNA sequences to specific locations on the substrate pad *via* Cu(I)-catalyzed azide/alkyne coupling. Multiple DNA sequences are patterned on the same substrate electrode through sequential washings of the surface and the addition of an alternate sequence of DNA with copper catalyst between the substrate and patterning pads. The strategy for the spatially resolved electrochemical activation of the catalyst is shown in Figure 3.3. While the substrate electrode was washed after patterning, residual

catalyst interacting with DNA was a concern. However, no change in DNA duplex melting temperatures in the presence of catalyst was observed (data not shown). Moreover, protein binding and hybridization were unaffected by catalyst, indicating that residual copper catalyst is not of great concern.

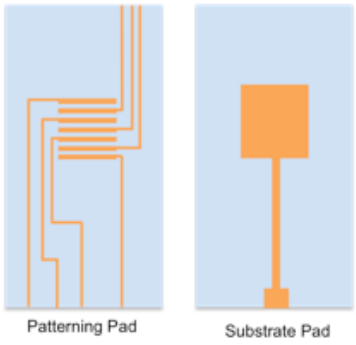

Figure 3.2 Design for patterning electrodes and substrate electrode. The patterning electrodes pad *(left)* contains four working electrodes that are individually-addressable interspersed with three reference electrodes. The substrate electrode pad *(right)* contains a single, large gold pad and a working electrode contact to the pad.

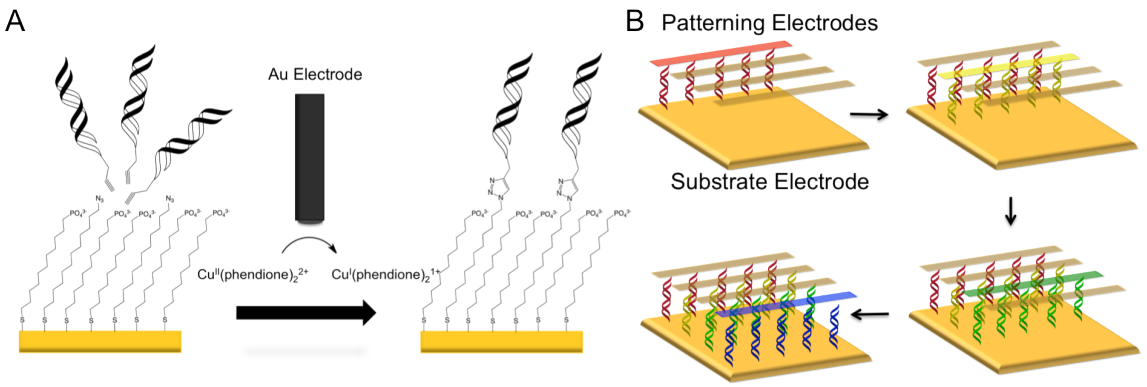

Figure 3.3 Selective activation for specific covalent attachment of DNA to particular locations. (A) An inert Cu(II) catalyst is electrochemically activated to an active Cu(I) species capable of catalyzing the [3+2] azide-alkyne cycloaddition between alkyne-modified DNA and an azide-terminated thiol monolayer. (B) Up to four different sequences of DNA can be patterned onto a single substrate pad through sequential catalyst activations.

Covalent attachment of DNA was confirmed by cyclic voltammetry (CV) at the substrate pad in the presence of 200 μM ferricyanide and 2 μM methylene blue (MB). Cyclic voltammetry at the substrate pad (i.e., from the bottom of the electrode surface) reveals a large, irreversible reduction peak at ~ -0.4 V, characteristic of DNA-mediated electrocatalysis of ferricyanide by methylene blue (Figure 3.4).[39] Although this voltammogram confirms that DNA is present on the surface, it provides no information on either the homogeneity of the DNA on the surface or the sequences of DNA present. Indeed, the bulk electrocatalytic signal in Figure 3.4 was obtained from a pad patterned with two strips of well-matched DNA and two strips of DNA containing a mismatch. Thus, while single-electrode measurements can provide some information about changes on a surface, they report only the bulk response averaged over the entire electrode, giving no information about the types of DNA on the surface, and providing no spatial resolution.

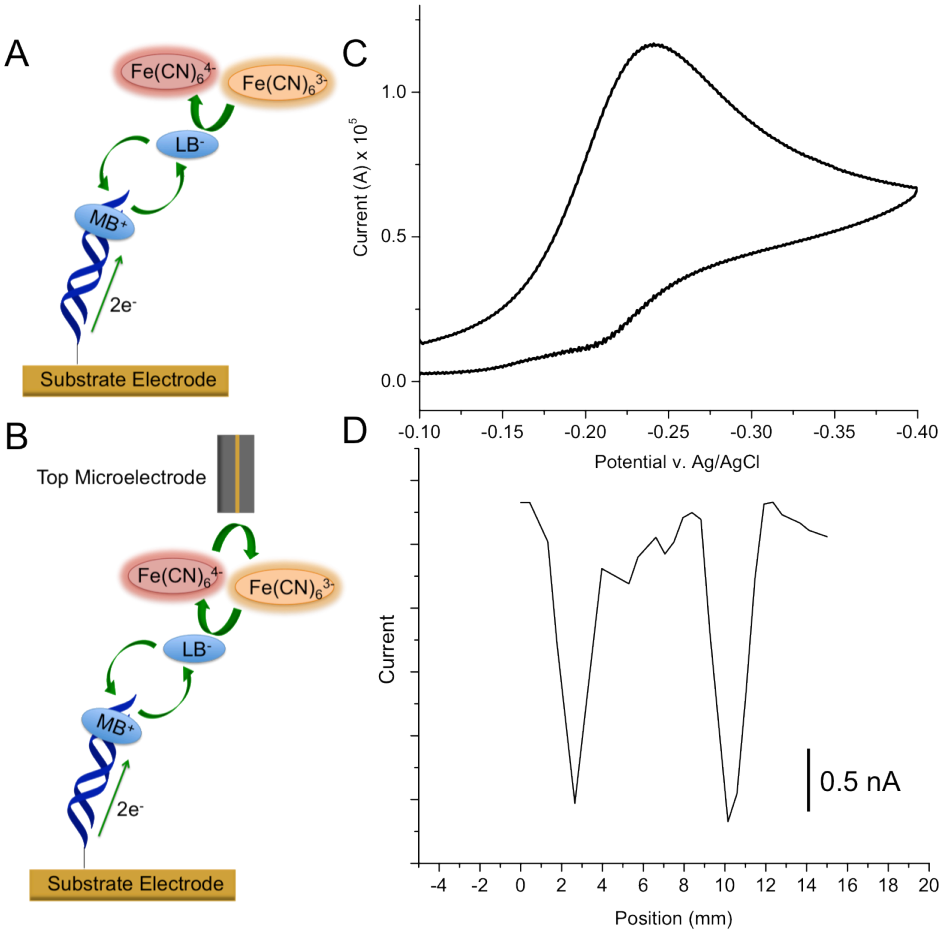

Figure 3.4 Comparison between bulk and spatially-defined electrochemical measurements. (A) One-electrode electrocatalysis. For well-paired DNA, methylene blue (MB) is reduced to leucomethylene blue (LB) through the DNA by the substrate electrode. LB can be reoxidized in solution to MB by ferricyanide, which is thereby reduced to ferrocyanide. (B) Two-electrode electrocatalysis. The second electrode functions both as a detector and a method of reoxidation of ferrocyanide to ferricyanide, thereby accelerating the electrocatalytic process described in (A). (C) Electrochemical data from a patterning pad containing two strips of well-matched DNA and two strips of DNA containing a single base mismatch. Electrochemical signals were obtained from electrocatalysis of 2 μM methylene blue and 200 μM ferricyanide in Tris buffer (10 mM Tris, 100 mM KCl, 2.5 mM $MgCl_2$, 1 mM $CaCl_2$, pH 7.6). The bulk electrochemical signal from the measurement of the substrate pad shows a classic electrocatalytic peak, indicating the presence of well-matched DNA on the electrode. (D) Electrochemical data from the two-electrode detection method. With this technique, the existence of two different sequences of DNA, one completely matched and one containing a mismatch, becomes apparent. The surface was scanned at ~0.6 mm/sec with a 100 μm gold microelectrode.

A 100-μm gold electrode positioned above the substrate electrode by a simple x,y,z-stage was subsequently employed as a secondary electrode to create a two-electrode detection system with spatial resolution for readout. DNA-mediated reduction of ferricyanide (via methylene blue electrocatalysis) results in the presence of ferrocyanide immediately above areas on the substrate electrode coated with intact DNA duplexes, and this ferrocyanide is readily detected at the probe (Figure 3.4). Thus measuring ferrocyanide oxidation at the microelectrode tip allows for spatial differentiation between the passivating layer and regions containing DNA on the substrate electrode. Notably, this method provides reproducible current outputs for multiple strips of a single DNA sequence (Figure 3.5), demonstrating a high level of reproducibility; the standard deviation for peak currents of DNA of the same sequence is 95 pA, or 1.5%. It should be noted that the full width half max of the DNA peaks is ~1 mm, the same width of the patterning electrodes, indicating minimal diffusive spreading of the catalyst upon activation. It should be noted that the width of the peaks depends on the speed of scanning, which was optimal at ~0.6 mm/sec. Some inconsistencies are observed because the scanning was performed manually. The dramatic attenuation of catalytic turnover at substrate locations featuring a single-base mismatch within the immobilized DNA is characteristic of a DNA-mediated process (Figure 3.4).

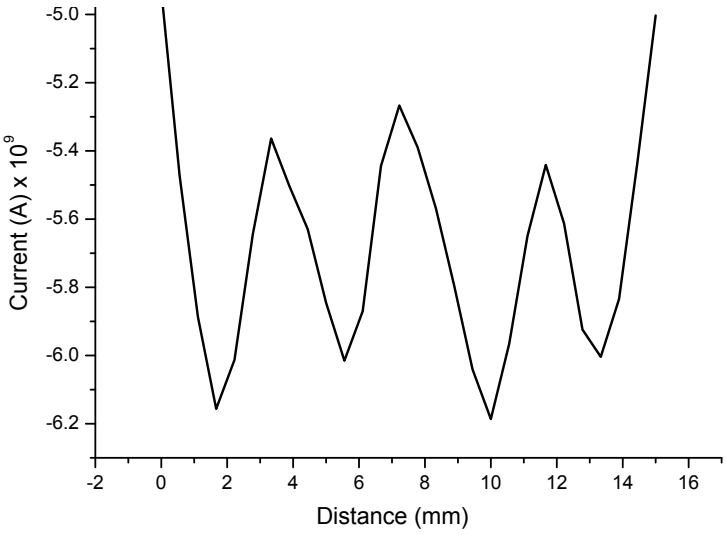

Figure 3.5 Patterning of a pad containing four strips of well-matched DNA. This was measured in 2 uM methylene blue and 200 uM ferricyanide in Tris buffer (10 mM Tris, 100 mM KCl, 2.5 mM $MgCl_2$, 1 mM $CaCl_2$, pH 7.6). As can be seen, the size and shape of the signals resulting the patterning of the same sequence four times is exceptionally consistent.

As the ultimate goal of this DNA-array technology is to detect biomolecules (e.g., proteins and nucleic acids), sensitive detection of proteins is essential. Protein binding was tested on this platform using TATA-binding protein (TBP), a subunit of the eukaryotic TFIID transcription factor, which kinks DNA by over 80° when bound to its TATA target sequence.[40] The K_D of this protein is in the nanomolar range (~3.3 nM), and detection limits near this concentration are ideal for TBP detection from biological samples. We have shown previously that TBP binding to duplexes containing a TATA sequence leads to attenuated CT, but does not affect electrocatalysis at duplexes lacking the TBP binding site.[15] Therefore, to test for selective TBP binding, we patterned strips of both TBP-binding sequences and non-binding sequences. Upon addition of 15 nM TBP to a substrate electrode patterned with two strips of well-matched DNA and two strips of TBP DNA, an almost complete loss of electrochemical signal occurs only at the location of the TBP sequences (Figure 3.6).

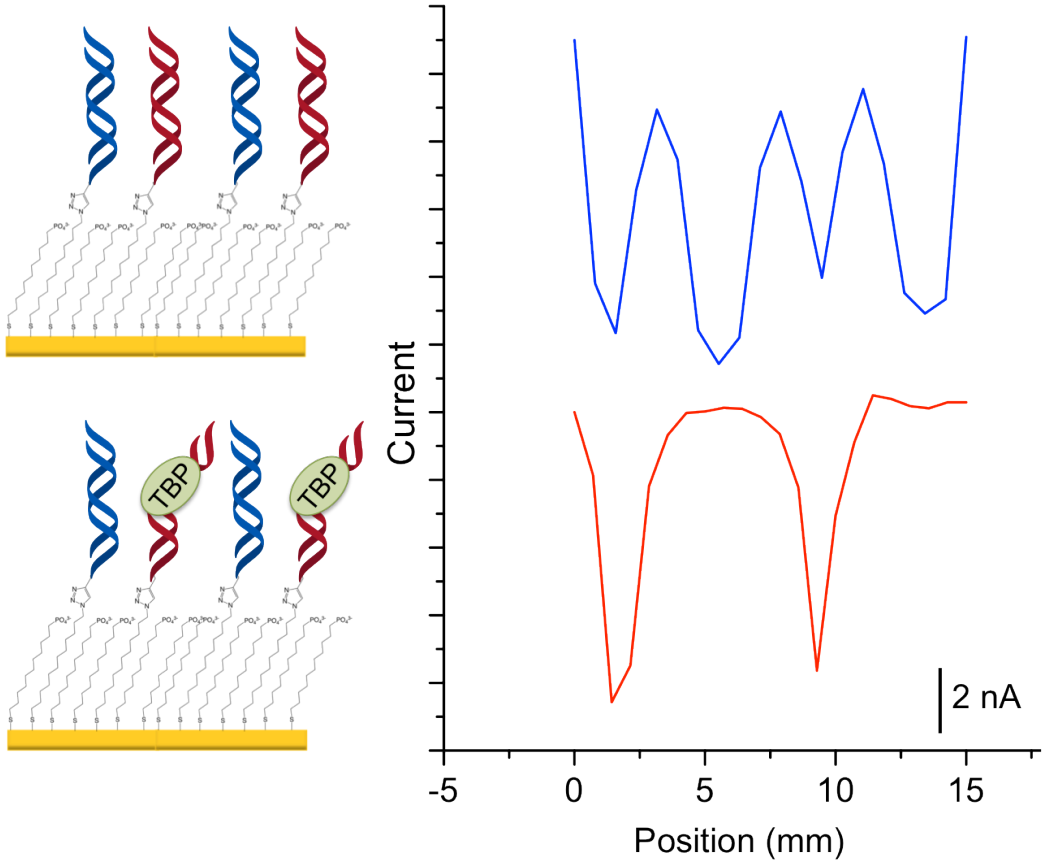

Figure 3.6 TBP detection on a patterned surface. Current increases negatively down the y-axis. The surface was patterned with two strips of well-matched DNA and two strips that contain a TBP binding site. The blue trace is a preliminary scan in 2 μM methylene blue and 200 μM ferricyanide before the addition of TBP but after a 30 minute incubation in 100 μM BSA to control for non-specific protein binding. The red trace is a scan after a 15-minute incubation with 15 nM TBP protein; the current corresponding to the TBP-binding sequences is reduced, while the locations corresponding to the well-matched sequence are unaffected.

This same detection strategy can also be employed to detect selective DNA hybridization. Two strips of well-matched DNA and two strips of DNA containing a CA mismatch were patterned onto an electrode surface. Electrochemically imaging the substrate from the top of the monolayer using the microelectrode via MB-catalyzed ferricyanide reduction yields the expected pattern of alternating high and low currents at the probe tip (Figure 3.7). The electrode was then dehybridized by heating the substrate pad in 65°C buffer for 15 minutes. A strand of DNA fully complementary to the alkynyl strand that was part of the original mismatch-containing duplex was subsequently incubated on the surface for 1 hour, resulting in the formerly mismatched sequences being well-matched and vice-versa. Rescanning the substrate electrode revealed almost complete reversal of signal locations, indicating that the majority of the DNA helices on the surface were dehybridized and rehybridized to an alternate complement (Figure 3.7). The ability to detect both protein-binding and hybridization events on the same platform highlights the utility of this DNA array for broad applications.

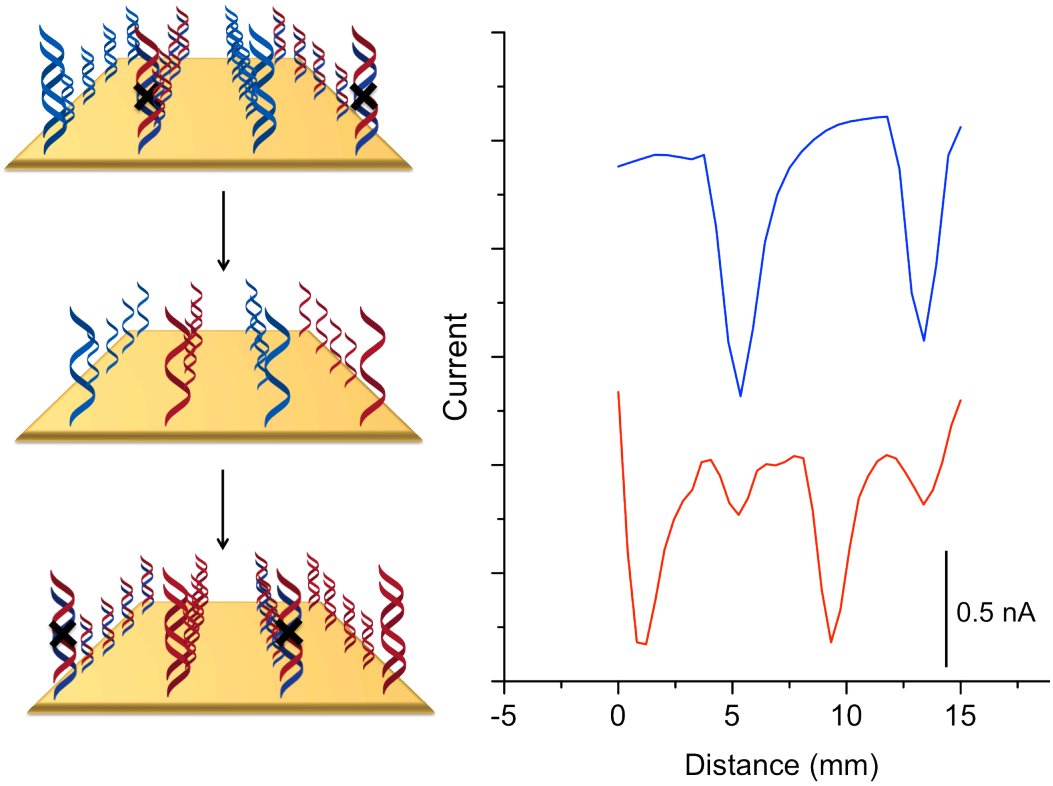

Figure 3.7 Oligonucleotide detection through dehybridization and hybridization. Current increases negatively down the y-axis. The surface was patterned with two strips of well-matched DNA and two strips that contain a mismatch. The blue trace is a preliminary scan in 2 μM methylene blue and 200 μM ferricyanide before dehybridization. The surface was subsequently soaked in phosphate buffer (5 mM phosphate, 50 mM NaCl, pH 7.0) at 65° C for 30 minutes. Single stranded oligonucleotides complementary to the formerly mismatched sequence heated to 65° C were added and allowed to cool to room temperature over 1 hour. The red trace shows the post-rehybridization data, where the mismatched sequences are now well-matched and the formerly well-matched now mismatched.

Discussion

Incorporating low-density DNA monolayers into a two-electrode platform enables sensitive detection of protein binding to DNA, as well as hybridization events, with spatial resolution on a surface. Multiple DNA probe sequences can be accurately grafted onto a single, azide-terminated substrate using readily available alkyne-labeled duplexes and a copper complex that is electrochemically activated to initiate click coupling. Exploiting DNA CT, electrochemical readout is inherently more sensitive and selective compared to assays that rely on electrostatic interactions of probe molecules to the phosphate backbone. Our platform effectively differentiates between fully complementary duplexes versus those that contain single-base mismatches, making it ideally suited for assays based on hybridization events. Using DNA CT, hybridization events are distinguished not based on minor thermodynamic differences of annealing but instead on the existence of a fully formed, entirely complementary duplex.

The ability to graft multiple DNA sequences onto a single substrate enables both incorporation of internal controls and a greatly simplified and standardized experimental platform. Unlike conventional multiplexed systems, our array requires no separate wells on the surface. This translates to the addition of a single sample of interest over the entire array simultaneously, ensuring identical experimental conditions for detection and reducing the necessary sample volume. Moreover, the single substrate electrode enables significantly more control over the incorporation of internal standards and makes comparisons between types of DNA on the array possible. This single-substrate platform also guarantees identical underlying monolayer conformations over the entire surface, leading to comparable DNA monolayers at different patterning sites.

The inherent advantages of DNA CT-based electrochemical readout coupled to a two-electrode fabrication/detection platform have resulted in the successful detection of well-matched and mismatched DNA on the same substrate electrode, as well as the selective binding of a DNA transcription factor. Oligonucleotide detection is easily accomplished with specificity, as illustrated through the switching of the location of mismatched strands on the substrate surface. This represents a completely new, sensitive biosensing platform, taking advantage of a two-electrode setup for both array formation and detection.

References

1. Chee, M., Yang, R., Hubbell, E., Berno, A., Huang, X. C., Stern, D., Winkler, J., Lockhart, D. J., Morris, M. S., and Fodor, S. P. (1996) Accessing genetic information with high-density DNA arrays, *Science 274*, 610-614.

2. Lockhart, D. J., and Winzeler, E. A. (2000) Genomics, gene expression and DNA arrays, *Nature 405*, 827-836.

3. Millan, K. M., and Mikkelsen, S. R. (1993) Sequence-selective biosensor for DNA based on electroactive hybridization indicators, *Anal. Chem. 65*, 2317-2323.

4. Abi, A., and Ferapontova, E. E. (2013) Electroanalysis of single-nucleotide polymorphism by hairpin DNA architectures, *Anal. and Bioanal. Chem. 405*, 3693-3703.

5. Ricci, F., Lai, R. Y., and Plaxco, K. W. (2007) Linear, redox modified DNA probes as electrochemical DNA sensors, *Chem. Commun.* 3768-3770.

6. Cederquist, K. B., and Kelley, S. O. (2012) Nanostructured biomolecular detectors: pushing performance at the nanoscale, *Curr. Opin. Chem. Biol. 16*, 415-421.

7. Boon, E. M., Ceres, D. M., Drummond, T. G., Hill, M. G., and Barton, J. K. (2000) Mutation detection by electrocatalysis at DNA-modified electrodes, *Nat. Biotechnol. 18*, 1096-1100.

8. Drummond, T. G., Hill, M. G., and Barton, J. K. (2003) Electrochemical DNA sensors, *Nat. Biotechnol. 21*, 1192-1199.

9. Kelley, S. O., Boon, E. M., Barton, J. K., Jackson, N. M., and Hill, M. G. (1999) Single-base mismatch detection based on charge transduction through DNA, *Nucleic Acids Res. 27*, 4830-4837.

10. Boal, A. K., and Barton, J. K. (2005) Electrochemical detection of lesions in DNA, *Bioconjug. Chem. 16*, 312-321.

11. Gorodetsky, A. A., Ebrahim, A., and Barton, J. K. (2008) Electrical detection of TATA binding protein at DNA-modified microelectrodes, *J. Am. Chem. Soc. 130*, 2924-2925.

12. Gorodetsky, A. A., Hammond, W. J., Hill, M. G., Slowinski, K., and Barton, J. K. (2008) Scanning electrochemical microscopy of DNA monolayers modified with Nile Blue, *Langmuir 24*, 14282-14288.

13. Gorodetsky, A. A., Buzzeo, M. C., and Barton, J. K. (2008) DNA-mediated electrochemistry, *Bioconjug. Chem. 19*, 2285-2296.

14. Boon, E. M., Salas, J. E., and Barton, J. K. (2002) An electrical probe of protein-DNA interactions on DNA-modified surfaces, *Nat. Biotechnol. 20*, 282-286.

15. DeRosa, M. C., Sancar, A., and Barton, J. K. (2005) Electrically monitoring DNA repair by photolyase, *Proc. Natl. Acad. Sci. USA 102*, 10788-10792.

16. Guo, X., Gorodetsky, A. A., Hone, J., Barton, J. K., and Nuckolls, C. (2008) Conductivity of a single DNA duplex bridging a carbon nanotube gap, *Nat. Nanotechnol. 3*, 163-167.

17. Pheeney, C. G., Guerra, L. F., and Barton, J. K. (2012) DNA sensing by electrocatalysis with hemoglobin, *Proc. Natl. Acad. Sci. USA 109*, 11528-11533.

18. Wang, H., Muren, N. B., Ordinario, D., Gorodetsky, A. A., Barton, J. K., and Nuckolls, C. (2012) Transducing methyltransferase activity into electrical signals in a carbon nanotube-DNA device, *Chem. Sci. 3*, 62-65.

19. Caruso, F., Rodda, E., Furlong, D. N., Niikura, K., and Okahata, Y. (1997) Quartz crystal microbalance study of DNA immobilization and hybridization for nucleic Acid sensor development, *Anal. Chem. 69*, 2043-2049.

20. Cheng, A. K., Sen, D., and Yu, H. Z. (2009) Design and testing of aptamer-based electrochemical biosensors for proteins and small molecules, *Bioelectrochemistry 77*, 1-12.

21. Schena, M., Shalon, D., Davis, R. W., and Brown, P. O. (1995) Quantitative monitoring of gene expression patterns with a complementary DNA microarray, *Science 270*, 467-470.

22. Kelley, S. O., Barton, J. K., Jackson, N. M., and Hill, M. G. (1997) Electrochemistry of methylene blue bound to a DNA-modified electrode, *Bioconjug. Chem. 8*, 31-37.

23. Chrisey, L. A., Lee, G. U., and O'Ferrall, C. E. (1996) Covalent attachment of synthetic DNA to self-assembled monolayer films, *Nucleic Acids Res. 24*, 3031-3039.

24. Levicky, R., Herne, T. M., Tarlov, M. J., and Satija, S. K. (1998) Using Self-Assembly To Control the Structure of DNA Monolayers on Gold: A Neutron Reflectivity Study, *J. Am. Chem. Soc. 120*, 9787-9792.

25. Murphy, J. N., Cheng, A. K., Yu, H. Z., and Bizzotto, D. (2009) On the nature of DNA self-assembled monolayers on Au: measuring surface heterogeneity with electrochemical in situ fluorescence microscopy, *J. Am. Chem. Soc. 131*, 4042-4050.

26. Yu, H. Z., Luo, C. Y., Sankar, C. G., and Sen, D. (2003) Voltammetric procedure for examining DNA-modified surfaces: quantitation, cationic binding activity, and electron-transfer kinetics, *Anal. Chem. 75*, 3902-3907.

27. Devaraj, N. K., Miller, G. P., Ebina, W., Kakaradov, B., Collman, J. P., Kool, E. T., and Chidsey, C. E. (2005) Chemoselective covalent coupling of oligonucleotide probes to self-assembled monolayers, *J. Am. Chem. Soc. 127*, 8600-8601.

28. Kang, D., White, R. J., Xia, F., Zuo, X., Vallee-Belisle, A., and Plaxco, K. W. (2012) DNA biomolecular-electronic encoder and decoder devices constructed by multiplex biosensors, *NPG Asia Mater. 4*, e1.

29. Lam, B., Das, J., Holmes, R. D., Live, L., Sage, A., Sargent, E. H., and Kelley, S. O. (2013) Solution-based circuits enable rapid and multiplexed pathogen detection, *Nat. Commun. 4*, 2001.

30. Slinker, J. D., Muren, N. B., Gorodetsky, A. A., and Barton, J. K. (2010) Multiplexed DNA-modified electrodes, *J. Am. Chem. Soc. 132*, 2769-2774.

31. Bard, A. J., Denuault, G., Friesner, R. A., Dornblaser, B. C., and Tuckerman, L. S. (1991) Scanning electrochemical microscopy: theory and application of the transient (chronoamperometric) SECM response, *Anal. Chem. 63*, 1282-1288.

32. Bard, A. J., Fan, F. R. F., Kwak, J., and Lev, O. (1989) Scanning electrochemical microscopy. Introduction and principles, *Anal. Chem. 61*, 132-138.

33. Wittstock, G. (2003) Imaging Localized Reactivities of Surfaces by Scanning Electrochemical Microscopy, In *Solid-Liquid Interfaces* (Wandelt, K., and Thurgate, S., Eds.), pp 335-364, Springer Berlin Heidelberg.

34. Zoski, C. G., Luman, C. R., Fernandez, J. L., and Bard, A. J. (2007) Scanning electrochemical microscopy. 57. SECM tip voltammetry at different substrate potentials under quasi-steady-state and steady-state conditions, *Anal. Chem. 79*, 4957-4966.

35. Leasen, S., Sritunyalucksana-Dangtip, K., Hodak, J., Srisala, J., Kulsing, C., and Veerasia, W. (2012) Using Electrochemical Impedance Spectroscopy of Methylene Blue and Ferricyanide for DNA Sensing Surface Characterization, In *Chemistry for Sustainable Development* (Gupta Bhowon, M., Jhaumeer-Laulloo, S., Li Kam Wah, H., and Ramasami, P., Eds.), pp 249-264, Springer Netherlands.

36. Turcu, F., Schulte, A., Hartwich, G., and Schuhmann, W. (2004) Label-free electrochemical recognition of DNA hybridization by means of modulation of the feedback current in SECM, *Angew. Chem. Int. Ed. 43*, 3482-3485.

37. Yamashita, K., Takagi, M., Uchida, K., Kondo, H., and Shigeori, T. (2001) Visualization of DNA microarrays by scanning electrochemical microscopy (SECM), *Analyst 126*, 1210-1211.

38. Goss, C. A., Charych, D. H., and Majda, M. (1991) Application of (3-mercaptopropyl)trimethoxysilane as a molecular adhesive in the fabrication of vapor-deposited gold electrodes on glass substrates, *Anal. Chem. 63*, 85-88.

39. Chaubey, A., and Malhotra, B. D. (2002) Mediated biosensors, *Biosens. Bioelectron. 17*, 441-456.

40. Nikolov, D. B., Hu, S. H., Lin, J., Gasch, A., Hoffmann, A., Horikoshi, M., Chua, N. H., Roeder, R. G., and Burley, S. K. (1992) Crystal structure of TFIID TATA-box binding protein, *Nature 360*, 40-46.

Chapter 4

Label-Free Electrochemical Detection of Human Methyltransferase from Tumors

Adapted from: Furst, A. L., Muren, N. B., Hill, M. G., and Barton, J. K. (2014) Label-Free Electrochemical Detection of Human Methyltransferase from Tumors, *Proc. Natl. Acad. Sci. USA 111*, 14985-14989.

A. L. Furst prepared all samples and collected and analyzed all data. N. B. Muren developed the electrochemical assay, tritium labeling assay, and cell lysis protocol.

Introduction

Epigenetic modifications, including DNA methylation, govern gene expression. Aberrant methylation by DNA methyltransferases can lead to tumorigenesis, so that efficient detection of methyltransferase activity provides an early cancer diagnostic. Current methods, requiring fluorescence or radioactivity, are cumbersome; electrochemical platforms, in contrast, offer high portability, sensitivity, and ease of use. We have developed a label-free electrochemical platform to detect the activity of the most abundant human methyltransferase, DNMT1, and have applied this method in detecting DNMT1 in crude lysates from both cultured human colorectal cancer cells (HCT116) and colorectal tissue samples.

DNA methylation powerfully influences gene expression in cells.[1, 2] DNA methyltransferases are responsible for maintaining a genomic pattern of methyl groups, which are covalently added to cytosine at predominantly 5′-CG-3′ sites. Although essential for many cellular processes, aberrant methylation is associated with cancer. In particular, abnormal activity of DNA methyltransferases can lead to hypermethylation, which can silence tumor suppressor genes and promote cancerous transformations.[3-6] The most abundant mammalian methyltransferase and an important diagnostic target is DNMT1, which preferentially methylates hemimethylated DNA using the cofactor *S*-adenosyl-L-methionine (SAM).[7-10] Current measurements of DNMT1 activity require [methyl-^{3}H]-SAM to observe radioactive labeling of DNA,[8, 11] or expensive fluorescence or colorimetric reagents with antibodies that require large instrumentation,[12, 13] both of which are significant obstacles that impede more widespread assessment of DNMT1 activity.

Traditionally, electrochemistry has been used to overcome such limitations for biomolecule detection, as electrochemical methods are low cost, portable, and require only modest instrumentation.[14, 15] However, electrochemical detection schemes have typically been restricted to measurements of highly purified samples because of the increased congestion and decreased accessibility of surface (vs. solution) platforms. Electrochemistry has been used to detect nucleic acids with high sensitivity and without the need for PCR amplification in bacterial lysate and serum,[16-20] but protein detection remains a challenge.[2, 21-23] In fact, although protein detection from simple serum has been accomplished,[24, 25] to date, no reported electrochemical systems have effectively detected active protein of any kind from crude cell lysate.

We have recently developed a unique electrochemical detection architecture aimed at overcoming the challenges associated with protein detection from complex biological samples. This multiplexed detection system involves a substrate plate consisting of a 15-electrode array and a complementary patterning and detection plate also containing a 15-electrode array, which combines low-density DNA monolayer patterning with the electrocatalytically amplified measurement of DNA charge transport (DNA CT) chemistry at a secondary electrode.[26] The low-density DNA monolayer enables protein access to the DNA even in highly congested lysate samples, while electrocatalytic signal amplification markedly increases sensitivity. We utilize measurements of DNA CT through the DNA helices in the monolayer because of the high sensitivity of this chemistry to perturbations in base stacking caused by mismatches, lesions, and protein binding.[27, 28] Methylene blue, a freely diffusing redox-active probe that is activated by DNA CT, interacts with the DNA stack and thereby reports on the

integrity of DNA CT through the monolayer. We use direct detection from the secondary electrode of the turnover of the electrocatalytic partner to methylene blue, ferricyanide, as a measurement of the amount of DNA charge transport occurring on the substrate electrode.

Here, for the first time, we demonstrate the effectiveness of this platform for the detection of human DNMT1 activity from crude lysates of colorectal tumor biopsies, utilizing a methylation-sensitive restriction enzyme to convert the methylation state of the DNA into an electrochemical signal. This strategy enables the detection of a methyl group, even though methylation itself does not significantly affect DNA CT (Figure 4.1).[29, 30] Electrodes patterned with DNA containing the preferred DNMT1 methylation site (a hemimethylated 5′-CG-3′ site) are first treated with the lysate sample. Electrodes are then treated with a restriction enzyme that is sensitive to methylation at this site. If the DNA is fully methylated by active DNMT1 in the lysate sample, the restriction enzyme does not cut the DNA, and there is an electrochemical signal owing to amplified DNA CT. If, in contrast, the DNA is not methylated by active DNMT1 in the lysate sample, the DNA remains hemimethylated (or unmethylated if this non-preferred substrate is used); the restriction enzyme can then cleave the DNA, significantly decreasing the amount of DNA on the surface, and thus diminishing the electrochemical signal generated from DNA CT. As our electrochemical platform uses electrocatalytic signal amplification involving a freely diffusing electrocatalyst (methylene blue), in contrast to earlier work,[29] the need for redox-labeled DNA is eliminated.

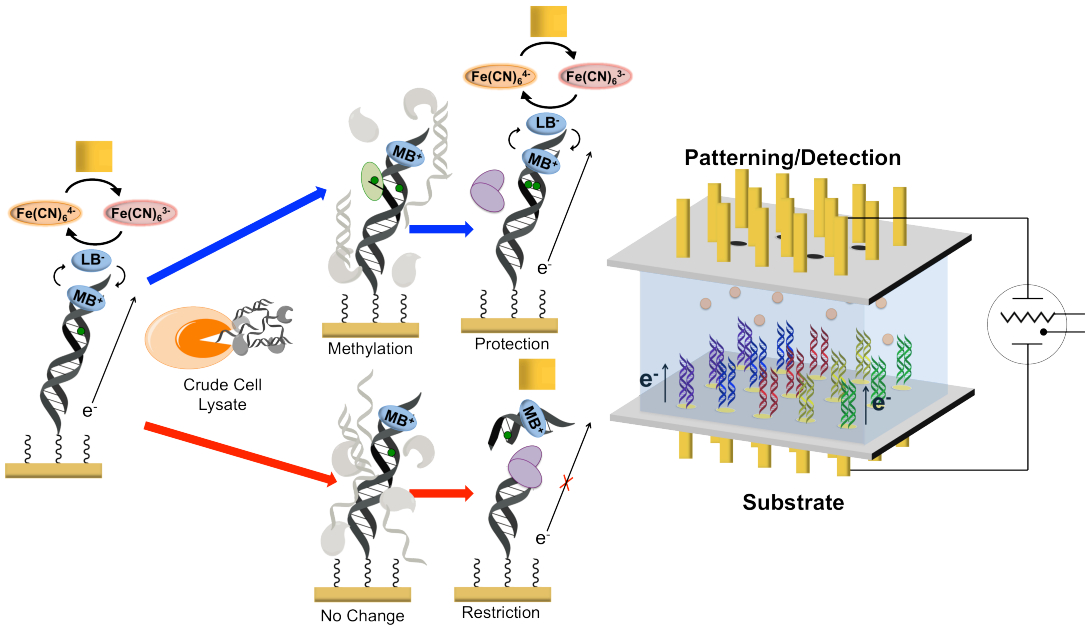

Figure 4.1 Electrochemical platform and scheme for the detection of human methyltransferase activity from crude cell lysates. *Left*: Overview of electrochemical detection scheme. Methyltransferase (green) is added to a surface either in its purified form or as a component of crude lysate, as shown on the left; a multitude of undesired biomolecules are added in the crude lysate mixture along with the methyltransferase of interest. The hemimethylated DNA on the electrode is either methylated (green dot) by the protein to a fully methylated duplex (blue arrows) or is not methylated (red arrows). A methylation-specific restriction enzyme, *BssH*II (purple), is then added. If the DNA is fully methylated, the electrochemical signal remains protected. However, if the DNA remains hemimethylated, it is cut by the restriction enzyme, and the signal is diminished significantly. *Right:* Electrochemical detection platform containing 15 electrodes (1 mm diameter each) in a 5x3 array. DNA is added to the substrate electrode by an electrochemically-activated click reaction initiated by the patterning electrode. Electrocatalytic detection is performed from the secondary (patterning) electrode.

Using this electrochemical platform and assay, we demonstrate the efficient detection of DNMT1 activity in crude lysates from both cultured human colorectal cancer cells (HCT116) and colorectal tissue samples. Femtomoles of DNMT1 in cellular samples are rapidly detected without the use of antibodies, fluorescence, or radioactive labels. Moreover, we distinguish colorectal tumor tissue from healthy adjacent tissue through differences in DNMT1 activity, illustrating the effectiveness of this two-electrode platform for clinical applications.

Materials and Methods

DNA Synthesis and Purification

Oligonucleotides were either synthesized on an Applied Biosystems 3400 DNA synthesizer or purchased from IDT. The terminal C6 alkyne moiety that was incorporated into the 5′ end of one of the strands was purchased from Glen Research. Complementary unmodified strands were purchased from IDT. DNA was deprotected and cleaved from solid support with ammonium hydroxide (60° C for 12 h). Following a preliminary round of HPLC, oligonucleotides were treated with 80% acetic acid in water for 20 minutes. Each oligonucleotide was purified by high-performance liquid chromatography (HPLC) using a gradient of acetonitrile and 50 mM ammonium acetate. Following purification, oligonucleotides were desalted by ethanol precipitation and quantified by ultraviolet-visible spectrophotometry based on their extinction coefficients at 260 nm (IDT Oligo Analyzer). Oligonucleotide masses were verified by matrix-assisted laser desorption (MALDI) mass spectrometry. DNA duplexes were formed by thermally annealing equimolar amounts of single-stranded oligonucleotides in deoxygenated phosphate buffer (5 mM phosphate, 50 mM NaCl, pH 7.0) at 90 °C for 5 minutes followed by slowly cooling to 25 °C.

The following sequences were prepared:

Alkyne: 5′-C_2-$(CH_2)_6$-GA CTG AGT ACT GCG CGC ACT GAT AGC-3′

Complement: 5′-GCT ATC AGT GCG CGC AGT ACT CAG TC-3′

Methylated Complement: 5′-GCT ATC AGT GCG C^mGC AGT ACT CAG TC-3′

The *BssHII* restriction site is shown in red.

Western Blot Analysis of Lysate for DNMT1

DNMT1 expression was confirmed by Western blot. Samples were mixed with Laemmli reagent and betamercaptoethanol and probe sonicated for 10 seconds, followed by heat inactivation at 90 °C for 5 minutes. Samples were loaded onto 4-12% polyacrylamide gels in MOPS buffer and run at 175 mV for 1.5 hours. Gels were subsequently transferred to membranes with a dry transfer procedure for 1.5 h. Membranes were then blocked with 5% milk in TBST at room temperature for 1 hour, followed by overnight incubation with a 1^{o} antibody in milk and 3% BSA (w/v) (1:2000 for DNMT1 (New England Biolabs) and 1:1000 for Lamin A (Santa Cruz Biotechnology)) for either DNMT1 or Lamin A detection. The membranes were then rinsed with TBST buffer. Membranes were incubated with goat anti-rabbit 2^{o} antibody (Abcam Incorporated)(1:7500 in 5% milk in TBST) for 1 hour and then rinsed with TBST, followed by scanning on an Odyssey infrared gel scanner. Resulting Western blots are shown in Figure 4.2.

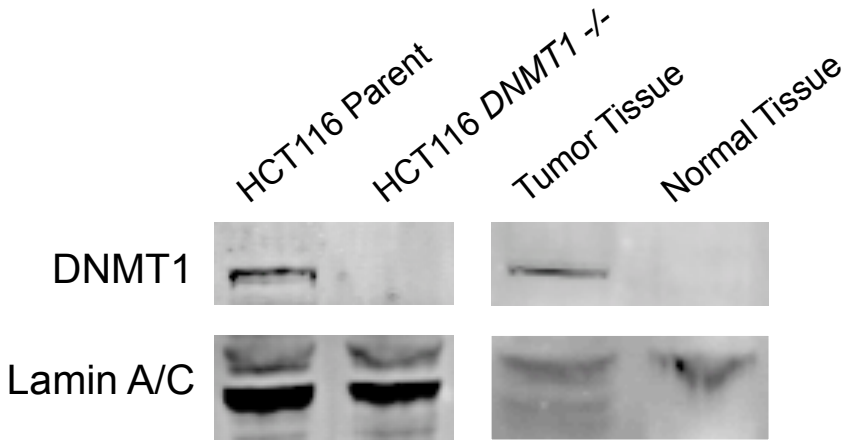

Figure 4.2 Western blot for DNMT1. Shown are gel lanes for HCT116 parent cell lysate, the HCT116 *DNMT1-/-* lysate, the tumor tissue lysate and the adjacent normal tissue lysate. The nuclear protein used as a loading control, Lamin A, is also shown for all samples. DNMT1 is only detectable from the HCT116 parent lysate and the tumor tissue lysate; no DNMT1 is observable in the HCT116 *DNMT1-/-* lysate or the normal tissue lysate.

^{3}H-SAM Methyltransferase Activity Assay

Methyltransferase activity was additionally tested using the conventional method of a ^{3}H-SAM incorporation activity assay. The activity assay followed a published protocol.[8,11] Briefly, 20 μL total reaction volumes were used for the ^{3}H-SAM activity assay. DNA (20 μM), identical to that used as a substrate for the electrochemical assay including the hexynyl terminus, was used. 0.5 μCi ^{3}H-SAM was added, and the reactions were run in DNMT1 activity buffer (50 mM Tris-HCl, 1 mM EDTA, 5% glycerol, pH 7.8). BSA (100 μg/mL) was included for the purified DNMT1 reaction, which was used as a positive standard, along with a negative standard that contained no protein. For the lysate samples, ~2 μL of lysate was included in the reaction mixture, bringing the total protein content for the reaction mixture to 3500 μg/mL. Reactions were incubated at 37° C for 2 h, followed by stopping the reaction with 30 μL of 10% TCA in water. The resulting solutions were spotted onto DE81 filter paper (Whatman) and air-dried for 15 minutes. Filter papers were then individually soaked in 10 mL of 50 mM Na_2HPO_4 for 15 minutes and rinsed with both 50 mM Na_2HPO_4 and 95% ethanol. Filter papers were then heated to 37° C to dry for 15 minutes before liquid scintillation counting. The DNMT1 assay, measured using radioactivity, is shown in Figure 4.3.

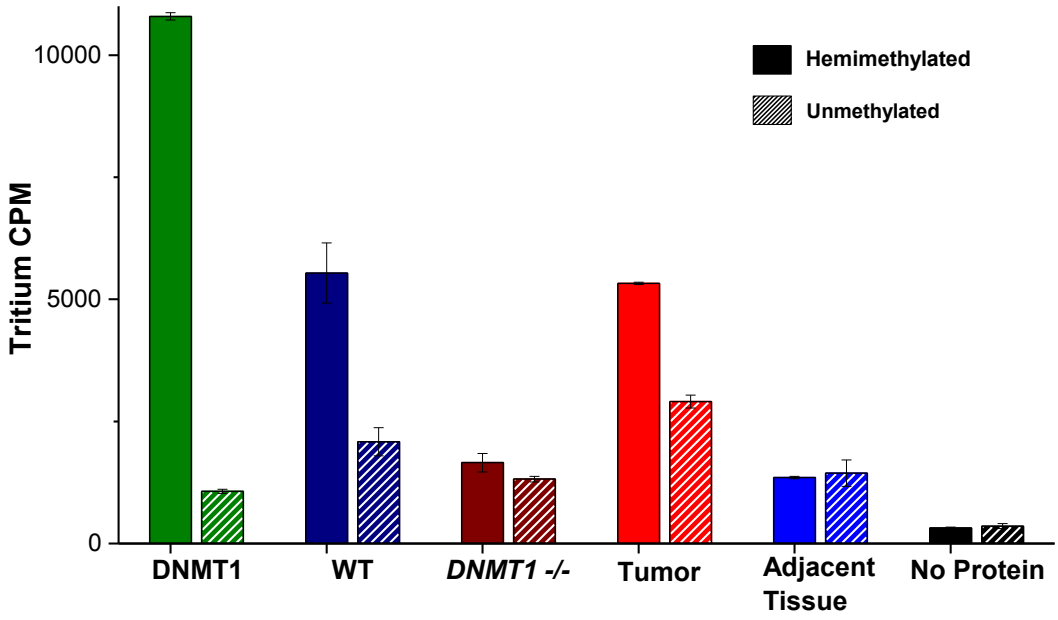

Figure 4.3 ^{3}H-SAM DNMT1 activity assay. The results of a ^{3}H-SAM DNMT1 activity assay are shown, with the counts per minute per sample given. In all cases, the solid bar is data from hemimethylated substrate, and the hashed bar is data from unmethylated substrate. In green is 65 nM DNMT1; in dark blue is parent HCT116 lysate, and in dark red is DNMT1-/- lysate. In red is the tumor lysate, and in blue is lysate from adjacent healthy tissue. In black is the negative control that contains no protein. Error bars represent triplicate scintillation measurements for two replicates of each experimental condition.

DNA Monolayer Formation

The two-electrode array was constructed as previously reported.[26] The multiplexed setup consisted of two complementary arrays containing 15 x 1 mm diameter gold rod electrodes embedded in Teflon. Gold surfaces were polished with 0.03 micron polish before monolayer assembly. Mixed monolayers were formed on one of the plates using an ethanolic solution of 1 M 12-azidododecane-1-thiol (C_{12}thiolazide) and 1 M 11-mercaptoundecylphosphoric acid (Sigma Aldrich). Surfaces were incubated in the thiol solution for 18-24 h, followed by rinsing with ethanol and phosphate buffer (5 mM phosphate, pH 7.0). The water-soluble $[Cu(phendione)_2]^{2+}$ (phendione=1,10-phenanthroline-5,6-dione) was synthesized by mixing two equivalents of phendione with copper sulfate in water. Covalent attachment of DNA to mixed monolayers containing 50% azide head group and 50% phosphate head group through electrochemically-activated click chemistry was accomplished by applying a sufficiently negative potential to the secondary electrode. Specifically, a constant potential of -350 mV was applied to a secondary electrode for 25 minutes, allowing for precise attachment of the appropriate DNA to a primary electrode. 40 μL of 100 μM catalyst and 80 μL of 50 μM DNA in Tris buffer (10 mM Tris, 100 mM KCl, 2.5 mM $MgCl_2$, 1 mM $CaCl_2$, pH 7.6) were added to the platform for covalent attachment.

Cell Culture and Lysate Preparation

HCT116 cells, either parent or *DNMT1*$^{-/-}$(Vogelstein Lab),[9] were grown in McCoy's 5A media containing 10% FBS, 100 units/mL penicillin, and 100 μg/mL

streptomycin in tissue culture flasks (Corning Costar, Acton, MA) at 37° C under a humidified atmosphere containing 5% CO_2.

Approximately 6 million cells were harvested from adherent cell culture by trypsinization, followed by washing with cold PBS and pelleting by centrifugation at 500*g* for 5 minutes. An NE-PER nuclear extraction kit (Pierce from Thermo Scientific) was used for cell lysis, with buffer then exchanged by size exclusion spin column (10 kDa cutoff; Amicon) into DNMT1 activity buffer (50 mM Tris-HCl, 1 mM EDTA, 5% glycerol, pH 7.8). Cell lysate was immediately aliquoted and stored at -80° C until use. A BCA assay (Pierce) was used to quantify the total amount of protein in the lysate. The total protein concentration at which the lysate was frozen was 3,500-5,000 μg/mL.

Tissue samples were obtained from CureLine. Colorectal carcinoma as well as healthy adjacent tissues were obtained. Approximately 150 mg of tissue were homogenized manually, followed by nuclear extraction, buffer exchange, storage, and quantification, as described above. The total protein concentration at which the lysate was frozen was 35,000-50,000 μg/mL.

Electrochemistry

All electrochemistry was performed on a bipotentiostat (BASinc.) with two working electrodes, a platinum wire counter electrode, and an AgCl/Ag reference electrode. Constant potential amperometry was performed for 90 seconds with an applied potential of 320 mV to the secondary electrode and -400 mV to the primary electrode relative to an AgCl/Ag reference electrode with a platinum counter electrode. All scans were performed in Tris buffer (10 mM Tris, 100 mM KCl, 2.5 mM $MgCl_2$, 1

mM $CaCl_2$, pH 7.6) with 4 μM methylene blue and 300 μM potassium ferricyanide. Scans were taken at each of the 15 secondary pin electrodes, and the reported variation in the data represents the standard error across three measurements of three electrodes, all at a given condition.

To incubate electrodes with desired proteins, a 1.5 mm deep Teflon spacer was clipped to the primary electrode surface. Each electrode is isolated in an individual well that holds 4 μL of solution. For methyltransferase activity detection, three electrodes on the device were always incubated with 65 nM DNMT1 with 160 μM SAM and 100 μg/mL BSA as a positive control. For electrodes incubated with lysate, lysate was either directly combined with SAM to a final SAM concentration of 160 μM or the lysate was diluted in DNMT1 activity buffer to the desired total protein concentration and subsequently combined with SAM to a final SAM concentration of 160 μM. For the tissue lysate, 50 μg/mL BSA was also added. Each electrode had the desired solution added to the well and incubated at 37° C for 1.5 h in a humidified container. The primary electrode array was then treated with 1 μM protease solution in phosphate buffer (5 mM phosphate, 50 mM NaCl, pH 7.0) for 1 h. The surface was then thoroughly rinsed with phosphate buffer (5 mM phosphate, 50 mM NaCl, pH 7.0) and scanned. The electrodes were subsequently incubated with the restriction enzyme *BssH*II at a concentration of 1500 units/mL for 1.5 h at 37° C in a humidified container. *BssH*II was exchanged into DNMT1 activity buffer by size exclusion column (10 kDa, Amicon). The electrodes were again rinsed with phosphate buffer and scanned.

Results and Discussion

Electrochemical Platform

Using a 15-pin setup, low-density DNA monolayers were formed on one set of electrode surfaces by DNA patterning from a secondary electrode. DNA substrates were optimized for length to balance on/off signal differential with the ability of proteins to access the binding site. For monolayer formation, thiol monolayers with 50% azide and 50% phosphate head groups first were prepared on the gold pins. We have previously characterized such low-density monolayers, and have found the total DNA coverage to be 20 pmol/cm^2.[31] Subsequently, specific DNA sequences were tethered to individual pins using electrochemically-activated Cu^{1+} click chemistry.[26] The secondary electrode activates the inert copper catalyst precursor only at specific locations on the primary electrode surface. Multiple sequences of DNA with different methylation states in the restriction enzyme binding site (either hemimethylated or unmethylated) were therefore patterned onto particular electrodes (Figure 4.1). The multiplexed array allows five experimental conditions to be run in triplicate, enabling simultaneous detection from healthy tissue and tumor tissue, along with the incorporation of a positive control of pure DNMT1.

Electrochemical measurements were obtained by constant potential amperometry over 90 seconds. Electrodes were measured after treatment with methyltransferase, either in its purified form or as a component of crude lysate, and again after treatment with 1500 units/mL of the restriction enzyme *BssH*II. Lysate was prepared from cultured cells through a simple treatment of cell disruption followed by buffer exchange. Purified DNMT1 was first used to establish the sensitivity and selectivity of this platform (Figure

4.4) and was subsequently included alongside lysate activity measurements as a positive control. The DNA-mediated signal remains fully ‘on’ after restriction when the electrode is preliminarily treated with a minimum of 65 nM DNMT1 protein on a hemimethylated DNA substrate in the presence of the SAM cofactor, although protein is easily detectable at a 15 nM concentration with 48±3% signal protection. For electrodes treated with 65 nM DNMT1 in the absence of additional SAM, only 33±5% signal protection is observed. Similarly, little DNA protection (31±6% signal protection) is observed with the unmethylated substrate. This is explained by the strong preference of DNMT1, as a maintenance methyltransferase, for a hemimethylated substrate.

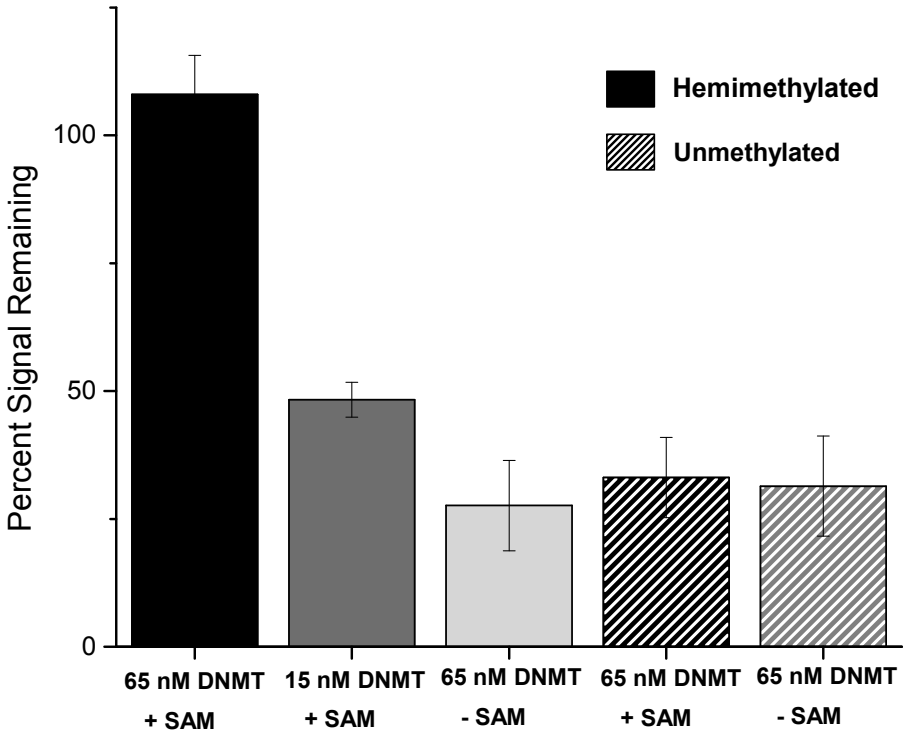

Figure 4.4 Substrate specificity and detection limits for purified DNMT1. The data are reported as the percent signal remaining by comparing the signal after protease treatment and after restriction enzyme treatment. DNMT1 (65 nM) on hemimethylated DNA with 160 μM SAM afforded full protection of the DNA on the surface (black), while electrodes treated with 15 nM DNMT1 on hemimethylated DNA with 160 μM SAM maintained 48±3% signal (dark grey). DNMT1 (65 nM) on hemimethylated DNA without SAM (light grey), on unmethylated substrate with 160 μM SAM (black hashed), or on unmethylated substrate without 160 μM SAM (grey hashed) showed no signal protection. The constant potential amperometry was performed for 90 seconds with an applied potential of 320 mV to the secondary electrode and -400 mV to the primary electrode relative to an AgCl/Ag reference electrode with a platinum auxiliary electrode. All scans were performed in Tris buffer (10 mM Tris, 100 mM KCl, 2.5 mM $MgCl_2$, 1 mM $CaCl_2$, pH 7.6) with 4 μM methylene blue and 300 μM potassium ferricyanide. Error bars represent the standard deviation over three measurements for three experiments.

Figure 4.5 shows the raw data collected for two individual electrodes treated with crude lysate, one in which the signal is 'on' in the presence of the SAM cofactor and one in which the signal is turned 'off' in the absence of cofactor, due to DNA restriction in the absence of methylation. Additionally, the reproducibility of the platform is shown (Figure 4.5), along with quantification of the 15 individual electrodes of a single assay. Interestingly, high concentrations of lysate were found to diminish the electrochemical signal, likely due to crowding on the DNA-modified electrode, and thus limiting access and binding of the methyltransferase of interest. Multiple concentrations of lysate were tested (Figure 4.6); a concentration corresponding to 4,000 cells per electrode was sufficiently dilute to allow access of DNMT1 to the DNA on the surface while still containing sufficient DNMT1 to produce measurable activity.

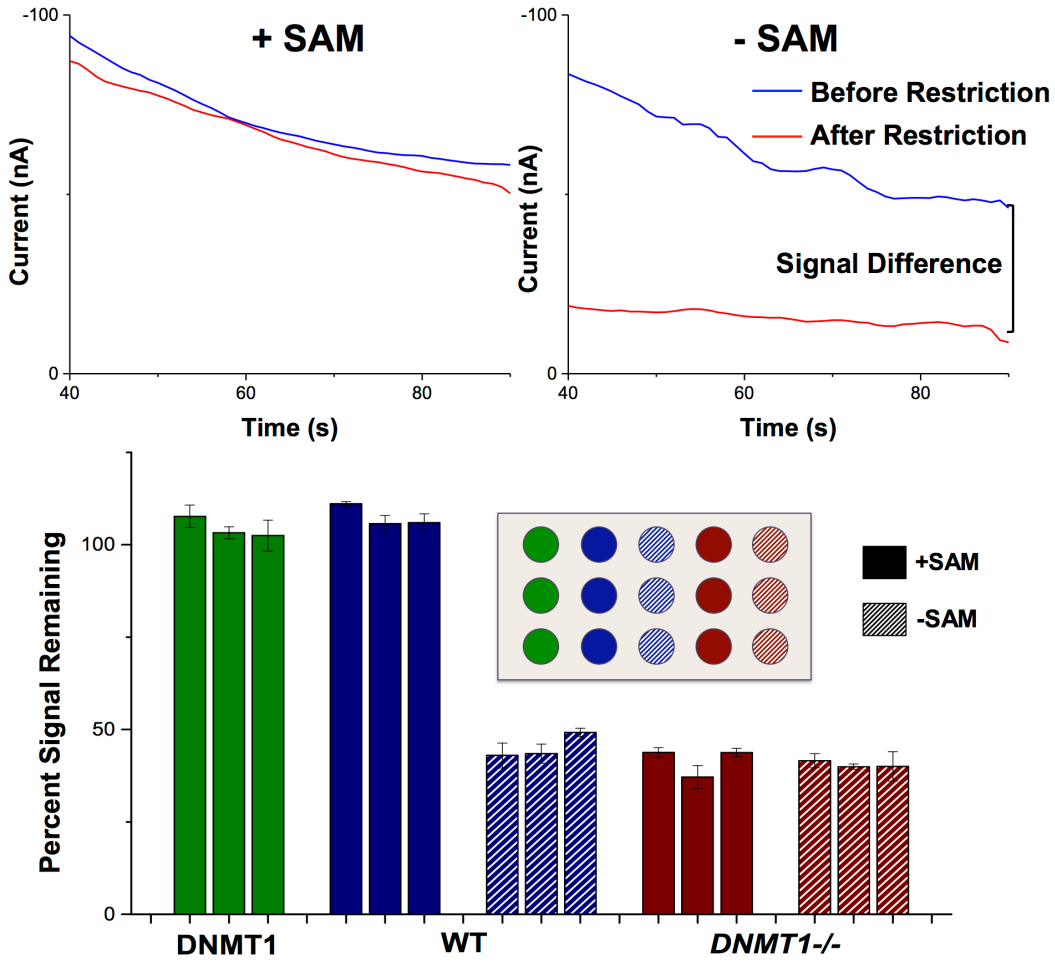

Figure 4.5 Detection and reproducibility of DNMT1 activity in cell lysates using electrochemical platform. *Top:* Raw data from single electrodes in the presence or absence of SAM cofactor. In blue is the preliminary scan after an electrode modified with hemimethylated DNA has been treated with parent lysate, followed by treatment with 1 µM protease in phosphate buffer, both at 37° C. In red is the scan after the electrode was treated with 1500 units/mL *BssH*II for 1.5 h at 37° C. On the left is the final scan from an electrode with 160 µM SAM added to the lysate; the signals essentially overlay, indicating an 'on' signal. On the right is the final scan from an electrode without SAM added to the lysate; this produces an 'off' signal. The constant potential amperometry was run for 90 seconds with an applied potential of 320 mV to the secondary electrode and -400 mV to the primary electrode. All scans were performed in Tris buffer (10 mM Tris, 100 mM KCl, 2.5 mM $MgCl_2$, 1 mM $CaCl_2$, pH 7.6) with 4 µM methylene blue and 300 µM potassium ferricyanide. *Bottom:* Reproducibility within the two-electrode multiplexed array. Orientation of the tested conditions on the 5x3 array is shown (inset) with circular electrodes colored to correspond with activity data represented in the bar graph. Both the electrodes treated with 65 nM purified DNMT1 on hemimethylated DNA with 160 µM SAM (green) and those treated with parent (WT) lysate in the presence of SAM (solid blue) show full signal protection. On electrodes

without added SAM (blue striped and red striped) and on *DNMT1* $^{-/-}$ lysate-treated electrodes in the presence of SAM (solid red), no signal protection is observed. Bar graph data are raw without standardization and error bars represent the standard deviation over three measurements.

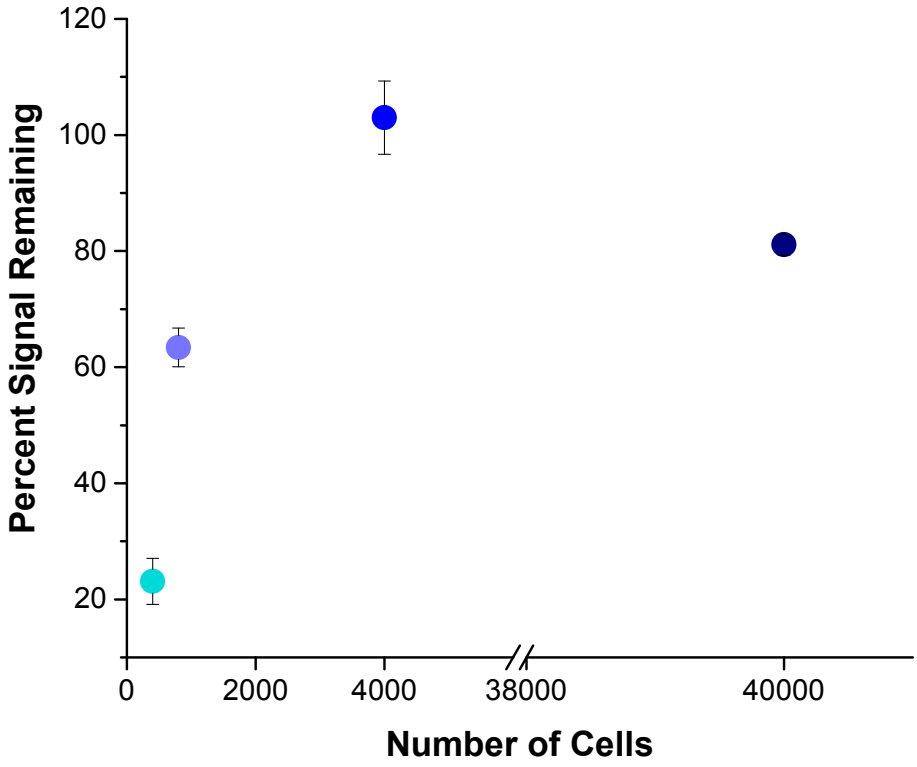

Figure 4.6 Signal protection from differing amounts of lysate. All electrodes on this array were modified with hemimethylated DNA, and values are normalized to 100% protection of the DNMT1 electrodes. All samples include 160 μM SAM. The darkest blue is lysate from approximately 40,000 cells. The subsequent points are from 4,000 cells, 800 cells, and 400 cells. Full protection is afforded from approximately 4,000 cells. The constant potential amperometry was performed for 90 seconds with an applied potential of 320 mV to the secondary electrode and -400 mV to the primary electrode relative to an AgCl/Ag reference electrode with a platinum counter electrode. All scans were performed in Tris buffer (10 mM Tris, 100 mM KCl, 2.5 mM $MgCl_2$, 1 mM $CaCl_2$, pH 7.6) with 4 μM methylene blue and 300 μM potassium ferricyanide. Error bars represent the standard error for three electrodes over three measurements.

To further combat signal decreases caused by undesired DNA-binding proteins, after electrodes are treated with lysate, a protease treatment step is incorporated to remove remaining bound protein before the electrochemical measurements. This protease step further ensures that there is no remaining protein bound either to the DNA or directly to the surface that could interfere with electrochemical measurements. Methyltransferase activity is then determined by the percent signal remaining after *BssH*II treatment. If the DNA is cut by the restriction enzyme, the signal is low, indicating little methyltransferase activity. It is noteworthy that the percent signal remaining is always non-zero because, even after restriction, a DNA fragment remains that can generate an electrochemical response with the noncovalent methylene blue redox probe; electrochemical amplification is proportional to the amount of bound methylene blue, and therefore to DNA length.

Differential Detection of DNMT1 Activity from Multiple Crude Cultured Cell Lysates

We then tested the ability of the platform to differentiate between lysate from a parent (HCT116 wild type) colorectal carcinoma cell line and a cell line that does not express DNMT1 (HCT116 *DNMT1*$^{-/-}$). As shown in Figure 4.7, specific detection of DNMT1 activity is dependent on both the methylation state of the substrate and the presence of the cofactor SAM. The 'signal on' specificity for the hemimethylated DNA substrate indicates unambiguous DNMT1 activity (maintenance methylation), and not activity by other human methyltransferases, DNMT3a or DNMT3b, which do not show this substrate preference (*de novo* methylation).[7] Signal is dependent on the presence of DNMT1 (purified or from parent lysate) as well as the cofactor SAM (Figure 4.7b) and

the hemimethylated substrate (Figure 4.7a). The remaining electrodes, treated either with parent lysate without SAM, or *DNMT1*$^{-/-}$ lysate independent of the cofactor, had significantly attenuated signals after restriction enzyme treatment.

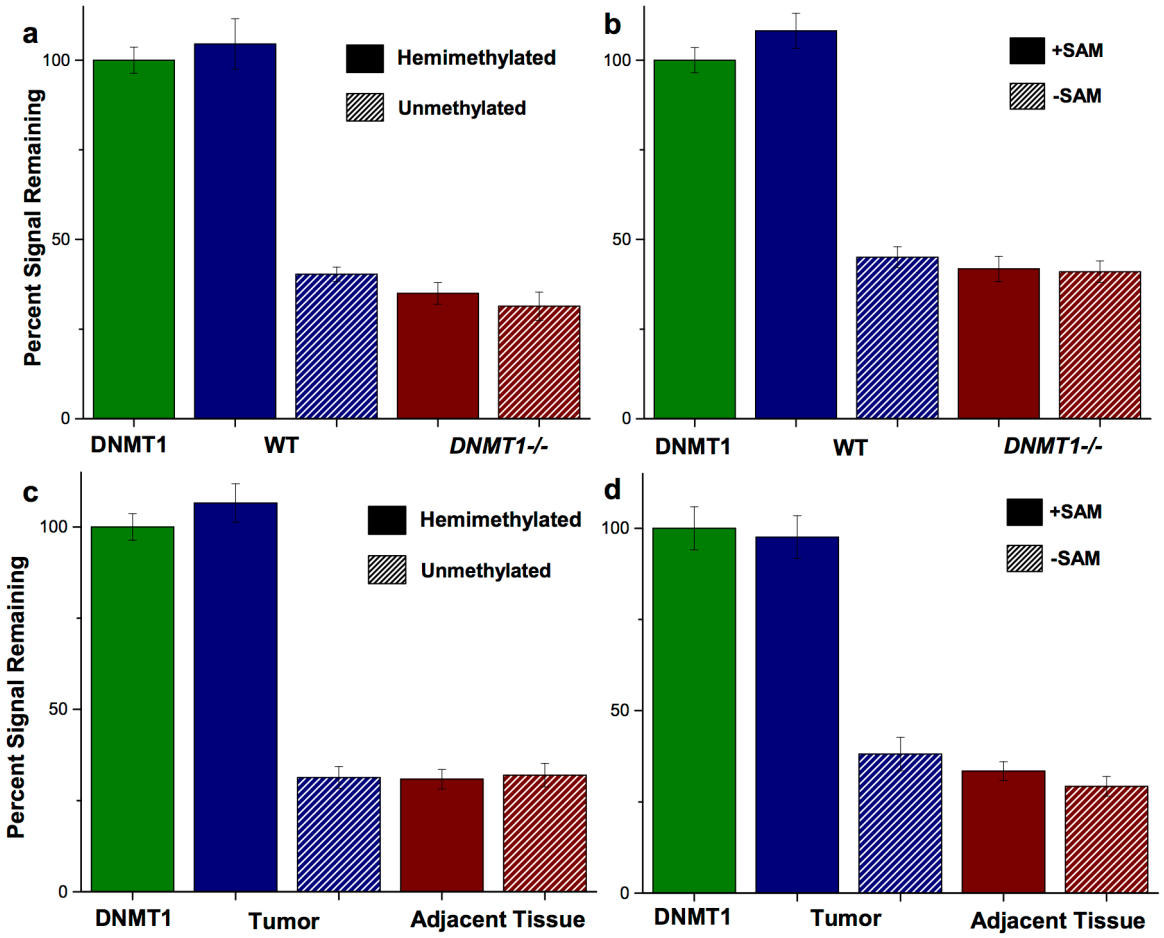

Figure 4.7 Dependence of lysate activity on the DNA substrate and cofactor. The positive control is 65 nM purified DNMT1 on hemimethylated DNA with 160 µM SAM (green). All values are normalized to 100% protection of the purified DNMT1 electrodes. Upper panels show cultured cell lysate substrate (a) and cofactor (b) dependence. Electrodes treated with parent (WT) lysate on the hemimethylated substrate in the presence of 160 µM SAM (blue) showed full signal protection, while on an unmethylated substrate or in the absence of SAM (striped blue) no signal protection is observed. Independent of conditions, electrodes treated with *DNMT1* $^{-/-}$ lysate (red solid and striped) showed no signal protection. Lower panels show biopsy tissue substrate (c) and cofactor (d) dependence. Electrodes treated with tumor lysate on the hemimethylated substrate in the presence of 160 µM SAM (blue) showed full signal protection, while on an unmethylated substrate or in the absence of SAM (striped blue) no signal protection is observed. Independent of conditions, electrodes treated with normal tissue lysate (red solid and striped) showed no signal protection. The data shown is the aggregation of three independent replicate experiments, with three electrodes per condition per experiment.

Detection of DNMT1 Activity from Human Tumor Tissue

Human biopsy tissue samples were similarly evaluated, and tumor tissue was readily distinguished from adjacent normal tissue (Figure 4.7). Tissue biopsy samples were purchased from a commercial source and were thus handled and stored using conventional methods (snap freezing in liquid nitrogen after removal and storage at -80° C for upwards of one month). The optimal amount of tissue for detection from these samples was found to be ~500 μg per electrode; typical colon punch biopsies yield 350 mg of tissue.[32] Samples of colorectal carcinoma tissue as well as the adjacent healthy tissue were prepared just as the cultured cell lysate was, and showed differential activity with our electrochemical platform. The tumor sample, which showed greater signal protection, was sensitive both to substrate and to cofactor, consistent with high DNMT1 methyltransferase activity, and similar to the cultured parent colorectal carcinoma cells. In contrast, the normal tissue sample showed low methyltransferase activity, as seen through the reduced electrochemical signal (Figure 4.7). These data clearly indicate that tumors can be effectively differentiated from healthy tissue through electrochemical DNMT1 measurement with our platform. By western blot, the relative abundance of DNMT1 in the tumor tissue as compared to healthy tissue was quantitatively consistent with the electrochemical results (Figure 4.2).

Lysate activities were also tested by a ^{3}H-SAM assay, and relative activities of the various samples were comparable to those determined electrochemically (Figure 4.3). However, as is typical for such radioactivity assays, activity measurements observed among trials of the ^{3}H-SAM assay were extremely variable, much more so than with the electrochemical platform. Activity differences between the tumor and healthy tissue

were seen only at concentrations of ~1 mg of tissue per sample, significantly higher than what is needed for electrochemical detection. The time required to obtain the data was additionally substantially longer.

Implications

DNMT1 is an important clinical diagnostic target due to its connection to aberrant genomic methylation, which is linked to tumorigenesis. Direct detection of methyltransferase activity from crude tissue lysates provides an early method of cancer screening and can also inform treatment decisions. However, current approaches for the detection of methyltransferase activity rely on radioactive or fluorescent labels, antibodies, and obtrusive instrumentation, which limit their application in laboratories and clinics. Although electrochemical approaches generally overcome these limitations, direct detection of proteins from crude samples remains challenging because of the complexity of crude biological lysates, as well as the sensitivity required to analyze the limited material of small clinical biopsy samples.

Our electrochemical assay for DNMT1 methylation effectively circumvents these problems. Methylation is detected through the presence or absence of DNA surface restriction followed by electrocatalytic amplification. We avoid clogging the platform through the formation of low-density DNA monolayers, enabling target DNA-binding proteins in the lysate ample access to the individual DNA helices on the surface. Our platform is also sensitive and selective without the use of radioactivity, fluorescence, or antibodies through the combination of electrocatalytic signal amplification and the sensitivity of DNA CT chemistry to report changes to the integrity of the DNA. This allows for detection of DNMT1 from both cultured colorectal carcinoma cells and tissue biopsy specimens. No difficult or time-consuming purification steps are necessary, and, for each electrode, only ~4000 cultured cells or ~500 μg tissue sample are required. Importantly, because of the multiplexed nature of this platform, we are able to assay for

substrate specificity while simultaneously measuring normal tissue and tumor tissue lysates. Therefore, with our platform, healthy tissue is easily distinguished from tumor tissue using very small amounts of sample. More generally, this work represents an important step in new electrochemical biosensing technologies.

References

1. Jones, P. A., and Takai, D. (2001) The role of DNA methylation in mammalian epigenetics, *Science 293*, 1068-1070.

2. Li, E., Beard, C., and Jaenisch, R. (1993) Role for DNA methylation in genomic imprinting, *Nature 366*, 362-365.

3. Baylin, S. B. (1997) Tying it all together: epigenetics, genetics, cell cycle, and cancer, *Science 277*, 1948-1949.

4. Heyn, H., and Esteller, M. (2012) DNA methylation profiling in the clinic: applications and challenges, *Nat. Rev. Genet. 13*, 679-692.

5. Jones, P. A., and Baylin, S. B. (2002) The fundamental role of epigenetic events in cancer, *Nat. Rev. Genet. 3*, 415-428.

6. Jones, P. A., and Laird, P. W. (1999) Cancer epigenetics comes of age, *Nat. Genet. 21*, 163-167.

7. Okano, M., Bell, D. W., Haber, D. A., and Li, E. (1999) DNA methyltransferases Dnmt3a and Dnmt3b are essential for de novo methylation and mammalian development, *Cell 99*, 247-257.

8. Pradhan, S., Bacolla, A., Wells, R. D., and Roberts, R. J. (1999) Recombinant human DNA (cytosine-5) methyltransferase. I. Expression, purification, and comparison of de novo and maintenance methylation, *J. Biol. Chem. 274*, 33002-33010.

9. Rhee, I., Bachman, K. E., Park, B. H., Jair, K. W., Yen, R. W., Schuebel, K. E., Cui, H., Feinberg, A. P., Lengauer, C., Kinzler, K. W., Baylin, S. B., and Vogelstein, B. (2002) DNMT1 and DNMT3b cooperate to silence genes in human cancer cells, *Nature 416*, 552-556.

10. Robert, M. F., Morin, S., Beaulieu, N., Gauthier, F., Chute, I. C., Barsalou, A., and MacLeod, A. R. (2003) DNMT1 is required to maintain CpG methylation and aberrant gene silencing in human cancer cells, *Nat. Genet. 33*, 61-65.

11. Jurkowska, R. Z., Ceccaldi, A., Zhang, Y., Arimondo, P. B., and Jeltsch, A. (2011) DNA methyltransferase assays, *Methods Mol. Biol. 791*, 157-177.

12. Dorgan, K. M., Wooderchak, W. L., Wynn, D. P., Karschner, E. L., Alfaro, J. F., Cui, Y., Zhou, Z. S., and Hevel, J. M. (2006) An enzyme-coupled continuous spectrophotometric assay for S-adenosylmethionine-dependent methyltransferases, *Anal. Biochem. 350*, 249-255.

13. Graves, T. L., Zhang, Y., and Scott, J. E. (2008) A universal competitive fluorescence polarization activity assay for S-adenosylmethionine utilizing methyltransferases, *Anal. Biochem. 373*, 296-306.

14. Drummond, T. G., Hill, M. G., and Barton, J. K. (2003) Electrochemical DNA sensors, *Nat. Biotechnol. 21*, 1192-1199.

15. Sadik, O. A., Aluoch, A. O., and Zhou, A. (2009) Status of biomolecular recognition using electrochemical techniques, *Biosens. Bioelectron. 24*, 2749-2765.

16. Besant, J. D., Das, J., Sargent, E. H., and Kelley, S. O. (2013) Proximal bacterial lysis and detection in nanoliter wells using electrochemistry, *ACS Nano 7*, 8183-8189.

17. Campbell, C. N., Gal, D., Cristler, N., Banditrat, C., and Heller, A. (2002) Enzyme-amplified amperometric sandwich test for RNA and DNA, *Anal. Chem. 74*, 158-162.

18. Cheng, J., Sheldon, E. L., Wu, L., Uribe, A., Gerrue, L. O., Carrino, J., Heller, M. J., and O'Connell, J. P. (1998) Preparation and hybridization analysis of DNA/RNA from E. coli on microfabricated bioelectronic chips, *Nat. Biotechnol. 16*, 541-546.

19. Das, J., Cederquist, K. B., Zaragoza, A. A., Lee, P. E., Sargent, E. H., and Kelley, S. O. (2012) An ultrasensitive universal detector based on neutralizer displacement, *Nat. Chem. 4*, 642-648.

20. Wang, F., Elbaz, J., Orbach, R., Magen, N., and Willner, I. (2011) Amplified analysis of DNA by the autonomous assembly of polymers consisting of DNAzyme wires, *J. Am. Chem. Soc. 133*, 17149-17151.

21. Liu, S., Wu, P., Li, W., Zhang, H., and Cai, C. (2011) An electrochemical approach for detection of DNA methylation and assay of the methyltransferase activity, *Chem. Commun. 47*, 2844-2846.

22. Wang, M., Xu, Z., Chen, L., Yin, H., and Ai, S. (2012) Electrochemical immunosensing platform for DNA methyltransferase activity analysis and inhibitor screening, *Anal. Chem. 84*, 9072-9078.

23. Wang, P., Wu, H., Dai, Z., and Zou, X. (2012) Picomolar level profiling of the methylation status of the p53 tumor suppressor gene by a label-free electrochemical biosensor, *Chem. Commun. 48*, 10754-10756.

24. Lai, R. Y., Plaxco, K. W., and Heeger, A. J. (2007) Aptamer-based electrochemical detection of picomolar platelet-derived growth factor directly in blood serum, *Anal. Chem. 79*, 229-233.

25. Sardesai, N. P., Barron, J. C., and Rusling, J. F. (2011) Carbon nanotube microwell array for sensitive electrochemiluminescent detection of cancer biomarker proteins, *Anal. Chem. 83*, 6698-6703.

26. Furst, A., Landefeld, S., Hill, M. G., and Barton, J. K. (2013) Electrochemical patterning and detection of DNA arrays on a two-electrode platform, *J. Am. Chem. Soc. 135*, 19099-19102.

27. Boon, E. M., Salas, J. E., and Barton, J. K. (2002) An electrical probe of protein-DNA interactions on DNA-modified surfaces, *Nat. Biotechnol. 20*, 282-286.

28. Muren, N. B., Olmon, E. D., and Barton, J. K. (2012) Solution, surface, and single molecule platforms for the study of DNA-mediated charge transport, *Phys. Chem. Chem. Phys. 14*, 13754-13771.

29. Muren, N. B., and Barton, J. K. (2013) Electrochemical assay for the signal-on detection of human DNA methyltransferase activity, *J. Am. Chem. Soc. 135*, 16632-16640.

30. Wang, H., Muren, N. B., Ordinario, D., Gorodetsky, A. A., Barton, J. K., and Nuckolls, C. (2012) Transducing methyltransferase activity into electrical signals in a carbon nanotube-DNA device, *Chem. Sci. 3*, 62-65.

31. Furst, A. L., Hill, M. G., and Barton, J. K. (2013) DNA-modified electrodes fabricated using copper-free click chemistry for enhanced protein detection, *Langmuir 29*, 16141-16149.

32. Melgar, S., Yeung, M. M., Bas, A., Forsberg, G., Suhr, O., Oberg, A., Hammarstrom, S., Danielsson, A., and Hammarstrom, M. L. (2003) Over-expression of interleukin 10 in mucosal T cells of patients with active ulcerative colitis, *Clin. Exp. Immunol. 134*, 127-137.

Chapter 5

A Multiplexed, Two-Electrode Platform for Biosensing based on DNA-Mediated Charge Transport

Adapted from: Furst, A. L., Hill, M. G., and Barton, J. K. (2015) A Multiplexed, Two-Electrode Platform for Biosensing based on DNA-Mediated Charge Transport, *Submitted.*

Introduction

Analytical methods for reliable biomolecule detection are becoming increasingly important with the continued discovery of disease-related biomarkers. Electrochemical nucleic acid-based assays,[1-10] particularly those that utilize DNA-mediated charge transport (DNA CT)[11, 12] are especially promising for sensing platforms. Devices based on DNA CT effectively report on the integrity of the π-stacked DNA bases; perturbations to the proper stacking, resulting from lesions, single nucleotide polymorphisms, or protein binding events that affect the base stack, attenuate the electrochemical signal. DNA CT has been employed successfully in the detection of a variety of biomolecules, including DNA fragments, chemically modified DNA, and DNA-binding proteins, many of which are not specifically detectable using alternative sensing platforms.[11, 13]

Substrates for DNA-based electrochemical systems typically are prepared by self-assembling thiolated DNA duplexes onto gold electrodes, followed by backfilling with an alkylthiol to passivate any remaining surface-exposed gold.[14-16] One major challenge with this methodology is the limited control over monolayer composition, both in the total amount of DNA assembled and its dispersion within the monolayer.[17-19] For biosensing applications, which rely on direct interactions between target biomolecules and the DNA duplexes attached to the electrode surface, homogeneous spacing between the DNA duplexes is critical to provide the target in solution adequate access to individual helices. Inevitably, clustering occurs with thiolated DNA. Recently, we demonstrated the utility of applying mixed alkylthiol monolayers doped with variable amounts of azide-terminated functional groups to gain more control over monolayer formation.[20] These monolayers are significantly more homogeneous than those prepared

using thiolated DNA. Additionally, coupling with copper-free click conjugation of cyclooctyne-labeled DNA yields surfaces containing evenly dispersed rather than clustered DNA with coverages that mirror the mole fraction of azide in the underlying film. The resulting monolayers allow greater access of DNA-binding proteins to individual helices within the films, permitting devices with greater sensitivity to these biomolecules.

While tethering DNA to surfaces with cyclooctynes provides a strong foundation for more controlled monolayer formation, ideally, DNA probe molecules would feature a simple terminal alkyne group to avoid additional synthetic steps. The well known Huisgen 1,3-dipolar cycloaddition ("click" reaction),[21] catalyzed by copper(I), has been used previously to form homogenous monolayers with terminal alkyne-labeled probe molecules.[22, 23] Indeed, because of the instability of copper(I) in aqueous solution and its reactivity with DNA,[24-26] electrochemical methods to generate copper(I) *in situ* from copper(II) precursors have been developed, and the coupling of alkyne-labeled oligonucleotides to azide-terminated surfaces *via* electrochemically induced click chemistry has been reported.[27-30]

We have now employed a multiplexed platform in which simple alkyne-labeled duplexes are coupled to azide-terminated surfaces by copper(I) species generated electrochemically *in situ* at a secondary working electrode positioned over the alkylthiol monolayer.[31] Our attempts to fabricate surfaces suitable for DNA CT using published methods with one working electrode were difficult: reliable electrochemical readout of DNA-mediated chemistry was hampered by interference from the irreversible products of copper(II) reduction at the modified electrochemical surface (likely adsorption of copper

films onto the electrode surface). Our new method[31] allows for the attachment of multiple DNA sequences onto a single electrode, with tight control over the probe-molecule spacing.[32] A multiplexed version of this methodology has enabled the sensitive detection of DNA methyltransferase activity directly from human tissue samples.[33]

Here we report the full characterization of this multiplexed, two working electrode platform that enables both catalyst activation and electrochemical readout from a secondary electrode. In addition to minimizing undesirable copper products at DNA-modified surfaces, we have found that readout of electrocatalytically generated reporter molecules at the secondary electrode greatly enhances the sensitivity and specificity of DNA CT assays. We have optimized the spacing between the primary and secondary electrodes such that we are no longer limited by the diffusion of the electrocatalytic components, and this mode of detection importantly eliminates large background signals. Indeed, this platform enables detection of single base mismatches as well as the selective and specific detection of two transcription factors, TATA binding protein (TBP) and CopG, with sensitivities greater than those achieved with single working electrode platforms.

Materials and Methods

Preparation of Surfaces and First Alkanethiol Monolayers

Gold surfaces were polished with 0.05 μm alumina slurries (Buhler) before monolayer assembly. Mixed monolayers were then formed on the substrate plate by self-assembly of 100 mM 12-azidododecane-1-thiol (C_{12} thiol azide) and 100 mM 11-mercaptoundecyl-phosphoric acid from an ethanolic solution. Surfaces were incubated in the thiol solution for 18-24 h, followed by rinsing with ethanol and phosphate buffer (5 mM phosphate, 50 mM NaCl, pH 7.0).

DNA Synthesis and Purification

Hexynyl-labeled oligonucleotides were synthesized on an Applied Biosystems 3400 DNA synthesizer, and were modified at the 5` end with a C6-alkyne reagent purchased from Glen Research, Inc. Complementary unmodified strands were purchased from IDT. DNA strands modified with Nile Blue at the 5` terminus were prepared as previously reported.[34] Briefly, DNA was synthesized with ultramild reagents (Glen Research, Inc) to prevent Nile Blue degradation, and 5-[3-acrylate NHS ester]-deoxy uridine was incorporated as the 5` terminal base. With DNA on the solid support, 10 mg/mL Nile Blue perchlorate in 9:1 *N,N*-dimethylformamide/*N,N*-diisopropylethylamine (Sigma Aldrich) was added and allowed to shake for 24 h. Beads were washed three times each with *N,N*-dimethylformamide, methanol, and acetonitrile. The DNA was removed from the solid support with 0.05 M potassium carbonate in methanol at ambient temperature for 24 h. Preparation of all oligonucleotides followed a reported protocol. For non-ultramild syntheses, DNA was deprotected and cleaved from the solid support

with ammonium hydroxide (60° C for 12 h). Following a preliminary round of high-performance liquid chromatography (HPLC) on a PLRP-S column (Agilent), oligonucleotides were treated with 80% acetic acid in water for 20 minutes. Each oligonucleotide was again purified by HPLC using a gradient of acetonitrile and 50 mM ammonium acetate. Oligonucleotides were then desalted by ethanol precipitation and quantified by ultraviolet-visible spectrophotometry based on their extinction coefficients at 260 nm (IDT Oligo Analyzer). Oligonucleotide masses were verified by matrix-assisted laser desorption (MALDI) mass spectrometry. DNA duplexes were formed by thermally annealing equimolar amounts of single-stranded oligonucleotides in deoxygenated phosphate buffer (5mM phosphate, 50 mM NaCl, pH 7.0) at 90° C for 5 minutes followed by slowly cooling to 25° C.

The following sequences were prepared:

Well Matched
Alkyne: H-C_2-$(CH_3)_6$-5'-GCT CAG TAC GAC GTC GA-3'
Complement: 3'-CGA GTC ATG CTG CAG CT-5'

Mismatched
Alkyne: H-C_2-$(CH_3)_6$-5'-GCT CAG TA*C* GAC GTC GA-3'
Complement: 3'-CGA GTC AT*A* CTG CAG CT-5'

TBP Binding Sequence
Alkyne: H-C_2-$(CH_3)_6$-5'-GGC GTC **TAT A**AA GCG ATC GCG A-3'
Complement: 3'-CCG CAG **ATA T**TT CGC TAC CGC T-5'

COPG Binding Sequence
Alkyne: H-C_2-$(CH_3)_6$-5'-AAC CG**T GCA** CTC AA**T GCA** ATC-3'
Complement: 3'-TTG GC**A CGT** GAG TT**A CGT** TAG-5'

The location of the mismatch is indicated in italics and with an underline, and the protein binding sites are shown in bold.

Design of Experimental Platform

The multiplexed, two-electrode array consisted of two ¼" Teflon blocks separated by a Teflon gasket of various thicknesses (Figure 5.1). Gold wires (1-mm diameter) were then inserted into holes drilled into the Teflon blocks to form complementary 5 x 3 electrode arrays on each block. Each pair of complementary electrodes was 5 mm from its nearest neighbor, providing the opportunity to isolate each pair into individual wells. The electrodes were sealed into the Teflon using superglue. The top array featured additional holes (1.5-mm diameter) to provide the reference and auxiliary electrodes access to the working solution. Spacers that separated the individual wells were constructed from 1.5 mm thick Teflon.

DNA Attachment to Alkanethiol Monolayers

A 10 mM aqueous $[Cu(phendione)_2]^{2+}$ (phendione=1,10-phenanthroline-5,6-dione solution was prepared by combining one equivalent of $CuSO_4$ (10 μmol, 15.9 mg) with two equivalents of phendione (20 μmol, 42.0 mg) in 10 mL of deionized H_2O. ESI-MS: 580.2 (calc: 580.0). The complex was additionally isolated as the PF_6^- salt. Prior to application to the electrode surface, the complex was diluted to a final concentration of 1 mM in Tris buffer (10 mM Tris, 100 mM KCl, 2.5 mM $MgCl_2$, 1 mM $CaCl_2$, pH 7.6). The catalyst solution was combined with 5`-labeled ethynyl DNA (final concentration of 25 μM), and a constant potential of -350 mV v. AgCl/Ag was applied to the sensing (top) electrode array to reduce the Cu(II) and initiate the coupling of the DNA to the azide-terminated monolayers. The potential was applied for 15 minutes. Multiple sequences of DNA were attached to the array through the sequential activation of different secondary

electrodes. For example, well matched and mismatched DNA were attached to the same array through the preliminary activation of secondary electrodes one through nine in the presence of well matched DNA, followed by rinsing of the platform and subsequent activation of secondary electrodes ten through fifteen in the presence of DNA containing a single-base mismatch.

Characterization of DNA-modified Monolayers

All electrochemical experiments were performed on a CHInstruments 760E bipotentiostat. For electrochemical impedance spectroscopy experiments, 400 μM potassium ferricyanide in phosphate buffer (5 mM phosphate, 50 mM NaCl, pH 7.0) was used. For all other experiments, electrochemistry was conducted in Tris buffer (10 mM Tris, 100 mM KCl, 2.5 mM $MgCl_2$, 1 mM $CaCl_2$, pH 7.6) with 4 μM methylene blue and 300 μM potassium ferricyanide; for experiments with covalent Nile Blue, methylene blue was omitted. For mismatch discrimination and protein binding experiments, constant potential amperometry was used, with potential applied for 90 s. The primary electrode was held at -400 mV v. AgCl/Ag, and the secondary electrode was held at 350 mV v. AgCl/Ag. A Pt wire was incorporated as a counter electrode.

TBP and CopG Experiments

TATA-Binding Protein (TBP) was purchased from ProteinOne, and CopG was purchased from Origene. Both proteins were stored at -80° C until use. MicroBiospin 6 columns (BioRad) were used to exchange the shipping buffer for Tris buffer (10 mM Tris, 100 mM KCl, 2.5 mM $MgCl_2$, 1 mM $CaCl_2$, pH 7.6). Prior to electrochemical

measurements with CopG and TBP, electrodes were incubated with 1 μM Bovine serum albumin (BSA) for 30 min, followed by rinsing with Tris buffer (10 mM Tris, 100 mM KCl, 2.5 mM $MgCl_2$, 1 mM $CaCl_2$, pH 7.6). Protein solutions (4 μL) were added to each electrode and incubated for 20 minutes at ambient temperature prior to measurement.

Results and Discussion

We have designed and fabricated an addressable, multiplexed biosensing array that features two sets of complementary electrodes separated by a thin film (Figure 5.1). The bottom electrodes, which compose the primary array, are modified with covalently bound DNA sequences dispersed within a mixed alkylthiol monolayer, while the top electrodes, which form the secondary array, are unmodified and are used both for activating a DNA-coupling catalyst and for the electrochemical readout.

Electrochemical Response of Coupling Catalyst

The electrode platform, electrocatalytic detection scheme, and coupling reaction are shown in Figure 5.1. The electrochemical initiation of azide/alkyne coupling via Cu(II) reduction has been explored previously.[35] While several chelating ligands for copper(I) click chemistry have been reported, our experiments have focused on the bipyridyl derivative 1,10-phenanthroline-5,6-dione (phendione), as this ligand is commercially available and yields a water-soluble complex. The cyclic voltammogram (CV) of $[Cu(phendione)_2][SO_4]$ in Tris buffer shows several copper-centered reductions between + 0.20 and -0.40 V *vs.* AgCl/Ag (Figure 5.2). Importantly, these processes are only partially chemically reversible. The CV also shows a coupled oxidative response with a shape characteristic of anodic stripping, suggesting that the electrochemical reactions result in the adsorption of at least some copper-containing species onto the electrode surface. The deposition of copper following electrochemical reduction is further

supported by the formation of a visible, black surface film following the application of potentials in the range of -0.30 to -0.40 V *vs.* AgCl/Ag.

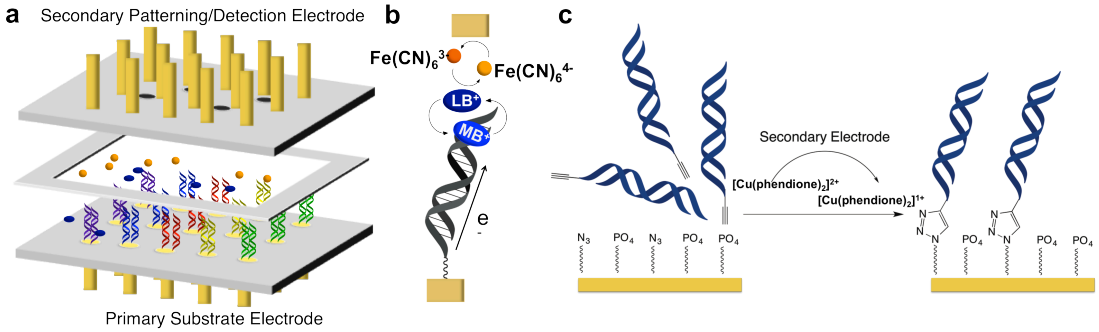

Figure 5.1 Multiplexed, two-electrode platform. a. The multiplexed platform contains two 5 x 3 arrays of 1 mm x 1.5 cm gold electrodes embedded in Teflon separated by a Teflon spacer to form a well for running solution. The secondary array (top) contains four holes into which reference and auxiliary electrodes can be inserted. A primary electrode array (bottom) forms the primary surface, and contains the same number and positioning of electrodes as the top array without holes. b. Electrocatalytic signal amplification occurs when a redox probe (blue oval) that interacts with the base stack of DNA is reduced *via* DNA-mediated CT. The probe then reduces an electron sink (orange ball) in solution, becoming reoxidized in the process. The reduced electron sink interacts with the secondary electrode, generating a current as it is reoxidized at the secondary electrode surface. c. DNA is covalently tethered to azide-containing monolayers on the substrate array by electrochemically activated click chemistry. A mixed monolayer containing azide head groups and phosphate head groups is formed on a gold surface. A solution of alkyne-modified DNA and the inert $[Cu(phendione)_2]^{2+}$ complex are added to the surface. Upon application of a sufficiently negative potential from the secondary electrode, the copper is reduced, yielding an active catalyst to covalently tether DNA to the mixed monolayer.

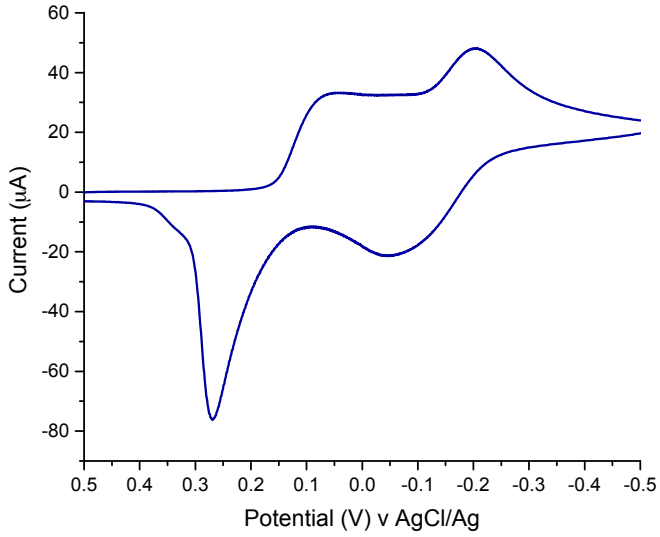

Figure 5.2 Electrochemistry of $[Cu(phendione)_2]^{2+}$. A cyclic voltammogram (CV) of $[Cu(phendione)_2]^{2+}$ was obtained in degassed Tris buffer (10 mM Tris, 100 mM KCl, 2.5 mM $MgCl_2$, 1 mM $CaCl_2$, pH 7.6) at a glassy carbon working electrode. CV was performed with a scan rate of 0.1 V/s against an AgCl/Ag reference electrode with a Pt counter electrode.

Formation of DNA Monolayers with Activation from Primary or Secondary Electrodes

To prepare DNA-modified surfaces for biomolecule detection assays, alkyne-labeled duplex DNA is attached to mixed thiol monolayers containing 50% azide and 50% phosphate head groups through electrochemically-activated click chemistry. An overview of the process of electrochemical click to attach DNA to an electrode, followed by DNA CT-facilitated current measurement, is shown in Figure 5.3. Based on previous studies, a 1:1 ratio of azide to phosphate head groups provides adequate spacing between the individual helices for substrate access, while maintaining a sufficient concentration of DNA on the surface for reliable detection.[20] Importantly, electrochemical titrations of methylene blue and ferricyanide individually, as well as mixtures of both methylene blue and ferricyanide together, established that these alkylthiol mixed monolayers remain effectively passivated to solutions of up to 8 μM methylene blue and 500 μM ferricyanide, showing no electrochemical signal at these concentrations (data not shown).

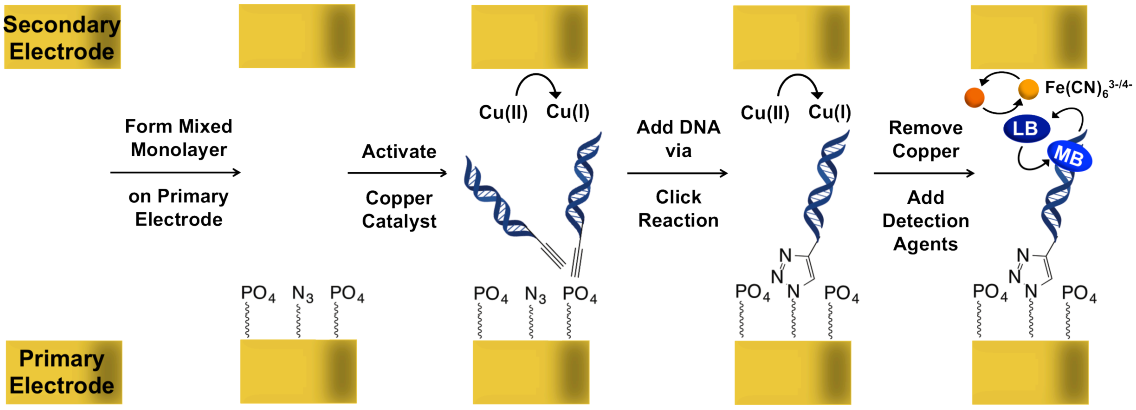

Figure 5.3 General strategy for monolayer formation and detection. First, a mixed alkanethiol monolayer is formed on the primary electrode array containing phosphate and azide head groups. Subsequently, a copper catalyst for click chemistry is activated at the secondary electrode to enable the click reaction to proceed between the surface-bound azides and alkyne-modified DNA. Finally, all copper is removed, and methylene blue and ferricyanide are added for electrochemical detection.

Solutions of $[Cu(phendione)_2]^{2+}$ (typically 1 mM) are used for the inert catalytic precursor; activation to Cu(I) is accomplished by applying a constant potential of -350 mV (vs. AgCl/Ag) to a secondary electrode for 15 minutes. As can be seen from the CVs in Figure 5.4, after copper activation and subsequent rinsing of the surface, no residual copper is evident on the surface.

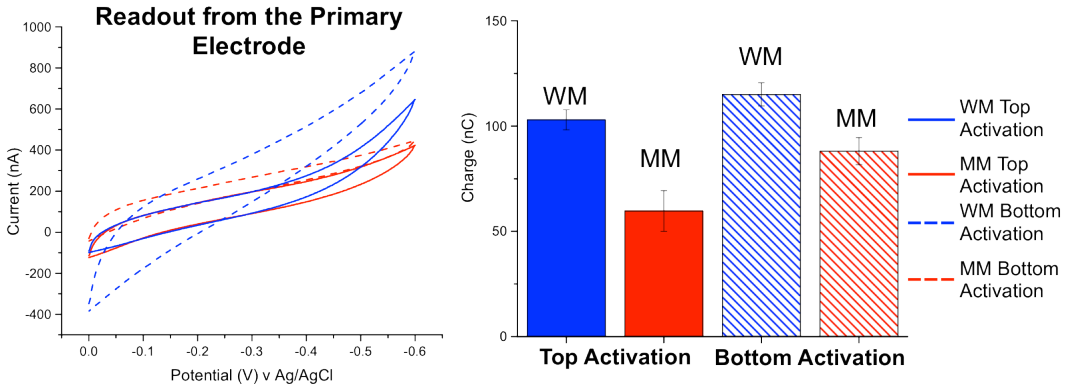

Figure 5.4 Effects of catalyst activation at the primary as compared to the secondary working electrodes with conventional detection from the DNA-modified electrode. (*Left*) Cyclic voltammetry (ν = 100 mV/s) of 4 μM MB / 300 μM $[K]_3[Fe(CN)_6]$ in Tris buffer, using the two-electrode multiplexed platform with a 127-μm spacer separating the primary- and secondary-electrode arrays. Data were recorded at four separate primary electrodes featuring an underlying 50/50 azide/phosphate monolayer, covalently modified with either well-matched (blue) or mismatched (red) alkyne-labeled DNA duplexes (18-mers). The solid traces were obtained at electrodes prepared by $Cu(phendione)_2^{2+}$ activation at the corresponding secondary electrodes, while the dashed traces were obtained by activating $Cu(phendione)_2^{2+}$ directly at the primary electrodes. (*Right*) Charges obtained by integrating the cyclic voltammograms. Electrodes prepared by catalyst activation at the secondary electrode display modest, though significantly better mismatch discrimination.

Cyclic voltammetry (CV) from the primary, DNA-modified electrode (DME) is a standard technique for electrochemical analysis of DNA CT through monolayers. Thus, CVs of DNA monolayers formed by catalyst activation at either the primary or the secondary electrode were acquired to evaluate monolayer characteristics. The CVs do not have the conventional redox couple from methylene blue on DMEs because of both the low coverage of DNA and the concentrations of the redox probe and electron sink required for detection at the secondary electrode. The CVs in Figure 5.4 also highlight complications arising from copper activation at the primary electrode; the details of mismatch analysis are described below. Most notably, background currents are larger at DNA-modified surfaces formed by activation at the primary electrode (primary electrode activation) versus the secondary electrode, likely due to a layer of copper precipitate on the DNA monolayer. This precipitate is only observable on the electrode used for catalyst activation. If the primary electrode is used for activation, copper precipitates on the DNA monolayer. Conversely, if the secondary electrode is used for activation, the copper precipitate occurs at that bare electrode surface and is easily removed by polishing the array prior to detection with this array. Copper activation at the primary electrode further yields surfaces that exhibit variable capacitances between well matched and mismatched DNA monolayers, indicating non-equivalent monolayer formation. The CVs from substrate electrodes patterned by a secondary electrode, in contrast, have consistent capacitance. Nevertheless, the difference in charge measured by well-matched DNA as compared to mismatched DNA, a hallmark of DNA CT, remains only moderate when these monolayers are measured from the primary electrode.

Electrochemical impedance spectroscopy (EIS)[36] was also performed to evaluate the effect of copper-film deposition on the electrochemical properties of DNA monolayers formed *via* $[Cu(phendione)_2]^{2+}$ reduction at either the primary or secondary electrode, as well as at bare gold electrodes and electrodes modified with only the underlying mixed alkylthiol monolayers. EIS was executed using ferricyanide and ferrocyanide, a standard method of label-free DNA detection, which is based on the amount of access the small molecule has to the electrode surface.[36, 37] Nyquist plots (Figure 5.5) constructed from data collected at these latter two surfaces display a small impedance arc, consistent with low surface capacitance and a response dominated mainly by diffusion of the small molecule to the surface.[36, 38-40] In contrast, the presence of DNA on the electrode surface partially blocks ferricyanide from interacting with the electrode, resulting in a significantly larger capacitive arc. Consistent with the CV data, the Nyquist plot from a DNA monolayer formed *via* catalyst activation from the substrate electrode shows a substantially larger (and less reproducible) arc, indicating higher electron-transfer resistance than that of the analogous DNA film prepared *via* activation from the secondary electrode. Presumably, deposition of copper-containing species following electrochemical reduction of $[Cu(phendione)_2]^{2+}$ further passivates the now heterogeneous surface from analytes in solution.

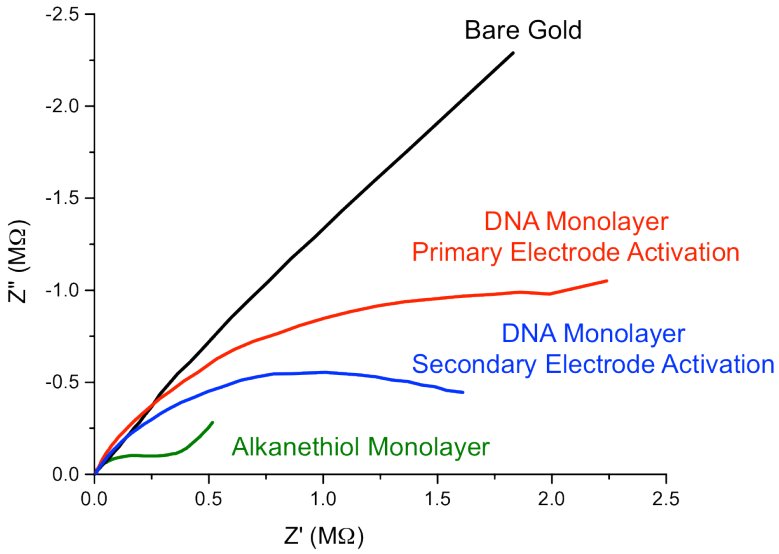

Figure 5.5 Nyquist plots of electrochemical impedance spectroscopy of differentially formed monolayers. Shown are results for a bare gold electrode (black), a mixed monolayer of azide and phosphate-terminated thiols (green), a DNA monolayer formed from $[Cu(phendione)_2]^{2+}$ catalyst activation from the secondary electrode (blue), and a DNA monolayer formed from the catalyst activation at the primary, substrate electrode (red). Conditions used for impedance spectroscopy were 400 μM ferrocyanide in phosphate buffer (5 mM phosphate, 50 mM NaCl, pH 7.0).

Electrochemical Readout at the Secondary versus Primary Electrode

To increase the sensitivity of DNA CT assays, we typically employ an electrocatalytic cycle using methylene blue (MB) and ferricyanide (Figure 5.1, 5.2).[12] Intercalated MB is reduced *via* DNA CT to leucomethylene blue (LB), which has a decreased affinity for DNA. Upon entering solution, the LB reduces freely diffusing ferricyanide to ferrocyanide, regenerating MB that re-intercalates into the film to begin the cycle again.

With a one working electrode system, the signal amplification afforded by the addition of the electron sink ferricyanide is limited to one turnover per ferricyanide molecule[39] Once ferricyanide is reduced to ferrocyanide in the vicinity of DNA monolayer, the effective concentration of electron sink at that location is very low, decreasing the signal amplification. In contrast, with a two working electrode system in which the electrodes are very close to one another, the effective concentration of ferricyanide is not depleted, as it is constantly replenished by the turnover of ferrocyanide at the secondary electrode. This ferrocyanide turnover enables more rounds of methylene blue turnover in a given amount of time with the two working electrode platform.

In fact, the incorporation of a secondary electrode enables the system to function as a collector-generator. The secondary electrode is held at a sufficiently positive potential to oxidize the ferrocyanide that is generated in solution as a result of the reduction of ferricyanide by LB following DNA CT. When the primary and secondary electrodes are sufficiently close, the current generated from the oxidation of ferrocyanide at the secondary electrode provides a significantly more amplified electrochemical signal than can be achieved in a one electrode system; the secondary electrode enables more

rounds of turnover in a given period of time than electrocatalysis with the primary electrode alone. If ferricyanide is reduced in solution by LB due to DNA-mediated reduction of MB, more ferrocyanide is present at the secondary electrode, where it is reoxidized to generate a large current at that electrode. In contrast, if no DNA CT occurs at the primary electrode, no current is generated at the secondary electrode, negating the need for background correction. Our platform can function as a collector-generator when starting with either ferrocyanide, as with conventional collector-generators, or ferricyanide, which is converted to ferrocyanide following DNA CT.

For this platform to effectively function as a collector-generator, the distance between the two sets of electrodes must be sufficiently close to ensure that the local concentration of ferricyanide is not depleted, while maintaining sufficient distance to obtain DNA-mediated signals. With scanning electrochemical microscopy (SECM), the optimal distance between the tip and the electrode surface is determined by an approach curve.[41, 42] We have similarly optimized the distance between our two working electrodes by varying the height of the Teflon spacer between the two arrays, with heights ranging from 50 μm to 1500 μm (Figure 5.6). Using ferricyanide and MB, the current as well as signal decrease upon incorporation of a single-base mismatch are measured.

Based on the currents obtained with the variation of spacer height, it may be the case that if the spacer is too close to the surface, our signals are no longer DNA-mediated. This is likely what is occurring with the 50 μm spacer, with which we do not see mismatch discrimination. The spacer that provides large currents while maintaining

DNA-mediated CT, as confirmed by mismatch discrimination, is the 127 μm spacer, which was therefore used for all experiments.

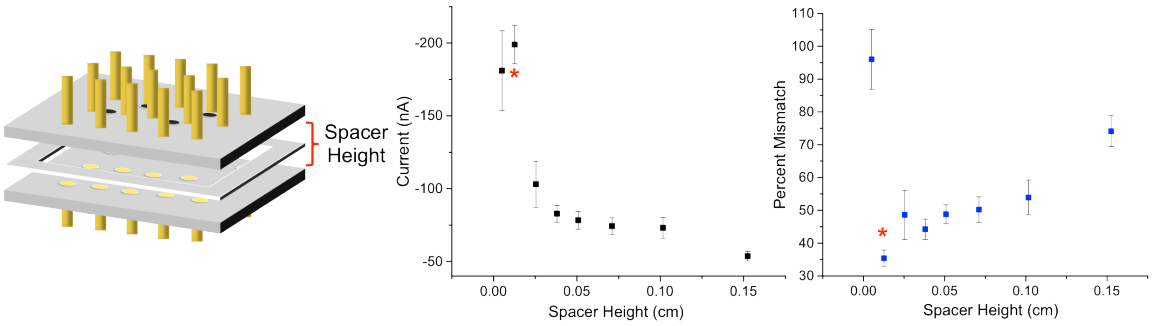

Figure 5.6 Optimizing the spacer height. Eight Teflon spacers of different heights were tested for electrochemical signal and mismatch discrimination. The spacer between the two electrode arrays establishes the gap between the two electrodes (left). The current from constant current amperometry obtained as a function of spacer height (center) is maximized with the 127 µm spacer (red asterisk). Mismatch discrimination as a function of spacer height (right) is reported as a ratio of the mismatched signal to the well matched signal, with maximal discrimination also observed with the 127 µm spacer (red asterisk). All electrochemistry was conducted in Tris buffer (10 mM Tris, 100 mM KCl, 2.5 mM $MgCl_2$, 1 mM $CaCl_2$, pH 7.6) with 4 µM methylene blue and 300 µM $K_3[Fe(CN)_6]$. 18-mer well matched and mismatched DNA was used.

As illustrated in Figure 5.7, we have also confirmed that our system functions as a collector-generator with both ferrocyanide and ferricyanide, which is important to ensure that time-resolved changes to the system are sensitively monitored.[41, 42] To test the collector-generator capabilities of the platform, generally the current at the secondary electrode is constantly monitored with an applied positive potential. Preliminarily, no potential is applied to the primary. After 15 seconds, a negative potential is applied to the DME. This causes a large amount of current to be immediately generated at the secondary electrode by electrocatalysis at the primary electrode. This initial burst of current, due to the rapid dissociation of a large amount of methylene blue that was intercalated into the DNA, depletes to a steady-state current as a cycle is established (Figure 5.7). When the secondary electrode is held at a positive, oxidizing potential and ferricyanide is used (Figure 5.7a), no current is evident before the potential is applied to the primary electrode. When ferrocyanide is monitored without a potential applied to the primary electrode, a small current is observed at the secondary electrode due to the preliminary oxidation of ferrocyanide to ferricyanide (Figure 5.7b). However, this small current quickly decreases as the ferrocyanide is depleted in the absence of DNA CT at the primary electrode. Once a potential is applied to the primary electrode with either ferricyanide or ferrocyanide, current is generated. This behavior mimics characteristic behavior of SECM substrates modified with a conductive film,[43-47] indicating that the DNA film on the primary electrode is conductive (due to DNA CT) and is responsible for the current output at the secondary electrode.

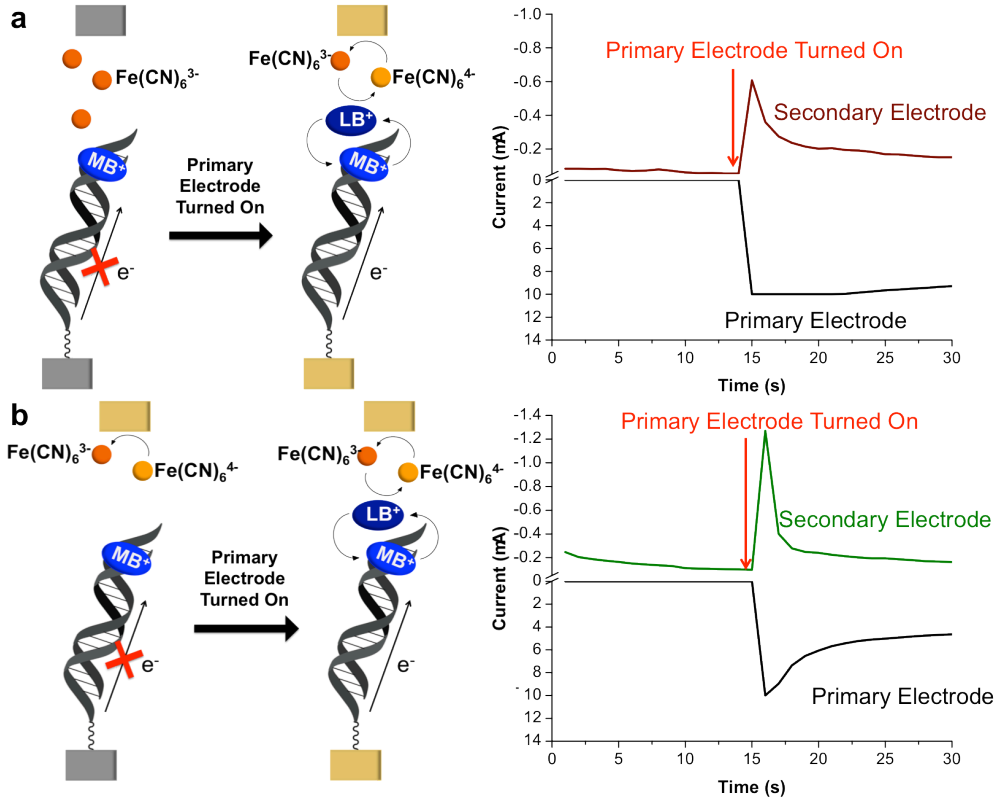

Figure 5.7 Detection strategy (*left*) and constant-potential amperometry assay (*right*) for DNA CT using the two-electrode detection platform. Electrochemical readout is carried out at a single, addressable electrode in the secondary array held at +0.35 V. In (**a**), the thin layer between the primary and secondary electrode arrays contains 4 μM MB and 300 μM $Fe(CN)_6^{3-}$. Because the applied potential is positive of the $Fe(CN)_6^{3-/4-}$ redox couple, there is no initial current (shown in red) at the secondary electrode. 15 seconds into the experiment, the entire primary electrode array (current shown in black) is activated at a potential of -0.40 V. This initiates the MB/$Fe(CN)_6^{3-}$ electrocatalytic cycle, and current begins to flow at the secondary electrode due to the re-oxidation of $Fe(CN)_6^{4-}$ generated at the primary array. For sensing applications, readout at the secondary electrode is measured only after a steady-state current is achieved (~ 30 s) to eliminate any complications arising from double-layer charging effects. The lower panel (**b**) shows the analogous experiment, except that the thin-layer solution initially contains 4 μM MB and 300 μM $Fe(CN)_6^{4-}$. When the secondary electrode is turned on at time zero, there is an initial current (shown in green) due to the oxidation of $Fe(CN)_6^{4-}$ to $Fe(CN)_6^{3-}$. This current rapidly approaches zero as the $Fe(CN)_6^{4-}$ is converted to $Fe(CN)_6^{3-}$ within the thin layer. At the 15-s mark, the primary array is turned on, and the assay proceeds as in (**a**).

Single-Base Mismatch Detection with Non-covalent and Covalent Redox Probes

The collector-generator experiment provides evidence that our DNA films are conductive, consistent with DNA CT processes. However, the key experiment demonstrating that this electrochemical process is mediated by transport through the DNA helix is electrochemical signal attenuation upon incorporation of a single-base mismatch. Single-base mismatch discrimination was previously discussed in the context of catalyst activation with detection at the primary electrode and spacer height. Additionally, evaluation of mismatches in DNA monolayers with detection at the secondary electrode was also tested with catalyst activation at both the primary and secondary electrodes. For this analysis, well matched and mismatched DNA monolayers were formed and evaluated side-by-side on the same electrode array with copper catalyst activation at either the primary or secondary electrode. Electrochemical responses were measured by constant potential amperometry with 4 μM MB and 300 μM ferricyanide for a time previously optimized to reach a steady-state current, 90 s.[33]

When constant potential amperometry is conducted from the secondary electrode, the advantages of both catalyst activation and electrochemical readout from this electrode are evident. The difference in current between well-matched and mismatched signals is large, and the current readout is very robust for monolayers formed by copper activation from a secondary electrode (Figure 5.8). In contrast, when monolayers are formed by copper activation from the primary electrode, the current is small, and mismatch discrimination is poor. The differences observed in signal size, consistency, and mismatch discrimination highlight the importance of catalyst activation from the secondary electrode. Furthermore, large signal differences obtained from secondary

electrode readout obviate the need for dramatic background subtractions, essentially providing an on/off sensor for mismatch detection.

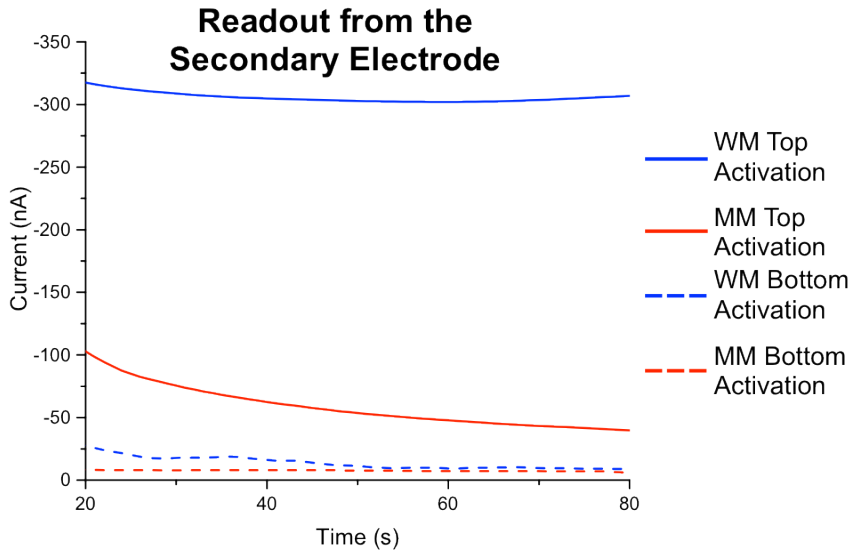

Figure 5.8 Mismatch detection with electrochemical readout at the secondary electrode. Constant-potential amperometry was conducted at the secondary electrodes with an applied potential of +0.35 V, while the primary-electrodes were held at -0.40 V in the presence of 4 μM MB and 300 μM $Fe(CN)_6^{3-}$. The blue traces represent currents measured at readout electrodes complementary to well-matched DNA sequences (18-mers) on the primary array, while the red traces represent the analogous currents generated at electrodes complementary to mismatched duplexes. For comparison (dashed lines), the identical assay was carried out on a separate array in which the DNA duplexes were conjugated *via* copper(II) activation directly at the primary electrodes; clearly, greater signal differential between well- *vs,* mismatched sequences occurs when monolayers are formed by catalyst activation at the secondary electrode. In these experiments, all primary-array electrodes were first modified with an underlying 50/50 azide/phosphate monolayer before DNA conjugation.

Additionally, we have investigated detection on this platform with a covalent redox probe, which may be favorable for some biomolecule detection applications. Nile Blue, a covalent reporter that is electronically conjugated to the DNA π-stack through the linker,[34] was found to successfully participate in electrocatalytic turnover, resulting in significant mismatch discrimination despite being covalently tethered to DNA (Figure 5.9). A 60±10% decrease in the current upon incorporation of a single base mismatch occurs with the covalent Nile blue redox probe, as compared to an 80±10% decrease with noncovalent methylene blue. This difference in mismatch discrimination is likely due to the fact that noncovalent methylene blue is not limited to one association per DNA, nor is it conformationally or spatially constrained as is the covalent Nile Blue. It is therefore unsurprising that MB yields larger signals and larger differential. This result is consistent with previous electrocatalytic mismatch discrimination, in which larger differentials are observed with free probes than with covalent probes.

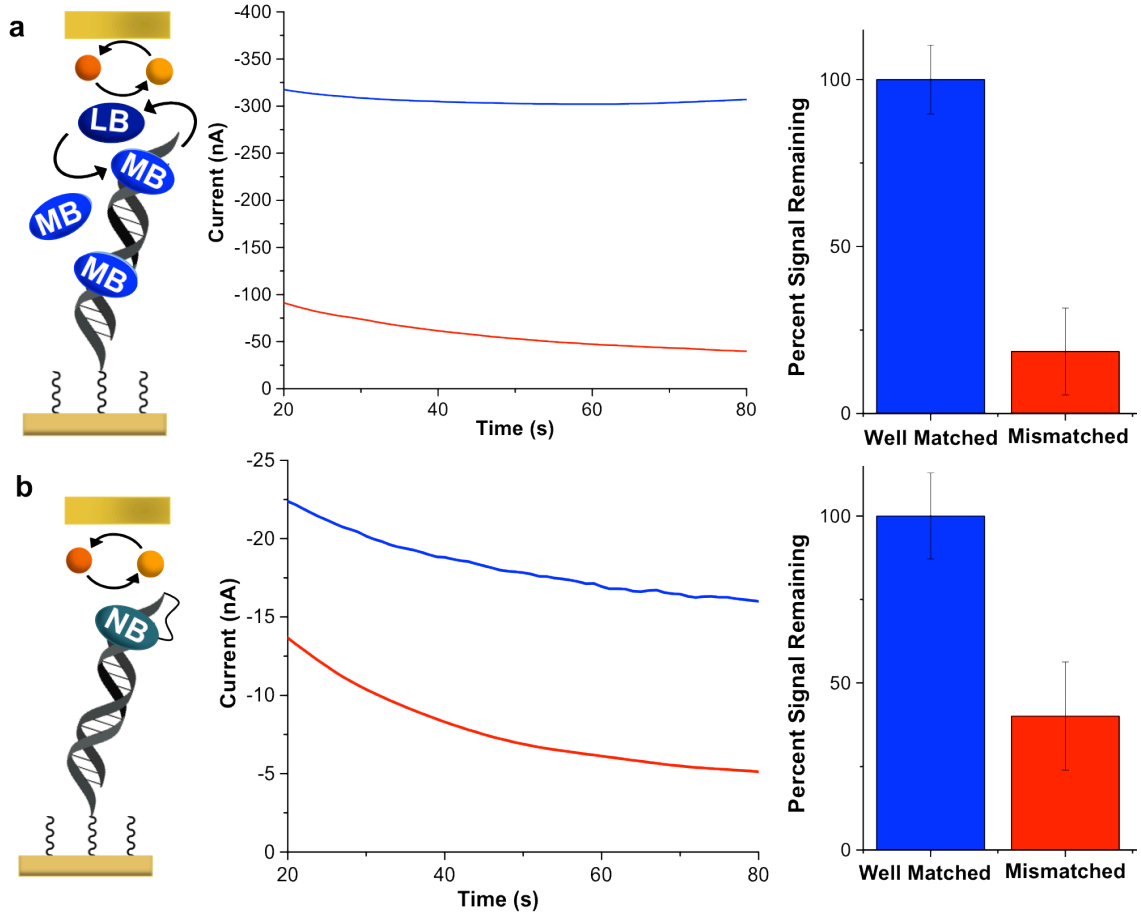

Figure 5.9 Comparison of mismatch discrimination recorded with the two-electrode platform using methylene blue *vs.* Nile blue redox reporters. (**a**) Electrochemical readout recorded at a secondary electrode during the electrocatalytic reduction of 400 μM $Fe(CN)_6^{3-}$ in the presence of 4 μM MB at primary electrodes modified with well-matched DNA duplexes (blue), and mismatched DNA duplexes (red). (**b**) The same assay, but with Nile blue covalently bound to the DNA probe sequences substituting for MB. Percent signal changes were calculated from the amperometry data recorded 90 seconds after initiation of the electrochemical readout.

Detection of DNA-binding Proteins

To establish the relevance of this platform for biomolecule detection, DNA-binding protein detection was also investigated with two transcription factors, TBP and CopG. Both bind to specific sequences of DNA, kink the duplex to a large degree, and are therefore capable of attenuating CT. The transcription factor TBP, TATA-binding protein, a subunit of the eukaryotic TFIID transcription factor, was previously employed as a measure of sensitivity for a DNA CT-based protein detection platform.[34, 48] This protein kinks DNA by over 80° when bound to its TATA target sequence with a K_D of 3.3 nM,[49] destacking the DNA bases and attenuating DNA CT.[20] Detection limits in the concentration range of the K_D support that a platform is sufficiently sensitive to detect protein binding. In the past, we have utilized covalent redox probes for protein detection, but the ease of detection with our two-electrode platform allows simple discrimination with non-covalent MB.

The multiplexed nature of our platform further enables the specific detection of multiple proteins simultaneously.We therefore additionally investigated the detection of the transcription repressor CopG, which binds DNA as a tetramer at an ACGTxxxxxACGT site, bending the helix up to 120°, with a nM binding affinity.[50-52] Each of these proteins was individually titrated onto monolayers to determine detection limits. Subsequently, specific detection of these proteins on the same multiplexed array was performed.

The titrations (Figure 5.10) indicate significant signal decreases, greater than 30%, associated with binding of both proteins at very low concentrations (10 nM), which, based on our extremely small volumes, translates to less than 50 femtomoles of protein.

From these titration curves, dissociation constants can be calculated for both proteins on our DMEs using a cooperative binding model (Hill model).[20] TBP has a surface K_D of 14±2 nM, and CopG has a surface K_D of 17±4 nM. Both TBP and CopG are therefore detectable at concentrations near their solution K_D's (3.3 nM and 10 nM, respectively).

We additionally specifically and selectively detected both of these proteins on the same multiplexed array. Each transcription factor was added to the array modified with three electrodes containing a non-binding sequence, six electrodes modified with DNA containing a TBP binding site, and six electrodes modified with DNA containing a CopG binding site. In this assay, one protein (either TBP or CopG) is added to the surface. Signal attenuation is then measured and compared to the non-binding sequence (the positive control). The surface is subsequently rinsed, and the second protein is added with measurement of the signal attenuation. In all cases, signal attenuation is only observed at DNA containing the binding sequence of the protein added, verifying changes are only due to the specific binding of a particular protein. Greater variability between protein detection experiments is observed in the dual protein detection experiments, as compared to the individual titrations, likely because of the added normalization of these data to a non-binding positive control sequence. This additional normalization is necessary for combined protein experiments to confirm that signal decreases are due to specific binding of one of the proteins.

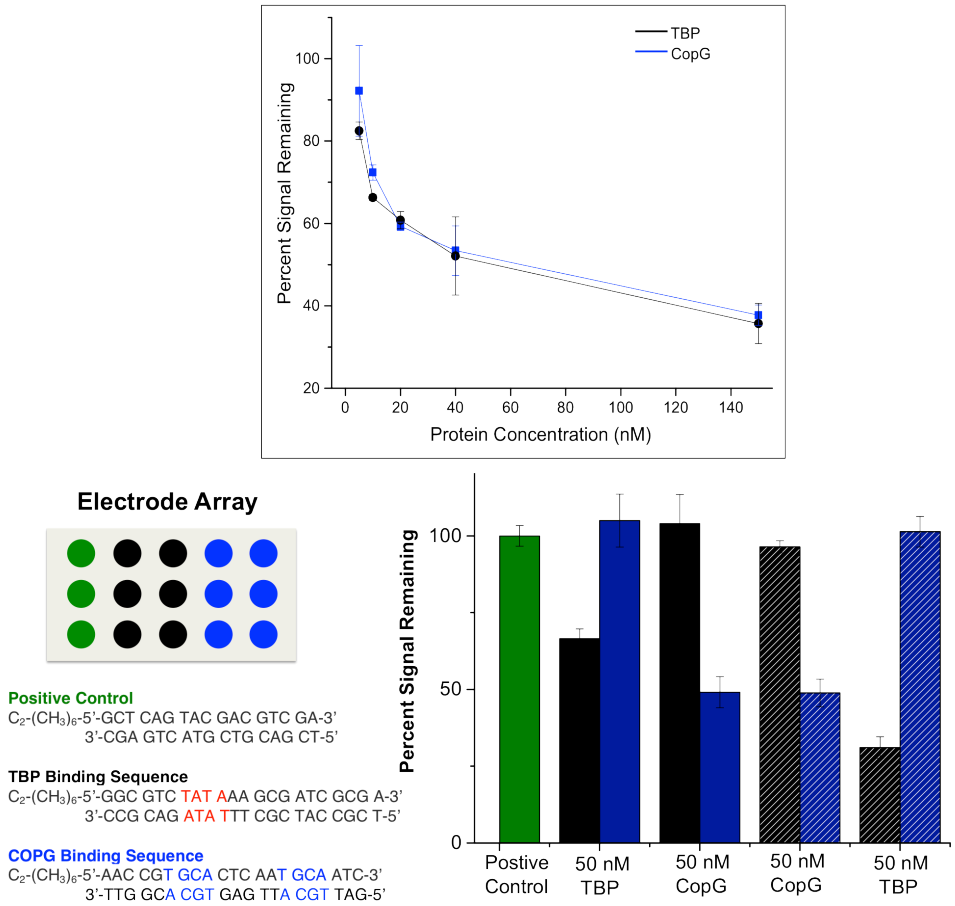

Figure 5.10 Titration of transcription factors TATA-binding protein (TBP) and CopG on two-electrode array. Each protein was titrated onto an array in concentrations ranging from 0 nM to 150 nM. Shown (top) is the percent electrochemical signal remaining from constant potential amperometry plotted as a function of protein concentration. The proteins caused significant signal decreases on the arrays in very low nanomolar concentrations. All electrochemistry was conducted in Tris buffer (10 mM Tris, 100 mM KCl, 2.5 mM $MgCl_2$, 1 mM $CaCl_2$, pH 7.6) with 4 μM methylene blue and 300 μM $K_3[Fe(CN)_6]$. Constant potential amperometry at the secondary electrode was conducted with an applied potential of 350 mV v. AgCl/Ag to the secondary electrode and -400 mV v. AgCl/Ag to the primary electrode for 90 seconds. Specific detection of transcription factors TBP and CopG on a single array is also shown (bottom right). Arrays are formed with six electrodes modified with DNA containing specific binding sites for each of the transcription factors TBP and CopG, as well as three electrodes containing positive control DNA that does not contain the binding site for either protein. A single protein was added to the surface at a 50 nM concentration, and the signal decrease for each sequence was monitored. The second protein was subsequently added, and signal decreases monitored. TBP detection followed by CopG detection is shown with solid bars, while CopG detection followed by TBP detection is shown with dashed bars. The

TBP binding sequence is represented by black, both in terms of the location of the electrodes modified with this sequence on the electrode array (bottom left, black circles) and in terms of the percent signal remaining for this sequence (bottom right, black bars). Independent of which protein was added first, signal decreases were only observed on the sequences to which the specific protein binds.

Implications

Although the copper(I)-catalyzed Huisgen cycloaddition[21] is attractive for biomolecule modification because of its bioorthogonality, issues with this reaction for DNA-based applications arise due to the instability of copper(I) complexes in aqueous solutions as well as their potential reactivity with DNA. One strategy to mitigate these complications is to generate Cu(I) *in situ* through electrochemical reduction of a more inert Cu(II) complex, although complications with this method may still arise (Figures 5.2, 5.4 and 5.8). These difficulties are easily surmounted, though, through the electrochemical activation of $[Cu(phendione)_2]^{2+}$ from a secondary working electrode, which minimizes the interference of degraded catalyst with the DNA film, as the copper precipitates on the bare, secondary electrode. Any catalyst precipitate on the secondary electrode array is easily removed through polishing prior to application of this array for detection.

In addition to enabling the formation of superior DNA monolayers, the second working electrode facilitates sensitive detection without the need for background corrections. In contrast to electrocatalytic signal amplification detected at the DME, in which amplification is limited by depletion of the local concentration of ferricyanide, a secondary electrode sufficiently close to the DME removes the dependence of the signal amplification on the diffusion of additional ferricyanide. As we demonstrate, this platform (Figures 5.1, 5.2) behaves as a collector-generator with either ferricyanide or ferrocyanide (Figure 5.7). Furthermore, large background corrections are unnecessary, as current only flows from the primary to the secondary electrode when a redox probe is reduced by DNA CT, and the current generated at the secondary electrode is wholly

dependent on the amount of DNA CT occurring at the primary electrode surface. Our signals were also confirmed to be DNA mediated through the detection of a single-base mismatch. Both covalent (Nile blue) and noncovalent (methylene blue) redox probes coupled to electrocatalytic signal amplification yielded significant signal attenuation upon incorporation of a single-base mismatch when probed from the secondary electrode by constant potential amperometry (Figures 5.8, 5.9).

For any nucleic acid platform, monitoring protein binding is an especially difficult challenge due to the required sensitivity and specificity, as well as the often-small signal differentials associated with binding. DNA CT-based platforms offer a unique opportunity for such detection, as proteins that destack DNA bases upon binding yield significant decreases in electrochemical signals. However, there is no guarantee that such detection is translatable to a two working electrode platform. In fact, we observe that this platform does enable the determination of sensitive and specific protein binding, both of a previously reported transcription factor, TBP, and a similar transcription factor, CopG, whose binding had not been previously evaluated by DNA CT. Indeed, we successfully detect femtomoles of both proteins at concentrations near their dissociation constants sequence-specifically.

The Two-Working Electrode Platform

Here, we have described an especially sensitive multiplexed, two working electrode platform for DNA CT-based electrochemical detection. This platform enables low density DNA monolayer formation and amplified electrochemical readout through the incorporation of a second working electrode. Catalyst activation at a secondary

electrode is essential to maintain the integrity of the DNA, as shown by EIS, CV, and constant potential amperometry. Detection from the secondary electrode is similarly necessary to provide high sensitivity without large background signals. These signals have further been confirmed to be DNA mediated by mismatch discrimination experiments. Importantly, this platform is capable of specifically detecting femtomoles of the transcription factors, TBP and CopG. This multiplexed, two-electrode detection platform thus broadens the scope and applications for detection using DNA CT.

References

1. Das, J., Cederquist, K. B., Zaragoza, A. A., Lee, P. E., Sargent, E. H., and Kelley, S. O. (2012) An ultrasensitive universal detector based on neutralizer displacement, *Nat. Chem. 4*, 642-648.

2. Gooding, J. J. (2002) Electrochemical DNA Hybridization Biosensors, *Electroanalysis 14*, 1149-1156.

3. Kelley, S. O., Mirkin, C. A., Walt, D. R., Ismagilov, R. F., Toner, M., and Sargent, E. H. (2014) Advancing the speed, sensitivity and accuracy of biomolecular detection using multi-length-scale engineering, *Nat. Nanotechnol. 9*, 969-980.

4. Lam, J. C. F., Aguirre, S., and Li, Y. (2010) Nucleic Acids as Detection Tools, In *The Chemical Biology of Nucleic Acids*, pp 401-431, John Wiley & Sons, Ltd.

5. Liu, J., Cao, Z., and Lu, Y. (2009) Functional nucleic acid sensors, *Chem. Rev. 109*, 1948-1998.

6. Pei, H., Lu, N., Wen, Y., Song, S., Liu, Y., Yan, H., and Fan, C. (2010) A DNA nanostructure-based biomolecular probe carrier platform for electrochemical biosensing, *Adv. Mater. 22*, 4754-4758.

7. Soleymani, L., Fang, Z., Sun, X., Yang, H., Taft, B. J., Sargent, E. H., and Kelley, S. O. (2009) Nanostructuring of patterned microelectrodes to enhance the sensitivity of electrochemical nucleic acids detection, *Angew. Chem. Int. Ed. 48*, 8457-8460.

8. Wang, J. (2002) Electrochemical nucleic acid biosensors, *Anal. Chim. Acta 469*, 63-71.

9. Yang, H., Hui, A., Pampalakis, G., Soleymani, L., Liu, F. F., Sargent, E. H., and Kelley, S. O. (2009) Direct, electronic microRNA detection for the rapid determination of differential expression profiles, *Angew. Chem. Int. Ed. 48*, 8461-8464.

10. Gorodetsky, A. A., Buzzeo, M. C., and Barton, J. K. (2008) DNA-mediated electrochemistry, *Bioconjug. Chem. 19*, 2285-2296.

11. Drummond, T. G., Hill, M. G., and Barton, J. K. (2003) Electrochemical DNA sensors, *Nat. Biotechnol. 21*, 1192-1199.

12. Furst, A., Hill, M. G., and Barton, J. K. (2014) Electrocatalysis in DNA Sensors, *Polyhedron 84*, 150-159.

13. Muren, N. B., Olmon, E. D., and Barton, J. K. (2012) Solution, surface, and single molecule platforms for the study of DNA-mediated charge transport, *Phys. Chem. Chem. Phys. 14*, 13754-13771.

14. Abi, A., and Ferapontova, E. E. (2012) Unmediated by DNA electron transfer in redox-labeled DNA duplexes end-tethered to gold electrodes, *J. Am. Chem. Soc. 134*, 14499-14507.

15. Kelley, S. O., Jackson, N. M., Hill, M. G., and Barton, J. K. (1999) Long-Range Electron Transfer through DNA Films, *Angew. Chem. Int. Ed. 38*, 941-945.

16. Levicky, R., Herne, T. M., Tarlov, M. J., and Satija, S. K. (1998) Using Self-Assembly To Control the Structure of DNA Monolayers on Gold: A Neutron Reflectivity Study, *J. Am. Chem. Soc. 120*, 9787-9792.

17. Murphy, J. N., Cheng, A. K., Yu, H. Z., and Bizzotto, D. (2009) On the nature of DNA self-assembled monolayers on Au: measuring surface heterogeneity with electrochemical in situ fluorescence microscopy, *J. Am. Chem. Soc. 131*, 4042-4050.

18. Ricci, F., Lai, R. Y., Heeger, A. J., Plaxco, K. W., and Sumner, J. J. (2007) Effect of molecular crowding on the response of an electrochemical DNA sensor, *Langmuir 23*, 6827-6834.

19. Sam, M., Boon, E. M., Barton, J. K., Hill, M. G., and Spain, E. M. (2001) Morphology of 15-mer duplexes tethered to Au(111) probed using scanning probe microscopy, *Langmuir 17*, 5727-5730.

20. Furst, A. L., Hill, M. G., and Barton, J. K. (2013) DNA-modified electrodes fabricated using copper-free click chemistry for enhanced protein detection, *Langmuir 29*, 16141-16149.

21. Huisgen, R., Grashey, R., and Sauer, J. (2010) Cycloaddition reactions of alkenes, In *The Alkenes (1964)*, pp 739-953, John Wiley & Sons, Ltd.

22. Collman, J. P., Devaraj, N. K., and Chidsey, C. E. (2004) "Clicking" functionality onto electrode surfaces, *Langmuir 20*, 1051-1053.

23. Gerasimov, J. Y., and Lai, R. Y. (2011) Design and characterization of an electrochemical peptide-based sensor fabricated via"click" chemistry, *Chem. Commun. 47*, 8688-8690.

24. Kazakov, S. A., Astashkina, T. G., Mamaev, S. V., and Vlassov, V. V. (1988) Site-specific cleavage of single-stranded DNAs at unique sites by a copper-dependent redox reaction, *Nature 335*, 186-188.

25. Meijler, M. M., Zelenko, O., and Sigman, D. S. (1997) Chemical Mechanism of DNA Scission by (1,10-Phenanthroline)copper. Carbonyl Oxygen of 5-Methylenefuranone Is Derived from Water, *J. Am. Chem. Soc. 119*, 1135-1136.

26. Shuman, M. S., and Woodward, G. P. (1977) Stability constants of copper-organic chelates in aquatic samples, *Environmental Science & Technology 11*, 809-813.

27. Canete, S. J., and Lai, R. Y. (2010) Fabrication of an electrochemical DNA sensor array via potential-assisted "click" chemistry, *Chem. Commun. 46*, 3941-3943.

28. Devaraj, N. K., Dinolfo, P. H., Chidsey, C. E., and Collman, J. P. (2006) Selective functionalization of independently addressed microelectrodes by electrochemical activation and deactivation of a coupling catalyst, *J. Am. Chem. Soc. 128*, 1794-1795.

29. Devaraj, N. K., Miller, G. P., Ebina, W., Kakaradov, B., Collman, J. P., Kool, E. T., and Chidsey, C. E. (2005) Chemoselective covalent coupling of oligonucleotide probes to self-assembled monolayers, *J. Am. Chem. Soc. 127*, 8600-8601.

30. Ripert, M., Farre, C., and Chaix, C. (2013) Selective functionalization of Au electrodes by electrochemical activation of the "click" reaction catalyst, *Electrochimica Acta 91*, 82-89.

31. Furst, A., Landefeld, S., Hill, M. G., and Barton, J. K. (2013) Electrochemical patterning and detection of DNA arrays on a two-electrode platform, *J. Am. Chem. Soc. 135*, 19099-19102.

32. Quinton, D., Maringa, A., Griveau, S., Tebello, N., and Bedioui, F. (2013) Surface patterning using scanning electrochemical microscopy to locally trigger a "click" chemistry reaction, *Electrochem. Commun. 31*, 112-115.

33. Furst, A. L., Muren, N. B., Hill, M. G., and Barton, J. K. (2014) Label-free electrochemical detection of human methyltransferase from tumors, *Proc. Natl. Acad. Sci. USA 111*, 14985-14989.

34. Gorodetsky, A. A., Ebrahim, A., and Barton, J. K. (2008) Electrical detection of TATA binding protein at DNA-modified microelectrodes, *J. Am. Chem. Soc. 130*, 2924-2925.

35. Hong, V., Presolski, S. I., Ma, C., and Finn, M. G. (2009) Analysis and optimization of copper-catalyzed azide-alkyne cycloaddition for bioconjugation, *Angew. Chem. Int. Ed. 48*, 9879-9883.

36. Ceres, D. M., Udit, A. K., Hill, H. D., Hill, M. G., and Barton, J. K. (2007) Differential ionic permeation of DNA-modified electrodes, *J. Phys. Chem. B 111*, 663-668.

37. Janek, R. P., Fawcett, W. R., and Ulman, A. (1998) Impedance spectroscopy of self-assembled monolayers on Au(111): Sodium ferrocyanide charge transfer at modified electrodes, *Langmuir 14*, 3011-3018.

38. Bard, A., and Faulkner, L. (2001) *Electrochemical Methods: Fundamentals and Applications*, John Wiley & Sons, Inc.

39. Boon, E. M., Barton, J. K., Bhagat, V., Nersissian, M., Wang, W., and Hill, M. G. (2003) Reduction of Ferricyanide by Methylene Blue at a DNA-Modified Rotating-Disk Electrode, *Langmuir 19*, 9255-9259.

40. Kafka, J., Pänke, O., Abendroth, B., and Lisdat, F. (2008) A label-free DNA sensor based on impedance spectroscopy, *Electrochimica Acta 53*, 7467-7474.

41. Fernandez, J. L., and Bard, A. J. (2003) Scanning electrochemical microscopy. 47. Imaging electrocatalytic activity for oxygen reduction in an acidic medium by the tip generation-substrate collection mode, *Anal. Chem. 75*, 2967-2974.

42. Martin, R. D., and Unwin, P. R. (1998) Theory and Experiment for the Substrate Generation/Tip Collection Mode of the Scanning Electrochemical Microscope:â€‰ Application as an Approach for Measuring the Diffusion Coefficient Ratio of a Redox Couple, *Anal. Chem. 70*, 276-284.

43. Liu, B., Bard, A. J., Li, C. Z., and Kraatz, H. B. (2005) Scanning electrochemical microscopy. 51. Studies of self-assembled monolayers of DNA in the absence and presence of metal ions, *J. Phys. Chem. B 109*, 5193-5198.

44. Turcu, F., Schulte, A., Hartwich, G., and Schuhmann, W. (2004) Label-free electrochemical recognition of DNA hybridization by means of modulation of the feedback current in SECM, *Angew. Chem. Int. Ed. 43*, 3482-3485.

45. Wain, A. J., and Zhou, F. (2008) Scanning electrochemical microscopy imaging of DNA microarrays using methylene blue as a redox-active intercalator, *Langmuir 24*, 5155-5160.

46. Whitworth, A. L., Mandler, D., and Unwin, P. R. (2005) Theory of scanning electrochemical microscopy (SECM) as a probe of surface conductivity, *Phys. Chem. Chem. Phys. 7*, 356-365.

47. Wierzbinski, E., Arndt, J., Hammond, W., and Slowinski, K. (2006) In situ electrochemical distance tunneling spectroscopy of ds-DNA molecules, *Langmuir 22*, 2426-2429.

48. Boon, E. M., Salas, J. E., and Barton, J. K. (2002) An electrical probe of protein-DNA interactions on DNA-modified surfaces, *Nat. Biotechnol. 20*, 282-286.

49. Hahn, S., Buratowski, S., Sharp, P. A., and Guarente, L. (1989) Yeast TATA-binding protein TFIID binds to TATA elements with both consensus and nonconsensus DNA sequences, *Proc. Natl. Acad. Sci. USA 86*, 5718-5722.

50. del Solar, G., Albericio, F., Eritja, R., and Espinosa, M. (1994) Chemical synthesis of a fully active transcriptional repressor protein, *Proc. Natl. Acad. Sci. USA 91*, 5178-5182.

51. del Solar, G. H., de al Campa, A. G., Perez-Martin, J., Choli, T., and Espinosa, M. (1989) Purification and characterization of RepA, a protein involved in the copy number control of plasmid pLS1, *Nucleic Acids Res. 17*, 2405-2420.

52. Gomis-Ruth, F. X., Sola, M., Acebo, P., Parraga, A., Guasch, A., Eritja, R., Gonzalez, A., Espinosa, M., del Solar, G., and Coll, M. (1998) The structure of plasmid-encoded transcriptional repressor CopG unliganded and bound to its operator, *EMBO J. 17*, 7404-7415.

Chapter 6

DNA Electrochemistry shows DNMT1 Methyltransferase Hyperactivity in Colorectal Tumors

Adapted from: Furst, A. L., and Barton, J. K. (2015) DNA Electrochemistry shows DNMT1 Methyltransferase Hyperactivity in Colorectal Tumors, *Submitted.*

Introduction

Colorectal cancer is the third most prevalent cancer worldwide, causing approximately 700,000 mortalities annually.[1] The investigation into the causes of this disease is especially important, as its diagnosis is on the rise among people under the age of 50, and one of the major causes of mortality from colorectal cancer is metastasis due to its late detection.[2] Many molecular factors have been found to contribute to the onset of this disease including a host of genetic mutations[3-6] and epigenetic modifications,[7-10] as well as the inactivation of DNA repair pathways.[11-13]

While many factors likely contribute to the initiation and development of colorectal cancer, epigenetic modifications are of special interest, as they are connected to the progression of a variety of cancers.[14, 15] DNA methylation in particular has garnered significant interest, as aberrant DNA methylation has been found to be a hallmark of many cancers,[16, 17] including colorectal cancer.[18] Both hypermethylation and hypomethylation are linked to tumorogenesis. However, genomic hypermethylation in particular is often found in colorectal cancer and has been linked to the methylation of tumor suppressor genes and genes that control the translation of DNA repair proteins, leading to their silencing and therefore tumorigenesis.[3, 19, 20]

In humans, there are two classes of methyltransferases: *de novo* methyltransferases (DNMT3a, DNMT3b, and DNMT3L) and maintenance methyltransferases (DNMT1). *De novo* methyltransferases are in relatively low copy number and are responsible for establishing methylation patterns on the genome, meaning that they have a large preference for unmodified DNA.[21] In contrast, DNMT1, the most abundant mammalian methyltransferase, is a maintenance methyltransferase responsible

for transferring the genomic methylation pattern from the parent DNA strand to the daughter strand during DNA replication.[22] Because of its vital role in maintaining genomic methylation patterns during DNA replication, DNMT1 may be important in these molecular transformations within the cell that lead to the development of colorectal cancer.

Despite the potential importance of DNMT1 activity in disease initiation and progression, there is currently no clinical test for its activity. Generally, quantitative PCR (qPCR), which can be used to quantify gene expression of this protein, is used as a correlative measurement for the total amount of DNMT1 present.[23] Other methods, such as bisulfite sequencing,[24, 25] are used to detect specific, disease-relevant methylation patterns for early clinical diagnosis. However, such techniques are very costly and have limited efficacy.[26] In order to obtain a direct measure of methyltransferase activity, the current laboratory gold standard involves radiolabeling DNA with a tritium-labeled methyl group.[27] This assay not only produces relatively high variability but also requires the use of radioactivity and specialized instrumentation for measurement, making it impractical for clinical use.

We have previously developed an electrochemical method for the assessment of DNMT1 activity from crude cultured cell and tissue lysate.[28] This assay is conducted on a multiplexed, two working electrode platform (Figure 6.1) that enables electrochemical readout from disperse DNA monolayers with signal amplification and no necessary background correction. Using this platform, low-density DNA monolayers are formed through electrochemical activation of an inert copper precatalyst into an active catalyst.[29]

Electrochemical readout is accomplished through the measurement of current generated from a catalytic cycle.

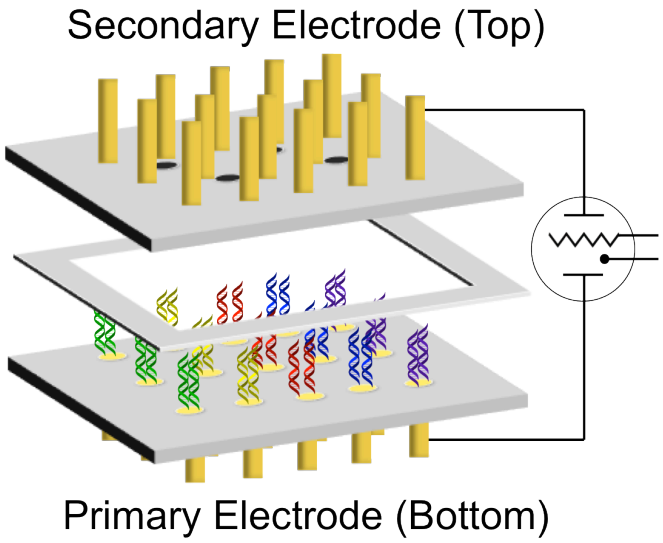

Figure 6.1 Electrochemical array for DNMT1 activity detection. The array contains two sets of fifteen gold electrodes, each embedded in a Teflon plate. Each electrode has a 1 mm diameter. The two complementary Teflon arrays are assembled with a 150 μm spacer between them, which was previously determined to be the optimal distance such that signals are not diffusion-limited.[28] The electrodes of the primary (bottom) array are modified with DNA of the desired sequences such that DNA-mediated charge transport is detectable. The electrodes of the secondary (top) array are bare for electrochemical detection.

In this cycle, DNA-mediated charge transport reduces an intercalative redox probe, methylene blue, to leucomethylene blue. This form of the probe has a reduced affinity for DNA, destacking from the helix and entering solution. In solution, leucomethylene blue reduces the ferricyanide electron sink to ferrocyanide, in turn becoming reoxidized to methylene blue. Amplified DNA-mediated electrochemical signals are generated without necessitating background correction through the detection of the current generated from the reoxidation of ferrocyanide at the secondary electrode array, which is proportional to the amount of ferrocyanide present (Figure 6.2). This cycling enables significant signal amplification, leading to very sensitive detection. This array combined with an electrochemical methyltransferase assay enables rapid detection, and requires no background correction or complex instrumentation. This assay requires only 500 μg of tissue per electrode, which is a significantly smaller sample than is currently removed with a biopsy.[28]

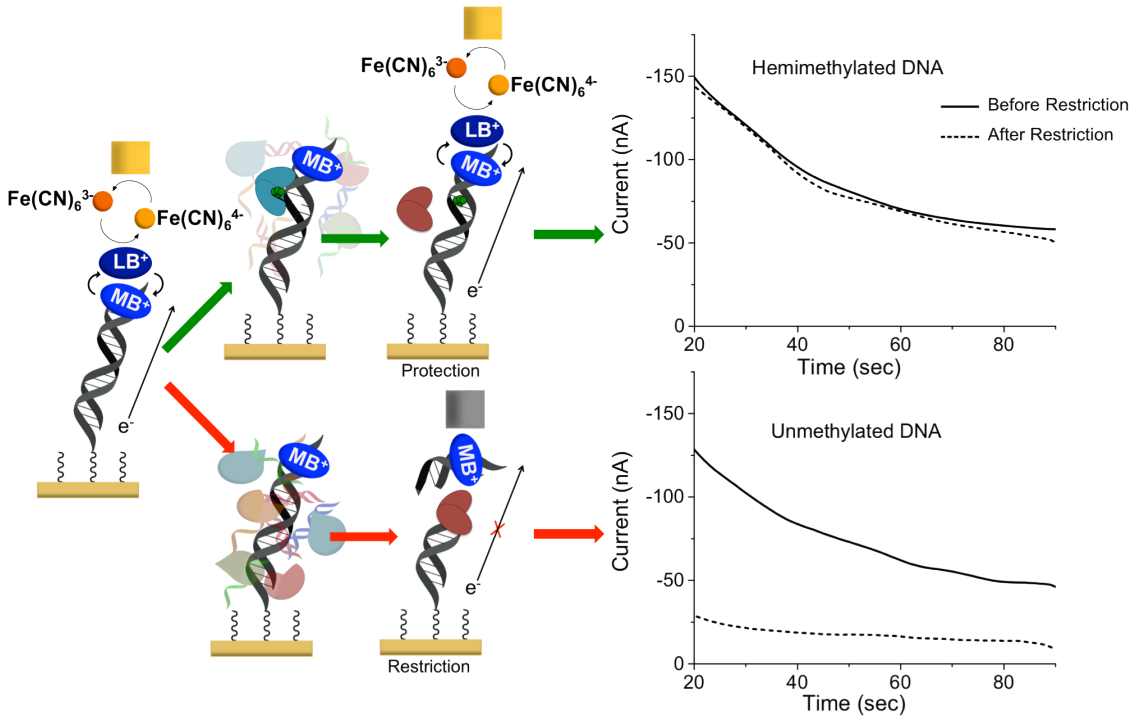

Figure 6.2 Signal-on electrochemical assay for DNMT1 detection. Left: The bottom (primary) electrode modified with a dilute DNA monolayer is responsible for generating electrochemical signals through DNA-mediated charge transport (CT) amplified by electrocatalysis. Methylene blue, a DNA intercalating redox probe, is reduced by DNA CT and enters solution as leucomethylene blue, where it can interact with an electron sink, ferricyanide. Upon interaction with leucomethylene blue, ferricyanide is reduced to ferrocyanide, reoxidizing the leucomethylene blue to methylene blue in the process. Current is generated and detected at the secondary electrode from the reoxidation of ferrocyanide. The current generated is proportional to the amount of ferrocyanide oxidized. To detect DNMT1, crude lysate is added to the electrode. If DNMT1 (blue) is capable of methylating DNA (green arrow), the DNA on the electrode becomes fully methylated. If the protein is not active, the DNA remains hemimethylated or unmethylated (red arrow). A methylation-specific restriction enzyme (*BssH*II) is then added that cuts the unmethylated or hemimethylated DNA (red arrow), significantly attenuating the electrochemical signal, while leaving the fully methylated DNA (green arrow) untouched. Constant potential amperometry (right) is used to measure the percent change before and after restriction enzyme treatment. If the restriction enzyme does not affect the DNA (top), the signals overlay. If, however, the restriction enzyme cuts the DNA, the signal is significantly attenuated (bottom). Constant potential amperometry is run for 90 s with a 320 mV potential applied to the secondary electrode and a -400 mV potential applied to the primary electrode relative to an AgCl/Ag reference. All scans are in Tris buffer (10 mM Tris, 100 mM KCl, 2.5 mM $MgCl_2$, 1 mM $CaCl_2$, pH 7.6) with 4 μM methylene blue and 300 μM potassium ferricyanide.

Using this platform, we evaluate DNMT1 activity in ten sets of tumor tissue and healthy adjacent tissue, as well as in cultured colorectal carcinoma and normal colon cells (Figure 6.3). Significantly more DNMT1 activity is observed electrochemically in the majority of the tumor samples as compared to their healthy tissue counterparts, making this assay promising as an early clinical diagnostic for cancerous transformations.

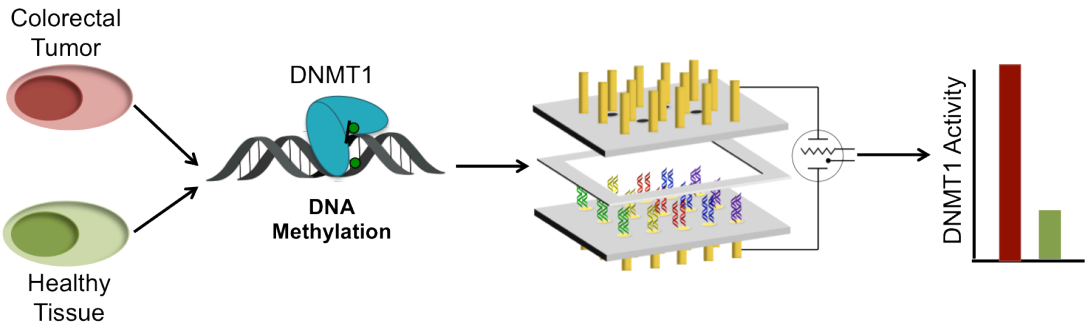

Figure 6.3 Overview of electrochemical DNMT1 analysis from tumors. Tumor and healthy tissues are lysed, and nuclear lysate is used to detect DNMT1 methyltransferase activity. The lysate is applied to a multiplexed, two working electrode platform that enables the conversion of methylation events into an electrochemical signal. Generally, we find hyperactivity of DNMT1 in tumor samples as compared to the healthy adjacent tissue.

Materials and Methods

DNA Synthesis and Purification

Hexynyl-modified oligonucleotides were synthesized on an Applied Biosystems 3400 DNA synthesizer, and unmodified complementary DNA was purchased from IDT. The terminal hexynyl moiety that was incorporated into the 5′ end of one of the strands was purchased from Glen Research. DNA was deprotected and removed from solid support with ammonium hydroxide (60° C for 16 h). Following a preliminary round of HPLC, oligonucleotides were treated with 80% acetic acid in water for 20 minutes. Each oligonucleotide was purified by high-performance liquid chromatography (HPLC) on a PLRP-S column (Agilent) with a gradient of acetonitrile and 50 mM ammonium acetate. Oligonucleotides were desalted by ethanol precipitation and quantified by ultraviolet-visible spectrophotometry based on their extinction coefficients at 260 nm (IDT Oligo Analyzer). Masses were verified by matrix-assisted laser desorption (MALDI) mass spectrometry. Based on the UV-Vis quantification of the DNA, DNA duplexes were formed by thermally annealing equimolar amounts of single-stranded oligonucleotides in deoxygenated phosphate buffer (5 mM phosphate, 50 mM NaCl, pH 7.0) at 90° C for 5 minutes followed by slowly cooling to 25° C.

The following sequences were prepared:

Alkyne: 5′-C_2-$(CH_2)_6$-GA CTG AGT ACT GCG CGC ACT GAT AGC-3′

Unmodified Complement: 5′-GCT ATC AGT GCG CGC AGT ACT CAG TC-3′

Methylated Complement: 5′-GCT ATC AGT GCG C^mGC AGT ACT CAG TC-3′

The *BssHII* restriction site is shown in red.

RT-qPCR

Total RNA was extracted from 30 mg of tissue and 3,000,000 cultured cells of each cell type. Tissue samples were homogenized in a total RNA extraction lysis buffer from a RNEasy kit (Qiagen). The total RNA extracted using this kit was eluted into a 300 μL of RNAse-free water.

Following RNA isolation, RT-PCR was performed to make a complete cDNA library using a Transcription First Strand cDNA Synthesis kit (Roche) and standard RT-PCR thermocycler conditions (C1000 Touch^{TM} Thermal Cycler, Bio-Rad). Total cDNA concentrations were determined by nanodrop. For these samples, 250 ng/μL of total DNA was used.

Three *DNMT1* primer sets were evaluated for consistency and reproducibility. *β-Actin* expression was evaluated to normalize the *DNMT1* results with primers from RealTime Primers; *GAPDH* was also evaluated as a housekeeping gene but was observed to be extremely variable between qPCR trials for the same samples. *DNMT1* primers were obtained from RealTime Primers, qSTAR and Genocopeiea. *DNMT1* primers from RealTime primers were found to have the most consistent results over multiple trials, and were therefore used for all tissue sample evaluation. Each sample was run in quadruplicate for RT-qPCR measurements. RT-qPCR was performed on a CFX 96 Real-Time PCR Detection system (Bio-Rad). RT-qPCR results were calculated using a relative quantification method, with the $\Delta\Delta C_t$ to determine fold excess of the mRNA between the adjacent normal and tumor tissue. Error was propagated through the experiment for four samples of each primer and sample set.

Cell and Tumor Preparation for ^{3}H and Electrochemistry

100 mg of each tissue sample was prepared as a crude cell lysate. Tissue samples were homogenized before nuclear isolation using a 3 mL homogenizer with 100 strokes of the pestle. Cultured cells were harvested upon confluence (approximately 7,000,000 cells) and taken directly to rinsing. Both tissue and cultured cells were rinsed with 1 mL phosphate buffer (5 mM phosphate, 50 mM NaCl, pH 7.0) and centrifuged. The tissue and cells were then prepared with a commercial NE-PER™ Nuclear and Cytoplasmic Extraction kit (Thermo Scientific). Following nuclear lysis, the lysate was buffer exchanged with a 10 kDa spin column into DNMT1 reaction buffer (50 mM Tris HCl, 1 mM EDTA, 5% glycerol, pH 7.8), flash frozen and stored at -80° C.

Once the nuclear lysate was aliquotted and frozen, total protein concentrations were determined using a bicinchoninic acid (BCA) assay kit (Pierce) for protein concentration. Concentrations of lysate were found to range from 1000-6000 μg/mL of protein.

^{3}H Assay

Tritium assays were performed using the protocol previously established in our lab.[30] The DNA used as a substrate for electrochemical measurements, with sequences provided in a previous section, including the hexynyl terminal modification, was used in this radioactive methyltransferase activity assay. 0.5 μCi ^{3}H-SAM with 20 μM DNA, 100 μg/mL of BSA, and lysate (final concentration of 500 μg/mL total protein) were combined to a total volume of 20 μL in DNMT1 reaction buffer (50 mM Tris HCl, 1 mM

EDTA, 5% glycerol, pH 7.8). Samples with purified DNMT1 (BPS Biosciences) were used as a positive standard, along with a negative standard with no methyltransferase. Reactions were incubated for 2 h at 37° C, followed by quenching with 30 μL of 10% TCA in water. The solutions were then spotted onto DE81 filter paper (Whatman) and air-dried for 15 minutes. Each filter paper was then washed by individually soaking it in 10 mL of 50 mM Na_2HPO_4 for 15 minutes, followed by rinsing with 50 mM Na_2HPO_4 and 95% ethanol. Filter papers were heated to 37° C and allowed to dry for 15 minutes before liquid scintillation counting. Fold excess for radioactive measurements of a given tumor set was determined by taking the ratio of the counts for the tumor lysate on the hemimethylated substrate to the tumor lysate on the unmethylated substrate divided by that same ratio for the normal tissue lysate.

Electrochemistry

Electrochemistry was performed on a bipotentiostat (CHInstruments 760E) with two working electrodes, a platinum counter electrode, and an AgCl/Ag reference electrode. Constant potential amperometry electrochemical measurements were recorded for 90 seconds with an applied potential of 320 mV to the secondary electrode and -400 mV to the primary electrode. Constant potential amperometry measurements were performed in Tris buffer (10 mM Tris, 100 mM KCl, 2.5 mM $MgCl_2$, 1 mM $CaCl_2$, pH 7.6) with 4 μM methylene blue and 300 μM potassium ferricyanide. Scans were taken individually at each of the 15 secondary pin electrode sets. The percent signal remaining data are reported as compared to pure DNMT1, with variation in the data representing the standard error across three measurements of three electrodes, all at a given condition.

To incubate electrodes with desired proteins, a 1.25 mm deep Teflon spacer was attached to the primary electrode surface with clips to form an isolated 4 μL volume well around each electrode. Generally, three electrodes on the device were incubated with 65 nM DNMT1, 160 μM SAM, and 100 μg/mL BSA as a positive control. For electrodes incubated with lysate, the lysate was diluted to a final concentration of ~200 μg/mL and directly combined with SAM to a final SAM concentration of 160 μM with 50 μg/mL BSA. Three electrodes modified with hemimethylated DNA were treated with tumor lysate and three treated with adjacent normal tissue lysate. Similarly, three electrodes modified with unmethylated DNA were incubated with tumor lysate and three with normal tissue lysate. Each electrode had 4 μL of the desired solution added to the well. The platform was incubated at 37° C for 1.5 h in a humidified container. The DNA monolayers were then treated with 1 μM protease solution in phosphate buffer (5 mM phosphate, 50 mM NaCl, pH 7.0) for 1 h, followed by thorough rinsing with phosphate buffer (5 mM phosphate, 50 mM NaCl, pH 7.0) and scanning by constant potential amperometry. The restriction enzyme *BssH*II was then added at a concentration of 1500 units/mL for 1.5 h at 37° C. *BssH*II was prepared by buffer exchange into DNMT1 reaction buffer (50 mM Tris HCl, 1 mM EDTA, 5% glycerol, pH 7.8) using a size exclusion column (10 kDa, Amicon). The electrodes were again rinsed with phosphate buffer and scanned. Results from three trials per tumor sample were aggregated and averaged. Fold excess for electrochemical measurements of a given tumor set was determined by taking the ratio of the percent signal remaining for the tumor lysate on the hemimethylated substrate to the tumor lysate on the unmethylated substrate divided by that same ratio for the normal tissue lysate.

Western Blot Analysis of Lysate for DNMT1

The relative amount of DNMT1 protein in each tumor set was established by Western blot. Samples were diluted to a final loading of 60 μg of protein per lane with DNMT1 reaction buffer (50 mM Tris HCl, 1 mM EDTA, 5% glycerol, pH 7.8) and Lammli reagent with betamercaptoethanol. Samples were probe sonicated for 10 seconds at 20% power, followed by boiling at 90° C for 5 minutes. Samples were loaded onto 4-12% polyacrylamide gels in MOPS SDS buffer (50 mM MOPS, 50 mM Tris base, 0.1% SDS, 1 mM EDTA, pH 7.7) and run at 175 mV for 2.5 hours at 4° C. Gels were subsequently transferred to membranes with a dry transfer procedure for 1.5 h. Membranes were blocked with 5% milk in TBST (20 mM Tris base, 150 mM NaCl, 0.1% Tween-20, pH 7.6) at room temperature for 1 hour, followed by overnight incubation with a 1^{o} antibody in 5% milk in TBST (1:1000 for DNMT1 (R & D) and 1:1000 for Lamin A (Santa Cruz)). The membranes were then rinsed with TBST buffer. Lamin A membranes were incubated with goat anti-rabbit 2^{o} antibody (Abcam) (1:5000 in 5% milk with 0.02% SDS in TBST) or Donkey Anti Sheep for DNMT1 (Santa Cruz) (1:5000) for 1 hour and then rinsed with TBST. Membranes were scanned on a Li-Cor Odyssey CLx infrared gel scanner, and bands were quantified using Image Studio software.

Results

DNMT1 Activity Measured Electrochemically

The electrochemical assay for DNMT1 activity involves the signal-on detection of methylation events on synthetic substrate DNA tethered to an electrode surface.[30] The process involves two steps: first, the pure methyltransferase or crude lysate is added to the surface. Subsequently, a methylation-specific restriction enzyme is used to cut any DNA that was not methylated during the previous treatment step. Successful methylation, resulting in protection from a methylation-specific restriction enzyme, maintains an electrochemical signal (Figure 6.2), while inactivity of the methyltransferase on the DNA-modified surface results in a significantly diminished electrochemical signal following restriction enzyme treatment.

When pure DNMT1 is titrated onto a DNA-modified electrode modified with hemimethylated DNA, a binding curve is generated, and a binding constant can be extracted based on the percent of the electrochemical signal that remains following restriction of the substrate DNA. A similar binding curve is generated from the addition of pure DNMT1 to the lysate of 4000 HCT116 *DNMT1*$^{-/-}$ cultured cells (the previously determined optimal lysate concentration for DNMT1 activity detection).[28] The titration data, along with the curve fit to the Hill binding model, are shown in Figure 6.4. Based on the inflection point of this curve, a K_D of pure DNMT1 on this DNA-modified electrode is found to be 31±1.3 nM, and 32±1.8 nM for pure DNMT1 in HCT116 *DNMT1*$^{-/-}$ lysate. These values are in good agreement with previously determined values for the K_D of DNMT1 in solution (26 nM).[31] A surface K_D on the same order as solution values indicates that not only is our platform especially sensitive for the detection of this

protein but also that the morphology of the DNA on our surface mimics the native substrate for the DNMT1 protein, allowing full access of the protein to the DNA bound to the surface.

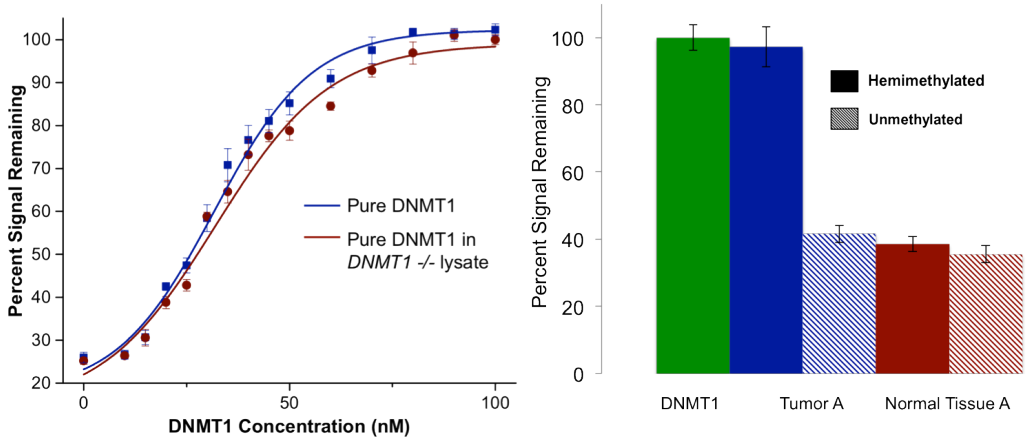

Figure 6.4 Detection of DNMT1 in pure form and from crude lysate. A titration of pure DNMT1 protein (*left*) demonstrates the sensitivity of this method of detection. In blue is shown the titration of pure DNMT1 on our electrodes, while in red is shown pure DNMT1 added to HCT116 *DNMT1*$^{-/-}$ cultured cell lysate. When the data are fit to a Hill binding model (fits shown as solid traces in plot), a K_D of 31±1.3 nM protein is extracted for pure DNMT1 and 32 nM±1.8 nM for DNMT1 added to lysate. The data from an array used to measure the DNMT1 activity from tumor A (*right*) show the differential between active lysate on electrodes and inactive lysate. The green bar shows electrodes treated with 65 nM pure DNMT1 as a positive control. The blue bars show electrodes treated with tumor A lysate on hemimethylated substrate (solid) and unmethylated substrate (dashed). The red bars show electrodes treated with adjacent normal tissue A lysate on hemimethylated DNA (solid) and unmethylated DNA (dashed). As can be seen, a significantly higher amount of signal protection is observed for the tumor tissue on the hemimethylated substrate than for the adjacent normal tissue on that substrate. The error bars show standard error across three electrodes.

Similarly, the differential signal protection from tumor and adjacent healthy tissue sets can be measured electrochemically. Ten tumor sets (A-J) were evaluated, and an example (tissue set A) is shown in Figure 6.4. Electrochemical data for this set show significant DNMT1 hyperactivity in the tumor sample as compared to the normal adjacent tissue over several replicates. With the data shown, an electrochemical assay using pure, isolated DNMT1 (green bar in Figure 6.4) is always included as a positive control. Also, it should be noted that the tumor lysate as well as the adjacent healthy tissue lysate are tested for methyltransferase activity using both a hemimethylated and an unmethylated DNA substrate. It is clear, even without normalization to the healthy adjacent tissue, that tumor A has significantly more DNMT1 activity than the healthy tissue. The incorporation of a comparison between the hemimethylated and unmethylated substrates, though, ensures that the activity we monitor is specific to DNMT1, and not to any *de novo* methyltransferases, given the noted preference of DNMT1 for a hemimethylated substrate.[32]

The data for each tissue set tested (A-J) have been aggregated into a single graph indicating the fold excess of DNMT1 activity in the tumor tissue as compared to the normal adjacent tissue (Figure 6.5). To calculate fold excess, each tumor and adjacent normal tissue has been normalized for the signal protection for the unmethylated DNA substrate to account for methylation that is not DNMT1-specific. Subsequently, the tumor tissue value is normalized to the adjacent healthy tissue, producing a ratio. If the fold excess is >1, then the DNMT1 activity in the tumor is higher than in the adjacent tissue. A fold excess of <1 indicates lower activity in the tumor relative to the healthy tissue, while a value of 1 indicates equivalent expression. As can be seen in Figure 6.5,

none of the tumors exhibits lower DNMT1 activity than their healthy tissue counterparts. In fact, the vast majority of the samples show significantly higher activity of DNMT1 when compared to the healthy tissue.

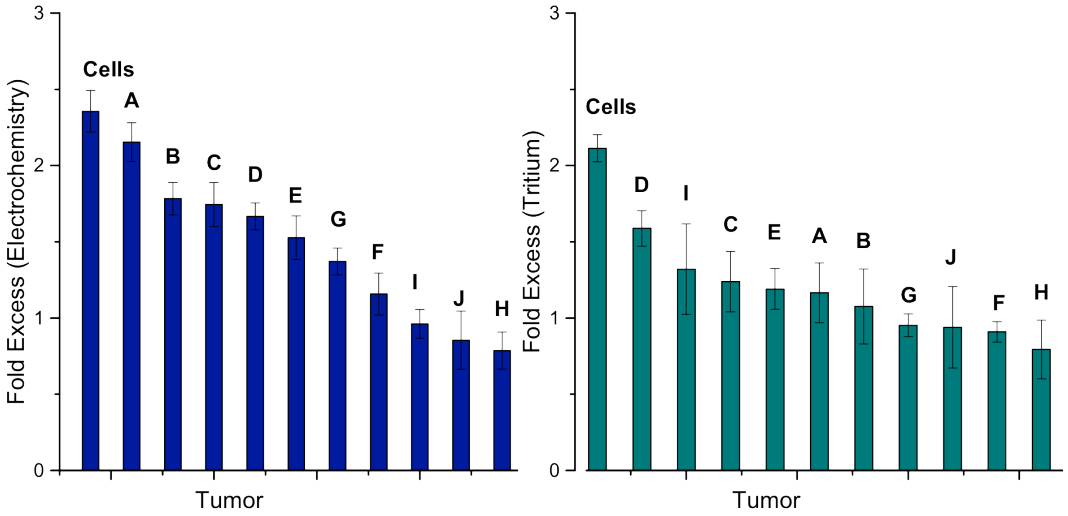

Figure 6.5 DNMT1 activity measured electrochemically and radioactively. The fold excess activity measured electrochemically (left) shows hyperactivity (fold excess > 1) in all but two of the tissue samples. Those that do not show hyperactivity show equivalent DNMT1 activity between tumor and normal tissue (fold excess ~1). When DNMT1 activity is measured with radioactive labeling (right), the same hyperactivity is not observed, likely because the measurement is convoluted by genomic DNA in the lysate samples. In both cases, the data for both the tumor and normal tissue on the hemimethylated substrate are first normalized to that of the unmethylated substrate, and the data for the tumor tissue are then normalized to the normal adjacent tissue. Each of the letters represents one of the tumor and healthy adjacent tissue sets, and the bar denoted 'cells' represents the result from the comparison between HCT116 colorectal carcinoma and healthy CCD-18Co colorectal cultured cells.

Radiometric Assay for DNMT1 Activity

In addition to measuring DNMT1 activity with our electrochemical assay, the current generally used radiochemical assay for DNMT1 activity[27] was used to assess the ten tumor samples. This assay involves the addition of substrate DNA and tritium-labeled S-Adenosyl methionine (SAM) cofactor, the source of methyl groups, to crude lysate or pure DNMT1. Protein activity is extrapolated from the amount of radioactive methyl groups added to the DNA following incubation, determined through scintillation counting of the samples in triplicate. Just as with the electrochemical assay, both hemimethylated and unmethylated substrate DNA were tested with the crude lysate for methylation. Analogously to the electrochemical assay, the resulting fold excess determination is calculated based on the ratio of hemimethylated substrate to unmethylated substrate counts for the tumor sample normalized to the hemimethylated divided by the unmethylated counts for the normal tissue. As can be seen in Figure 6.5, although the trend in fold excess activity is similar for tritium labeling as for electrochemistry, the extent of hyperactivity is diminished across all samples. Additionally, the majority of the samples have essentially statistically equivalent activity measured in this manner. This is, in part, due to the correction for the activity on unmethylated DNA. In this assay, genomic DNA from the lysate remains in the reaction mixture and is therefore capable of being methylated and contributing to the overall activity, even though it is not the target substrate. This seems to have led to higher activity in the unmethylated substrate samples for the tumors in many cases, which, when corrected, may lead to overall lower fold excess activity. The values that simply compare the hemimethylated tumor counts to their normal tissue counterparts are shown in Figures

6.6 and 6.7. Because of this significant difference in fold excess of DNMT1 activity, tritium labeling of DNA appears to be a less precise measurement of specific DNMT1 activity from lysate than electrochemical measurements.

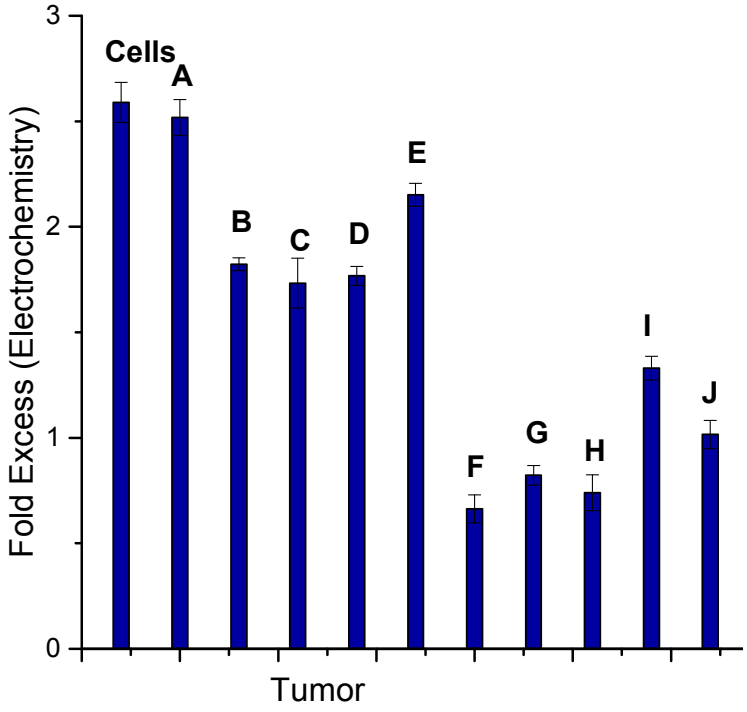

Figure 6.6 DNMT1 activity measured electrochemically without normalization to the unmethylated substrate. The fold excess activity measured electrochemically shows hyperactivity in all but two of the tissue samples. Those that do not show hyperactivity have equivalent DNMT1 activity between tumor and normal tissue. The data for activity on the hemimethylated substrate for the tumor tissue are normalized to that of the normal adjacent tissue.

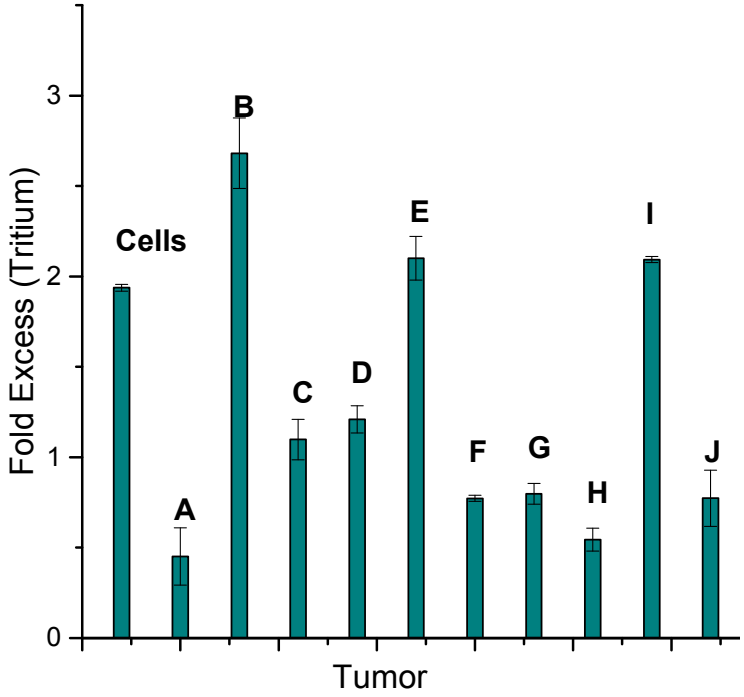

Figure 6.7 DNMT1 activity measured with radioactivity. The fold excess activity measured with radioactive labeling does not show similar hyperactivity in the tumor sample as when measured electrochemically. The data for activity on the hemimethylated substrate for the tumor tissue are normalized to that of the normal adjacent tissue.

DNMT1 Expression Measured by RT-qPCR

Currently, the most common method to analyze methyltransferases from lysate is through evaluation of genomic expression of the methyltransferase of interest. Thus, as a baseline with which to compare our electrochemical data, the expression of the *DNMT1* gene in each tumor and adjacent healthy tissue sample was evaluated by reverse transcription-quantitative PCR (RT-qPCR). A relative quantification method was used to determine the fold excess of *DNMT1* gene expression in the tumor sample as compared to the adjacent normal tissue sample. For each set of samples, the relative abundance of *DNMT1* is first normalized to the expression of *β-Actin* in each sample, followed by comparison between the normal tissue and tumor tissue. A fold excess of *DNMT1* from each tumor and normal tissue pair is calculated, and a value of >1 indicates higher expression in the tumor as compared to the normal tissue, <1 indicates lower expression in the tumor as compared to the healthy tissue, and a value of 1 indicates equivalent expression.

Multiple primer sets were evaluated for consistency over multiple trials, and the most consistent results were obtained with RealTime Primers, which were used for both *DNMT1* and *β-Actin* quantification by RT-qPCR. As can be seen in Figure 6.8, there is a large degree of variability among the ten tumor sets regarding the overexpression of *DNMT1* in the tumors as compared to the normal adjacent tissues. Sample B has the most significant upregulation, with a 22±5 fold excess of *DNMT1* expression, while sample G has significant downregulation of *DNMT1* in the tumor sample, with a fold excess of 0.3±0.1. Overall, no trends were observed with regards to the expression of *DNMT1* among these samples; tumors A, B, E, and F, as well as the HCT116 cells

compared to the CCD-18Co cells, all have significant upregulation of *DNMT1* in the tumor tissue. Samples C, D, and I have equivalent *DNMT1* expression compared to adjacent tissue, while samples G, H, and J have significant downregulation of *DNMT1* in the tumors.

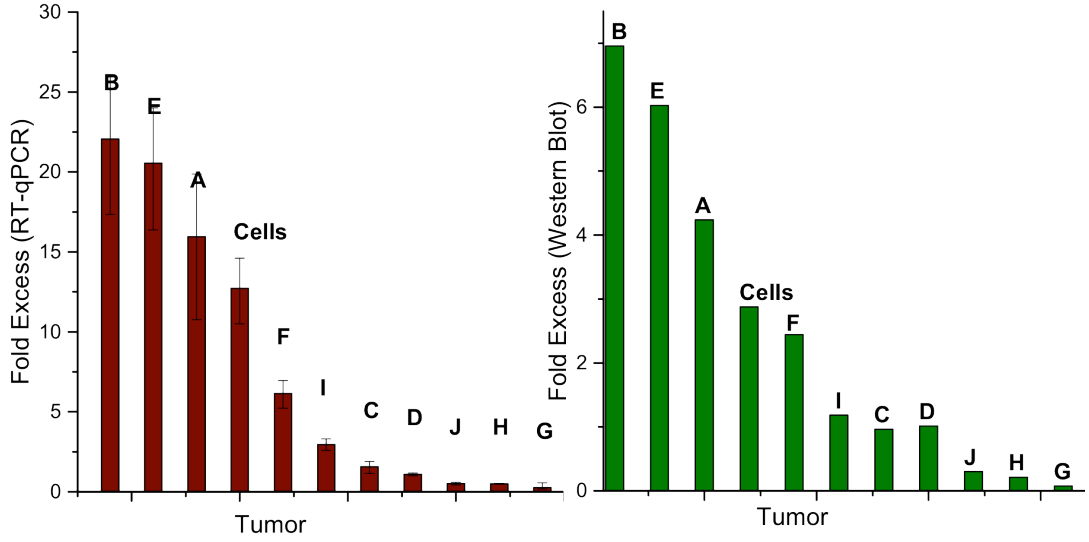

Figure 6.8 *DNMT1* expression and DNMT1 protein quantification. The fold excess *DNMT1* expression is determined with RT-qPCR (left), which shows just as many samples with overexpression of *DNMT1* in the tumor (fold excess > 1) as with equivalent expression (fold excess ~1) and underexpression (fold excess < 1). The RT-qPCR expression data for *DNMT1* expression in the tumor tissue are normalized to that of the normal adjacent tissue. The error represents the standard error across four replicates. The DNMT1 protein content (right), determined by Western blot, follows the same trend as the fold excess *DNMT1* expression; overexpression in the tumor sample correlates to more protein in that sample as compared to the normal adjacent tissue. The same trends are observed for those samples with equivalent expression and underexpression. For DNMT1 protein quantification, the measured intensity of the DNMT1 band is normalized to the Lamin A loading control, and subsequently, data for the tumor tissue are normalized to the normal adjacent tissue. Each of the letters represents one of the tumor and healthy adjacent tissue sets, and the bar denoted 'cells' represents the result from the comparison between HCT116 colorectal carcinoma and healthy CCD-18Co cultured cells.

Protein Content Measured by Western Blot

In addition to *DNMT1* expression evaluated by RT-qPCR, the total DNMT1 protein content of each tissue sample was evaluated by Western blotting. Total nuclear protein (60 μg) was added to each lane, and the amount of DNMT1 protein in the tumor tissue as compared to the healthy adjacent tissue was determined through quantification of the bands resulting from the Western blot (Figure 6.8). Again, a large amount of variability is observed in the total amount of DNMT1 within each lysate sample. The bands for DNMT1 protein as well as the nuclear protein Lamin A, used as a loading control, are given in Figure 6.9. Importantly, the ratio of DNMT1 in the tumor as compared to the normal adjacent tissue correlates directly to the fold excess of the *DNMT1* gene expression quantified by RT-qPCR.

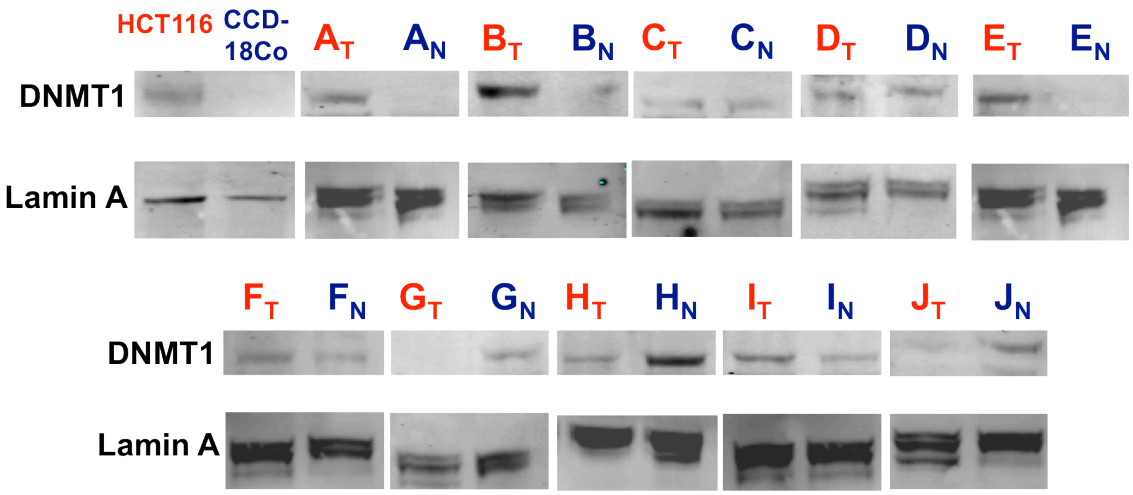

Figure 6.9 Western blots used for quantification. Shown are the bands used for quantification of differential DNMT1 protein content in the tumor as compared to normal tissue. The top bars show the DNMT1 in each tissue set as well as cell lysate. The bottom bars show the loading control, Lamin A, to which each DNMT1 concentration is normalized. 60 µg of protein per lane were loaded onto the gels. 1^o antibody for DNMT1 (R & D) and Lamin A (Santa Cruz) is incubated overnight. Goat anti-rabbit 2^o antibody (Abcam) or Donkey Anti Sheep for DNMT1 (Santa Cruz) is subsequently incubated, followed by imaging. Quantification is performed with Li-COR Odyssey Image Studio software.

Figure 6.10 then compares our electrochemical measurement of activity for the various tumor samples normalized to the adjacent healthy tissue, with *DNMT1* expression also normalized. Remarkably, as is evident in the Figure, there is no correlation between expression levels and resultant activity. While, for example, sample D has comparable expression levels in the tumor and adjacent tissue, the protein is found to be hyperactive electrochemically. In the case of sample B, the high activity seen electrochemically appears instead to be a function of the very high expression levels. Thus the electrochemical measurements allow a clear determination of methyltransferase activity associated with a given sample, and comparisons with expression and/or Western blotting permit the evaluation of whether the high activity in a given tumor sample results from high protein content or protein hyperactivity. The electrochemical assay is seen to provide the most direct measure of DNMT1 activity, and not simply its cellular abundance.

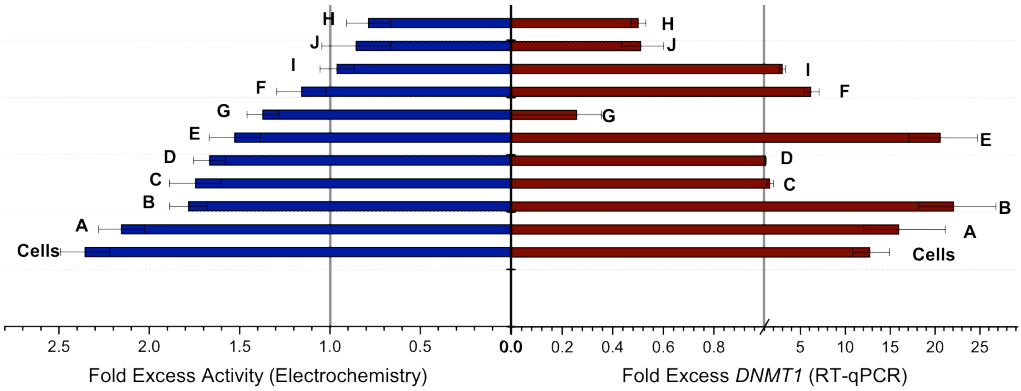

Figure 6.10 Direct comparison between DNMT1 activity measured electrochemically and *DNMT1* expression. The two bar graphs directly compare the fold excess protein activity (blue) measured electrochemically and the fold excess gene expression (red). There is no correlation evident between the amount of expression of *DNMT1* and the eventual activity of DNMT1 found in the tissue.

Discussion

The electrochemical platform developed for the measurement of DNMT1 activity allows the detection of this protein from crude cultured cell and colorectal tissue lysates. However, the utility of this platform for potential clinical diagnostic applications rests in the analysis of many samples. Here, ten tumor samples and adjacent healthy tissue have been evaluated. Our electrochemical platform facilitates extremely sensitive protein detection, with femtomole detection limits for the DNMT1 protein.[28] Furthermore, the electrochemical assay is a signal-on method of detection, ensuring specific DNMT1 discrimination from a host of proteins, DNA and RNA fragments found in crude lysates. Importantly, measurements of methyltransferase activity using the hemimethylated versus unmethylated substrate distinguishes the methyltransferase activity as associated with DNMT1 versus other methyltransferases, since only DNMT1 is preferentially active on the hemimethylated substrate.[32]

From the electrochemical analysis of the ten samples tested, in addition to lysate from cultured colorectal carcinoma cells, a pattern was found to emerge. Hyperactivity in the tumor samples as compared to the normal tissue is clearly found in the majority of tissue specimens analyzed. Furthermore, the few samples that did not show hyperactivity in the tumor tissue have equal activity between the tumor and healthy tissue. We therefore observe hyperactivity of DNMT1 in the majority of the measured tumor samples. In fact, a one-way ANOVA analysis of variance between the tumor and normal adjacent tissue DNMT1 activity was performed. We found a confidence level of $p < 0.05$, indicating a 95% confidence that the DNMT1 activity in the tumor tissues is different from the healthy adjacent tissues.

Currently, the most prevalent method of methyltransferase activity measurement is a radioactivity assay involving the application of tritium-labeled SAM cofactor to the methyltransferase of interest in pure form or in a mixture from crude lysate.[28] Substrate DNA is added to the reaction, and activity is measured based on scintillation counts resulting from tritium-labeled methyl groups added to DNA. This assay is also used here as a comparison to our electrochemical assay. The results from this activity assay, however, show less hyperactivity in the tumor samples as compared to the electrochemical assay. Indeed, the radioactivity assay does not show for most samples a statistically clear hyperactivity of DNMT1 in tumorous tissue. This lack of a clean correlation is likely due to methylation of genomic DNA present in the lysate, which is inseparable from measurements of the methylation of the synthetic, target DNA added to the reaction. Tritium labeling, therefore, does not provide a pure measurement of DNMT1 activity on a target substrate when measured from lysate, as methylation of native DNA can affect the levels of methylation measured, and therefore, the ratio of methylation on hemimethylated versus unmethylated substrates. It is especially important to note that this is not a problem with our electrochemical assay, as the only DNA methylation events that contribute to the electrochemical signal are those that occur on the target DNA in the electrochemical device. Noteworthy also is that the tritium-based assay is not suitable for clinical applications due to the large amounts of reagents required and the necessity of radioactivity for detection.

Perhaps more important in the context of clinical relevance is the comparison of DNMT1 activity measurements to the primary method currently applied in analysis of clinical samples: gene expression of the *DNMT1* gene by RT-qPCR. Many studies have

focused on correlations between the expression of this methyltransferase gene and tumorigenesis.[23, 33-35] However, upon analysis of the ten sample sets involved in this study, no such correlation is observed. There are just as many samples that have upregulation of *DNMT1* in tumors as equivalent expression and underexpression. We also observe no correlation between the activity of DNMT1 in a sample and its gene expression level as measured by RT-qPCR. Thus while RT-qPCR has potential applications for general research regarding methyltransferases, in and of itself it is insufficient as a diagnostic to identify potentially tumorous transformations.

Western blotting for total DNMT1 protein content in the lysate samples yields similar results as RT-qPCR. The DNMT1 protein levels are found to correlate to the expression of *DNMT1*, but not to the activity of the protein measured electrochemically. This finding indicates that it is not simply the amount of protein present that is responsible for the hyperactivity in the tumor samples observed electrochemically. Other post-translational factors must influence the activity of DNMT1.[36, 37]

If one considers the various sources of changes in protein activity, it is understandable that the electrochemical assay, which directly measures the methyltransferase activity on a hemimethylated target, would yield the clearest diagnostic for DNMT1 as a source of epigenetic change within a given tissue. Measurement of protein activity is closest in time and space to the epigenetic changes responsible for cancerous transformation, certainly as compared to the measurement of mRNA for the methyltransferase, which reflects effects on transcription, and even measurements of the abundance of protein, reflecting the status of DNMT1 following translation. What is key for cancerous transformation is the activity of the methyltransferase itself, turning on and

off particular genes as a result of methylation. The fact that only some of the tumorigenic changes in a sample depend on the amount of DNMT1, measured by Western blot or expression levels, underscores that point; tumorigenic changes are also seen to depend upon enzymatic hyperactivity of a given DNMT1. In developing assays for epigenetic changes as a source of tumorigenic change, this point needs to be kept in mind. In sum, then, using our electrochemical data, it is clear that tumorigenesis does indeed correlate with DNMT1 hyperactivity, and hence the electrochemistry provides a useful early and sensitive diagnostic for cancerous transformation.

Significance

We have developed an electrochemical platform based upon DNA charge transport for the measurement of DNMT1 activity from crude lysate samples. Using this platform to analyze ten colorectal carcinoma samples, as well as cultured colorectal carcinoma cells, we find a direct correlation between hyperactivity of DNMT1 and tumorous tissue. Significant hyperactivity of the protein is found in the majority of samples. This hyperactivity does not correlate with either overexpression or total amount of DNMT1 within the sample. Instead, significant enzyme hyperactivity is frequently evident. Furthermore, DNMT1 hyperactivity as an indicator of cancerous transformation, measured electrochemically, is not cleanly observed with the current standard techniques of DNMT1 analysis, including tritium labeling, RT-qPCR, and Western blotting. Thus our electrochemical platform has the potential to provide a sensitive method of detecting DNMT1-related cancerous transformations and with greater reliability than current DNMT1 analysis techniques.

References

1. Forman, D., Bray, F., Brewster, D. H., Gombe, M. C., Kohler, B., Piñeros, M., Steliarova-Foucher, E., Swaminathan, R., and Ferlay, J. (2013) Cancer Incidence in Five Continents, Vol. X electronic version., Lyon, IARC.

2. Mandelblatt, J., Andrews, H., Kao, R., Wallace, R., and Kerner, J. (1996) The late-stage diagnosis of colorectal cancer: demographic and socioeconomic factors, *Am. J. Pub. Health 86*, 1794-1797.

3. Fearon, E. R., and Vogelstein, B. (1990) A genetic model for colorectal tumorigenesis, *Cell 61*, 759-767.

4. Lengauer, C., Kinzler, K. W., and Vogelstein, B. (1997) Genetic instability in colorectal cancers, *Nature 386*, 623-627.

5. Liu, B., Nicolaides, N. C., Markowitz, S., Willson, J. K., Parsons, R. E., Jen, J., Papadopolous, N., Peltomaki, P., de la Chapelle, A., Hamilton, S. R., and et al. (1995) Mismatch repair gene defects in sporadic colorectal cancers with microsatellite instability, *Nat. Genet. 9*, 48-55.

6. Vogelstein, B., and Kinzler, K. W. (2004) Cancer genes and the pathways they control, *Nat. Med. 10*, 789-799.

7. Feinberg, A. P., and Tycko, B. (2004) The history of cancer epigenetics, *Nat. Rev. Cancer 4*, 143-153.

8. Frigola, J., Song, J., Stirzaker, C., Hinshelwood, R. A., Peinado, M. A., and Clark, S. J. (2006) Epigenetic remodeling in colorectal cancer results in coordinate gene suppression across an entire chromosome band, *Nat. Genet. 38*, 540-549.

9. Jones, P. A., and Baylin, S. B. (2002) The fundamental role of epigenetic events in cancer, *Nat. Rev. Genet. 3*, 415-428.

10. Jones, P. A., and Laird, P. W. (1999) Cancer epigenetics comes of age, *Nat. Genet. 21*, 163-167.

11. Bronner, C. E., Baker, S. M., Morrison, P. T., Warren, G., Smith, L. G., Lescoe, M. K., Kane, M., Earabino, C., Lipford, J., Lindblom, A., and et al. (1994) Mutation in the DNA mismatch repair gene homologue hMLH1 is associated with hereditary non-polyposis colon cancer, *Nature 368*, 258-261.

12. Leach, F. S., Nicolaides, N. C., Papadopoulos, N., Liu, B., Jen, J., Parsons, R., Peltomaki, P., Sistonen, P., Aaltonen, L. A., Nystrom-Lahti, M., and et al. (1993) Mutations of a mutS homolog in hereditary nonpolyposis colorectal cancer, *Cell 75*, 1215-1225.

13. Lynch, H. T., and de la Chapelle, A. (2003) Hereditary colorectal cancer, *New Engl. J. Med. 348*, 919-932.

14. Esteller, M. (2008) Epigenetics in cancer, *New Engl. J. Med. 358*, 1148-1159.

15. Sharma, S., Kelly, T. K., and Jones, P. A. (2010) Epigenetics in cancer, *Carcinogenesis 31*, 27-36.

16. Baylin, S. B., and Herman, J. G. (2000) DNA hypermethylation in tumorigenesis: epigenetics joins genetics, *Trends in Genet. 16*, 168-174.

17. Esteller, M. (2007) Cancer epigenomics: DNA methylomes and histone-modification maps, *Nat. Rev. Genet. 8*, 286-298.

18. Toyota, M., Ahuja, N., Ohe-Toyota, M., Herman, J. G., Baylin, S. B., and Issa, J. P. (1999) CpG island methylator phenotype in colorectal cancer, *Proc. Natl. Acad. Sci. USA 96*, 8681-8686.

19. Esteller, M., Corn, P. G., Baylin, S. B., and Herman, J. G. (2001) A gene hypermethylation profile of human cancer, *Cancer Res. 61*, 3225-3229.

20. Esteller, M., Toyota, M., Sanchez-Cespedes, M., Capella, G., Peinado, M. A., Watkins, D. N., Issa, J. P., Sidransky, D., Baylin, S. B., and Herman, J. G. (2000) Inactivation of the DNA repair gene O6-methylguanine-DNA methyltransferase by promoter hypermethylation is associated with G to A mutations in K-ras in colorectal tumorigenesis, *Cancer Res. 60*, 2368-2371.

21. Okano, M., Bell, D. W., Haber, D. A., and Li, E. (1999) DNA methyltransferases Dnmt3a and Dnmt3b are essential for de novo methylation and mammalian development, *Cell 99*, 247-257.

22. Bestor, T. H. (2000) The DNA methyltransferases of mammals, *Human Molec. Genet. 9*, 2395-2402.

23. el-Deiry, W. S., Nelkin, B. D., Celano, P., Yen, R. W., Falco, J. P., Hamilton, S. R., and Baylin, S. B. (1991) High expression of the DNA methyltransferase gene characterizes human neoplastic cells and progression stages of colon cancer, *Proc. Natl. Acad. Sci. USA 88*, 3470-3474.

24. Toyota, M., Ho, C., Ahuja, N., Jair, K. W., Li, Q., Ohe-Toyota, M., Baylin, S. B., and Issa, J. P. (1999) Identification of differentially methylated sequences in colorectal cancer by methylated CpG island amplification, *Cancer Res. 59*, 2307-2312.

25. Zou, H., Yu, B., Zhao, R., Wang, Z., Cang, H., Li, D., Feng, G., and Yi, J. (2002) Detection of aberrant p16 methylation in the serum of colorectal cancer patients, *Chinese J. Preventive Med. 36*, 499-501.

26. Munteanu, I., and Mastalier, B. (2014) Genetics of colorectal cancer, *J. Med. and Life 7*, 507-511.

27. Fraga, M. F., and Esteller, M. (2002) DNA methylation: a profile of methods and applications, *BioTechniques 33*, 632, 634, 636-649.

28. Furst, A. L., Muren, N. B., Hill, M. G., and Barton, J. K. (2014) Label-free electrochemical detection of human methyltransferase from tumors, *Proc. Natl. Acad. Sci. USA 111*, 14985-14989.

29. Furst, A., Landefeld, S., Hill, M. G., and Barton, J. K. (2013) Electrochemical patterning and detection of DNA arrays on a two-electrode platform, *J. Am. Chem. Soc. 135*, 19099-19102.

30. Muren, N. B., and Barton, J. K. (2013) Electrochemical assay for the signal-on detection of human DNA methyltransferase activity, *J. Am. Chem. Soc. 135*, 16632-16640.

31. Lee, B. H., Yegnasubramanian, S., Lin, X., and Nelson, W. G. (2005) Procainamide is a specific inhibitor of DNA methyltransferase 1, *J. Biol. Chem. 280*, 40749-40756.

32. Hermann, A., Goyal, R., and Jeltsch, A. (2004) The Dnmt1 DNA-(cytosine-C5)-methyltransferase methylates DNA processively with high preference for hemimethylated target sites, *J. Biol. Chem. 279*, 48350-48359.

33. De Marzo, A. M., Marchi, V. L., Yang, E. S., Veeraswamy, R., Lin, X., and Nelson, W. G. (1999) Abnormal regulation of DNA methyltransferase expression during colorectal carcinogenesis, *Cancer Res. 59*, 3855-3860.

34. Girault, I., Tozlu, S., Lidereau, R., and Bieche, I. (2003) Expression analysis of DNA methyltransferases 1, 3A, and 3B in sporadic breast carcinomas, *Clin. Cancer Res. 9*, 4415-4422.

35. Peng, D. F., Kanai, Y., Sawada, M., Ushijima, S., Hiraoka, N., Kosuge, T., and Hirohashi, S. (2005) Increased DNA methyltransferase 1 (DNMT1) protein expression in precancerous conditions and ductal carcinomas of the pancreas, *Cancer Sci. 96*, 403-408.

36. Rountree, M. R., Bachman, K. E., and Baylin, S. B. (2000) DNMT1 binds HDAC2 and a new co-repressor, DMAP1, to form a complex at replication foci, *Nat. Genet. 25*, 269-277.

37. Smallwood, A., Esteve, P. O., Pradhan, S., and Carey, M. (2007) Functional cooperation between HP1 and DNMT1 mediates gene silencing, *Genes & Development 21*, 1169-1178.

Chapter 7

Development of Glassy Carbon Flow-through Cells for Biomolecule Analysis

M. G. Hill contributed to the design and construction of the flow-through cell.

Introduction

Biomolecule detection involving DNA charge transport (DNA CT) has enabled the analysis of a variety of targets, including nucleic acids,[1, 2] DNA-binding proteins,[3-5] and epigenetic modifications.[6] In fact, such platforms have enabled the sensitive and selective analysis of the human methyltransferase, DNMT1, from crude tumor lysate.[7] As this assay has the potential to function as a clinical diagnostic, increasing the efficiency and ease of use will greatly increase its utility. One major component of increasing the efficiency of this system is to decrease the amount of sample necessary for detection. To achieve detection from smaller sample volumes without significantly altering detection assay itself, it is necessary instead to modify the electrode platform utilized for detection through the incorporation of microfluidics into the platform.

Microfluidics, the manipulation of fluids over micrometer to millimeter length scales, is ideal for biomolecule analysis, as it requires minimal reagent and provides a large surface area-to-volume ratio for measurements.[8] Microfluidics platforms enable accurate, rapid operation with multiplexing for the simultaneous analysis of multiple clinical samples and targets.[9] Biological applications of microfluidic devices range from high-throughput pharmaceutical analysis[10] to lab-on chip analysis of blood glucose levels.[11] Such platforms are advantageous, as they enable sample preparation and analysis in a single device, minimizing the amount of sample and the level of sample preparation required. Additionally, electrochemical detection is compatible with microfluidics platforms; common electrochemical methods incorporated into microfluidics platforms include potentiometry,[12] amperometry,[13] and conductometry,[14] in addition to electrophoretic separations.[15]

Although a multitude of biomarkers have been connected to tumorogenesis, DNA methylation has recently garnered significant interest because of its role in gene expression.[16-21] Specifically, DNA methyltransferase activity detected electrochemically is a viable method to monitor potential cancerous transformations. Tight control over DNA methylation in cells is vital, as methylation patterns strongly affect gene expression.[22] DNA methyltransferases maintain a specific genomic methylation pattern by the covalent methylation of cytosine at 5′-CG-3′ sites. Aberrant activity of DNA methyltransferases can cause hypermethylation, silencing tumor suppressor genes and promoting cancerous transformations.[23-26] The most abundant mammalian methyltransferase is DNMT1, a maintenance methyltransferase that preferentially methylates hemimethylated DNA using the cofactor *S*-adenosyl-L-methionine (SAM).[27, 28] In the Barton lab, we have recently developed an electrochemical assay for the specific detection of DNMT1 activity from crude cultured cell and human tissue lysate.[7] This assay employs a methylation-sensitive restriction enzyme to convert the methylation state of the DNA into an electrochemical signal, thereby enabling the detection of a methyl group, even though methylation itself does not significantly affect DNA CT.

Although our two working electrode platform requires a minimal amount of lysate for detection, all of the preparation of the lysate must be performed macroscopically external to the platform. Furthermore, while nucleic acid sensors have been incorporated into microfluidic platforms,[29] the electrodes involved in detection remain planar, limiting the surface area to volume ratio. Additionally, the sensitivity, specificity, and selectivity of DNA-mediated charge transport (DNA CT) have yet to be applied to microfluidics-based biomolecule detection. We have developed an electrochemical flow-through cell

in which the electrodes themselves form the fluidics channels. The devices, fabricated from glassy carbon, silver, and Kel-F, have a total volume of less than 5 μL with two working electrodes, each with an area of 4.7 mm^2.

Methods and Materials

Unless otherwise stated, all reagents were purchased from Sigma Aldrich.

Glassy Carbon Flow-Through Cells

Glassy carbon cells were fabricated in a stepwise manner. Glassy carbon working electrodes and silver pseudoreference electrodes, as well as Kel-F endcaps, were fabricated in the Caltech machine shop. Glassy carbon electrodes were milled from 10 cm x 10 cm x 1.5 mm glassy carbon sheets (Bayville Chemical) to final dimensions of 6 mm x 6 mm x 1.5 mm with a 1 mm diameter hole drilled through the center. A diamond grit drill bit (National Diamond Lab) with wet drilling was used to form the hole in the electrodes.

A 10 cm x 10 cm x 1 mm sheet of silver foil was used to form the silver pseudoreference electrode. The silver electrodes were formed to 6.2 mm x 6.0 mm x 1 mm, again with a 1 mm hole in the center. The Kel-F pieces were 6 mm^3 with a 1 mm hole in the center.

Before fabrication, the faces containing the holes of both the glassy carbon and the silver electrodes were coated with Super Corona Dope (MG Chemicals). One face of the Kel-F pieces was roughed with P50 grit sandpaper to ensure that the epoxy remains affixed. The holes were then aligned, and the pieces are sandwiched together and affixed with 5-minute epoxy. One Kel-F piece, followed by a glassy carbon and a silver piece were added, followed by the second glassy carbon electrode and a final Kel-F piece were connected. The epoxy was allowed to harden with the devices in a vice.

To form electronic connections between the potentiostat and the electrodes, silver epoxy was painted in a thin strip on the top of each electrode (two glassy carbon working electrodes and the silver pseudoreference electrode). 0.25 mm diameter silver wire was connected to each electrode with the silver epoxy. It is vital at this point that the silver epoxy and the wires are isolated to a particular electrode. If any crossover occurs, the device will short circuit.

To create a flow cell through this piece, 1 mm outer diameter HPLC tubing (IDEX Health and Science, LLC) was inserted into the Kel-F until it reached the glassy carbon working electrode. A sharp was then inserted into the tubing to enable facile connection to a syringe. Electrochemical readout with this platform was performed by connecting the flow-through cell to a potentiostat via each of the silver wire leads previously attached to the cell. The silver in the center acts as a pseudoreference electrode, and a Pt counter electrode was inserted into the HPLC tubing output from the device.

Synthesis of 4-azidobenzene Diazonium Tetrafluoroborate

Protocol adapted from Evrard et al. 2008.[30] An aqueous solution of $NaNO_2$ (90 mg, 1.3 mmol) in 0.5 mL H_2O at 4° C was added dropwise to a solution of 4-azidoaniline hydrochloride (200 mg, 1.18 mmol) in 2 mL 1 M HCl on ice. The resulting solution was stirred at 4° C for 1 h. 1.5 mL of a saturated aqueous solution of $NaBF_4$ was then added, forming a light brown precipitate. The solid was filtered and rinsed with 2 x 6 mL diethyl ether. The product was purified by recrystallization in diethyl ether from

acetonitrile. The product is an off-white powder, which was stored under vacuum. ESI-MS: calc'd: 145.18 found: 145.8 $[M]^+$.

Glassy Carbon Rod Electrode Modification

Preliminary experiments with aniline attachment to glassy carbon were performed on glassy carbon rod electrodes (3.0 mm diameter) (Bioanalytical Systems, Inc.). Glassy carbon electrodes were prepared by polishing the electrodes with 300 grit sandpaper, followed by 0.3 micron diamond polish on a cloth polishing pad, and finally 0.05 micron silica polish. Electrodes were then sonicated in aqueous solution for 5 minutes.

Aniline and its derivatives were attached to glassy carbon either using an *in situ* diazonium formation method[31] or with activation of a pre-formed diazonium salt. For *in situ* formation, either 1 mM or 10 mM total aniline was dissolved in 0.1 M tetrabutylammonium tetrafluoroborate containing 4% 1M HCl. The solutions were chilled to 4° C and degassed on an ice bath, followed by the addition of 1 mM or 10 mM sodium nitrite with continued argon bubbling on ice. The diazoium was tethered to the glassy carbon through electrochemical activation, either by cyclic voltammetry (CV) or by constant potential amperometry (CPE). Generally, CV's were scanned from 500 mV to -1000 mV v AgCl/Ag for various numbers of scans. Additionally, CPE was run at -750 mV v AgCl/Ag for 120 seconds.

Electrochemical surface modification of glassy carbon electrodes using 4-azidobenzene diazonium tetrafluoroborate[30] was performed in a similar manner to the *in situ* method. 1.3 mM 4-azidobenzene diazonium tetrafluoroborate in 0.1 M HCl was degassed and cooled to 4° C. Electrodeposition was achieved through either CPE for 120

s at -800 mV v AgCl/Ag or cyclic voltammetry from 500 mV to -800 mV v AgCl/Ag at 50 mV/s for four scans.

Passivation against both methylene blue and ferricyanide were tested by scanning the modified glassy carbon electrodes in phosphate buffer (5 mM phosphate, 50 mM NaCl, pH 7.0) containing various concentrations of methylene blue or $[Fe(CN)_6]^{3-}$. Multiple combinations of 4-azidoaniline with aniline, p-nitroaniline, 4-aminobenzoic acid, or p-phenylenediamine were tested for passivation against methylene blue and $[Fe(CN)_6]^{3-}$.

Coupling of ethynyl ferrocene to surfaces was effected using copper-catalyzed click chemistry. Copper catalyst was activated by ascorbic acid. Ascorbic acid dissolved in water was added to ethynyl ferrocence and thoroughly degassed. $CuSO_4$, $[Cu(bathophen)_2]^{2+}$ (bathophen = Bathophenanthrolinedisulfonic acid), $[Cu(phendione)_2]^{2+}$ (phendione= 1,10-Phenanthroline-5,6-dione), or $[Cu(TBTA)]^{2+}$ (TBTA= Tris[(1-benzyl-1H-1,2,3-triazol-4-yl)methyl]amine) was independently degassed. Just before clicking to the electrode, copper solution was added to the ascorbic acid and ethynyl ferrocene. The final concentrations of all components in 2:1:1 H_2O: DMSO:EtOH were 300 μM ascorbic acid, 25 μM copper, and 25 μM ethynyl ferrocene. Rod electrodes were soaked in 25 μL of the clicking solution for varying times between one and two hours, followed by rinsing with water. Residual copper was removed by soaking the electrodes in 1 mM EDTA in pH 8.0 phosphate buffer (5 mM PO_4, 50 mM NaCl, pH 8.0).

Glassy Carbon Flow-through Cell Modification

Glassy carbon flow-through cells were modified with diazonium salts in the same manner as the rod electrodes. Briefly, aniline derivatives were attached to glassy carbon using an *in situ* diazonium formation method.[31] 1 mM azidoaniline was dissolved in 0.1 M tetrabutylammonium tetrafluoroborate containing 4% 1M HCl. The solution was chilled to 0° C and degassed on an ice bath, followed by the addition of 1 mM sodium nitrite with continued argon bubbling on ice. The diazoium solution was added to the device *via* syringe, and was tethered to one of the glassy carbon working electrodes through electrochemical activation by CV. CVs were run by scanning from 500 mV to -850 mV for between 2 and 4 scans.

Electrochemical click on the flow-through cell was performed through the addition of 25 μM $[Cu(bathophen)_2]^{2+}$ and 25 μM ethynyl ferrocene in 1:1 water : ethanol. A 0.25 mm diameter silver wire was inserted into the cell, and a -350 mV potential was applied to the wire for 10 minutes.

Results and Discussion

Fabrication of Flow-through Cells

A basic four-electrode set-up contains two working electrodes, a reference electrode, and an auxiliary electrode. A flow-through cell combines these elements, along with a path for liquid flow. An overview of the setup is shown in Figure 7.1. Briefly, the set-up contains a path for fluidics that runs through a sandwich structure comprised of insulating material, glassy carbon working electrodes, a silver pseudoreference electrode, and a Pt wire counter electrode. This overall schematic allows for incredibly small sample volumes compared to macroscopic electrodes. While a single inlet and outlet are shown, these devices can be multiplexed and combined in parallel to perform detection of multiple analytes simultaneously.

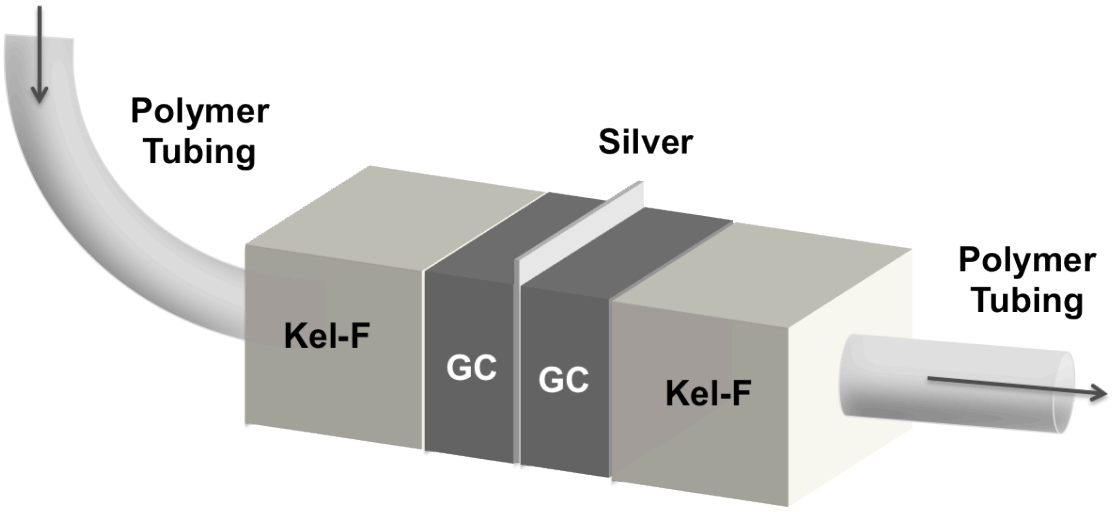

Figure 7.1 Flow-through cell configuration. A 1 mm diameter hole is created through all of the materials to form a channel through which analyte solution is added for detection. The glassy carbon electrode flow-through cell is comprised of two Kel-F ends, two glassy carbon working electrodes, and a silver foil pseudoreference electrode sandwiched between the two working electrodes. Analyte is added to the device through polymer tubing attached to the Kel-F pieces.

Working Electrode Fabrication

A microfluidic detection device should use materials that are cost-effective, easily manipulated, and well characterized. Glassy carbon (GC) was chosen as the electrode fabrication material for several reasons. The relative cost of GC compared to precious metals is extremely low. Additionally, it can be easily milled into a variety of shapes, including the incorporation of cylindrical interior surfaces, something that is not easily accomplished with other carbon materials such as HOPG and carbon paste. Yet, GC remains a robust material with a multitude of surface modification methods available.[31-37]

The GC working electrodes were individually designed to maximize the surface area-to-volume ratio, while maintaining fluidics dimensions compatible with commercially available supplies, including drill bits and tubing. With that in mind, the electrodes were optimized to a small square of dimensions 6 mm x 6 mm x 1.5 mm, with a 1 mm diameter hole through the 6 mm x 6 mm face. This yields an electrode with a surface area of 4.7 mm^2, but a volume of only 1.2 μL. Additionally, this 1 mm diameter hole is on the order of the smallest commercially available diamond drill bits.

Silver was chosen to act as a pseudoreference for similar reasons; AgCl/Ag references are an industry standard reference electrode, and the cost of silver foil is relatively low compared to other precious metals. The silver foil was milled to the same dimensions as the GC electrodes, with one edge slightly longer. This extra length creates an overhang of the silver foil upon assembly of the flow-through cell, which helps to prevent the working electrodes from making electrical contact with the silver foil upon attachment of silver wires with silver epoxy. The silver wires connected to the individual electrodes in the flow-through cell enable their connection to a potentiostat. Kel-F was

chosen to seal the ends of the flow-through cell because of its durability and resistance to a variety of solvents.

Flow-through Cell Assembly

When constructing electrodes, it is vital to prevent electrical contact between the electrode surfaces. Both GC electrodes and the silver electrode were coated in Super Corona Dope, an electrical insulator used to both insulate and protect electronic components on circuitry boards. The device is fabricated from one Kel-F piece attached to one GC electrode, followed by the silver electrode, a second GC electrode, and finally, the second Kel-F cap. These pieces were adhered to one another using 5-minute epoxy and allowed to dry in a vice to prevent leaking and to ensure that the hole in each material remained properly aligned.

After drying, silver wires were connected to each of the electrodes in the flow through cell using silver epoxy to enable connection with the potentiostat. It is important to note that the silver epoxy must be isolated to a particular electrode. If the epoxy makes electrical contact with multiple electrodes, the cell will short circuit. Finally, to complete the device, polymer tubing with a 1 mm outer diameter and a 0.58 mm inner diameter was inserted into the Kel-F piece until it reached the GC electrode. A sharp was inserted into the distal end of the tubing to enable facile connection of a syringe. Photographs of the setup are shown in Figure 7.2.

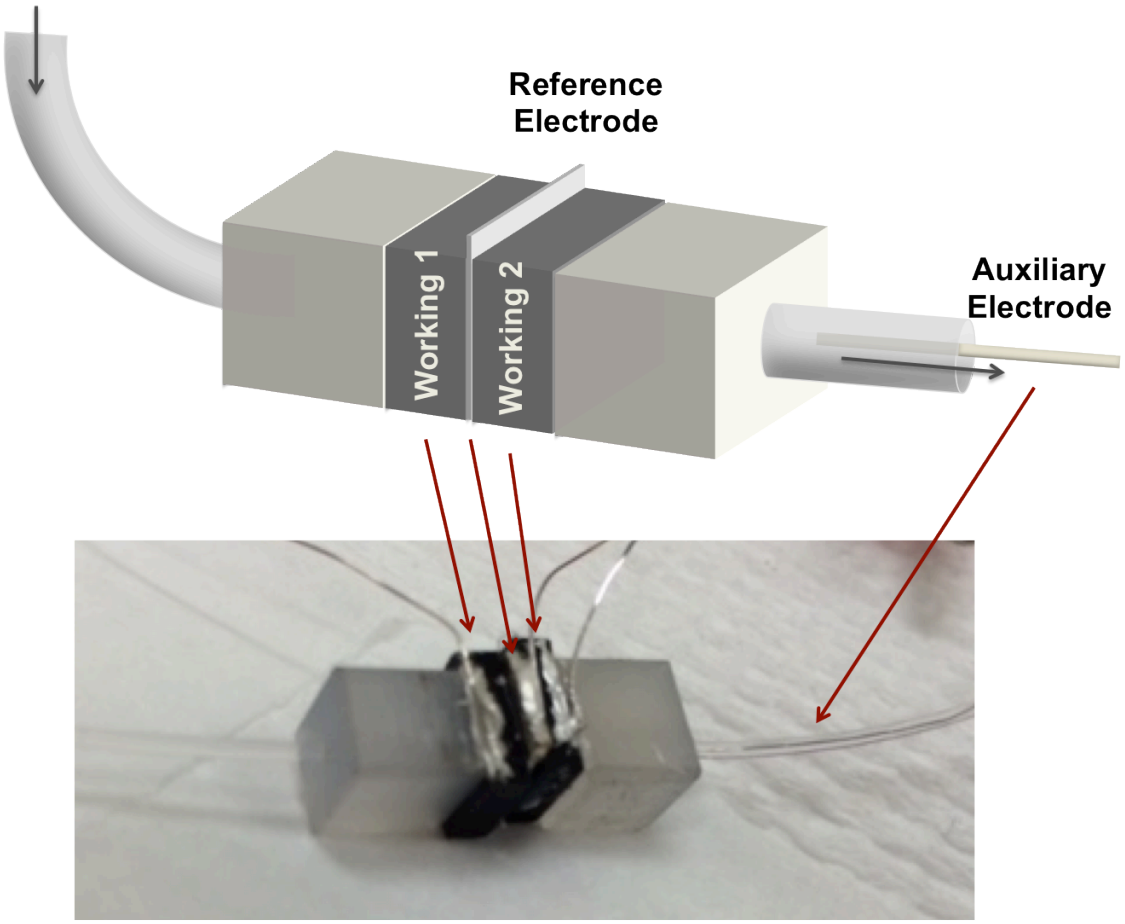

Figure 7.2 Assembled glassy carbon flow-through cell. A cartoon of all components of the cell are shown *(top)*, with the two glassy carbon working electrodes and an integrated silver pseudoreference electrode between them. A platinum auxiliary electrode is inserted into the terminal polymer tubing. A photograph of the assembled cell (*bottom*) shows all of the flow-through cell components with silver lead wires attached to each electrode *via* conductive silver epoxy.

To mimic previously designed platforms that incorporate a secondary working electrode for detection, two working electrodes were incorporated into the flow-through cell.[5, 7] This platform design enables DNA-mediated electrocatalysis between methylene blue and ferricyanide at the first working electrode. Methylene blue is reduced to leucomethylene blue, and can, in turn reduce ferricyanide in solution to ferrocyanide, regenerating the oxidized methylene blue in the process. A second working electrode incorporated into a fluidics device enables the ferrocyanide to be transported to the secondary working electrode, where it can be reoxidized to ferricyanide. The reoxidation of ferrocyanide at the secondary electrode will generate a current proportional to the amount of ferrocyanide in solution, which is a direct measure of the amount of DNA CT occurring at the primary electrode. Before DNA CT-based detection is attempted with this platform, however, the fundamentals of glassy carbon surface modification must be established.

Surface Modification of Glassy Carbon Rod Electrodes

Aniline-based modifications are the most prevalent and well established glassy carbon modification methods.[30-32, 34, 36, 37] The general procedure for covalent aniline attachment to carbon surfaces is to convert the aniline to a diazonium, followed by electrochemical generation of a radical through the loss of N_2 (Figure 7.3).

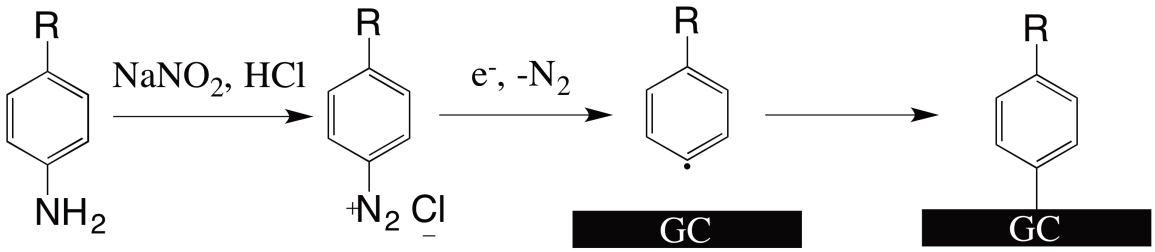

Figure 7.3 Diazonium formation and glassy carbon surface modification. An aniline derivative is first converted to a diazonium salt upon treatment with sodium nitrite under acidic conditions. Following diazonium formation, an aryl radical is formed electrochemically, which is capable of covalent attachment to carbon surfaces.

This aryl radical then reacts to form a carbon-carbon bond with the surface. Two main methods exist to generate the diazonium: it is either formed and isolated[30] before electrodeposition or it is generated *in situ*.[31] Both techniques involve the formation of the diazonium with sodium nitrite at 4° C, followed by conversion of the diazonium to an aryl radical electrochemically.

Many conditions are reported for the electrochemical deposition of anilines onto carbon electrode surfaces,[31-33, 35-37] but the most common techniques are cyclic voltammetry (CV) and constant potential amperometry (CPE).[30] Using CV, aniline derivatives were activated under various conditions to verify the activation in the flow-through device (Figure 7.4). By CV, multiple irreversible reductive peaks are observable. On GC rod electrodes (Figure 7.4, top left) with *in situ* diazonium formation, these peaks occur at -0.4 and -0.8 V (vs AgCl/Ag), and with pre-formed diazonium salts (Figure 7.4, bottom left), the peaks occur at -0.2 V and -0.5 V (vs AgCl/Ag). While these peaks occur at slightly different potentials, this is likely due to differences between the solvents and the other components present in solution for activation. On the flow-through electrodes (Figure 7.4, top right), peaks are observed at -0.1 V and -0.5 V (vs AgCl/Ag). Importantly, after the first scan, the intensities of these peaks decrease significantly, and the potential of remaining peaks shifts slightly negative. This phenomenon is consistent with the formation of a grafted azidobenzene layer on the carbon electrode,[30] indicating that our device is capable of electrochemical aniline deposition.

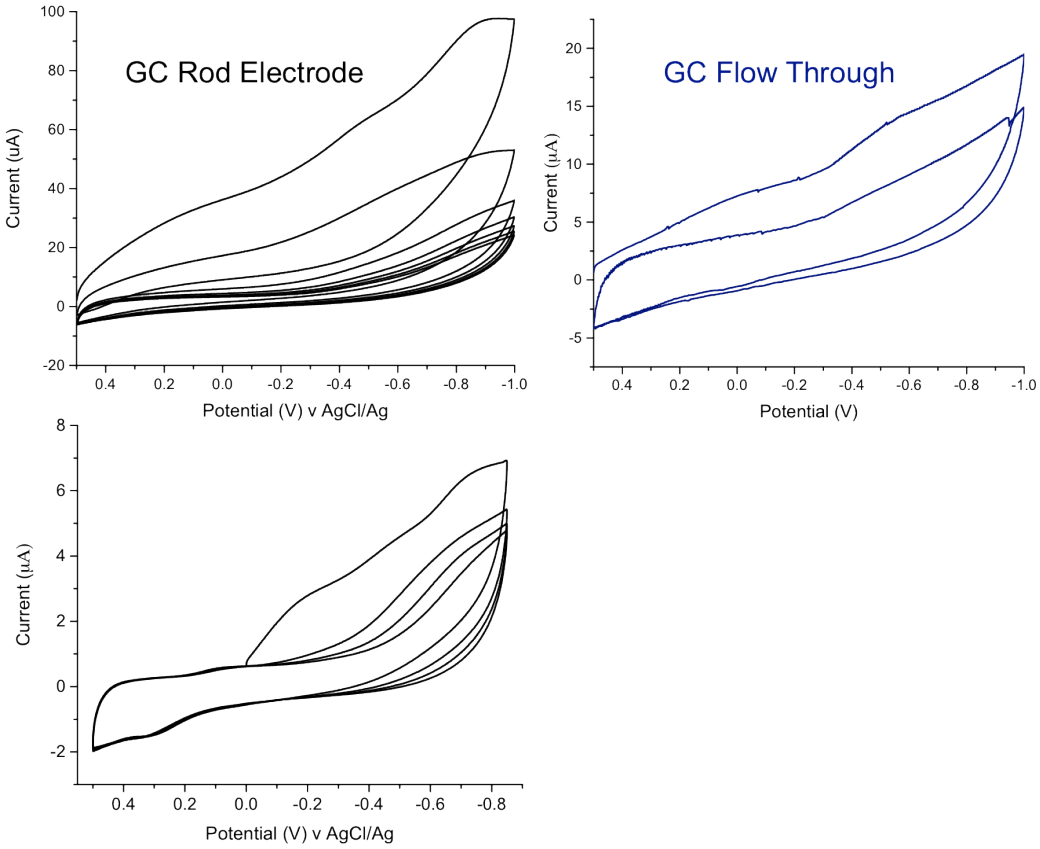

Figure 7.4 Electrochemical modification of glassy carbon surfaces with 4-azidobenzene diazonium salt. Shown are activations on rod electrodes (*left*) and on flow-through cells (*right*). *In situ* diazonium formation (*top*) yields two very similar sets of cyclic voltammograms for the rod electrodes and the flow-through cells. The pre-formed diazonium salt used to modify a glassy carbon electrode (*bottom*) has slightly different peak characteristics as compared to the *in situ* formation. However, in all cases, after the preliminary scan, a significant decrease in current is observed, indicating coupling to the carbon surface. For *in situ* diazonium formation, the electrochemistry was obtained with degassed 1 mM aniline in 0.1 M tetrabutylammonium tetrafluoroborate containing 4% 1M HCl at 4° C, with 1 mM sodium nitrite added. In the case of the pre-formed diazonium salt, surface modification is performed with 1.3 mM aniline in degassed 0.1 M HCl at 4° C. Scan rate: 0.1 V/s.

Modified Glassy Carbon Rod Electrode Passivation against Ferricyanide and Methylene Blue

With the eventual goal of performing DNA CT-based detection on these flow-through cells, it is vital that monolayers formed be passivated against electrocatalytic components. A family of aniline derivatives (4-azidoaniline, aniline, 4-aminobenzoic acid, p-phenylenediamine, and 4-nitroaniline) (Figure 7.6) was tested for passivation against the redox-active species commonly used for DNA CT electrocatalysis, methylene blue and ferricyanide.[38] All of the aniline derivatives yielded modified surfaces that were passivated against ferricyanide in excess of 500 μM (data not shown), a significantly higher concentration than is necessary for DNA-mediated electrocatalysis. However, the same was not true for passivation against methylene blue.

Methylene blue titrations against the same family of aniline derivatives were performed (Figure 7.5). On electrodes modified with 4-azidoaniline and aniline, methylene blue had a higher binding affinity than on bare GC electrodes, with electrochemical signals apparent at a concentration of 500 nM (methylene blue signals are detectable on bare GC at 1.5 μM). 4-aminobenzoic acid modified electrodes were well passivated against methylene blue until 2 μM DNA, which is below the necessary concentration for DNA binding. Finally, surfaces modified with either 4-nitroaniline or p-phenylenediamine were extremely well passivated against methylene blue with no detectible binding below 10 uM (Figure 7.5).

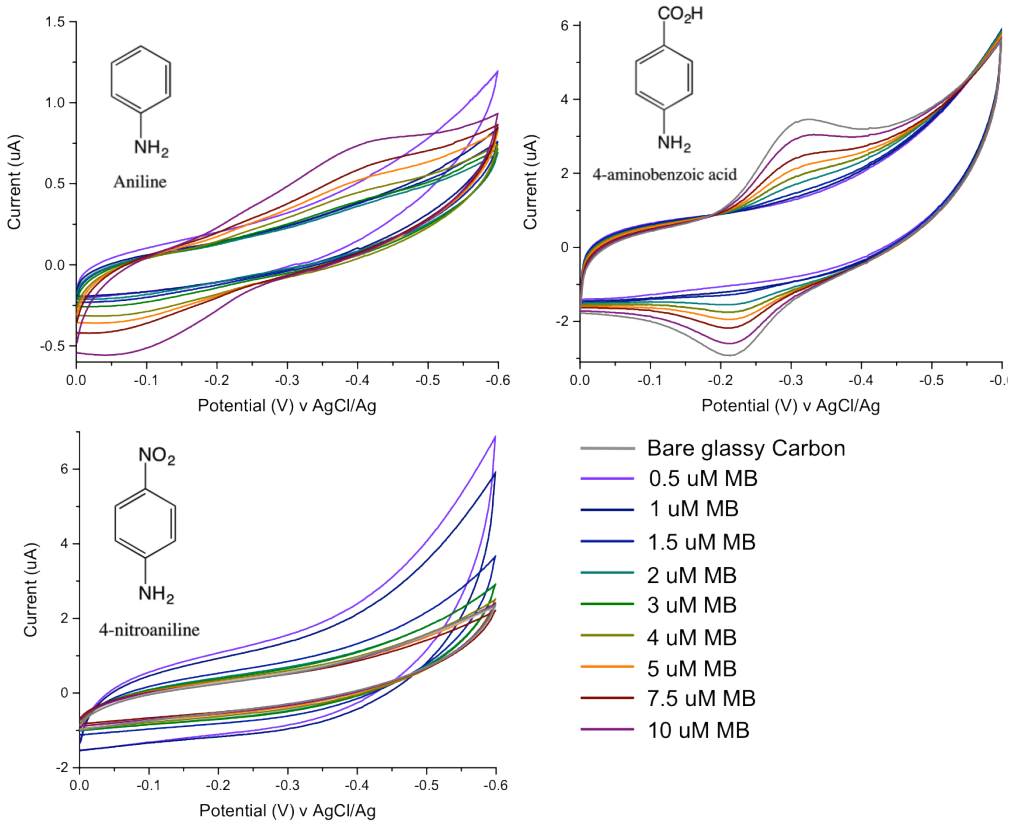

Figure 7.5 Methylene blue titration with modified glassy carbon electrodes. Shown is an electrode modified with aniline alone (*top left*), on which methylene blue signals are observed at 500 nM concentrations. 4-aminobenzoic acid is slightly better passivated, with methylene blue signals apparent at 2 µM (*top right*). Finally, the best passivation is observed with 4-nitroaniline (*bottom left*), which is passivated against methylene blue at concentrations in excess of 10 µM. All titrations were performed in Tris buffer (10 mM Tris, 100 mM KCl, 2.5 mM $MgCl_2$, 1 mM $CaCl_2$, pH 7.6). Scan rate: 0.1 V/s.

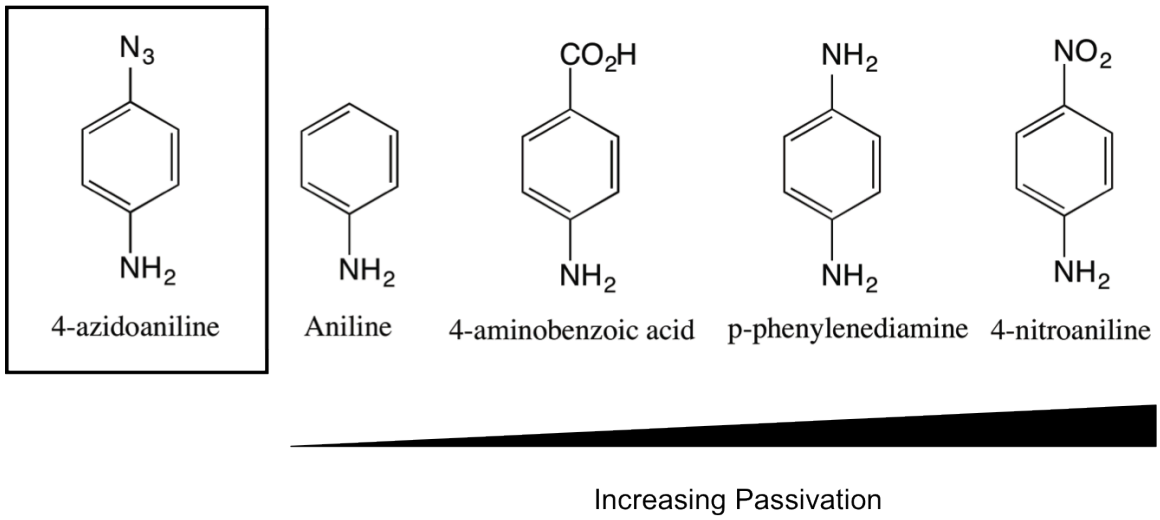

Figure 7.6 Aniline derivatives evaluated for methylene blue passivation ability. Each compound is used to functionalize a glassy carbon electrode. Methylene blue is titrated onto the monolayers to determine the maximum concentration at which the modified electrodes are passivated. The order of passivation, from least passivated to most passivated, is shown from left to right.

It is important to note, however, that we were unable to click ethynyl ferrocene onto the GC electrodes modified with a mixture of azidoaniline and either *p*-phenylenediamine or 4-nitroaniline, the two compounds that yielded passivation against methylene blue. This result will be discussed further in the following section.

Functionalization of Modified Glassy Carbon Rod Electrodes

To form DNA-modified glassy carbon electrodes, DNA must be covalently tethered to azidoaniline-modified GC electrodes. To evaluate the ease of performing the click reaction on such monolayers, ethynyl ferrocene was used as a model alkyne complex, as it is inherently electrochemically active, and provides a large electrochemical signal upon successful coupling. The general method of ethynyl ferrocene covalent attachment to modified GC electrodes is shown in Figure 7.7.

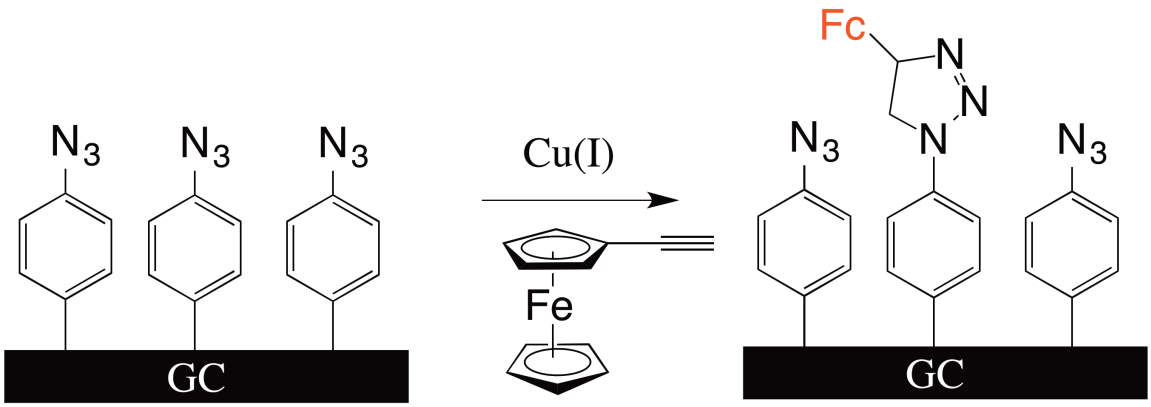

Figure 7.7 Functionalization of modified glassy carbon electrodes with ethynyl ferrocene (Fc). In the presence of a copper (I) source, ethynyl ferrocene is covalently tethered to glassy carbon electrodes modified with azidoaniline through click chemistry.

Preliminary attempts to tether ethynyl ferrocene to modified GC utilized mixed aniline modified electrodes. 50% of the aniline in solution for attachment was 4-azidoaniline, and 50% was an alternative aniline derivative shown in Figure 7.6. The ability to tether ethynyl ferrocene was found to be inversely proportional to the ability of the aniline derivative to block methylene blue. This result suggests that free methylene blue cannot be used for electrocatalysis with this flow-through device because glassy carbon modifications are insufficiently passivated against the redox-active molecule, resulting in direct surface reduction of methylene blue instead of DNA-mediated reduction. Therefore, a covalent redox probe may be necessary for electrocatalysis with this platform; many are compatible with both DNA CT and electrocatalysis.[4, 39]

Ethynyl ferrocene was successfully tethered to a mixed aniline and 4-azidoaniline surface using click chemistry. To directly compare the efficacy of copper(I) sources for this click reaction, GC electrodes were either modified with 50% aniline and 50% 4-azidoaniline or 100% 4-azidoaniline. Four copper sources were tested for their ability to catalyze the click reaction between the electrode surface and ethynyl ferrocene: $[Cu(phendione)_2]^{2+}$, $[Cu(bathophen)_2]^{2-}$, $CuSO_4$, and $[Cu(TBTA)]^{2+}$. The copper compounds were reduced with ascorbic acid, and ethynyl ferrocene coupling to surfaces was allowed to proceed for 90 minutes. The results of these coupling attempts are shown in Figure 7.8. In all cases, ethynyl ferrocene coupling is observed. The lighter color for all copper compounds is coupling to the 50% aniline/50% 4-azidoaniline modified surface, while the darker is coupling to the 100% 4-azidoaniline modified surface.

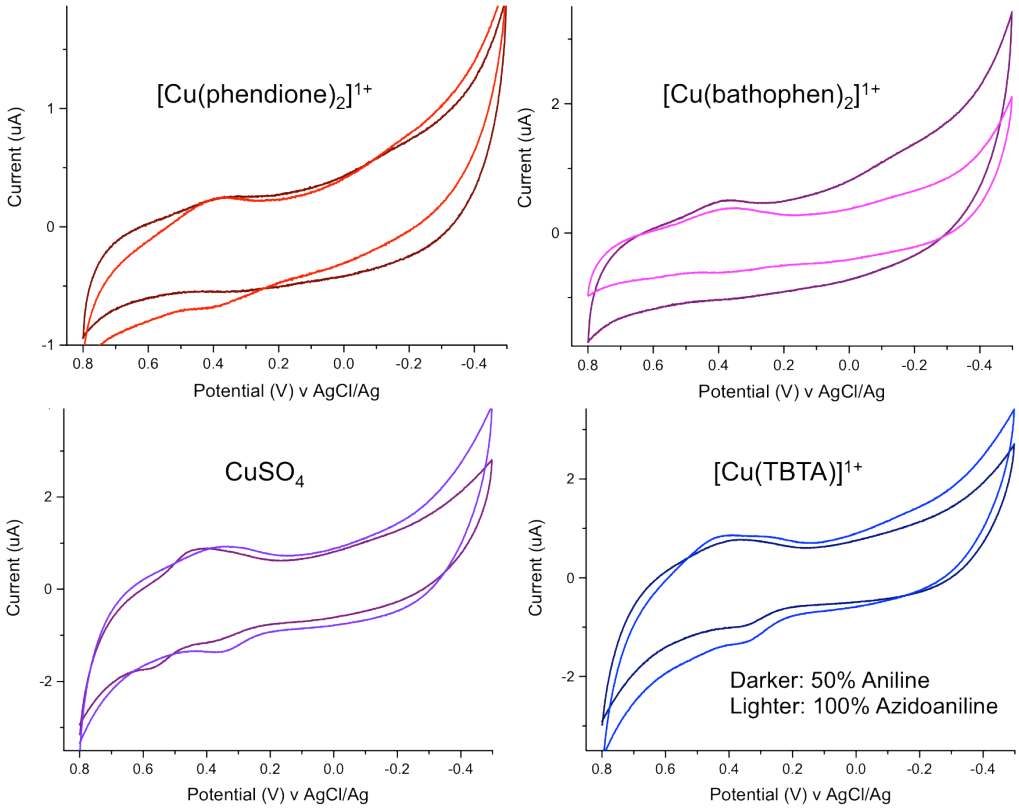

Figure 7.8 Ethynyl ferrocene coupling to modified glassy carbon electrodes. In all cases, the light color is the result of coupling to an electrode modified with 50% aniline/50% azidoaniline, while the darker is the result of coupling to a 100% azidoaniline-modified electrode. As can be seen, more efficient coupling is observed on the 50% aniline-modified electrodes. Scans were obtained in Tris buffer (10 mM Tris, 100 mM KCl, 2.5 mM $MgCl_2$, 1 mM $CaCl_2$, pH 7.6). Scan rate: 0.1 V/s.

Two issues arose with attempts to couple ethynyl ferrocene to modified GC surfaces using ascorbic acid-reduced copper compounds: first was optimization of the total amount of azidoaniline coupled to the modified GC surface, and second was optimization of the copper compound used for ethynyl ferrocene attachment. Based on the amount of ethynyl ferrocene coupled, the 50% aniline/50% azidoaniline-modified electrodes enable more efficient surface coupling with all of the copper sources. This result is consistent with what we have previously observed: more access to surface modifications through better spacing enables more efficient interaction between the surface modifications and the molecules in solution.[5, 7, 40]

Additionally, though, issues arose with the removal of copper complexes from the GC surface following activation. Some copper compounds are not as easily removed from electrode surfaces following coupling, and can result in electroactive species that remain on the electrode surfaces. As can be seen in Figure 7.9, copper signals are apparent with almost all compounds, except $[Cu(TBTA)]^{2+}$. This result is problematic for both eventual DNA attachment and electrochemical detection with monolayers formed using this technique. However, upon treatment of electrodes with EDTA (Ethylenediaminetetraacetic acid), a strong chelator of copper, the electrochemical copper signals were no longer observable. Results from a 20 minute EDTA treatment are shown in Figure 7.9.

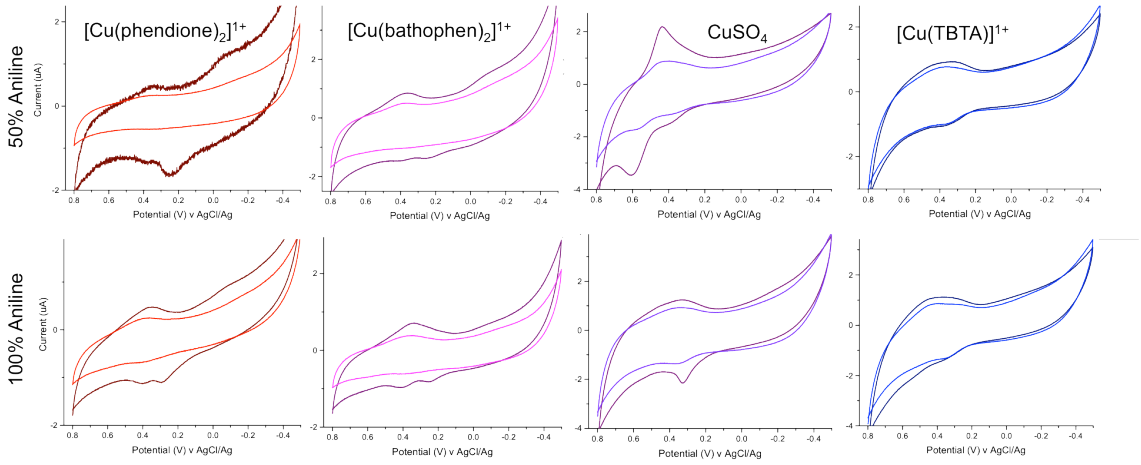

Figure 7.9 Ethynyl ferrocene-modified glassy carbon electrodes upon treatment with EDTA. Four sources of copper are evaluated for the ability to tether ethynyl ferrocene to an electrode modified with 50% aniline/50% azidoaniline (*top*) and coupling to a 100% azidoaniline-modified electrode (*bottom*). Before EDTA treatment (*darker colors*), copper contamination is apparent on the majority of electrodes. Following EDTA treatment (*lighter colors*), the copper signals are no longer present, indicating chelation and removal by EDTA. Scans were obtained in Tris buffer (10 mM Tris, 100 mM KCl, 2.5 mM $MgCl_2$, 1 mM $CaCl_2$, pH 7.6). Scan rate: 0.1 V/s.

Further study will optimize the glassy carbon modification procedure for applications on the flow-through cell. Similarly, conditions for copper-catalyzed click will be evaluated to determine the optimal method for DNA coupling.

Conclusions

For clinically relevant biomolecule detection, not only should a sample be easy to prepare and analyze, but small volumes are key to minimize invasiveness. We have previously established platforms for the detection of methyltransferases from crude tissue lysate. However, to apply this assay clinically, both the ease of sample preparation and speed of detection must be increased. The most efficient technique to meet both of these requirements is microfluidics. We have developed a device that uses inexpensive commercially available materials. This device enables flow through within the electrodes, minimizing the sample volumes required, while also maximizing the surface area-to-volume ratio of the electrodes, which are made of glassy carbon. This flow-through cell differs from traditional nucleic acid electrodes because it is cylindrical, as opposed to common planar electrodes.

To verify that the structure of these cylindrical electrodes does not affect performance, aniline was electrochemically deposited on both glassy carbon rod electrodes and the flow-through device, and the two different electrode shapes were found to behave similarly. The flow-through cell additionally incorporates the ability to control the density of surface functionalization through mixed aniline surface modification. A second working electrode is incorporated into the flow-through cell, facilitating detection in the same manner as the two working electrode detection platform previously shown to enable especially sensitive detection. A family of aniline derivatives was used to test passivation against common electrocatalytic agents. Surfaces are fully passivated against 500 μM ferricyanide; however, they are not passivated against even

very low concentrations (500 nM in some cases) of free methylene blue, indicating the need for a covalent electrochemical probe.

Click attachment of ethynyl ferrocene, and subsequently DNA, to these modified surfaces is being optimized on glassy carbon rod electrodes and will be applied to the flow-through device. This flow-through device behaves similarly to rod electrodes while significantly reducing the sample volume required for the electrode areas. This device is easily manipulated to enable multiplexing, and the cylindrical GC electrode surface is easily modified for rapid attachment of aniline derivatives. The ease of modification of this device will enable a multitude of new detection platforms with covalently-tethered duplex DNA attached to the surface to facilitate DNA-mediated detection of particular analytes from sub-μL sample volumes.

References

1. Boon, E. M., Ceres, D. M., Drummond, T. G., Hill, M. G., and Barton, J. K. (2000) Mutation detection by electrocatalysis at DNA-modified electrodes, *Nat. Biotechnol. 18*, 1096-1100.

2. Kelley, S. O., Boon, E. M., Barton, J. K., Jackson, N. M., and Hill, M. G. (1999) Single-base mismatch detection based on charge transduction through DNA, *Nucleic Acids Res. 27*, 4830-4837.

3. Gorodetsky, A. A., Hammond, W. J., Hill, M. G., Slowinski, K., and Barton, J. K. (2008) Scanning electrochemical microscopy of DNA monolayers modified with Nile Blue, *Langmuir 24*, 14282-14288.

4. Gorodetsky, A. A., Ebrahim, A., and Barton, J. K. (2008) Electrical detection of TATA binding protein at DNA-modified microelectrodes, *J. Am. Chem. Soc. 130*, 2924-2925.

5. Furst, A., Landefeld, S., Hill, M. G., and Barton, J. K. (2013) Electrochemical patterning and detection of DNA arrays on a two-electrode platform, *J. Am. Chem. Soc. 135*, 19099-19102.

6. Muren, N. B., and Barton, J. K. (2013) Electrochemical assay for the signal-on detection of human DNA methyltransferase activity, *J. Am. Chem. Soc. 135*, 16632-16640.

7. Furst, A. L., Muren, N. B., Hill, M. G., and Barton, J. K. (2014) Label-free electrochemical detection of human methyltransferase from tumors, *Proc. Natl. Acad. Sci. USA 111*, 14985-14989.

8. Mu, X., Zheng, W., Sun, J., Zhang, W., and Jiang, X. (2013) Microfluidics for manipulating cells, *Small 9*, 9-21.

9. Kumaresan, P., Yang, C. J., Cronier, S. A., Blazej, R. G., and Mathies, R. A. (2008) High-throughput single copy DNA amplification and cell analysis in engineered nanoliter droplets, *Anal. Chem. 80*, 3522-3529.

10. Whitesides, G. M. (2006) The origins and the future of microfluidics, *Nature 442*, 368-373.

11. Srinivasan, V., Pamula, V. K., and Fair, R. B. (2004) Droplet-based microfluidic lab-on-a-chip for glucose detection, *Anal. Chim. Acta 507*, 145-150.

12. Werdich, A. A., Lima, E. A., Ivanov, B., Ges, I., Anderson, M. E., Wikswo, J. P., and Baudenbacher, F. J. (2004) A microfluidic device to confine a single cardiac myocyte in a sub-nanoliter volume on planar microelectrodes for extracellular potential recordings, *Lab Chip 4*, 357-362.

13. Cai, X., Klauke, N., Glidle, A., Cobbold, P., Smith, G. L., and Cooper, J. M. (2002) Ultra-low-volume, real-time measurements of lactate from the single heart cell using microsystems technology, *Anal. Chem. 74*, 908-914.

14. Pumera, M., Wang, J., Opekar, F., Jelinek, I., Feldman, J., Lowe, H., and Hardt, S. (2002) Contactless conductivity detector for microchip capillary electrophoresis, *Anal. Chem. 74*, 1968-1971.

15. Effenhauser, C. S., Bruin, G. J., Paulus, A., and Ehrat, M. (1997) Integrated capillary electrophoresis on flexible silicone microdevices: analysis of DNA restriction fragments and detection of single DNA molecules on microchips, *Anal. Chem. 69*, 3451-3457.

16. Baylin, S. B., and Herman, J. G. (2000) DNA hypermethylation in tumorigenesis: epigenetics joins genetics, *Trends in Genet. 16*, 168-174.

17. De Marzo, A. M., Marchi, V. L., Yang, E. S., Veeraswamy, R., Lin, X., and Nelson, W. G. (1999) Abnormal regulation of DNA methyltransferase expression during colorectal carcinogenesis, *Cancer Res. 59*, 3855-3860.

18. Esteller, M. (2008) Epigenetics in cancer, *New Engl. J. Med. 358*, 1148-1159.

19. Esteller, M., Corn, P. G., Baylin, S. B., and Herman, J. G. (2001) A gene hypermethylation profile of human cancer, *Cancer Res. 61*, 3225-3229.

20. Esteller, M., Fraga, M. F., Paz, M. F., Campo, E., Colomer, D., Novo, F. J., Calasanz, M. J., Galm, O., Guo, M., Benitez, J., and Herman, J. G. (2002) Cancer epigenetics and methylation, *Science 297*, 1807-1808; discussion 1807-1808.

21. Feinberg, A. P., and Tycko, B. (2004) The history of cancer epigenetics, *Nat. Rev. Cancer 4*, 143-153.

22. Li, E., Beard, C., and Jaenisch, R. (1993) Role for DNA methylation in genomic imprinting, *Nature 366*, 362-365.

23. Baylin, S. B. (1997) Tying it all together: epigenetics, genetics, cell cycle, and cancer, *Science 277*, 1948-1949.

24. Heyn, H., and Esteller, M. (2012) DNA methylation profiling in the clinic: applications and challenges, *Nat. Rev. Genet. 13*, 679-692.

25. Jones, P. A., and Baylin, S. B. (2002) The fundamental role of epigenetic events in cancer, *Nat. Rev. Genet. 3*, 415-428.

26. Jones, P. A., and Laird, P. W. (1999) Cancer epigenetics comes of age, *Nat. Genet. 21*, 163-167.

27. Rhee, I., Bachman, K. E., Park, B. H., Jair, K. W., Yen, R. W., Schuebel, K. E., Cui, H., Feinberg, A. P., Lengauer, C., Kinzler, K. W., Baylin, S. B., and Vogelstein, B. (2002) DNMT1 and DNMT3b cooperate to silence genes in human cancer cells, *Nature 416*, 552-556.

28. Robert, M. F., Morin, S., Beaulieu, N., Gauthier, F., Chute, I. C., Barsalou, A., and MacLeod, A. R. (2003) DNMT1 is required to maintain CpG methylation and aberrant gene silencing in human cancer cells, *Nat. Genet. 33*, 61-65.

29. Das, J., Cederquist, K. B., Zaragoza, A. A., Lee, P. E., Sargent, E. H., and Kelley, S. O. (2012) An ultrasensitive universal detector based on neutralizer displacement, *Nat. Chem. 4*, 642-648.

30. Evrard, D., Lambert, F., Policar, C., Balland, V., and Limoges, B. (2008) Electrochemical functionalization of carbon surfaces by aromatic azide or alkyne molecules: a versatile platform for click chemistry, *Chemistry 14*, 9286-9291.

31. Baranton, S., and Belanger, D. (2005) Electrochemical derivatization of carbon surface by reduction of in situ generated diazonium cations, *J. Phys. Chem. B 109*, 24401-24410.

32. Actis, P., Caulliez, G., Shul, G., Opallo, M., Mermoux, M., Marcus, B., Boukherroub, R., and Szunerits, S. (2008) Functionalization of glassy carbon with diazonium salts in ionic liquids, *Langmuir 24*, 6327-6333.

33. Bahr, J. L., Yang, J., Kosynkin, D. V., Bronikowski, M. J., Smalley, R. E., and Tour, J. M. (2001) Functionalization of carbon nanotubes by electrochemical reduction of aryl diazonium salts: a bucky paper electrode, *J. Am. Chem. Soc. 123*, 6536-6542.

34. Casella, I. G., and Guascito, M. R. (1997) Electrocatalysis of ascorbic acid ion the glassy carbon electrode chemically modified with polyaniline films, *Electroanalysis 9*, 1381-1386.

35. Liu, G. Z., Liu, J. Q., Bocking, T., Eggers, P. K., and Gooding, J. J. (2005) The modification of glassy carbon and gold electrodes with aryl diazonium salt: The impact of the electrode materials on the rate of heterogeneous electron transfer, *Chem. Phys. 319*, 136-146.

36. Ortiz, B., Saby, C., Champagne, G. Y., and Belanger, D. (1997) Carbon electrode modified with substituted phenyl grow: Useful electrode materials for sensors, *Abstr. Pap. Am. Chem. Soc. 213*, 51-ANYL.

37. Saby, C., Ortiz, B., Champagne, G. Y., and Belanger, D. (1997) Electrochemical modification of glassy carbon electrode using aromatic diazonium salts .1. Blocking effect of 4-nitrophenyl and 4-carboxyphenyl groups, *Langmuir 13*, 6805-6813.

38. Boon, E. M., Barton, J. K., Bhagat, V., Nersissian, M., Wang, W., and Hill, M. G. (2003) Reduction of Ferricyanide by Methylene Blue at a DNA-Modified Rotating-Disk Electrode, *Langmuir 19*, 9255-9259.

39. Pheeney, C. G., Guerra, L. F., and Barton, J. K. (2012) DNA sensing by electrocatalysis with hemoglobin, *Proc. Natl. Acad. Sci. USA 109*, 11528-11533.

40. Furst, A. L., Hill, M. G., and Barton, J. K. (2013) DNA-modified electrodes fabricated using copper-free click chemistry for enhanced protein detection, *Langmuir 29*, 16141-16149.

Chapter 8

Thymine Dimers for DNA Nanocircuitry Applications

Introduction

Current technology for the production of nanoscale electronics relies on a top-down approach involving lithography to pattern chips. However, this technology is reaching a limit; on such small scales, problems such as charge leakage through imperfections in the insulation occur, resulting in burnout of the circuit.[1, 2] An alternative to current lithographic techniques is a bottom-up approach, which relies on single molecules to act as the conductive wires in the circuit. Molecular wires circumvent the majority of issues associated with miniaturization of circuitry components because each wire is completely self-contained.[3]

Molecular wires are thus a significant improvement over lithography for applications on the nano and sub-nanoscale. However, these wires have their own problems, especially with their implementation for commercial production. Molecular wires must have uniform lengths and conductive properties, functionalized termini, and the ability to conduct charge over nanoscale distances.[1, 3] These stringent criteria severely limit the current applications of molecular wires.

Most molecular wires fall into three categories: conjugated hydrocarbons, carbon nanotubes, and porphyrin oligomers.[4] While examples of these molecules have all been shown capable of acting as molecular wires, each also has drawbacks. Conjugated hydrocarbons are often difficult to uniformly synthesize and terminally functionalize, carbon nanotubes cannot be produced on a large scale with uniform conductive properties, and porphyrin oligomers cannot be readily synthesized into oligomers longer than several monomers.[4] The difficulty with manufacturing these molecular wires on a large scale with uniform properties has prohibited their broad applicability in circuitry.

In contrast, DNA is uniformly and efficiently synthesized with a variety of easily incorporated terminal functionalizations on a large scale. Furthermore, DNA has the unique ability to conduct electrons through its π-stacked bases, a phenomenon known as DNA charge transport (DNA CT). This unique property, in addition to the ease of synthesis and functionalization, imbues DNA with the qualities necessary to act as a component of a molecular circuit. Importantly, DNA has a shallow distance dependence, with a β value determined to be less than 0.05 (an ideal molecular wire has a β value of 0).[4] DNA CT is both robust and sensitive; charge transport has been shown to occur through 100 base pairs, 34 nm, with signal sizes comparable to those found for 17 base pair duplexes.[4] The ease of synthesis combined with the shallow distance dependence makes DNA ideal for potential applications as molecular wires.

In addition to its conductive properties, DNA has structural characteristics that increase its value as a potential component of a molecular circuit. Because of its dependence on the structure of DNA, DNA CT is highly sensitive to perturbations in the base stack. Any alterations that lead to destacking of the bases, including a mismatched base pair,[5] a damaged base,[6] or a DNA binding protein that kinks or bends the DNA, significantly attenuates the DNA-mediated electrochemical signal.[7, 8] Thus, any reversible DNA damage product has the potential to function as an internal switch. The inherent directionality of DNA further allows for specificity in terminus functionalization; the 5' and 3' ends of DNA can easily be modified independently to enable specific tethering within a circuit using orthogonal tethering methods.

The Barton group has extensively studied the basic properties of DNA CT by probing DNA self-assembled monolayers (SAMs) electrochemically.[5, 9-13] DNA

monolayers are assembled on gold surfaces through a terminal alkanethiol linker that forms a gold-sulfur bond with the electrode.[11, 14] The density of the assembled DNA can be somewhat controlled with the addition of magnesium chloride to the assembly solution of DNA.

DNA CT can be directly measured through a redox-active probe covalently linked to the complementary strand of DNA. Importantly, the probes must be well coupled to the π-stack in order to report DNA CT. The two main covalent probes currently employed by our group are Methylene Blue and Nile Blue (Figure 8.1). These probes differ in their mechanism of interaction with the base stack; Nile Blue is electronically coupled to the duplex through direct conjugation with the modified uracil to which it is appended (Figure 8.1B).[13] In contrast, Methylene Blue, tethered to the DNA by a long alkyl linkage, interacts with the base stack through direct intercalation with the bases (Figure 8.1A).[15] Both of these probes are used in the research described.

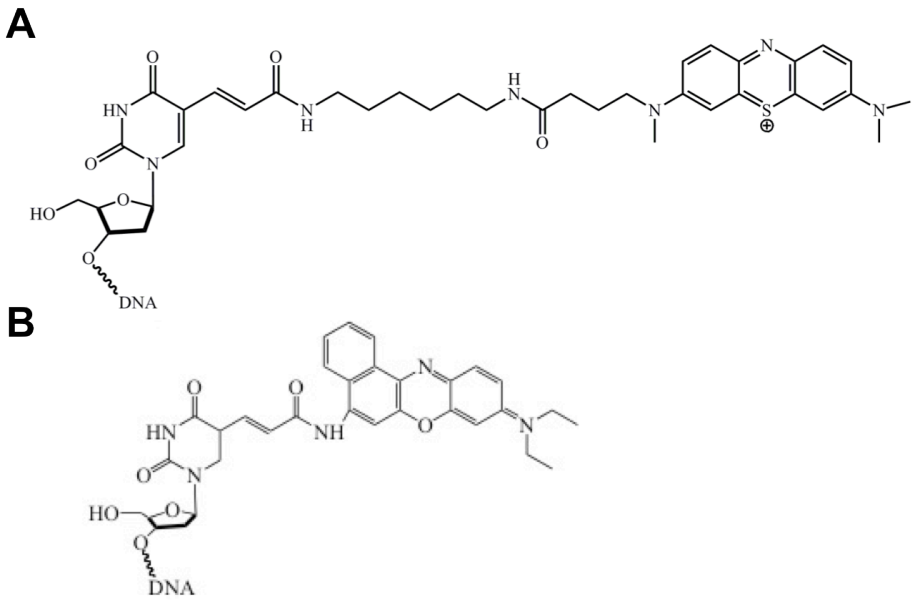

Figure 8.1 Common covalent redox reporters for DNA CT on gold surfaces. The methylene blue (*top)* is connected to the DNA through a long alkyl linker. The synthetically modified methylene blue is attached to the base through amide bond formation with an amine-modified terminal base. This probe is capable of intercalating into the DNA base stack because of the flexible tether. The covalent Nile Blue moiety (*bottom*) is tethered to a modified uracil base. Because this probe lacks a long, flexible tether, it reports on charge transport through the conjugated tether to the DNA.

In order to probe DNA CT effectively for its applications to molecular circuitry, multiple experimental conditions with redundancy are required. Single gold rod electrodes are therefore insuffucient for such complex experiments. The Barton group has developed a multiplexed platform for simultaneous analysis of DNA CT through multiple DNA films on the same surface.[13] Multiplexed chips contain 16 individually addressable gold electrodes that can be divided into four quadrants (Figure 8.2). Electrodes are patterned onto silicon wafers using a two-step photolithographic technique. The multiplexed electrode areas are defined using photoresist followed by metal evaporation, and the individual electrodes are isolated through the addition of an insulating layer of SU-8 photoresist. Each electrode contains the working electrode area, leads, and contact pads around the exterior of the chip that enable each electrode to be addressed individually. This is advantageous over the single gold electrodes previously employed because four types of DNA can be assembled and measured on the same surface with four replicates simultaneously. This platform has opened significant avenues for pursuing both molecular wire-based and biosensing applications for DNA.

As DNA has been established to have all of the features of an effective molecular wire, the question of increasing the complexity of DNA circuitry components arises: what circuitry components could be directly incorporated into DNA nanowires through the exploitation of DNA's natural structure? Here, the progress made toward the development of a reversible switch for DNA CT is described.

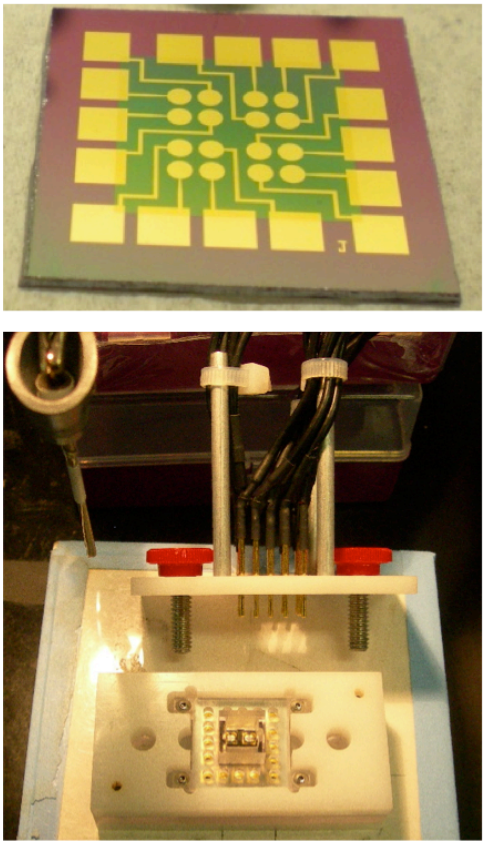

Figure 8.2 Multiplexed chip platform. Multiplexed chip (*top*) contains sixteen individually addressable electrodes divided into four quadrants. The electrodes are centered on the silicon wafer with the pads for connection around the exterior. The clamp (*bottom*) contains sixteen leads connected to a multiplexer. The clamp on the chip divides the electrodes into four quadrants with a single well to contain the electrolyte solution.

Reversible switches are the simplest circuitry component to incorporate as additional complexity into DNA-based nanostructures. The Barton group has demonstrated that DNA lesions that disrupt the π-stack attenuate DNA CT,[6, 7, 16-19] but circuitry-based applications require completely reversible, precise, controlled, and robust switching. One method of achieving these criteria is through the formation of the reversible DNA damage product, a thymine-thymine cyclobutane dimer.

Thymine dimers are formed through [2+2] cycloadditions between adjacent thymine bases on the same strand of DNA, forming a covalently-bound cyclobutane dimer (Figure 8.3). The major photoproduct formed has the *cis-syn* dimer, which is the stereochemistry shown in Figure 8.3. The thymine dimer lesion causes a 30° bend toward the major groove of a DNA duplex[20] and therefore attenuates DNA CT (Figure 8.4).[6] In nature, thymine dimers are formed upon photoexcitation of the DNA with UV light.[21] Because the adjacent thymines are identical, they are capable of forming an exciton and subsequently, an excimer. These states are specific to interactions between identical components of a complex. The ability of adjacent thymines to form such excited intermediates is one of the reasons that thymine dimers are the most common form of DNA photodamage.[22] UV irradiation is not optimal for the formation of thymine dimers in a laboratory environment because it can cause additional, nonspecific damage. Controlled thymine dimer formation is therefore performed in the laboratory with the aid of the triplet sensitizer acetophenone.[22]

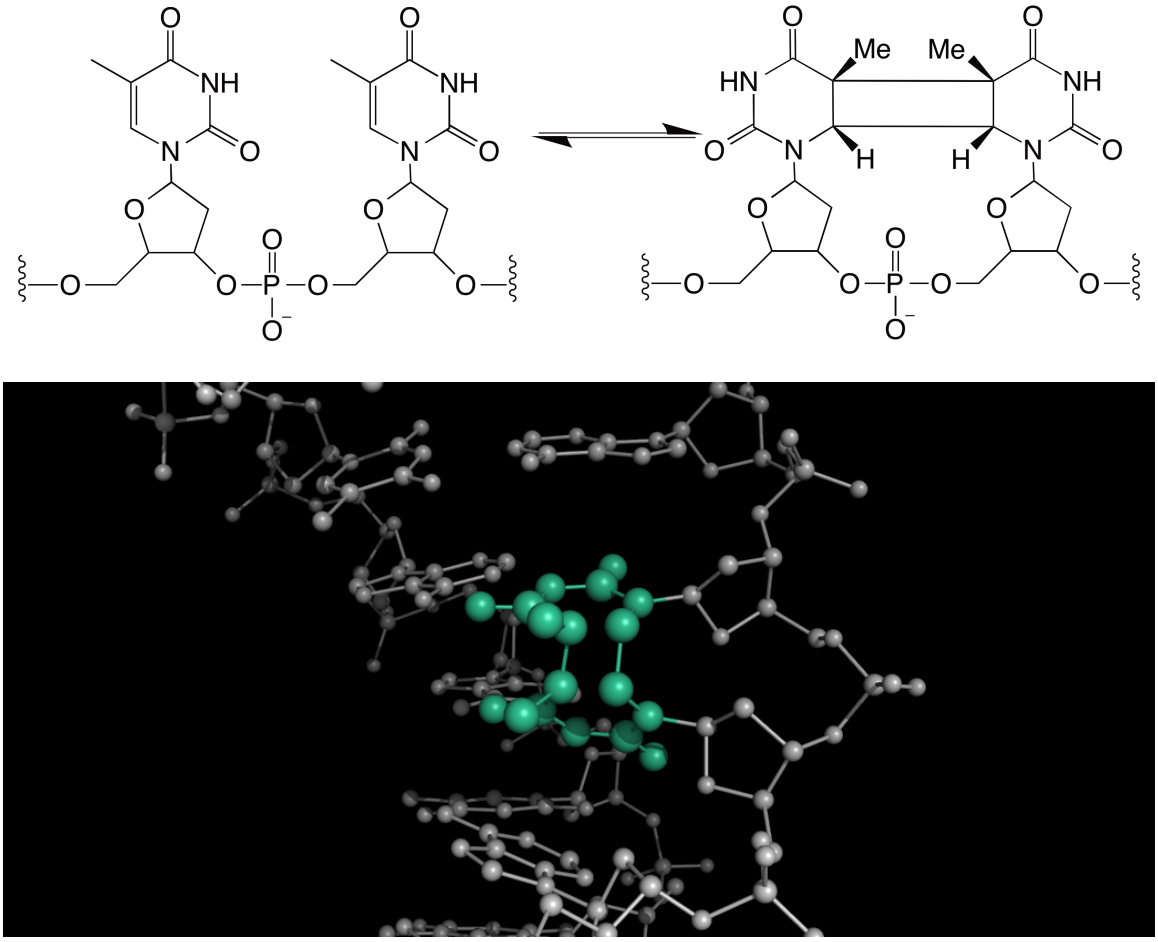

Figure 8.3 Thymine dimer formation. Top: Cyclobutane formation between adjacent thymine bases on the same strand of DNA. Bottom: Crystal structure of cyclobutane formation between adjacent bases on a single strand of DNA. Damaged bases (green) are overlaid onto undamaged (purple). The thymine dimer, shown in green, causes a significant pucker in the bases.

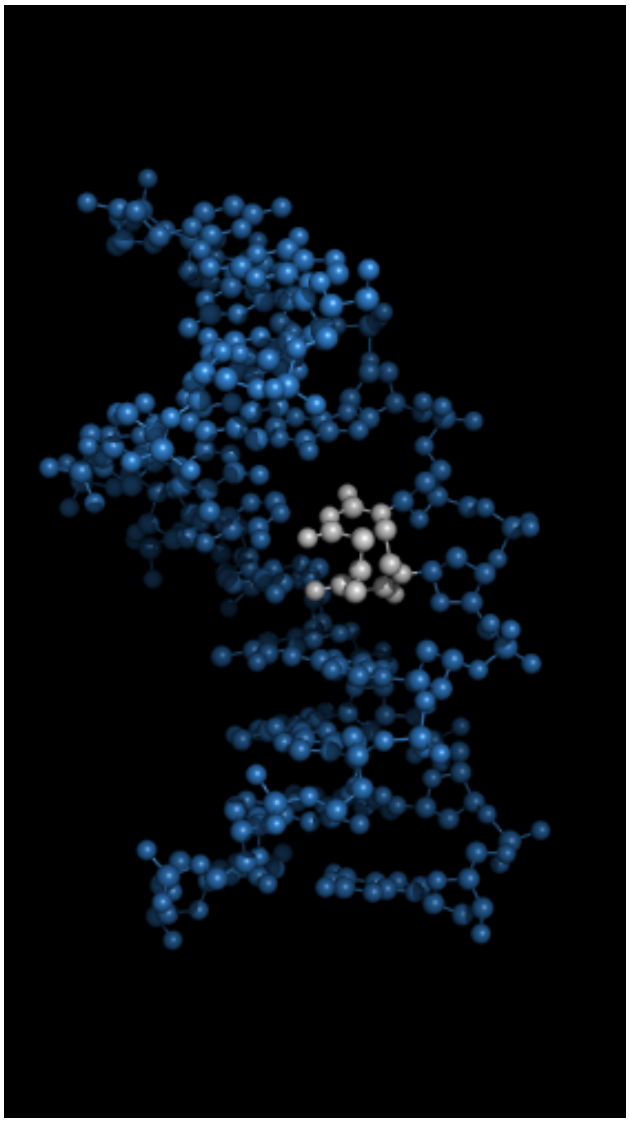

Figure 8.4 Crystal structure of a DNA duplex containing a thymine dimer. As can be seen from the thymine dimer (grey) formed on a single strand of the duplex, this damage product causes a significant kink in the DNA, with a distortion of over 30°.[20]

There are three major methods of thymine dimer repair: photocycloreversion with 254 nm light,[23] repair by the enzyme photolyase,[6] or repair by irradiation with a small molecule such as the organic intercalator naphthalene diimide (NDI)[24] or a rhodium(III) intercalator (Figure 8.5). Previous work in our group has demonstrated that the rhodium(III) intercalator, $Rh(phi)_2bpy^{3+}$, upon excitation with visible light, yields complete repair of thymine dimers.[25, 26] When the metal complex is photoexcited, an electron hole is injected into the DNA duplex, which breaks the cyclobutane dimer bonds, reejecting the electron hole and reforming two native thymine bases. These small rhodium complexes are advantageous for molecular switching, as they intercalate nonspecifically and can mediate thymine dimer repair over long distances. However, all previous studies with such metal complexes were performed in solution. Thus, experimentation to determine the efficacy of these complexes for thymine dimer repair on surfaces must be fully investigated to determine if the properties of this compound are equivalent on a surface to those of the compound in solution.

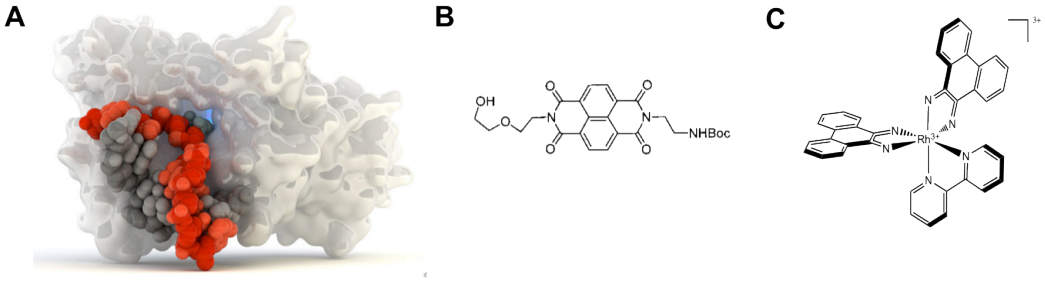

Figure 8.5 Modes of thymine dimer repair. A. The photolyase enzyme flips the dimerized bases out of the base stack to repair the cyclobutane.[34] B. The organic intercalator naphthalene diimide (NDI) is capable of repairing 27% of thymine dimers in solution. C. The rhodium intercalator, $Rh(phi)_2bpy^{3+}$ nonspecifically intercalates into the base stack and can repair 100% of thymine dimers in solution.

To date, our lab has focused on studying thymine dimer repair electrochemically on a surface using the enzyme photolyase. DNA containing a pre-formed thymine dimer was used to form a self-assembled monolayer (SAM) on a single gold electrode. The system was monitored for the growth of a signal upon addition of photolyase, an enzyme that repairs thymine dimers. However, the reversibility of this process on a surface over multiple cycles was never investigated, nor were chemical methods of repair.

Here, we work to develop a thymine dimer-based photochemical switch on multiplexed chips (Figure 8.6). Applying multiplexed chips to the development of photoswitches would enable the creation of complex switching patterns with the incorporation of internal controls (Figure 8.7). In addition to testing thymine dimer formation and repair, multiple redox probes, MB', NB and $Rh(phi)_2bpy'^{3+}$ are tested for applications in this system, as MB' and NB each act as more than a simple redox probe and interfere with switching conditions.

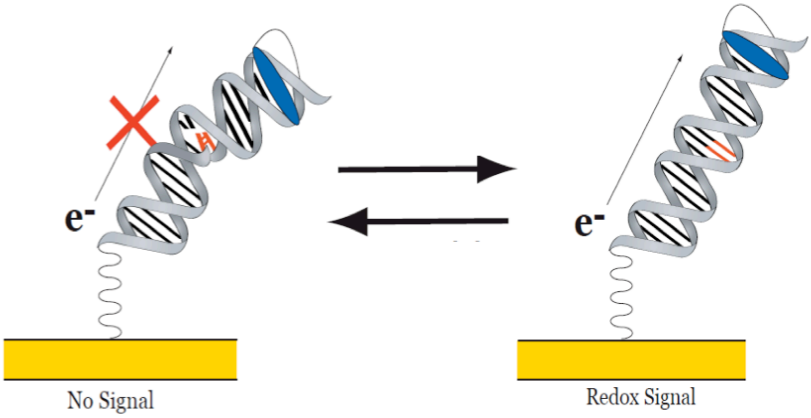

Figure 8.6 Thymine dimer formation and repair on multiplexed chips. DNA modified with an alkanethiol at the terminus of one strand and a redox probe at the terminus of the complementary strand form a film on a gold surface. Reversible thymine dimer formation and repair are used to modulate the electrochemical signal output from the system. Upon formation of a thymine dimer, the DNA helix is severely kinked, thereby significantly attenuating the electrochemical signal. Upon repair of the cyclobutane dimer, the electrochemical signal should return. Because mild conditions are used for thymine dimer formation, the reversibility of this process over multiple cycles is possible.

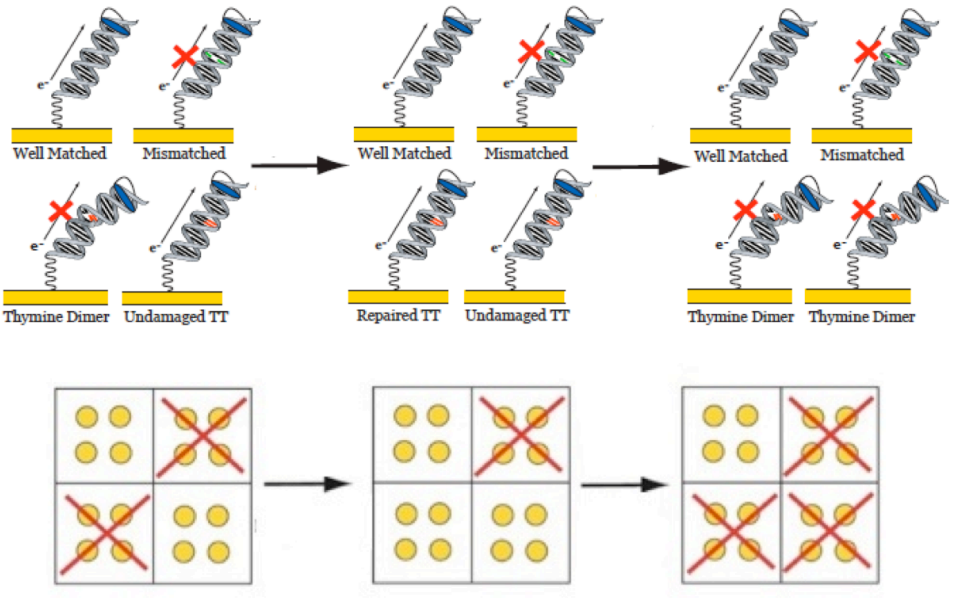

Figure 8.7 Overview of switching patterning on surfaces. Using multiplexed chips, up to four types of DNA can be observed simultaneously. A quadrant of well-matched DNA and a quadrant of mismatched DNA serve as controls for the on signal and off signal, respectively. Initially, one quadrant can contain DNA with a preformed thymine dimer (quadrant 4) and one quadrant containing a thymine dimer parent duplex (quadrant 3). Initially, quadrants 2 and 4 will have attenuated signals; however, upon thymine dimer repair on the surface, signal should be restored to quadrant 4. Then, under thymine dimer formation conditions, signal should be attenuated for quadrants 3 and 4. Thus thymine dimer switches can be used to create complex patterns of switching on surfaces.

Materials and Methods

DNA Synthesis

All reagents for DNA synthesis, including modified nucleotides and the C_6 thiol linker, were purchased from Glen Research.[27] Oligonucleotides were synthesized on an Applied Biosystems 3400 DNA synthesizer using standard phosphoramidite chemistry on a solid CPG support. Three DNA duplexes were designed for this work: a well-matched duplex, a duplex containing a CA mismatch, and a thymine dimer parent strand duplex containing adjacent thymine bases on one strand (Figure 8.8). For duplexes to be used in electrochemical experiments, the 5' end of one strand was modified with a C_6 S-S thiol linker, and the 5' end of the complementary strand was modified for redox reporter conjugation. Unless otherwise stated, after synthesis, DNA was cleaved from the solid support by incubation at 60° C with concentrated NH_4OH for 12 hours, followed by drying, resuspension in phosphate buffer (5.0 mM phosphate, 50 mM NaCl, pH 7.0), and HPLC purification with the dimethoxytrityl (DMT) group remaining. After deprotection, the DNA was again HPLC purified, desalted, and characterized by MALDI-TOF mass spectrometry.

Complementary DNA strands were quantified using UV/vis absorption at 260 nm. Equimolar amounts of each strand were prepared as a 50 μM solution in phosphate buffer (5.0 mM phosphate, 50 mM NaCl, pH 7.0) and annealed on a thermocycler by heating to 90°C followed by cooling to room temperature.

Well Matched
Redox Probe-5'-TGC ACA TGC ATG TGT GC-3'
3'-ACG TGT ACG TAC ACA CG-5'-SH

Mismatched
Redox Probe-5'-TGC ACA TGC ACG TGT GC-3'
3'-ACG TGT ACG TAC ACA CG-5'-SH

Parent Thymine Dimer
Redox Probe-5'-TCG ACG TGC AAC TGA GC-3'
3'-AGC TGC ACG TTG ACT CG-5'-SH

Figure 8.8 Sequences of DNA used for testing thymine dimer formation and repair. A CA mismatch, indicated with red text, is included in one of the sequences to observe its effect on signal attenuation. The sequence of the parent thymine dimer strand contains two adjacent thymine bases on one strand that have the potential to dimerize.

Thiol-Containing DNA Synthesis

Following standard synthesis and DMT-on HPLC purification, the disulfide terminus was reduced to a free thiol by suspending the sample in Tris buffer (50 mM Tris, pH 8.4) with DTT (100 mM) for 45 minutes. The sample was filtered through a Nap5 column prior to repurification by HPLC.

Nile Blue-modified DNA Synthesis[27]

DNA to contain Nile Blue (NB) was synthesized with Ultramild CE phosphoramidites and a terminal NHS-ester carboxy dT incorporated at the 5' end. While still attached to solid support, a saturated solution of NB (Sigma Aldrich) (150 mg NB in DCM with 10% DIEA) was added to the oligos. The columns were agitated for 24 h followed by rinsing with 5 mL each of DCM, methanol, and ACN. Cleavage from solid support was achieved with potassium carbonate (0.05M) in methanol for 12 h. DNA was purified and analyzed as previously described.

Methylene Blue-modified DNA Synthesis[15]

Methylene Blue (MB'), a modified form of the methylene blue dye containing a flexible alkyl tether and a terminal carboxylic acid, was synthesized in the Barton group. MB' was prepared for coupling to DNA by NHS ester activation. 8 mg (0.022 mmol) of MB' was combined with 9.3 mg (0.045 mmol) N,N'-dicyclohexylcarbodiimide and 5.2 mg (0.045 mmol) N-hydroxysuccinimide in 1 mL anhydrous DMF. The reaction was stirred for 24 h, followed by solvent removal under reduced pressure. Activation was

confirmed by ESI-MS in acetonitrile: water: acetic acid (1:1:0.1) (454.5 g/mol; calc'd 454.54 g/mol). The activated ester was resuspended in 50 μL DMSO.

DNA to be coupled to MB' was synthesized with a 5'-terminal amino-modified C6 dT phosphoramidite. The DNA was cleaved from solid support, deprotected, and HPLC-purified as previously described. Following desalting, the oligonucleotides were suspended in 200 μL of 0.1 M $NaHCO_3$, pH 8.3, and the MB'-ester in DMSO was added to the oligonucleotides in 10x excess. The reaction was shaken for 24 h, followed by a final round of HPLC purification. MALDI-TOF was used to confirm the formation of MB'-DNA.

Rhodium Conjugation to the 5' DNA Terminus

Coupling $Rh(phi)_2bpy'^{3+}$ (phi = 9, 10-phenanthrene quinone diimine; bpy' = 4-butyric acid-4'-methyl bipyridyl) to the 5' terminus of DNA was performed as described by Holmlin et al.[26] DNA was synthesized on large pore solid support (2000 Å) with the terminal protecting DMT group on the 5' end removed on the synthesizer. The DNA-beads (2x1.0 μmol) were subsequently added to glass cylinders containing a coarse frit and stopcock. The beads were washed 3 x 3 mL dry dioxane followed by the addition of 50 mg (308 μmol) carbonyl diimidazole (CDI) in 1 mL dioxane. The cylinder was purged with Ar(g) and shaken for 1 h. The beads were again washed with 5 x 3 mL dioxane. 36 mg (240 μmol) diaminononane in 1 mL 9:1 dioxane:H_2O was subsequently added to the vessel, which was shaken for 30 minutes followed by washing with 9:1 dioxane:H_2O, dioxane and methanol. 10 mg (13.3 μmol) $Rh(phi)_2bpy'^{3+}$, 1.9 mg (14.7 μmol) hydroxybenzotriazole (HOBt), 4.4 mg (11.6 μmol) O-Benzotriazole-N,N,N',N'-

tetramethyl-uronium-hexafluoro-phosphate (HBTU), and 80 μL N,N-diisopropylethylamine (DIEA) were added to the reaction vessel in 1 mL anhydrous DMF. The reaction was allowed to proceed for 24 h, followed by washing with DMF and methanol before cleavage from the solid support with incubation at 60° C with concentrated NH_4OH for 12 h. The DNA was purified by HPLC, and both isomers of the $Rh(phi)_2bpy$'-DNA were collected. Tethering to the DNA was verified with MALDI-TOF and CD Spectroscopy.

$Rh(phi)_2bpy^{3+}$ Synthesis

$Rh(bpy)Cl_4^-$ was prepared according to previously reported procedures (Figure 8.9).[26] To a 25 mL schlenk flask was added $Rh(bpy)Cl_4^-$ (762 mg, 1.901 mmol) and trifluoromethanesulfonic acid (HOTf) (6.75 mL, 7.632 mmol) under Ar(g) and allowed to stir overnight. The product was ether precipitated. In a 250 mL round bottom flask, $Rh(bpy)(OTf)_4^-$ (1.2727 g, 1.42 mmol) and 100 mL concentrated NH_4OH were refluxed at 45°C for 30 minutes. $[Rh(bpy)(NH_3)_4]^{3+}$ (1.1163 g, 1.16 mmol) was added to a 500 mL round bottom flask with phenanthraquinone (0.534 g, 2.552 mmol)and 1 mL of 1N NaOH in 75% ACN/25% H_2O. The product was purified with a cation exchange column followed by an anion exchange column (87 mg, 6%). ^1H NMR (300 MHz, DMSO): δ 13.87 (s, 2H), 13.37 (s, 2H), 8.95 (d, J = 7.8 Hz, 2H), 8.66 (d, J = 5.6 Hz, 2H), 8.63 – 8.45 (m, 10H), 7.88 (t, J = 8.1 Hz, 6H), 7.66 (t, J = 7.5 Hz, 4H) ESI-MS: calc: 667.54 ($M+H^+$) obs: 669.2 ($M+H^+$).

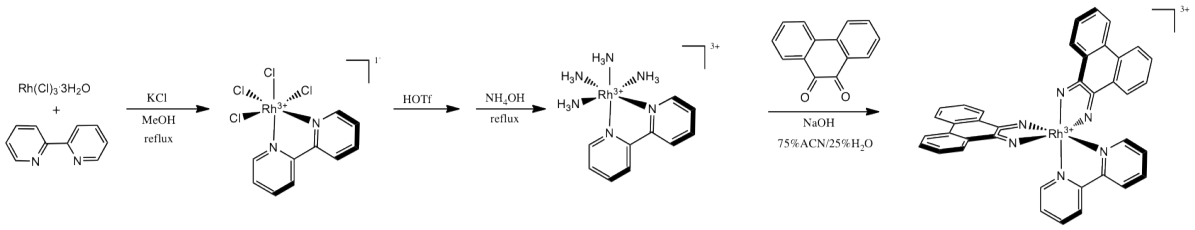

Figure 8.9 Synthesis of $Rh(phi)_2bpy^{3+}$. The bpy ligand is first added to the metal center. Subsequently, the chlorides are exchanged for ammines, followed by attachment of the two phi ligands.

Thymine Dimer Formation and Repair in Solution

Solutions of DNA duplexes of varying concentrations, either with or without a covalently tethered redox probe, were prepared in phosphate buffer (5.0 mM phosphate, 50 mM NaCl, pH 7) in a 1.7 mL Eppendorf with varying amounts of acetophenone. The solutions were irradiated with a 1000W HgXe lamp (Newport, Oriel) outfitted with a monochromator. For thymine dimer formation trials, 330 nm irradiation was used; 30 μL aliquots were taken at various times and run on HPLC to monitor the progression of cyclobutane formation.

To test thymine dimer repair with $Rh(phi)_2bpy^{3+}$, the metal complex was added directly to the eppendorf containing the acetophenone and DNA The sample was irradiated at 400 nm, and 30 μL aliquots were again taken and monitored by HPLC to determine the degree of thymine dimer repair.

DNA-modified Electrode Preparation

Multiplexed chips fabricated in Caltech facilities were used for electrochemical experiments.[13] Chips contain 16 electrodes (2 mm^2 area) divided into four quadrants. Low-density DNA monolayers (25 μM duplex, no Mg^{2+}) and high-density DNA monolayers (25 μM duplex, 100 mM Mg^{2+}) were assembled on the surface using DNA containing a thiol modifier at the terminus of one strand and a redox-active probe at the terminus of the complementary strand. DNA was incubated on the surface for 20-24 h in a humid environment, followed by thorough washing with phosphate buffer. The surface was then passivated with 1mM mercaptohexanol (MCH) in phosphate buffer with 5% glycerol for 45 minutes, followed again by washing with phosphate buffer.

Thymine Dimer Formation and Repair Attempts on Surfaces

Multiplexed chips to be used for thymine dimer formation and repair experiments contained one quadrant of well-matched DNA, one quadrant of mismatched DNA and two quadrants of thymine dimer parent DNA. After DNA monolayer formation, 200 μL of a solution of degassed acetophenone in phosphate buffer, pH 7, was added to the surface. The well of the clamp for the multiplexed chips, shown in the bottom panel of Figure 2, was covered by a microscope cover slide and sealed with adhesive putty. The surface was irradiated by redirecting the beam from the 1000 W HgXe lamp (Newport, Oriel) and monochromator 90° using a mirror angled at 45° so the multiplexed chip could be irradiated vertically. After irradiation at 330 nm with acetophenone, the chip was washed and scanned in phosphate buffer and TBP buffer. A solution of $Rh(phi)_2bpy^{3+}$ was then added to the chip, which was again covered with a cover slip and sealed with adhesive putty, and irradiated at 400 nm.

Electrochemical Measurements

After surface passivation, the central well of the clamp was filled with phosphate buffer. A three-electrode setup was used for electrochemical measurements, with both the Ag/AgCl reference (Cypress) and platinum auxiliary electrodes submerged in the buffer solution. Electrochemical measurements were performed with a 16-channel multiplexer and a CHI620D Electrochemical Analyzer (CH Instruments) in either phosphate buffer (5.0 mM phosphate, 50 mM NaCl, pH 7.0) or spermidine buffer (5.0 mM phosphate, 50 mM NaCl, 4 mM $MgCl_2$, 4 mM spermidine, 50 μM EDTA, 10%

glycerol, pH 7.0). Unless otherwise stated, cyclic voltammetry (CV) data were collected at 100 mV/s scan rate and square wave (SWV) data at 15 Hz.

Results and Discussion

Thymine Dimer Formation and Repair in Solution

Before electrochemical experiments, conditions for optimized, selective thymine dimer formation and repair were established in solution. To selectively form thymine dimers over other potential photoproducts upon DNA irradiation, a triplet sensitizer, acetophenone, was employed. This small molecule allows selective access to the triplet excited state of thymine because thymine is the only base with a triplet excited state lower in energy than the excited state of acetophenone. Irradiation of the DNA duplex at the peak absorbance of acetophenone, 330 nm, should cause no damage. The progression of thymine dimer formation and any other potential damage to the DNA duplex was monitored by HPLC, as the retention time of DNA containing a thymine dimer is significantly earlier than undamaged DNA (Figure 8.10).

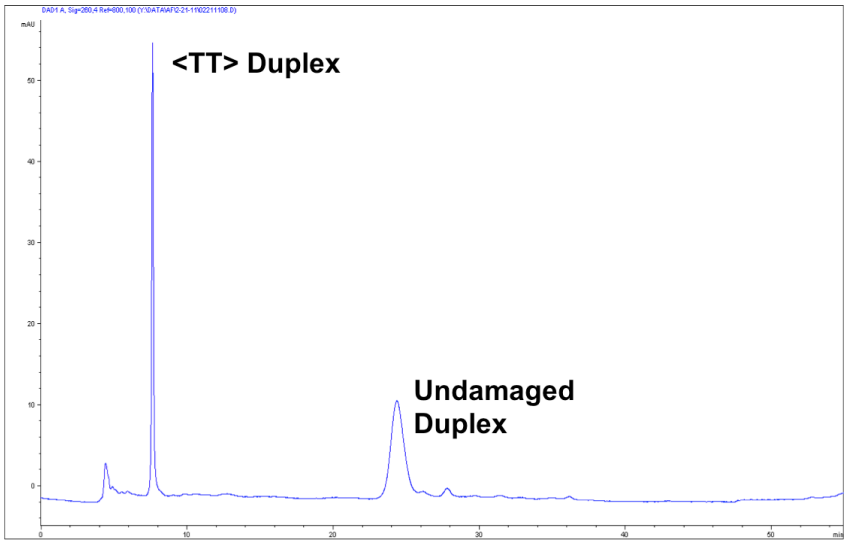

Figure 8.10 HPLC trace of thymine dimer formation. HPLC of the parent thymine dimer DNA is shown after irradiation. Both the parent duplex and the dimerized duplex are observed in this trace, with the thymine dimer-containing peak eluting significantly earlier than undamaged, parent DNA.

Initial controls were performed to ensure that irradiation of DNA without acetophenone did not damage the duplex. Additionally, irradiation of the well-matched duplex was undertaken to ensure that this duplex is not damaged upon irradiation with acetophenone. While irradiation trials confirm that minimal damage occurrs to DNA irradiated at 330 nm without acetophenone, a relatively large amount of DNA damage (~15%) was observed upon irradiation of the well-matched strand, which contains no adjacent thymines, in the presence of acetophenone. The damage observed is likely due to adjacent cytosines and thymines, which form photoadducts between the bases connected by a single bond. To avoid this undesired photodamage, the well-matched duplex (WM) was redesigned to ensure that the sequence no longer contained adjacent thymines and cytosines. Minimal damage is observed in the new sequence upon irradiation in the presence of acetophenone.

Conditions for specific thymine dimer formation with unmodified DNA were then optimized to produce the maximum amount of dimerization with minimal irreversible DNA damage. The optimum conditions are 30 μM DNA with 3.6 mM acetophenone irradiated for 8 hours. Degassing the sample before irradiation is vital in order to minimize nonspecific damage. To confirm the optimal conditions, thymine dimer formation was monitored by HPLC, as shown in Figure 8.11. As can be seen, with the progression of time, the earlier-eluting peak containing the dimerized thymines increases in size as the later-eluting peak, which contains the undamaged duplex, decreases in size.

As the metal complex $Rh(phi)_2bpy^{3+}$ is known to be capable of thymine dimer repair, conditions were also optimized for thymine dimer repair in solution with $Rh(phi)_2bpy^{3+}$. The metal complex was added directly to the DNA solution containing

acetophenone and irradiated at 400 nm. Optimal repair is observed when the concentration of the metal complex was twice that of the DNA. In the presence of the $Rh(phi)_2bpy^{3+}$ complex (Figure 8.12), it can be seen that the dimer-containing peak decreases in size, while the undamaged peak increases in size. This trend is the inverse of what is observed by HPLC under thymine dimer formation conditions, indicating successful repair of the photodamage product by the metal complex.

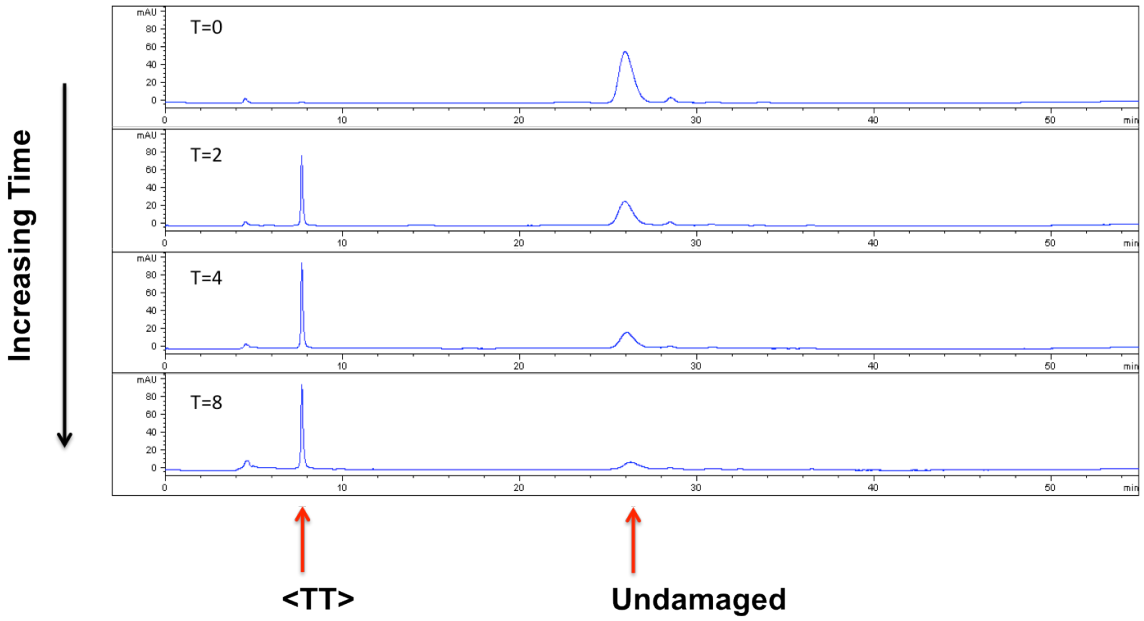

Figure 8.11 Thymine dimer formation under optimized conditions. As time progresses, the cyclobutane dimer peak increases in size, while the undamaged DNA peak decreases in size. The time reported on the left is in hours of irradiation under conditions of 30 μM DNA and 3.6 mM acetophenone in a sample that was degassed before irradiation at 330 nm on a 1000 W HgXe lamp outfitted with a monochromator.

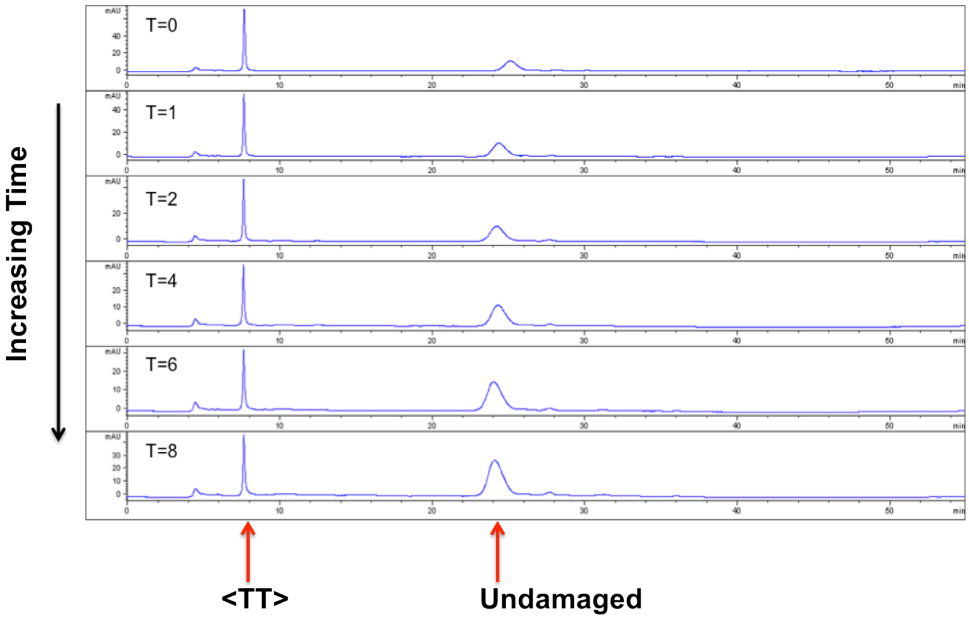

Figure 8.12 Thymine dimer repair under optimized conditions. As time progresses, the cyclobutane dimer peak decreases in size, while the undamaged DNA peak returns. The time reported on the left is in hours of irradiation. The conditions were 30 μM DNA and 60 μM $Rh(phi)_2bpy^{3+}$ in a sample irradiated at 400 nm on a 1000 W HgXe lamp outfitted with a monochromator.

Electrochemical Experiments with Thymine Dimer Formation and Repair

As the solution phase experiments demonstrate successful thymine dimer formation and repair in solution, attempts at thymine dimer formation and repair on surfaces were also made. DNA modified with a MB' redox probe was first used for electrochemical measurements of thymine dimer formation and repair on an electrode surface. Experiments were conducted with multiplexed chips, and one quadrant of the chip was modified with WM DNA, a second with mismatched DNA (MM), and the final two with parent thymine dimer (<TT>) DNA. Initial conditions for thymine dimer formation and repair on the surface were based on the previously optimized acetophenone and $Rh(phi)_2bpy^{3+}$ conditions for solution-phase thymine dimer formation and repair.

Two issues are immediately evident from experiments with thymine dimer formation and repair on surfaces. First, no selectivity in signal reduction is observed for the <TT> DNA over the WM DNA. In both cases, upon irradiation with acetophenone, significant signal decreases are observed (80-95%) (Figure 8.13). As is seen from the CV scans of the well-matched (left) and parent <TT> DNA (right) in Figure 8.13, no selective signal attenuation is observed in the parent <TT> DNA. The large signal decrease observed in both sequences of DNA indicates that the signal decrease is not due to the selective formation of thymine dimers; this result is likely due to irreversible damage to both sequences of DNA. As this level of damage is not observed in the solution experiments involving DNA without a redox probe, these results point to the MB' redox probe as a potential source of damage.

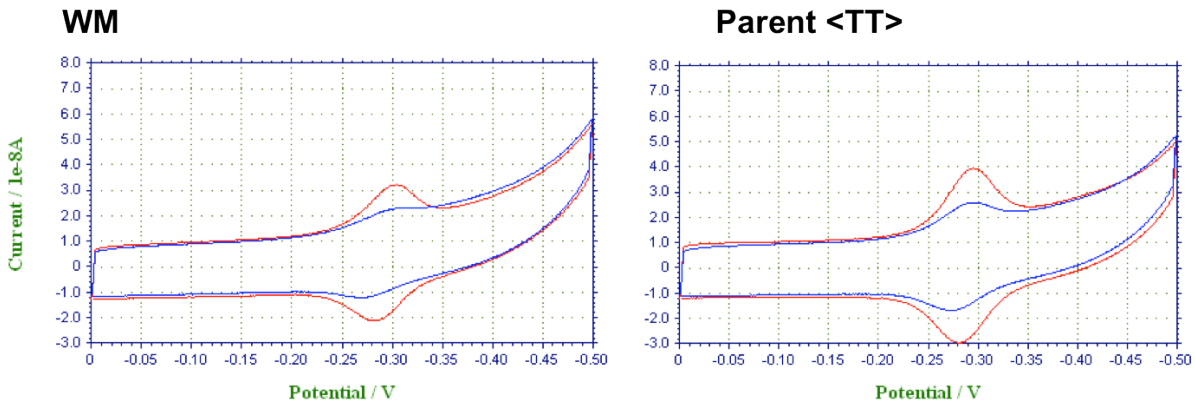

Figure 8.13 Cyclic voltammogram of MB'-modified DNA on multiplexed chips. Both before irradiation (red trace) and after irradiation in the presence of acetophenone (blue trace) are shown. Irradiation proceeded at 330 nm in the presence of 3.6 mM acetophenone for 2 hours. Cyclic voltammograms of the well-matched duplex (*left*) show significant signal attenuation, which is not expected. Nearly the same attenuation is observed in the sequences that are capable of forming thymine dimers (*right*).

A second issue arose upon attempting thymine dimer repair on multiplexed chips. After the addition of $Rh(phi)_2bpy^{3+}$ to the surface, followed by irradiation, a large, irreversible reductive peak is consistently observed, regardless of washing conditions (Figure 8.14). Many attempts were made using a variety of solvent conditions for washing, including high-salt phosphate buffer, 3 M NaCl in H_2O, 3 M NH_4OAc in H_2O, 3 M KPF_6, acetonitrile, and ethanol, to reduce the large peak. However, all were unsuccessful. Repassivating the surface was also attempted. After the surface was irradiated with acetophenone and washed, 1 mM MCH in phosphate buffer with 5% glycerol was added to the surface for 45 minutes and washed before the addition of $Rh(phi)_2bpy^{3+}$. The irreversible signal is still observed after the $Rh(phi)_2bpy^{3+}$ solution was removed from the surface and the surface was washed.

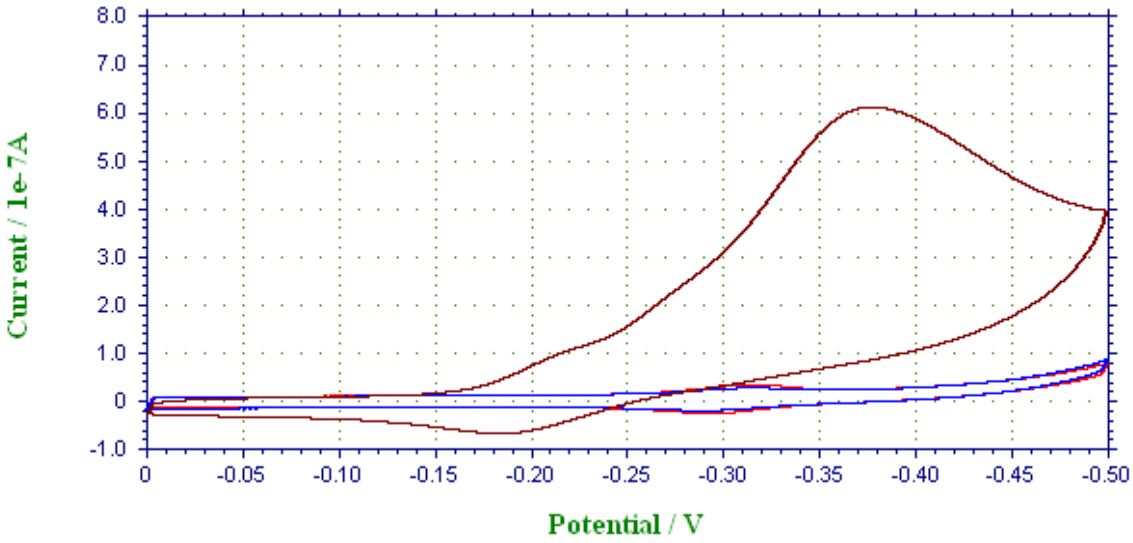

Figure 8.14 $Rh(phi)_2bpy^{3+}$ signal on multiplexed chips. After $Rh(phi)_2bpy^{3+}$ is added to a quadrant of a multiplexed chip containing well-matched DNA, a large irreversible signal is observed (brown trace). Both the initial scan of the surface (red trace) and after the surface is irradiated with acetophenone (blue trace) show only the reversible methylene blue signal. After the surface was irradiated with $Rh(phi)_2bpy^{3+}$ and thoroughly washed, the large, irreversible peak from the $Rh(phi)_2bpy^{3+}$ metal complex remains (brown trace).

To verify that $Rh(phi)_2bpy^{3+}$ is the source of the irreversible peak, a quadrant of a multiplexed chip with a bare gold surface and one containing only a MCH monolayer were each incubated with $Rh(phi)_2bpy^{3+}$, followed by washing. An irreversible reductive peak similar to those previously observed was found for both the bare gold and MCH surfaces. Because of these findings, free $Rh(phi)_2bpy^{3+}$ is not a viable option as a thymine dimer repair agent for experiments on surfaces.

Thymine Dimer Formation and Repair in Modified DNA in Solution

Because of the extreme amount of signal attenuation observed for both the WM and <TT> duplexes on surfaces, the effect of the redox probe under thymine dimer formation conditions was investigated in solution by HPLC. When MB'-DNA is irradiated, significant amounts of non-specific damage consistently occur both in the presence and absence of acetophenone. Similar results are obtained for unmodified DNA with a 1:1 ratio of free methylene blue in solution (Figure 8.15). This damage is likely caused by methylene blue forming reactive oxygen species in solution, which indiscriminately damage DNA. MB' is therefore incompatible as a redox probe for a DNA switch.

Free Methylene Blue

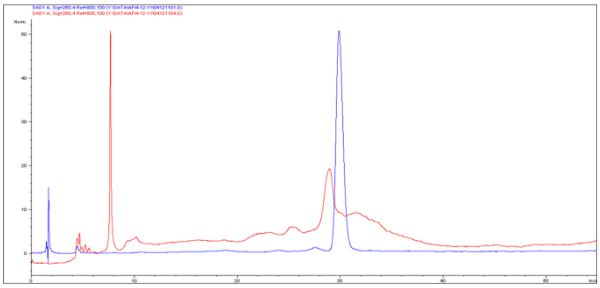

Covalent Methylene Blue

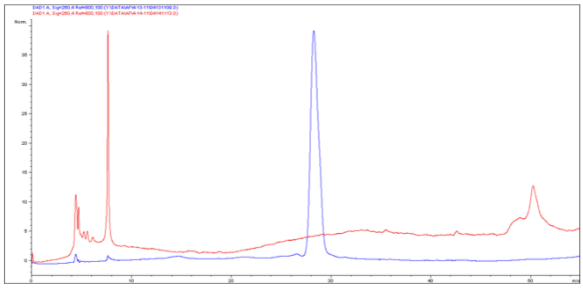

Figure 8.15 Damage to free DNA by irradiation in the presence of methylene blue. In the absence of acetophenone, degassed samples of DNA in phosphate buffer were irradiated at 330 nm for 4 hours (*left*). The blue trace is an HPLC trace of the DNA before irradiation; the red trace is after 4 hours of irradiation. Both a 1:1 ratio of free MB to DNA (*left*) and covalently-tethered MB' (*right*) exhibited significant amounts of nonspecific damage.

As methylene blue is not a viable option for this platform, an alternative redox probe, Nile Blue (NB), was also tested. When NB-DNA was irradiated in the absence of acetophenone, no DNA damage is observed. When NB-DNA is irradiated in the presence of acetophenone, the NB probe loses its color, changing from blue to colorless, indicating damage to the probe under these conditions. As the redox probe must be stable to conditions used for thymine dimer formation and repair, NB was also rejected as a redox probe for this application (Figure 8.16)

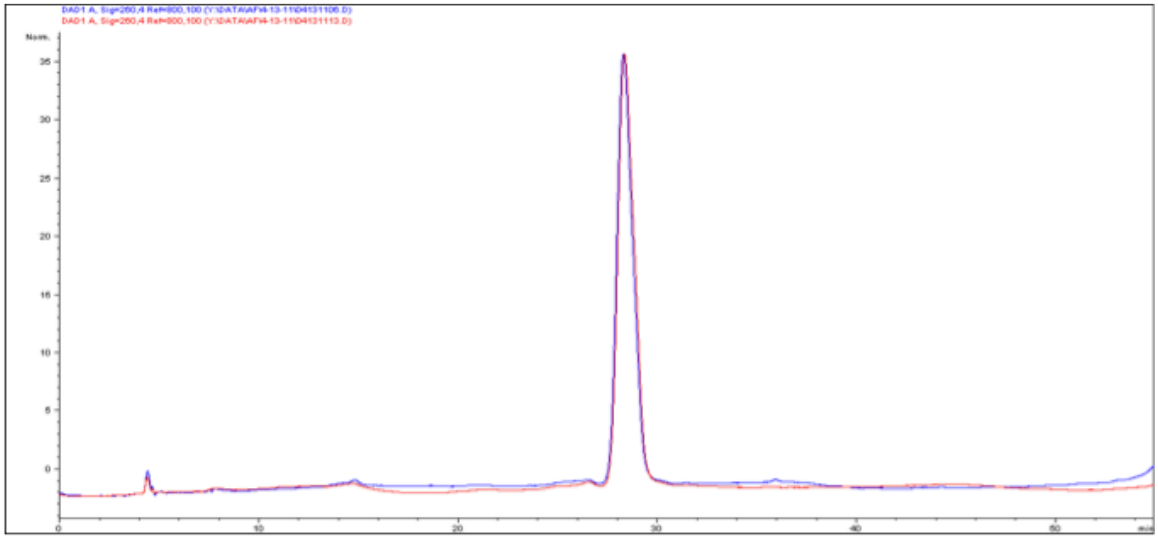

Figure 8.16 Nile blue-modified DNA irradiated at 330 nm. Nile blue covalently attached to DNA is irradiated in the absence of acetophenone for 4 h. The blue trace is at t=0 h, and the red is at t=4 h. No DNA damage is observed.

$Rh(phi)_2bpy'^{3+}$ as a Covalent Redox Probe: Synthesis and Initial Studies

As neither MB' or NB is suitable as a redox probe for the photoswitch system, we sought to utilize $Rh(phi)_2bpy'^{3+}$ (Figure 8.17), a variant of the metal complex known to repair thymine dimers. This complex was also shown to be stable in the presence of acetophenone. These qualities enable the metal complex to potentially function as both a redox probe and repair agent. Additionally, as the complex is covalently tethered to the DNA, issues with direct surface reduction of the complex should be minimized. Before proceeding with covalent linkages, $Rh(phi)_2bpy'^{3+}$ was tested to ensure that it is both stable to 330 nm irradiation in the presence of acetophenone and maintains its ability to repair thymine dimers after acetophenone irradiation. Finally, the ability of thymine dimers to form in the presence of this complex was also evaluated. Thymine dimer formation and repair in solution was undertaken with $Rh(phi)_2bpy'^{3+}$ present in both irradiation steps. The rhodium complex is stable to conditions for thymine dimer formation and repairs thymine dimers with 400 nm irradiation following its irradiation with acetophenone. Covalent tethering was therefore undertaken to enable the $Rh(phi)_2bpy^{3+}$ complex to act as both a repair agent for thymine dimers and a redox reporter.

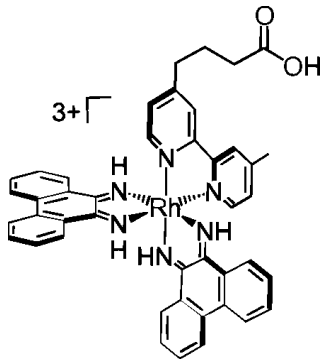

Figure 8.17 Structure of $Rh(phi)_2bpy'^{3+}$ to be coupled to the DNA. Coupling to both the phosphate backbone and a modified uracil base are possible.

Two modes of covalent linkage of the rhodium complex to the DNA were undertaken. Coupling to the phosphate backbone of DNA with a C9 amine linker as well as to a C6 amino-modifed uracil base incorporated into the terminus of the DNA duplex were tested. The $Rh(phi)_2bpy'^{3+}$ is a racemic mixture of Δ- and Λ-isomers. The Δ isomer intercalates into the base stack much more strongly than the Λ isomer. Racemic $Rh(phi)_2bpy'^{3+}$ was successfully coupled to the phosphate backbone of DNA using a previously-developed protocol from our group.[14] However, the yields for this coupling are extremely low (~10%). Coupling $Rh(phi)_2bpy'^{3+}$ directly to the modified uracil base was found to be no more successful. Coupling attempts were made with the DNA both on solid support and free in solution with coupling reagents including HBTU and HOBt, HATU, EDC, and PyBOP, as well as NHS ester activation of the $Rh(phi)_2bpy'^{3+}$.

The $Rh(phi)_2bpy'^{3+}$ coupled to the backbone of DNA is a racemic mixture of Δ- and Λ-isomers. When coupled to the DNA backbone, the Δ- and Λ-isomers have different HPLC retention times and can be distinguished by CD spectroscopy. Figure 8.18 shows the CD spectra of each of the isomers conjugated to DNA isolated by HPLC. Each isomer was isolated by HPLC to test individually on the multiplexed chips.

The DNA strand conjugated to the rhodium complex was annealed to a thiolated complement and allowed to self-assemble on the gold surface. To determine if the signals observed are DNA mediated, both WM and MM DNA of each isomer were prepared. Mismatch discrimination is observed for both the Δ- and Λ-isomers, indicating that at least a portion of the DNA signals observed are DNA mediated (Figure 8.19). However, the larger signal present for the Λ isomer indicates that, despite the mismatch

discrimination observed, the signal is likely not DNA mediated. This is further supported by the irreversibility of all of the rhodium electrochemical signals observed.

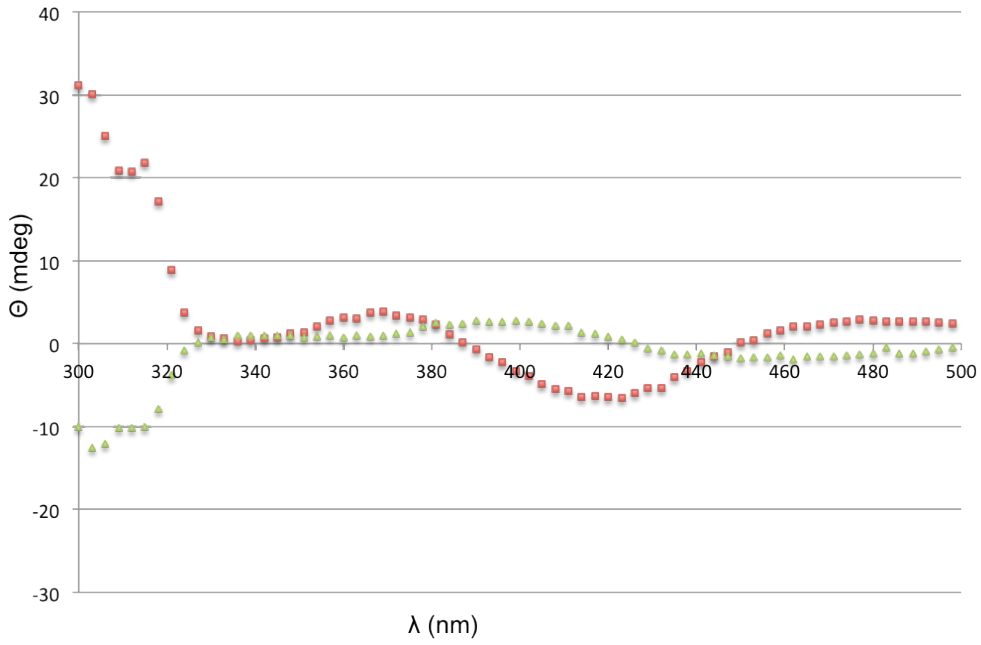

Figure 8.18 CD spectra of the Δ- and Λ-isomers of $Rh(phi)_2bpy^{3+}$ coupled to the backbone of DNA. The Λ isomer is shown in red, and the Δ isomer is shown in green.

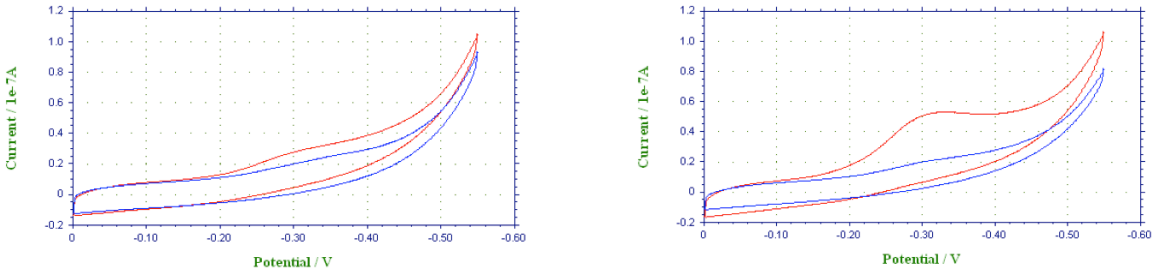

Figure 8.19 Electrochemistry of backbone-coupled $Rh(phi)_2bpy^{3+}$. The CVs shown were taken at a scan rate of 50 mV/s. In both cases, scans were collected in TBP buffer. The well-matched duplex (*red*) showns an irreversible reductive signal, while the mismatched duplex (*blue*) shows no electrochemical signal. The Δ isomer (*left*) shows a significantly smaller signal for the well-matched DNA than the Λ isomer (*right*).

Conclusions

As DNA is known to be an effective molecular wire over long distances, efforts have been made to add functionality to DNA in order to build circuitry components. The simplest component of a circuit is a switch. We therefore made efforts to develop such a circuitry component through the formation and repair of thymine dimers, which have been shown to attenuate DNA CT. Solution-phase switching of the formation and repair of thymine dimers has been developed; thymine dimer formation with the triplet sensitizer, acetophenone, and repair with a rhodium intercalator, $Rh(phi)_2bpy^{3+}$, is robust in solution. However, moving to DNA tethered to solid support has proved difficult. Multiple redox probes are non-innocent in the thymine dimer formation and repair process, and the rhodium complexes have been found to generate an electrochemical signal, interfering with readout. Although using covalent $Rh(phi)_2bpy'^{3+}$ to act as both a redox reporter and method of thymine dimer repair appears to be a simple solution, the signals obtained from this tethered compound are not reversible and do not appear to be DNA-mediated. Future work on this project will benefit from better surface passivation techniques, including the application of 11-mercaptoundecylphosphoric acid as a passivating agent. Additionally, low-density monolayers formed by click chemistry to tether the DNA will provide better spacing between the helices, which may facilitate thymine dimer formation.

References

1. Robertson, N., and McGowan, C. A. (2003) A comparison of potential molecular wires as components for molecular electronics, *Chem. Soc. Rev. 32*, 96-103.

2. Tour, J. M. (2000) Molecular electronics. Synthesis and testing of components, *Acc. Chem. Res. 33*, 791-804.

3. James, D. K., and Tour, J. M. (2005) Molecular wires, *Topics in Curr. Chem. 257*, 33-62.

4. Slinker, J. D., Muren, N. B., Renfrew, S. E., and Barton, J. K. (2011) DNA charge transport over 34 nm, *Nat. Chem. 3*, 228-233.

5. Kelley, S. O., Boon, E. M., Barton, J. K., Jackson, N. M., and Hill, M. G. (1999) Single-base mismatch detection based on charge transduction through DNA, *Nucleic Acids Res. 27*, 4830-4837.

6. DeRosa, M. C., Sancar, A., and Barton, J. K. (2005) Electrically monitoring DNA repair by photolyase, *Proc. Natl. Acad. Sci. USA 102*, 10788-10792.

7. Boon, E. M., Salas, J. E., and Barton, J. K. (2002) An electrical probe of protein-DNA interactions on DNA-modified surfaces, *Nat. Biotechnol. 20*, 282-286.

8. Gorodetsky, A. A., Ebrahim, A., and Barton, J. K. (2008) Electrical detection of TATA binding protein at DNA-modified microelectrodes, *J. Am. Chem. Soc. 130*, 2924-2925.

9. Drummond, T. G., Hill, M. G., and Barton, J. K. (2003) Electrochemical DNA sensors, *Nat. Biotechnol. 21*, 1192-1199.

10. Jackson, N. M., and Hill, M. G. (2001) Electrochemistry at DNA-modified surfaces: new probes for charge transport through the double helix, *Curr. Opin. Chem. Biol. 5*, 209-215.

11. Kelley, S. O., Barton, J. K., Jackson, N. M., McPherson, L. D., Potter, A. B., Spain, E. M., Allen, M. J., and Hill, M. G. (1998) Orienting DNA Helices on Gold Using Applied Electric Fields, *Langmuir 14*, 6781-6784.

12. Kelley, S. O., Jackson, N. M., Hill, M. G., and Barton, J. K. (1999) Long-Range Electron Transfer through DNA Films, *Angew. Chem. Int. Ed. 38*, 941-945.

13. Slinker, J. D., Muren, N. B., Gorodetsky, A. A., and Barton, J. K. (2010) Multiplexed DNA-modified electrodes, *J. Am. Chem. Soc. 132*, 2769-2774.

14. Kelley, S. O., Barton, J. K., Jackson, N. M., and Hill, M. G. (1997) Electrochemistry of methylene blue bound to a DNA-modified electrode, *Bioconjug. Chem. 8*, 31-37.

15. Pheeney, C. G., and Barton, J. K. (2012) DNA electrochemistry with tethered methylene blue, *Langmuir 28*, 7063-7070.

16. Boal, A. K., and Barton, J. K. (2005) Electrochemical detection of lesions in DNA, *Bioconjug. Chem. 16*, 312-321.

17. Boon, E. M., Ceres, D. M., Drummond, T. G., Hill, M. G., and Barton, J. K. (2000) Mutation detection by electrocatalysis at DNA-modified electrodes, *Nat. Biotechnol. 18*, 1096-1100.

18. Gorodetsky, A. A., Buzzeo, M. C., and Barton, J. K. (2008) DNA-mediated electrochemistry, *Bioconjug. Chem. 19*, 2285-2296.

19. Guo, X., Gorodetsky, A. A., Hone, J., Barton, J. K., and Nuckolls, C. (2008) Conductivity of a single DNA duplex bridging a carbon nanotube gap, *Nat. Nanotechnol. 3*, 163-167.

20. Park, H., Zhang, K., Ren, Y., Nadji, S., Sinha, N., Taylor, J. S., and Kang, C. (2002) Crystal structure of a DNA decamer containing a cis-syn thymine dimer, *Proc. Natl. Acad. Sci. USA 99*, 15965-15970.

21. Schreier, W. J., Schrader, T. E., Koller, F. O., Gilch, P., Crespo-Hernandez, C. E., Swaminathan, V. N., Carell, T., Zinth, W., and Kohler, B. (2007) Thymine dimerization in DNA is an ultrafast photoreaction, *Science 315*, 625-629.

22. Lamola, A. A., and Eisinger, J. (1968) On the mechanism of thymine photodimerization, *Proc. Natl. Acad. Sci. USA 59*, 46-51.

23. Holman, M. R., Ito, T., and Rokita, S. E. (2007) Self-repair of thymine dimer in duplex DNA, *J. Am. Chem. Soc. 129*, 6-7.

24. Nunez, M. E., Noyes, K. T., Gianolio, D. A., McLaughlin, L. W., and Barton, J. K. (2000) Long-range guanine oxidation in DNA restriction fragments by a triplex-directed naphthalene diimide intercalator, *Biochemistry 39*, 6190-6199.

25. Dandliker, P. J., Nunez, M. E., and Barton, J. K. (1998) Oxidative charge transfer To repair thymine dimers and damage guanine bases in DNA assemblies containing tethered metallointercalators, *Biochemistry 37*, 6491-6502.

26. Holmlin, R. E., Dandliker, P. J., and Barton, J. K. (1999) Synthesis of metallointercalator-DNA conjugates on a solid support, *Bioconjug. Chem. 10*, 1122-1130.

27. Gorodetsky, A. A., Green, O., Yavin, E., and Barton, J. K. (2007) Coupling into the base pair stack is necessary for DNA-mediated electrochemistry, *Bioconjug. Chem. 18*, 1434-1441.

Chapter 9

Summary and Perspective

Detection of biologically relevant targets, including small molecules, proteins, and nucleic acids, is vital for both fundamental research as well as clinical and field diagnostics. Sensing strategies that feature biological substrates for analyte capture provide a natural foundation for bioassays, owing to the inherent molecular-recognition nature of substrate-ligand binding. Nucleic acid-based platforms in particular comprise an especially robust and flexible class of sensors, capable of detecting a variety of small-molecule, protein, and DNA/RNA targets.[1-5]

Protein targets, in particular, have garnered significant interest because of their roles in the initiation and development of many diseases, including cancer. While DNA arrays using fluorescence-based technology have changed the way we probe gene expression and the variations therein that lead to disease, they generally cannot directly detect proteins. Additionally, they inherently require expensive optical systems for readout and exhibit significant signal variability.

DNA-based electrochemistry, in contrast, enables fast, facile detection of a variety of biomolecules, with high sensitivity, low cost, and the capacity to incorporate multiplexing.[1-5] All of these features are vital for the clinical applicability of a detection platform. Many DNA-modified electrodes employ the same strategies for detection as fluorescence-based sensors, but with the added sensitivity and lower complexity of electrochemistry (i.e., hybridization with labeled targets,[6-8] structural changes to a DNA hairpin to turn on a signal,[2, 5, 9] and impedance measurements[10, 11]). These similarities in detection strategies lead many of these platforms to have the same issues as the fluorescence-based assays, including non-specific hybridization interactions, yielding false positive signals and difficulty directly detecting protein activity.

If the intrinsic structural and electronic properties of DNA are harnessed, the sensitivity and selectivity of DNA-based electrochemical detection is significantly increased.[12, 13] One especially sensitive method of detection relies on the phenomenon known as DNA-mediated charge transport (DNA CT). DNA CT is based on the ability of electrons to flow through the stacked, aromatic bases that comprise the core of DNA. The structure of the stacked DNA bases is very similar to the structure of the known conductor, graphene; the vertical rise between the aromatic bases, as between the layers of graphene, is 3.4 Å, which is sufficiently small to enable the π orbitals of the DNA bases to overlap, creating a conduit for electron flow. The ability of DNA to conduct charge through its core was initially shown with excited-state solution experiments,[14, 15] and this process was found to be efficient over long distances on fast time scales. Importantly, this process is extremely sensitive to anything that disturbs the π stacking of the DNA bases.[16-20]

For DNA CT to be an effective method of biomolecule detection, the DNA must be anchored to provide a handle for detection. DNA-modified gold electrodes provide a solid support and simple electrochemical readout to facilitate detection by DNA CT. Conventionally, DNA-modified electrodes are formed from the self-assembly of thiolated DNA duplexes on gold electrode surfaces. These monolayers have enabled single-base mismatch and lesion detection, irrespective of sequence context.[17, 21] DNA-mediated electrochemistry also offers a sensitive means to monitor protein activity at low concentrations. Proteins that perturb the base stack or chemically modify DNA are easily detected by DNA CT-based platforms, including methyltransferases, photolyases, and transcription factors. Selectivity is governed by the sequence-specificity of the protein.[22-

[24] Self-assembly of thiolated DNA for DNA film formation has enabled the detection of a variety of biomolecules, but little control is afforded with this method over the spacing between individual DNA helices.[25] Increased access for biological targets to bind, particularly in congested, crude lysate samples, is a critical parameter for sensitive, relevant biomolecule detection. The importance of interhelical spacing was previously demonstrated by the effect of DNA deflection angles on nanostructured microelectrodes. Increasing the deflection angle between helices enabled significantly lower detection limits of oligo targets.[1-3]

In this thesis work, we have improved i) control over the morphology of DNA monolayers and ii) platforms to facilitate sensitive biomolecule detection. We first utilized copper-free click chemistry to better control the density and homogeneity of DNA monolayers. Subsequently, we applied click chemistry-based formation of low-density DNA monolayers to the patterning of DNA arrays. The platform developed for DNA array formation also incorporated a secondary electrode for detection, which, when coupled with electrocatalysis, enabled especially sensitive protein and nucleic acid detection. This platform was subsequently multiplexed for simultaneous detection from multiple biological samples. When a signal-on assay for methyltransferase detection was combined with this electrochemical platform, methyltransferase activity from crude tissue lysates was detected. Differential activity between tumor tissue and healthy adjacent tissue was consistently observed when measured with this platform. We have increased the control over DNA monolayer morphology and combined this control with improved sensitivity to facilitate detection of an important cancer biomarker from clinical samples.

Extensive characterization of conventional thiolated DNA monolayers has confirmed their inhomogeneity. Some control over the total amount of DNA assembled is obtained by varying the ionic strength of the assembly solution. Thiolated DNA monolayers contain some regions of very high DNA density and other regions with little to no DNA, making biomolecule detection difficult, as different regions of the surface will respond differently to the addition of biomolecules.

To improve the morphology of DNA monolayers, we first developed a method of monolayer formation using copper-free click chemistry, which enables control over the amount of DNA assembled. Extremely low-density DNA monolayers, with as little as 5% total surface coverage of DNA, have been formed. These DNA-modified electrodes (DMEs) were fully characterized both visually and electrochemically, and were found to be significantly more homogeneous than traditional thiol-modified DNA monolayers. Furthermore, these monolayers support greater accessibility to individual DNA helices, resulting in more sensitive detection of the transcriptional activator TATA-binding protein (TBP), with detection limits on the order of the dissociation constant of the protein. The improved DNA helix accessibility, and therefore sensitivity, afforded by these DNA monolayers reflects their general utility for electrochemical sensor development.

We further developed click chemistry-based DNA monolayer formation to create patterned DNA arrays, which facilitate direct comparisons between multiple sequences of DNA on a single electrode surface. These arrays are electrochemically formed and addressed with a two-electrode platform. Electrochemical activation of a copper catalyst at a particular location on a bare secondary electrode precisely places multiple sequences

of DNA onto a single, substrate electrode surface. The incorporation of a secondary microelectrode with electrocatalytic signal amplification for electrochemical readout provides improved sensitivity with spatial resolution of the DNA array on the primary electrode surface. We have applied this two-electrode platform to form DNA arrays that enable differentiation between well-matched and mismatched sequences, detection of TATA-binding protein, and sequence-selective DNA hybridization, all with greater control than was previously available.

Multiplexing of this two working electrode platform has enabled simultaneous and specific detection of multiple proteins. In this platform, which contains two complementary electrode arrays, DNA duplexes are patterned onto the primary electrode array, while the secondary array is used for DNA patterning and biomolecule detection. Particular sequences of DNA are specifically placed on the primary electrode array using electrochemically-activated click chemistry. We have found that catalyst activation at the bare secondary electrode array is essential to maintain the integrity of the DNA monolayer. The deleterious effects of catalyst activation at the DNA-modified electrode have been confirmed by impedance spectroscopy, cyclic voltammetry, and constant potential amperometry. Electrochemical readout at the secondary electrode has further eliminated the need for large background corrections, as current is only generated at the secondary electrode when DNA CT occurs at the primary electrode. We expanded our protein detection capabilities with this platform through the sensitive detection of the transcription factors TATA-binding protein and CopG on the same electrode array with sequence specificity.

Clinically relevant detection with this two working electrode platform was established by incorporating an electrochemical signal-on methyltransferase activity assay. Epigenetic modifications, namely DNA methylation, have been found to necessitate tight regulation in the cell to prevent the development of cancer.[26-28] As such, abnormal DNA methyltransferase activity has been connected to the development and progression of cancer. However, detection methods to assess methyltransferase activity from crude tumor samples are limited because they rely on radioactivity or fluorescence and require bulky instrumentation.[29, 30] We developed an electrochemical platform for the label-free detection of the activity of the most abundant human methyltransferase, DNMT1, that enables measurements from crude cultured colorectal cancer cell lysates (HCT116) and biopsied tumor tissues. We specifically and selectively measured DNMT1 activity within these congested cellular samples using this platform and, based on differences in DNMT1 activity, we can distinguish colorectal tumor tissue from healthy adjacent tissue.

As differences in DNMT1 activity between tumor tissue and healthy adjacent tissue were measureable with our platform, we evaluated ten sets of tumors to determine the clinical relevance of this technology. With our multiplexed, two working electrode platform, we have found a direct correlation between higher DNMT1 activity and tumorous tissue. In the majority of samples analyzed, the tumorous tissue had significantly higher DNMT1 activity than the healthy adjacent tissue. No such correlation was observed in measurements of *DNMT1* expression by quantitative PCR, DNMT1 protein abundance by Western blotting, or DNMT1 activity using a radiometric

DNA labeling assay. Our electrochemical platform provides a direct measure of DNMT1 activity in crude, clinically relevant samples.

DNA CT-based electrochemical sensors offer many advantages over other nucleic acid sensors. The inherent sensitivity of CT to small perturbations in the base stack of DNA has enabled the detection of proteins, nucleic acids, and even epigenetic DNA modifications. With conventional DNA-modified electrodes, however, we have been limited to the detection of purified biomarkers. It has been especially rewarding to have developed platforms that enable detection from clinically relevant crude samples, a great step toward real-world applications of these DNA sensors. The platforms described here offer a basis for further development, with the goal of methyltransferase analysis on a single-cell level, detection of the epigenetic modification hydroxymethylation, and the further application of this technology to the development of assays that could provide better diagnostics for disease.

References

1. Cederquist, K. B., and Kelley, S. O. (2012) Nanostructured biomolecular detectors: pushing performance at the nanoscale, *Curr. Opin. Chem. Biol. 16*, 415-421.

2. Das, J., Cederquist, K. B., Zaragoza, A. A., Lee, P. E., Sargent, E. H., and Kelley, S. O. (2012) An ultrasensitive universal detector based on neutralizer displacement, *Nat. Chem. 4*, 642-648.

3. Das, J., and Kelley, S. O. (2013) Tuning the bacterial detection sensitivity of nanostructured microelectrodes, *Anal. Chem. 85*, 7333-7338.

4. Kang, D., White, R. J., Xia, F., Zuo, X., Vallee-Belisle, A., and Plaxco, K. W. (2012) DNA biomolecular-electronic encoder and decoder devices constructed by multiplex biosensors, *NPG Asia. Mater. 4*, e1.

5. Lai, R. Y., Plaxco, K. W., and Heeger, A. J. (2007) Aptamer-based electrochemical detection of picomolar platelet-derived growth factor directly in blood serum, *Anal. Chem. 79*, 229-233.

6. Caruso, F., Rodda, E., Furlong, D. N., Niikura, K., and Okahata, Y. (1997) Quartz crystal microbalance study of DNA immobilization and hybridization for nucleic Acid sensor development, *Anal. Chem. 69*, 2043-2049.

7. Cheng, J., Sheldon, E. L., Wu, L., Uribe, A., Gerrue, L. O., Carrino, J., Heller, M. J., and O'Connell, J. P. (1998) Preparation and hybridization analysis of DNA/RNA from E. coli on microfabricated bioelectronic chips, *Nat. Biotechnol. 16*, 541-546.

8. Gooding, J. J. (2002) Electrochemical DNA Hybridization Biosensors, *Electroanalysis 14*, 1149-1156.

9. Kelley, S. O., Mirkin, C. A., Walt, D. R., Ismagilov, R. F., Toner, M., and Sargent, E. H. (2014) Advancing the speed, sensitivity and accuracy of biomolecular detection using multi-length-scale engineering, *Nat. Nanotechnol. 9*, 969-980.

10. Kafka, J., PÃ¤nke, O., Abendroth, B., and Lisdat, F. (2008) A label-free DNA sensor based on impedance spectroscopy, *Electrochimica Acta 53*, 7467-7474.

11. Leasen, S., Sritunyalucksana-Dangtip, K., Hodak, J., Srisala, J., Kulsing, C., and Veerasia, W. (2012) Using Electrochemical Impedance Spectroscopy of Methylene Blue and Ferricyanide for DNA Sensing Surface Characterization, In *Chemistry for Sustainable Development* (Gupta Bhowon, M., Jhaumeer-Laulloo, S., Li Kam Wah, H., and Ramasami, P., Eds.), pp 249-264, Springer Netherlands.

12. Gorodetsky, A. A., Buzzeo, M. C., and Barton, J. K. (2008) DNA-mediated electrochemistry, *Bioconjug. Chem. 19*, 2285-2296.

13. Muren, N. B., Olmon, E. D., and Barton, J. K. (2012) Solution, surface, and single molecule platforms for the study of DNA-mediated charge transport, *Phys. Chem. Chem. Phys. 14*, 13754-13771.

14. Holmlin, R. E., Dandliker, P. J., and Barton, J. K. (1997) Charge Transfer through the DNA Base Stack, *Angew. Chem. Int. Ed. 36*, 2714-2730.

15. Holmlin, R. E., Dandliker, P. J., and Barton, J. K. (1999) Synthesis of metallointercalator-DNA conjugates on a solid support, *Bioconjug. Chem. 10*, 1122-1130.

16. Kelley, S. O., Barton, J. K., Jackson, N. M., and Hill, M. G. (1997) Electrochemistry of methylene blue bound to a DNA-modified electrode, *Bioconjug. Chem. 8*, 31-37.

17. Kelley, S. O., Boon, E. M., Barton, J. K., Jackson, N. M., and Hill, M. G. (1999) Single-base mismatch detection based on charge transduction through DNA, *Nucleic Acids Res. 27*, 4830-4837.

18. Murphy, C. J., Arkin, M. R., Ghatlia, N. D., Bossmann, S., Turro, N. J., and Barton, J. K. (1994) Fast photoinduced electron transfer through DNA intercalation, *Proc. Natl. Acad. Sci. USA 91*, 5315-5319.

19. Murphy, C. J., Arkin, M. R., Jenkins, Y., Ghatlia, N. D., Bossmann, S. H., Turro, N. J., and Barton, J. K. (1993) Long-range photoinduced electron transfer through a DNA helix, *Science 262*, 1025-1029.

20. Slinker, J. D., Muren, N. B., Renfrew, S. E., and Barton, J. K. (2011) DNA charge transport over 34 nm, *Nat. Chem. 3*, 228-233.

21. Boon, E. M., Ceres, D. M., Drummond, T. G., Hill, M. G., and Barton, J. K. (2000) Mutation detection by electrocatalysis at DNA-modified electrodes, *Nat. Biotechnol. 18*, 1096-1100.

22. Gorodetsky, A. A., Ebrahim, A., and Barton, J. K. (2008) Electrical detection of TATA binding protein at DNA-modified microelectrodes, *J. Am. Chem. Soc. 130*, 2924-2925.

23. Muren, N. B., and Barton, J. K. (2013) Electrochemical assay for the signal-on detection of human DNA methyltransferase activity, *J. Am. Chem. Soc. 135*, 16632-16640.

24. DeRosa, M. C., Sancar, A., and Barton, J. K. (2005) Electrically monitoring DNA repair by photolyase, *Proc. Natl. Acad. Sci. USA 102*, 10788-10792.

25. Murphy, J. N., Cheng, A. K., Yu, H. Z., and Bizzotto, D. (2009) On the nature of DNA self-assembled monolayers on Au: measuring surface heterogeneity with electrochemical in situ fluorescence microscopy, *J. Am. Chem. Soc. 131*, 4042-4050.

26. Jones, P. A., and Baylin, S. B. (2002) The fundamental role of epigenetic events in cancer, *Nat. Rev. Genet. 3*, 415-428.

27. Jones, P. A., and Laird, P. W. (1999) Cancer epigenetics comes of age, *Nat. Genet. 21*, 163-167.

28. Jones, P. A., and Takai, D. (2001) The role of DNA methylation in mammalian epigenetics, *Science 293*, 1068-1070.

29. Heyn, H., and Esteller, M. (2012) DNA methylation profiling in the clinic: applications and challenges, *Nat. Rev. Genet. 13*, 679-692.

30. Jurkowska, R. Z., Ceccaldi, A., Zhang, Y., Arimondo, P. B., and Jeltsch, A. (2011) DNA methyltransferase assays, *Methods Mol. Biol. 791*, 157-177.